UNIVERSITY OF LIVERPOOL

DUAL-STIMULI RESPONSIVE NANOGELS FOR INJECTABLE DRUG DELIVERY IMPLANTS

Adam R. Town

April 2018

Thesis submitted in accordance with the requirements

of the University of Liverpool for the degree of Doctor in Philosophy

ACKNOWLEDGEMENTS

Firstly, I'd like to begin by acknowledging my supervisor Tom. As the first person to join the McDonald group, his excellent supervision and mentoring throughout my PhD has proved invaluable. He has improved my skillset immeasurably, and without this support the body of research that makes up this PhD would also have been more limited in its extensiveness. His keen interest to help and support all the members of our research group (and others) inspired me to pass on this enthusiasm in the training and supervision of others as the research group has expanded.

Secondly, I'd like to thank my partner Paul, and all my family, particularly my mum and dad, who have always supported me through the challenges and setbacks I've faced with the encouragement that I'd get to the end successfully.

Many thanks also go to my secondary supervisor, Steve Rannard, for the advice, equipment access, and other opportunities and resources he provided. I'd also like to thank Esther Garcia-Tunon Blanca and Janine Kavanagh for their help understanding rheological data, Marco Giardiello for the supply of solid drug nanoparticles, Riaz Akhtar for AFM imaging, Dr Michael Briggs for HPLC support, and Rohan Gurjar and Marco Siccardi for cytotoxicity work.

I'd also like to thank my research group, and the larger nanomedicine group for all their help and support, as well as the vast number of external collaborators, and people in the department, who lent their help or offered advice in one way or another. There are too many examples to list them all here! Some of these people include Edyta, who was not only a great person to work with day to day, but honoured me with the invitation to attend her wedding in Poland. I'd also like to thank Chung, whose diligent work on a 4th year undergraduate project under my supervision greatly helped inform my own research. Also of note is the social support provided by Jess Smith, Jess Taylor, Steph Edwards, Prof. Peter Myers and many others. After a hard day in the lab, these people could always be counted on to lighten the mood, whether it be Peter, who recently celebrated his 35th birthday for the second time by dancing on tables at Bongo's Bingo, a trip to Berlin with Steph after a conference in Dresden, or spontaneous drinks with the two Jess's, and joint runs around Sefton park to break up thesis writing.

I'd also like to thank the Royal Society of Chemistry, Macro Group UK, and the Society of Chemical Industry for the financial support they provided to enable myself to attend conferences. Finally thanks goes to the Engineering and Physical Sciences Research Council, who provided the funding for the opportunity to undertake this PhD in the first place.

ABSTRACT

Chronic conditions are on the rise due to an ageing and increasing global population. Medication adherence to treat chronic conditions is low, with good adherence on average ≤ 50% across a wide range of chronic conditions. Poor adherence is estimated to cost between $100 and $300 billion of avoidable health care costs annually in the US alone. One was to tackle this issue is the use of implants, which provide sustained release of drug over a long time period, removing the reliance on daily oral medication. In situ forming implants are particularly of interest as they can be injected through a standard gauge needle, reducing pain and discomfort for the patient. They are injected as a liquid and then solidify at the injection site.

Three different solidification methods were explored to allow a dispersion of poly(N-isopropylacrylamide) nanogels to act as an in situ forming implant for drug delivery. Two of these solidification methods were based on the modification of existing methods and utilised the modification of the nanogel behaviour with the incorporation of comonomers of acrylic acid and allylamine. The stabiliser polyvinylpyrrolidone (PVP) was included in the synthesis of these nanogels to attempt to aid nanogel dispersion and formulation with a drug payload. A third novel method of solidification was found to work successfully and so was developed and investigated further. This was based on the aggregation of poly(N-isopropylacrylamide) nanogels to rapidly form a drug depot at an injection site in response to both physiological temperature and ionic strength, giving a new in situ forming implant. Nanogels without surfactant, with sodium dodecyl sulphate (SDS), and with PVP were synthesised to determine if this would effect the suitability of the nanogels to undergo triggered aggregation under the correct conditions.

The system was found to be easy to inject, and could be used to deliver hydrophobic drug or hydrophobic drug formulated into solid drug nanoparticles. Unlike the majority of in situ forming implants, a low burst release of drug payload was achievable, < 3.4 wt%, and sustained release was possible for over 120 days. The rate of release could also be tuned by altering the ratio of two different nanogels used to create the depot formulation which has not previously been demonstrated. One of these nanogels contained the comonomer allylamine alongside the monomer N-isopropylacrylamide. This gave a depot with a higher water content and more porosity. Release was also shown to occur through Fickian diffusion. The nanogels were also found not to exhibit any cytotoxicity. Nanogels of different sizes were also synthesised, and it was found that these exhibited different phase behaviour and rheological properties. The rate of drug release from the depot could also be tuned by the size of the nanogel used, which has not previously been demonstrated. Finally nanogels were synthesised with the degradable cross-linking agent N,N'-bis(acryloyl)cystamine (BAC). This allows a depot to degrade into polymeric fragments once it has served its purpose. Alongside BAC, the comonomer N-isopropylmethacrylamide (NIPMAM) was utilised to reduce

non-degradable cross-linking formation. The NIPAM and NIPMAM monomers were used to create core-shell nanogels. The ratio of each monomer used gave nanogels with a tuneable aggregation temperature. The nanogels were shown to be fully degradable into polymeric fragments beyond the lower detection limit of dynamic light scattering when the count rate of the nanogel dispersion was monitored using DLS. The degradation rate was also very sensitive to temperature, with degradation shown to take place at a much slower rate as temperature increased from 25 °C up to 40 °C, where the nanogels are deswollen and more hydrophobic in nature. This could potentially allow a depot to degrade slowly over a period of months, allowing it to provide a sustained release of drug over this time period, whilst also being fully degradable into polymeric fragments when subjected to an average body temperature of 37 °C.

CONTENTS

Chapter 1 – Introduction

Chapter 2 - Exploration of In Situ Forming Implant Concepts Based on Poly(N-isopropylacrylamide) Nanogels

ABBREVIATIONS

AFM	Atomic Force Microscopy
M_W	Average Molecular Weight
CS	Core-Shell
DSC	Differential Scanning Calorimetry
K	Dissolution Constant
DLS	Dynamic Light Scattering
FTIR	Fourier-transform Infrared Spectroscopy
HPLC	High Performance Liquid Chromatography
H_d	Hydrodynamic Diameter
R_h	Hydrodynamic Radius
ISFI	In Situ Forming Implant
kDa	Kilodaltons
LDE	Laser Doppler Electrophoresis
G''	Loss Modulus
LCST	Lower Critical Solution Temperature
MEC	Minimum Effective Concentration
MTC	Minimum Toxic Concentration
MWCO	Molecular Weight Cut Off
NMR	Nuclear Magnetic Resonance
PDA	Photo Diode Array
PdI	Polydispersity Index
LDE	Laser Doppler Electrophoresis
PDA	Photo Diode Array
R_g	Radius of Gyration
ρ	Shape Factor
SANS	Small Angle Neutron Scattering
SDN	Solid Drug Nanoparticle
SEM	Scanning Electron Microscopy
UV	Ultraviolet
UV-Vis	Ultraviolet-Visible Spectroscopy
G	Wire Gauge (e.g. 18G)

CHEMICAL ABBREVIATIONS

MeCN	Acetonitrile
AcA	Acrylic Acid
ATP	Adenosine 5′-Triphosphate
AlA	Allylamine
TPGS	D-α-Tocopheryl Polyethylene Glycol Succinate
D_2O	Deuterium Oxide
DTT	Dithiothreitol
GSH	Glutathione
GSSG	Glutathione Disulphide
HBSS	Hank's Balanced Salt Solution
HCl	Hydrochloric Acid
LPV	Lopinavir
MTT	Methylthiazolyldiphenyl-Tetrazolium Bromide
NIPAM	N-isopropylacrylamide
NIPMAM	N-isopropylmethacrylamide
BAC	N,N'-bis(acryloyl)cystamine
BIS	N,N'-methylenebisacrylamide
OR	Oil Red
PBS	Phosphate Buffered Saline
PolyNIPAM	Poly(N-isopropylacrylamide)
PolyNIPMAM	Poly(N-isopropylmethacrylamide)
PS	Polystyrene
PVA	Poly(Vinyl Alcohol)
PVP	Polyvinylpyrrolidone
KPS	Potassium Persulfate
NaCl	Sodium Chloride
SDS	Sodium Dodecyl Sulphate
NaOH	Sodium Hydroxide
THF	Tetrahydrofuran
TSP	Trimethylsilylpropanoic acid

PRESENTATIONS AND PUBLICATIONS

Publications:

Dual-stimuli responsive injectable microgel/solid drug nanoparticle nanocomposites for release of poorly soluble drugs. A. R. Town, M. Giardiello, R. Gurjar, M. Siccardi, M. E. Briggs, R. Akhtar, T. O. McDonald. Nanoscale, 2017, 9, 6302–6314.

Tuning HIV drug release from a nanogel-based in situ forming implant by changing nanogel size. A. R. Town, J. Taylor, K. Dawson, E. Niezabitowska, N. M. Elbaz, A. Corker, E. Garcia-Tuñón and T. O. McDonald. Journal of Materials Chemistry B, 2019, 7, 373–383.

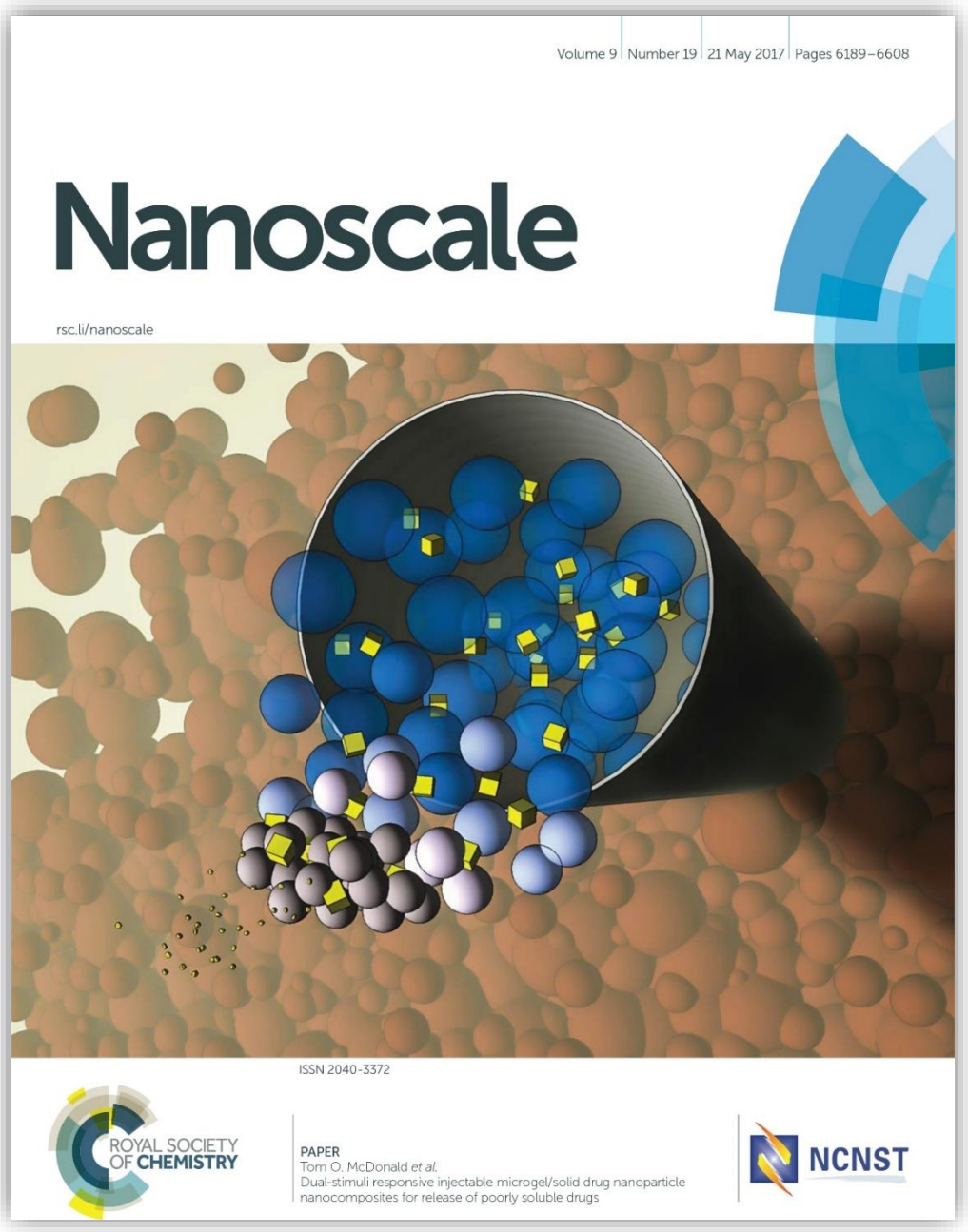

Oral Presentations:

254th ACS National Meeting (Washington D.C., 2017) - American Chemical Society

Young Researchers Meeting (Edinburgh, 2017) - Macro Group UK

10th World Biomaterials Congress (Montreal, 2016)

Young Researchers Meeting (Swansea, 2016) – British Society for Nanomedicine

Poster Presentations:

European Nanomedicine Meeting (London, 2017) – British Society for Nanomedicine

Non-Newtonian Club Meeting (Liverpool, 2017) – British Society of Rheology

Young Researchers Meeting (Liverpool, 2016) - Macro Group UK

Congress of the EPF (Dresden, 2015) - European Polymer Federation

Young Researchers Meeting (Liverpool, 2015) – British Society for Nanomedicine

Travel Bursaries and Awards:

Rideal Travel Bursary (2017) - Society of Chemical Industry and Royal Society of Chemistry

D.H. Richards Memorial Bursary (2015) - Macro Group UK

Chapter 1

Introduction

1.1. The Rise of Chronic Conditions

One of mankind's greatest, and often overlooked achievements is the development of modern healthcare. This has been a big contributor to life expectancy, which has risen consistently for over a century, giving us all the gift of a longer life.[1] In the record holding country (Japan), female life expectancy has risen at a rate of 3 months per year for the last 160 years.[1] This trend is mirrored in other industrialised nations, and is predicted to carry on well into the future.[2] However, this rise in life expectancy presents another set of challenges for scientist to address, that is the rise in chronic diseases as people live longer. Chronic diseases are defined and summarised by the U.S. National Center for Health Statistics as lasting 3 months or more, generally not being curable by medication, nor simply disappearing over time.[3] Chronic diseases become more prevalent in a population with age, so as life expectancy rises, so does chronic disease.[4] Over 50% of people over the age of 65 have more than one chronic disease, compared to a much lower rate for younger people.[4] With the median age of the entire world's population predicted to rise far into the future,[5] the number of people living with chronic diseases will also carry on rising. This rise is enhanced not only by people living longer, but also by the fact that the world's population is continually growing,[6] further accelerating this problem in the future if it is not addressed.

1.2. Adherence

Many chronic diseases are managed through patient self-medication, where a patient must take medication appropriately without direct professional medical assistance to achieve the best therapeutic outcome.[7] This most frequently takes the form of oral medication, taken once or multiple times a day, for the remainder of that patients lifetime, because of its simplicity and convenience over other administration routes.[7] The measure of a patients ability to adhere to medical advice in regards to their self-medication regime is termed medication adherence.[8] If medication dosages are missed by the patient, they are considered to be less adherent than 100% adherence, where a patient takes their medication exactly as prescribed, also known as non-adherent.[9] Adherence itself is much broader that simply adherence to medication. It can also be a measure of ability to seek medical attention, fill prescriptions, obtain immunisations, attending follow-up appointments and execute behavioural changes.[10] Adherence can be understood better with as example: in Europe, only 28% of patients

being treated for diabetes achieve good glycaemic control. However this figure is a combination of adherence measurements. These include adherence to a good diet (behavioural adherence), as well as medication adherence, which for diabetes still only lies at 67.5%[11], despite diabetes being a potentially fatal condition.[12] The focus of this thesis lies on medication adherence rather than adherence as a whole, and so from now on adherence refers specifically to medication adherence, which is generally the most widely researched and important of the forms adherence can take.

1.2.1. Medication Adherence

Medication adherence is vital in the treatment of many chronic conditions such as HIV, diabetes, cancer, hypertension, coronary heart disease, depression, and mental conditions, however mean patient adherence rates range anywhere from poor to near complete adherence depending on the disease, geographical location and a number of other factors. Surprisingly, in developed countries, good adherence in patients with chronic diseases is measured to average only 40-50% across a range of conditions,[13,14] and although the accuracy of these generalised adherence averages for all chronic conditions has been questioned,[15] adherence is still clearly much lower than desired. The highest mean adherence in a review of 508 studies into 17 diseases was found to lie at 88.3% for HIV.[11] The seriousness of this value is difficult to comprehend until taking into consideration that successful management of HIV requires adherence > 95%, and so good adherence is critical.[16] Medication adherence is also important in many other chronic conditions such as diabetes, where poor adherence leads to increased morbidity and mortality.[17] Rates of adherence are also found to be much lower in chronic conditions than acute ones, dropping most dramatically after the first 6 months of therapy.[18,19] Likewise medication adherence drops dramatically when patients are required to take an increasing number of daily medication doses. With over half of patients not intentionally missing doses, this effect is mainly down to the difficulty of remembering to take multiple doses at different times in the day, every day, for long periods.[20] There are also many other factors which have an effect on medication adherence which can be broadly grouped into external, provider and patient factors. In patient factors alone lies demographical, sociocultural and behavioural reasons. Just a few interesting examples of the many barriers to adherence include

stress, cognitive function, health literacy, age, sex, employment status and income of the patient.[21,22]

1.2.2. The Impact of Poor Adherence

Patients need to be adherent to their medication regimen for a number of reasons. The most obvious and important being the increase in morbidity and mortality with poor adherence.[23] There is also the avoidable healthcare cost burden placed on the healthcare system from increased service utilisation, such as increased hospital admissions.[24] In the US alone this is estimated to total $100 and $300 billion of avoidable health care costs annually to due poor adherence.[25] We can also consider why adherence is important therapeutically on a physiological level, which requires a little more detail to understand as a concept, and is the underlying reason for increased morbidity, mortality and healthcare cost.

1.2.3. Therapeutic Effect of Poor Adherence

When a patient is required to take repeated doses of medication at set intervals of time, it is because a steady state of drug at a certain plasma concentration is required in the body.[26] When a patient takes their first dose of medication orally, this will lead to a spike of maximum drug plasma concentration (C_{max}) at time (t_{max}), figure 1.1 (i).[27] The concentration of drug then decreases over time and is quantified by the elimination half-life ($t_{1/2}$).[28] This then reaches a trough known as (C_{min}), which is the minimum concentration reached before the next dose is administered, figure 1.1 (ii). Upon subsequent doses C_{max} and C_{min} are greater, and continue to increase until a steady state is reached, usually at 4 to 5 times the $t_{1/2}$ of the drug, figure 1.1 (iii).[29] To maintain this steady state the patient must maintain the correct dosage amount and interval.

The steady state concentration required is determined by the therapeutic index of the drug. The therapeutic index is the ratio of the lethal concentration to the therapeutic concentration of a particular drug in the body.[30] Hence safer drugs have a higher index. The most effective drug dose and frequency to reach the steady state concentration required can be simulated through pharmacokinetic (PBPK) models,[31,32] and is based on a large set of parameters, which include solubility, potency and bioavailability of a drug, metabolism rate, formulation of the drug and administration route.[33] The actual steady state concentration can also be determined from patient blood samples.[34] The

steady state concentration should fall in a concentration range known as the therapeutic window. This is bound by a maximum and minimum concentration, known as the minimum toxic concentration (MTC) and minimum effective concentrations (MEC) respectively, (figure 1.1).[35] This window gives a range where drug is considered to act therapeutically; C_{max} and C_{min} should ideally fall within this window.

An example using a hypothetical 'Patient X' (who is suffering from a chronic illness and taking a daily oral medication) can be used to demonstrate the importance of medication adherence for chronic conditions in terms of the therapeutic window. If patient X misses or delays medication doses, then the drug concentration will fall below the MEC and out of therapeutic window into the sub therapeutic range, figure 1.1 (iv), particularly for drugs with a narrow therapeutic index.[36] Other than halting the therapeutic action of the drug, this can also have more profound consequences for some conditions. An example of this is in the treatment of HIV, where drug resistance to highly active antiretroviral therapy (HAART) can develop in the sub therapeutic range, leading to failure of the treatment, and limiting options available for future treatments each time a treatment fails.[37,38] There is also the potential for a patient to overdose on medication, which is caused by factors such as poor health literacy,[21] where medication adherence is then classed as > 100%. (i.e. the patient takes more than the prescribed dose).[39] Using patient X's poor health literacy as an example, they may think "I missed my last pill, I'll take two pills this time to catch up". Unfortunately, in this case, patient X doesn't realise it, but the effect is to take the drug concentration over the MTC, and above the therapeutic window, figure 1.1 (v). Hopefully patient X avoids a dose great enough to cause death, however they now experience unwanted side effects as the drug reaches a toxic level.[40] This causes patient X to decide to stop taking their medication because it's making them feel much worse than the chronic condition they are suffering from, figure 1.1 (vi). This could result in an expensive hospital admission to stabilise the patient.[41] Achieving good medication adherence avoids these issues.

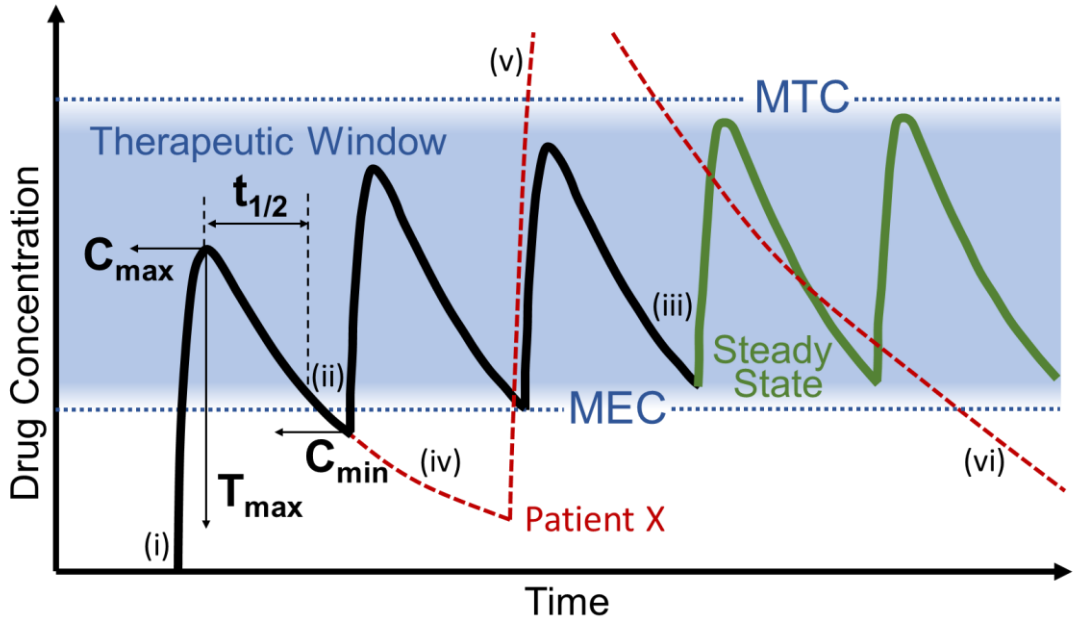

Figure 1.1 Illustration of drug concentration over time with repeated oral dosage of medication *for complete medication adherence:* (i) first dose, (ii) second dose, (iii) point at which a steady stated of drug concentration is reached, and *irregular medication adherence of patient X:* (iv) deviation of drug concentration into sub therapeutic region with missed dose, (v) deviation of drug concentration into toxic range, (vi) drug clearance from body as patient ceases to follow drug regimen.

1.2.4. Solutions to Poor Medication Adherence

Over the decades there have been a wide range of strategies to improve medication adherence, which all have the aim of maintaining a drug concentration within the therapeutic window. Some more pragmatic approaches include simplifying the patients medicine regimen, medication aids, Short Message Service (SMS) reminders, and introducing a collaborative approach at the level of prescribing.[9,42] Some easily overlooked solutions also include simply proving better transport and pharmacy parking for patients. Mail order pharmacy removes the influences of collecting medication prescriptions on adherence from the equation. Hence it has been shown to give a reduction in emergency department visits in the treatment of conditions such as diabetes over more traditional pharmacy routes.[43] Interventions involving pharmacists, behavioural specialists, and nursing staff have also been utilised to try to improve medication adherence rates.[44,45] These can take the form of behavioural, educational, integrated care, self-management and risk communication interventions.[46,47] Simple interventions somewhat increase adherence for short term treatments, however even when interventions were more complex, they were found to be much less effective in dealing with chronic conditions, with little perceived improvement across a range of

studies.[43] Successful methods for improving medication adherence are generally complex, labour intensive, and single approaches are not suitable for all patients or conditions, leaving room for new innovative strategies.[48] These strategies potentially come in the form of new technological approaches to improving adherence, this includes a concerted effort to leverage big data and the internet of things (IOT) to utilise devices such smartphones (mHealth) and virtual assistants (e.g. Amazon Alexa and Google Assistant).[14,49] A technological approach has also been taken towards mail order pharmacy, incorporating it into a system of blockchain technology, which can utilise data sharing to create "adherence profiles", cryptocurrency incentives, and customised reminders for patients to improve adherence.[50] These new approaches are either still in development, or have only recently been employed, so they have not yet been studied and scrutinised to an appropriate level to make any claims as to their effectiveness.

1.3. Long Acting Release

One way to improve medication adherence is to remove the reliance on the patient to take either daily or more frequent medication doses. This has been shown to improve adherence by avoiding issues such as 'pill fatigue' and missed doses.[51,52] This is achieved through long acting drug delivery systems, where dosing can be as infrequent as monthly, quarterly or yearly. This is also referred to as controlled release, because the controlled rate of release of drug gives a plasma concentration which remains constant or slowly decreases within the therapeutic window in comparison to the peaks and troughs of frequent oral dosing, figure 1.2.[53,54] Ideally, release is zero order, to maintain a constant rate of release, although other release kinetics can still provide viable long acting release.[55] Development of long acting drug release began with implantable drug delivery systems in the 1930's for veterinary use,[56] however the technology did not reach mainstream development for human use, and commercialisation, until the 1960's and 1970's respectively with the inception of companies dedicated to controlled release such as Alza and Elan. Early devices were macroscopic, non-injectable and non-degradable,[57] which along with subcutaneous implants also took the form of mucosal inserts and topical patches.[57] Whilst reasonably practical for mucosal and topical usage, they required invasive microsurgery to locate and remove from a subcutaneous site. Drug delivery devices have since become increasingly more sophisticated, and are now available in the form of injectable and biodegradable formulations;[58] these include polymeric implants,[59] microspheres/particles,[60,61] hydrogels,[62] and oils.[58]

Commercially available implantable systems include Vitrasert® which was approved by the FDA in 1996 for the treatment of AIDS-related cytomegalovirus (CMV) retinitis. This consists of a reservoir of the drug ganciclovir coated in polyvinyl alcohol (PVA) and ethylene vinyl acetate (EVA) and located intravitreally. Delivery of drug is possible for 5-8 months with zero-order release,[63] and replaces weekly injections.[64] This was shown to limit the progression of CMV retinitis three times longer than intravenous injection.[65] However this requires invasive surgery for implantation and removal. Another example of a commercially available implant is a Lupron depot®, which is a microparticle depot used to treat cancer and other conditions via intramuscular injection.[66] The leuprolide hormone is encapsulated in poly(lactic-co-glycolic acid) microspheres, with long acting release allowing the frequency of injections to be lowered.[67]

Overall implantable systems can be significantly more convenient for the patient, reduce morbidity and mortality, and also reduce healthcare costs by avoiding the effects of poor adherence such as hospital admissions. Long acting release has also proved particularly effective for patients with psychological dysfunctions, where oral medication compliance can be less than 40%,[68] or patients with drug addictions where a large stock of tablets cannot be provided.[69,70]

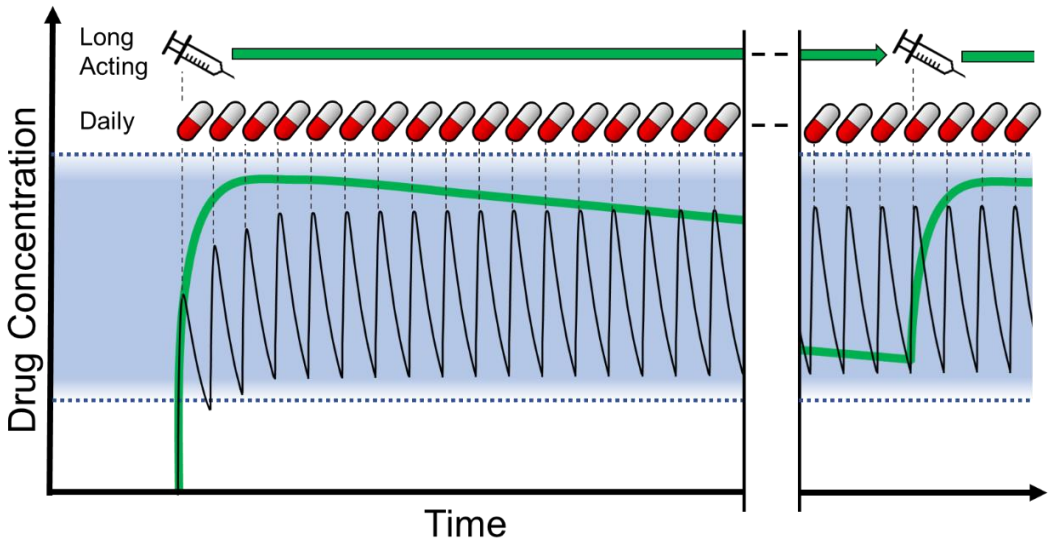

Figure 1.2 Illustrative comparison of drug concentration over time with repeated daily oral dosage of medication (black line) and a long acting injectable formulation (green line).

1.3.1. Routes of Administration of Long Acting Systems

Long acting systems are most commonly administered through intravenous, intramuscular and subcutaneous routes,[71] although oral, nasal and transdermal delivery is also possible with certain limitations.[72] For example controlled release medications using the convenience of the oral administration route are available,[73] however they are not truly long acting, because they still require frequent dosage. This is because the majority of a drug is absorbed in the small intestine, where the length of transit time is on average only eight hours.[74] Hence an orally administered drug can only be employed for a short time as it migrates through the gastrointestinal tract. Long acting release will ideally therefore use an alternative method for drug delivery, where a longer release period can be obtained. For example intravenous injections are able to provide extended drug release during systemic circulation of a drug carrier.[75,76] Alternatively, the long acting system can be administered intramuscularly or subcutaneously, to form a drug delivery depot, which allows delivery on a prolonged timescale from weeks to years.[77] A drug depot is a site where a localized mass of drug is stored and released at a controlled rate usually from a subcutaneous, intradermal or intramuscular site; replacing many doses with one dose for a given period of time. This allows the concentration of drug in the body to remain within the therapeutic window for a prolonged period of time. This is achieved by tuning the release rate from the drug depot to counter the rate of elimination of the drug from the body.[78]

1.3.2. Subcutaneous and Intramuscular Administration Considerations

There are a number of important considerations for long acting systems which are administered intramuscularly or subcutaneously. First of all, the biocompatibility of biomaterials used in this way is multifaceted. They must be chemically inert, noncarcinogenic, hypoallergenic, and avoid a large inflammatory response.[79] Otherwise issues such as platelet adhesion, tissue damage, or infection are all possible.[54,80] Inflammatory response can also have an effect on drug release rate, for example the formation of a fibrous capsule of collagen fibrils around the depot can modify the in vivo release rate.[81,82] Even without an inflammatory response the release rate observed *in vitro* and *in vivo,* for example in subcutaneous tissue, can differ due to the local *in vivo* environment.[83] Hence it is important to consider the impact of the local environment on the *in vitro – in vivo* release rate correlation. This correlation is very difficult to predict, and although predictions can be made for specific depot

formulations of drug, often animal models are used to determine *in vivo* release rates.[84] The *in vivo* release rate at a subcutaneous or intramuscular site also effects the pharmacokinetics (distribution and fate) of a drug delivered from a depot. The pharmacokinetics are dependent on the release rate of drug as well as many other factors such as free drug in the surrounding tissue, metabolites, drug degradation, drug bound to tissue and proteins, and absorption via blood or the lymphatic system into systemic circulation.[85] However this can be simplified in the categorisation by Washington *et al*. when the pharmacokinetics are controlled by the depot when drug release from the depot is slow (Type I), and release rate is limited by the pharmacokinetic absorption rate when depot drug release is fast (Type II).[86] Drug release from a depot can also occur by different mechanisms depending on the chemistry of the biomaterials used to form the depot. This includes diffusion controlled, chemically controlled, solvent-activated and modulated-release, where drug release is controlled by stimuli such as pH, ionic strength or temperature.[87]

1.3.3. Criteria for a Successful Long Acting System

Alongside the above considerations, a long acting release injection or implant must meet a large set of criteria to be viable. Criterion that a delivery technology can prove inadequate against include: a) the length of the release period/release rate of drug, b) the amount of burst release that occurs, c) the percentage drug loading that can be achieved, d) mechanical stability, e) ease of administration, f) cytotoxicity and inflammation response, g) drug stability, and h) cost of the technology.[88–90] It is important to assess long acting delivery technologies against this criteria during development. There is also no single solution which is suitable for the entire long acting release market; the treatment of different conditions for example requires a different rate of drug delivery to achieve a therapeutic dose. Some examples of how depots can be modified in development to achieve each of the above desired criteria include: a) changing the viscosity of an oil used in a drug loaded oil depot to change the release rate of drug from the depot,[91,92] b) performing surface coating, or surface drug extraction on a depot to prevent burst release,[90] c) changing the size of poly(lactic-co-glycolic acid) (PLGA) microspheres used in long acting drug delivery to increase drug loading,[93] d) the inclusion of a second material, such as the addition of chitosan to bovine serum albumin based hydrogels to increase the mechanical stability of the depot,[94] e) adding a rheological modifier, such as the addition of

N-methyl pyrrolidone to l-alanine based implants, to reduce the viscosity and allow easier administration of an injectable depot,[95] f) using a depot coating such as a layer of poly(*N*-isopropylacrylamide) (polyNIPAM) nanogels to reduce inflammation response to a depot,[96] g) including stabilising agents such as small sugars to increase the stability of biopharmaceutical drugs within a depot,[97] and finally h) using low cost materials and a simple manufacturing process such as in systems based on sucrose acetate isobutyrate to reduce the overall cost of the technology.[98] Therefore, although a drug delivery technology may not be appropriate for clinical usage after initial development due to a large set of criteria it must meet, there are usually many opportunities to continue the development of a promising long acting injection or implant to improve its performance.

1.4. In Situ Forming Implants (ISFIs)

One delivery system of current interest is *in situ forming implants* (ISFIs).[99] An ISFI consists of an injectable low viscosity solution which once inside the body is able to transform into a gel or solid depot, (figure 1.3).[98] The main advantage of an ISFI over other long acting implants is its comparatively less invasive and less painful administration, due to the ability of being able to inject a low viscosity liquid through a standard gauge needle, so that local anaesthesia and surgical intervention are not required.[99] Due to the less invasive administration, it is also useful for the ISFI to be degradable, as then the depot does not have to be surgically removed after having served its purpose. Kang *et al.* were able to demonstrate a degradable depot which was also biocompatible, formed from the thermo gelation of a diblock copolymer consisting of polyethylene glycol block, and a random copolymer block of polycaprolactone (PCL) and poly-L-lactic acid (PLLA).[100] By changing the ratio of PCL to PLLA, the rate of degradation could be tuned, with *in vivo* studies showing degradation of the depot to be tuneable from a range of weeks to months.[100] ISFI systems also provide a relatively extensive period of sustained release, compatibility with a wide range of drugs and relatively simplified manufacturing and low production cost.[98] For the drug leuprolide (used to treat prostate cancer, breast cancer, endometriosis, uterine fibroids, and early puberty), an ISFI has been demonstrated clinically to be effective for a 6 month time span, meaning only 2 injections a year are required, allowing patients to improve their medication adherence.[101] Many other drugs have also been successfully released from ISFIs,[102] and they also show

suitability in the delivery of fragile drugs, biopharmaceuticals, and drugs with short half-lives.[97] Amiram *et al.* showed that a glucagon-like peptide used in the treatment of diabetes could be fused to a thermally sensitive elastin-like polypeptide which forms a depot at body temperature. This allowed a 120 fold increase in therapeutic effect duration, in which blood glucose level was reduced.[103] ISFIs are also useful where localised drug delivery is required.[104] Kilicarslan *et al.* showed that mucoadhesive sodium carboxymethyl cellulose and carbopol polymers could be combined with poly(lactide-co-glycolide) (PLGA) to give an ISFI capable of releasing the drug metronidazole locally to treat periodontal pockets. The depot was also degradable, and the rate of drug release could also be tuned depending upon the composition of the depot.[105] Compared to other delivery technologies, ISFIs can however also suffer from various issues. These include a large burst release of drug,[106] potential toxicity of materials,[107] cytotoxicity and inflammation response,[54] long-term stability of the drugs,[108] and finally variation in the shape of the implant formed, which leads to a variation in the amount of drug released.[98] However these issues can be avoided in ISFIs. Shikanov *et al.* synthesised the polyesteranhydride poly(sebacic-co-ricinoleic acid), which solidified when in contact with water. Minimal burst release of the drug paclitaxel was observed from this depot material, whilst it was also degradable, and showed minimal inflammation response.[109]

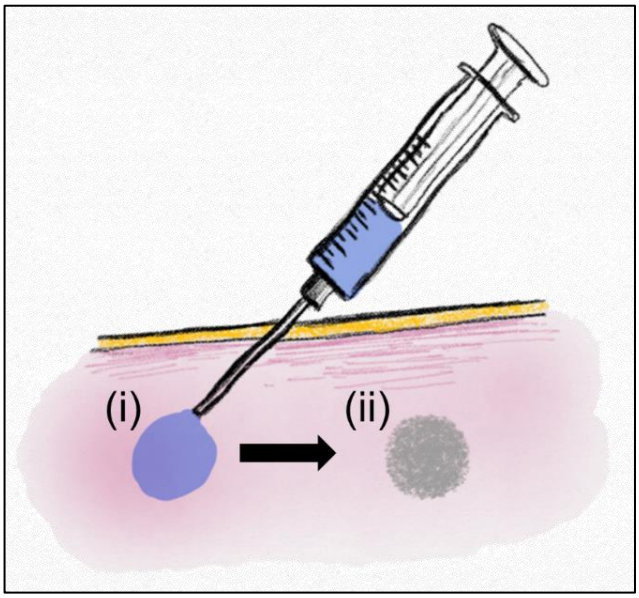

Figure 1.3 Illustration of an in situ forming implant (ISFI). (i) a low viscosity liquid is injected through a standard hypodermic needle into a subcutaneous or intramuscular site, (ii) a trigger causes the liquid to solidify, forming a depot which can give a sustained release of drug over time.

1.4.1. Solidification triggers used in ISFIs

A range of ISFI systems have been developed, which achieve in situ gelation or solidification by different triggers. Some of these triggers include in situ physical or chemical cross-linking,[107,108] solidifying organogels,[110,111] and in situ phase separation via pH, solvent exchange or temperature.[89]

In situ physical cross-linking occurs via hydrogen bonds or charge interactions. As an example, Balakrishnan and Jayakrishnan demonstrated that the gelation of alginates can occur in the presence of borax to provide the basis for an ISFI which was both biodegradable and biocompatible, with the system also being used to demonstrate the encapsulation of hepatocyte cells.[112] Mekhail *et al.* used guanosine 5′-diphosphate as an anionic cross-linking agent to trigger the gelation of chitosan in 1.6 seconds using electrostatic attractions,[113] which is much faster that the gelation of other chitosan system, which can require over 30 minutes to gelate,[114] allowing potential burst release and flow to surrounding tissues.

In situ chemical cross-linking can be achieved with cross linking agents in situ. An example of this is the in situ polymerisation of poly(propylene fumarate)-diacrylate with the initiator benzoyl peroxide, where the formation of chemical cross-linking in situ allows solidification.[115] However like many in situ polymerisations, there are potential toxicity issues due to the reactive nature of the polymerisation species. In the case of the reactive initiator benzoyl peroxide, there is the potential to promote tumour growth.[116] There are, however, non-cytotoxic methods to induce in situ chemical cross-linking, such as the use of cross-linking agents which are activated by biological triggers. For example, Saeed *et al*. showed that non-cytotoxic chemical cross-linking using di-sulphide bonds and vinyl groups could be triggered by the biological reductant glutathione. It is also possible to trigger chemical cross-linking via photo-initiation. Ono *et al.* modified chitosan to contain lactose and azide moieties. UV light could then be used to trigger photoreactive azide groups to undergo cross-linking, forming a hydrogel within 30 to 60 seconds. The hydrogel also acted as a tissue adhesive.[117] This was then demonstrated to inhibit tumour growth in mice when the antitumour drug paclitaxel was incorporated.[118] One potential drawback for photo cross-linked systems is the low penetration depth possible with irradiated light,[98] and the potential modification of some drugs by high energy radiation.[119]

Another way to trigger solidification is in the use of organogels, which are able to self-assemble and hence gelate through intermolecular interactions, such as hydrogen bonding, π-π stacking, and electrostatic interactions.[111] Gelation can be triggered by heating the organogel and then allowing it to cool at the injection site, or through solvent exchange.[111] Example of the two triggers can be demonstrated with the organogelator N-stearoyl L-alanine methyl ester. Vintiloiu *et al*. showed that as the organogelator cools it gelates via the self-assembly driven by Van der Waals interactions and hydrogen bonding.[120] Plourde *et al.* showed that solvent exchange in the same gelator allowed it to self-assemble into a fibre like structure. This allowed the release of therapeutic peptide for 14 to 25 days.[95]

Finally a range of ISFIs which phase separate based on various different triggers have been demonstrated. A change in pH can be used to trigger solidification, as demonstrated by Chenite *et al*. in the formation of a gel like precipitate for chitosan based implants, due to chitosan being a pH-dependant cationic polymer.[121] Solvent exchange can also be used to trigger solidification. Some organic solvents such as dimethyl sulfoxide and N-Methyl-2-pyrrolidone have limited a limited toxicity,[104,122] and so are utilised in solvent exchange systems.[104] Here, an injection consists of a water insoluble polymer, which contains a solvent the polymer is soluble in. When the solvent diffuses into the surrounding aqueous environment and vice versa, the polymer precipitates to form a depot. However the time taken for these systems to solidify often leads to a large burst release of drug.[104] Dunn *et al*. demonstrated poly(lactic-co-glycolic acid) could be used to create an ISFI based on solvent exchange,[123] with the particular polymer also approved by the FDA for therapeutic devices, due to its biodegradability and biocompatibility.[124] Finally, in situ phase separation can be triggered by a change in temperature. Jeong *et al*. showed that a poly(ethylene glycol)-poly(lactic acid-co-glycolic acid)-poly(ethylene glycol) block copolymer transitioned from a sol to a gel at physiological temperature due to the formation of a hydrophobic core driving micellular arrangement.[125]

Kempe and Mäder summarised that an ideal ISFI should be of low viscosity to allow injection, allow simple drug loading, contain only biodegradable and biocompatible material, good system stability, and low initial burst release and low variability of drug release over time.[98] However, ISFI's which have previously been developed generally suffer from one or more issues,[98] with burst release of drug being a particularly prevalent issue across a range of delivery systems.[110]

1.5. Nanogels

A very recent area of interest for in situ forming implants is the application of nanogels to form depots.[126] A nanogel is a series of cross-linked polymer chains which form a nano-sized particle containing a network of polymers, which has the ability to be swollen by a good solvent, (figure 1.4).[127] Nanogels form a disperse phase of discrete polymeric particles and so exhibit properties of both colloids and gels, and act as an intermediate between branched and macroscopically linked systems.[128] They are often termed microgels in literature,[129] as first coined by Baker,[130] and synthesised by Staudinger and Husemann.[131] There does not seem to be a clear consensus in the literature with regards to the terms used to refer to different sizes of cross-linked swollen nanoparticles, with nanogel and microgel being used interchangeably. Generally, the term microgel is favoured for larger particles and vice versa for nanogels. Whilst the majority of nanogels in literature fall below 100 nm, there are examples of nanogels being defined as particles of less than 200 nm,132 and also examples of nanogels above 200 nm,133 300 nm,134 400 nm135 and up to 500 nm.136 Hence the term nanogel is used in this thesis, as the nanogels under investigation were generally in the range of 30 to 1000 nm in diameter, so it was felt the prefix ‘nano’ was a better representation for the particles under discussion, as they fall below a micrometer in size.

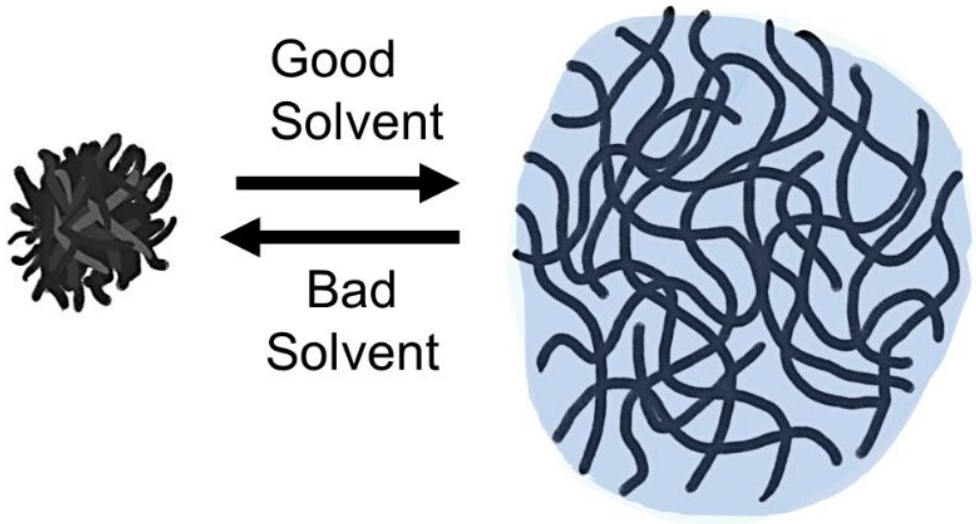

Figure 1.4 Illustration of a nanogel in a bad solvent (collapsed) and good solvent (swollen by solvent).

1.5.1. Nanogel Applications

The properties of nanogels allow them to be used in a range of useful applications. One example of a nanogel is polystyrene latex, which can be swollen with an organic solvent such as tetrahydrofuran (THF). This reversible swelling behaviour can be used to allow encapsulation of a hydrophobic compound in the nanogel particles.[137] Although all nanogels are responsive to solvent environment, they can also exhibit other properties which can be exploited. Depending on the material they are composed of they may also be able to reversibly respond to other environmental stimuli such as temperature, pH and ionic strength.[127] In terms of drug delivery, nanogels have been demonstrated to both encapsulate and release many different bioactive compounds,[136] whilst also achieving targeted delivery by taking advantage of their responsive behaviour.[138] Used at a high enough concentration, or as two populations of oppositely charged particles, they can also achieve the viscosity of a bulk gel when swollen with solvent, but with shear thinning behaviour.[139] This allows them to act as an injectable material.[140] One such use is mouldable tissue engineering scaffolds.[141,142] Most nanogels used in nanomedical applications are hydrogels. Hydrogels consist of a water-soluble polymer network containing a large amount of water.[143] Cross-linking between the polymer chains prevents the network from dissolving. They are distinguishable from other bulk gels by the fact that their high water content and biocompatibility make them ideal for biological applications such as drug delivery, tissue engineering and bionanotechnology.[144,145] Increasingly ‘smart’ hydrogels, with environmentally sensitive properties are being employed.[146] When hydrogels take on the particulate form of a nanogel they have a much higher surface-to-volume ratio,[126] and a much faster response to environmental changes than a bulk hydrogel.[147] Hence hydrogel based nanogels are often more useful smart materials than their bulk counterparts.

1.5.2. Nanogel Based In Situ Forming Implants

A range of injectable nanogels have recently been demonstrated for use in drug delivery systemically, however as the research area is still in its infancy examples of injectable nanogels being specifically employed for depot formation as an ISFIs are very limited.[126] Oppositely charged particles can be synthesised, which are able to interact and self-assemble to from a nano-network through electrostatic forces.[148]

Gu *et al*. demonstrated glucose-mediated insulin delivery was possible using dextran based nanogels coated with oppositely charged polymers, allowing the particles to self-assemble at the injection site through electrostatic interactions.[149] Injection of the material is possible because the weak electrostatic interactions can be disrupted by shear during injection of the material.[141] However with surface charge potentially having a cytotoxic effect,[150] this could present a barrier to the commercial deployment electrostatic of charge interaction-based approaches. Thermo-gelation of chitosan particles in situ has also been demonstrated by Hsiao *et al*. to deliver the hydrophilic anti-epilepsy drug ethosuximide,[151] as well as in the treatment of diabetes.[152] Chen *et al*. have also demonstrated the self-assembly of ketal derivative polymers to form a micellar nanogel depot for the delivery of the drug paclitaxel.[153] Finally Nakai *et al*. demonstrated that salt induced aggregation of hyaluronic acid based nanogels could be used to create a solid depot in situ, with high protein loading and low denaturation possible using nanogels.[154]

1.6. PolyNIPAM Nanogel Based In Situ Forming Implants

An interesting nanogel which has been demonstrated for use as an ISFI in a small number of studies is a nanogel formed of the thermo-responsive polymer poly(N-isopropylacrylamide) (polyNIPAM), (figure 1.5).[127]

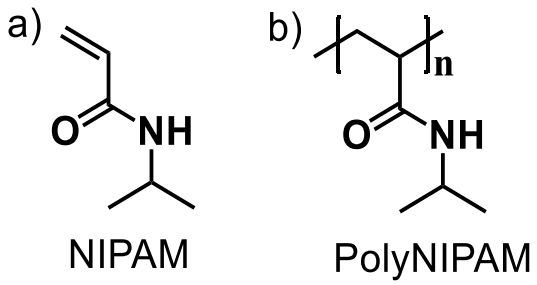

Figure 1.5 Chemical structure of a) the monomer N-isopropylacrylamide (NIPAM) and b) the corresponding polymer poly(N-isopropylacrylamide) (polyNIPAM).

PolyNIPAM nanogels are able to respond to a rise in temperature above around 34 °C.[155] As this response lies between room temperature and body temperature, and these nanogels have also been shown to reduce inflammation response when coating other drug depots,[96] these nanogels could potentially be used to develop an ISFI which is able to meet all the required criteria to reach clinical success. Huang *et al*.

synthesised two species of polyNIPAM nanogels using 10 mol% of allylamine and acrylic acid respectively as comonomers. This gave polyNIPAM-co-allylamine and polyNIPAM-co-acrylic acid nanogels, which had a hydrodynamic diameter of 372 nm and 640 nm respectively at 21 ° C. Glutaric dialdehyde and adipic acid dihydrazide were used to covalently cross-link each of the two nanogel species, allowing the formation of a three-dimensional gel network, (figure 1.6, a). Unlike bulk polyNIPAM hydrogel, these networks were able to give sustained release of dextran. The rate of release was also tuneable using a range of dextran molecular weights, due to the mesh size of the cavities formed in between the nanogels covalently linked together to form the three-dimensional gel network.[156] However, this system would have to be implanted rather than injected, and so would lose the less invasive administration benefits of an ISFI. Wang *et al*. showed than thermoresponsive polyNIPAM nanogels with an acrylamide comonomer were injectable, and able to gelate under physiological conditions.[157] These nanogels had a hydrodynamic diameter in the range of 200 to 300 nm at 25 °C, with nanogels synthesised with less than 5 mol% of cross-linking agent showing more abrupt thermoresponsive deswelling in response to an increase in temperature. The nanogels were shown to be able to undergo phase transitions between a swollen gel, shrunken gel, and liquid, depending on the concentration and temperature of the nanogel dispersion, (figure 1.6, b). However, in terms of drug delivery significant burst release of anticancer drug Bleomycin was seen from a concentrated dispersion of the nanogels (13% w/v), with up to 50% of cumulative drug release occurring in the first 5 hours.[157] Similar burst release issues were seen in the release of 5-Fluorouracil from thermoresponsive polyNIPAM nanogels synthesised with the same acrylamide comonomer, to give nanogels with a diameter of 230 nm. The release of the biomacromolecule bovine serum albumin was also assessed, and reached a plateau of 20% cumulative release, likely due to the large protein remaining entrapped between the nanogels. In order to measure drug release from this nanogel, an 8.3% (w/v) dispersion loaded with drug was prepared in a flat bottom test tube, forming a gel phase at 37 °C. Release medium was then added on top of the gel phase and replaced at sampling intervals, (figure 1.6, c).[158] Finally Xiong *et al*. showed polyNIPAM nanogels with acrylic acid comonomer were able to gelate in situ in response to a change in both temperature and pH. Nanogels with a diameter in the range of 100 to 900 nm were created using varying amount of acrylic acid comonomer

in the synthesis (0 – 32.9 mol%), with the nanogel diameter also dependant on pH as well as temperature. When the nanogels were used as a drug depot, *in vivo* studies showed the nanogels had good biocompatibility and syringability.[159] However, with no way for the nanogels to degrade, the depot would have to be removed surgically after having served its purpose unless a degradable version of the nanogels was developed.

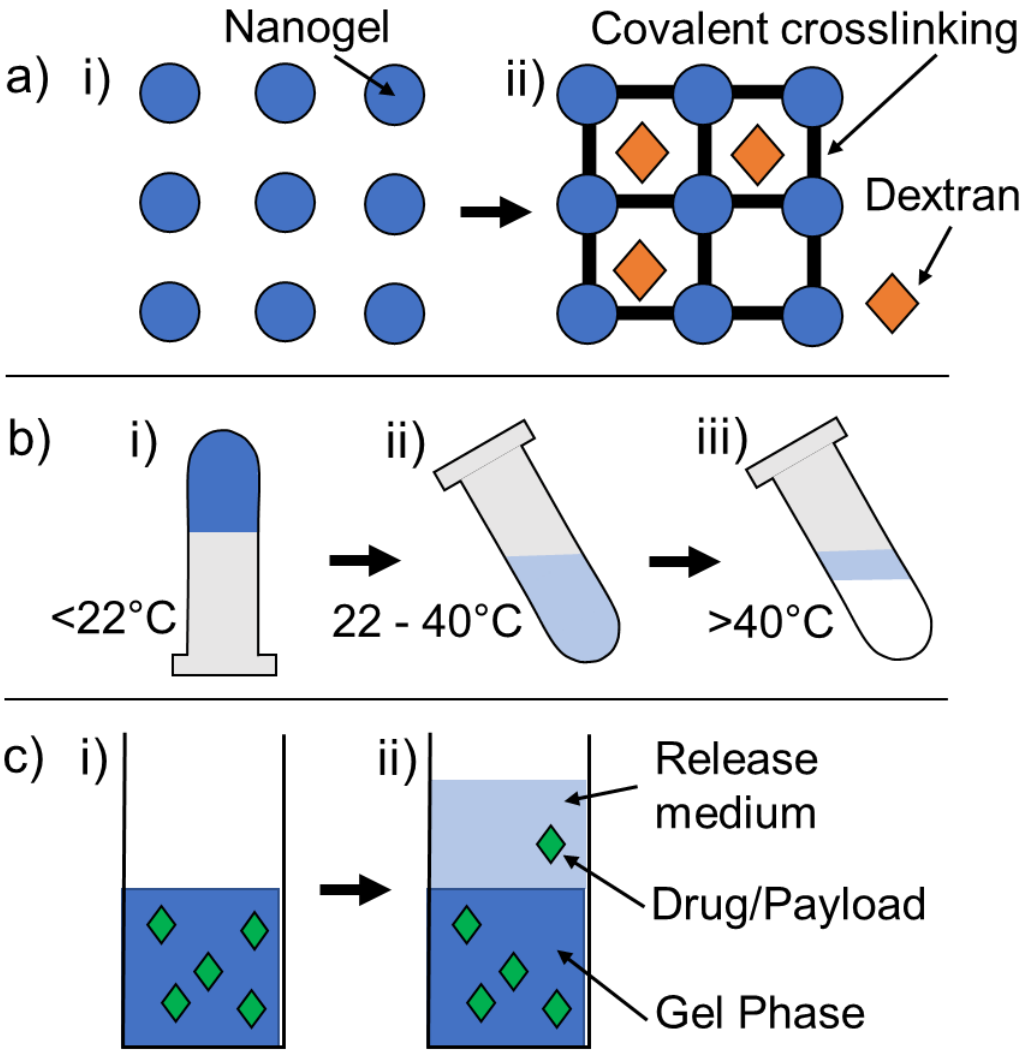

Figure 1.6 Illustrations of polyNIPAM based in situ forming implants, a) two dimensional representation of a i) nanogel dispersion and ii) covalent cross-linking of the nanogels, allowing release of dextran contained in the mesh of the three dimensional structure.[156] b) concentrated nanogel dispersion as i) a swollen gel, ii) a liquid, and iii) a shrunken gel.[157] c) *in vitro* drug release i) from the gel phase of a concentrated nanogel dispersion at 37 °C, ii) after the introduction of release media to allow drug release from the gel phase.[158]

1.6.1. PolyNIPAM Nanogel Behaviour

PolyNIPAM nanogels are one of the most highly studied nanogels based on a hydrogel.[127] PolyNIPAM nanogels were first discovered by a student of Pelton in 1984.[160] The reason for such an interest in this particular nanogel is its temperature sensitive properties. Properties such as size, charge density, colloidal stability, light scattering and hydrophobicity all gradually change with temperature, however around the volume phase transition temperature (VPTT), these properties become very sensitive to a small change in temperature. This VPTT is around 34 °C,[155] with some dependence on factors such as the cross-linker structure and cross-linking density,[161,162] and is the temperature where the nanogel acquires the largest and sharpest hydrodynamic diameter change, (figure 1.7).[163] This is close to the lower critical solution temperature (LCST) of linear polyNIPAM of 32 °C.[164] This gives a very defined transition in particle size and other properties as it crosses the VPTT. Below the VPTT polyNIPAM exists in a swollen state in which the network is fully expanded and swollen by water molecules giving a colloidal hydrogel.[129] Favourable hydrogen bonding interactions exist between the amide groups of the polyNIPAM units and water.[165] Upon heating above the VPTT this hydrogen bonding is increasingly disrupted, so that the water becomes a poorer solvent and the chains begin to collapse expelling most of the water molecules in the process to form a hard sphere.[129] This causes the switch to inter- and intra- polymer hydrogen bonding and polymer-polymer hydrophobic interactions in the nanogel particles.[127] Hence the dramatic change in particle properties and the ability to switch the hydrogel 'on and off' with temperature.

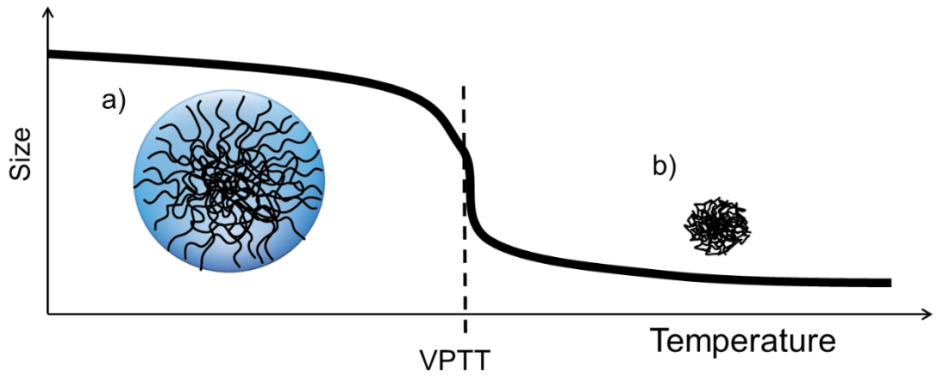

Figure 1.7 Swelling behaviour of poly(NIPAM) nanogel dispersed in water, a) swollen hydrogel particle below the volume phase transition temperature (VPTT), b) collapsed dehydrated particle above the VPTT, water expelled from network upon collapse.

This is of importance in biomedical applications, as the VPTT lies close to body temperature, and so a dramatic change in material properties can be exploited. One such example of this is in a drug delivery application. The drug naltrexone can be loaded into swollen polyNIPAM nanogel particles, and then becomes entrapped as the polymer network collapses as the particles reach body temperature, which is above their LCST. This combined with the switch to a more hydrophobic environment in the collapsed nanogel greatly decreases the release rate of the drug.[166] The nanogel exhibits a "smart" response to its environment.

1.6.2. PolyNIPAM Nanogel Synthesis

PolyNIPAM nanogels are usually synthesised by precipitation or dispersion polymerisation.[167] In a typical precipitation polymerisation the monomer N-isopropylacrylamide (NIPAM) along with a cross-linking agent such as N,N'-methylenebisacrylamide (BIS) is dissolved in water. This is then heated above the LCST of polyNIPAM, followed by the addition of a thermal free radical initiator such as potassium persulfate (KPS). As the chain begins to propagate they reach a length at which they precipitate through homogeneous nucleation into colloidally unstable precursor (primary) particles.[168] It has be shown that polyNIPAM only requires three oligomer units to phase separate,[169] hence the nucleation process to precursor particles happens within minutes, ensuring a narrow particle size distribution.[127] These precursor particles then undergo coagulative association with other precursor particles, until they finally reach colloidal stability as larger polymer particles.[168] It is the charge of the ionic initiator on the chain end of the polymers which determines when colloidal stability is reached, and hence the critical particle size. The hydrophilic chain ends concentrate at the surface of the particle and so surface charge density increase as the particle grows to the point where colloidal stability is reached,[129] (figure 1.8, a). Dispersion polymerisation is able to take advantage of ionic or steric stabilisers. These are able to impart greater colloidal stability to the precursor particles, reducing the amount of precursor particles that must coagulate to reach a colloidal stability particle.[170] Hence the final particle size is smaller and tuneable depending on the amount of stabiliser used, (figure 1.8, b). Tuning particle size was shown to be possible via electrostatic stabilisation by Pelton *et al*. by varying the amount of ionic sodium dodecyl sulphate (SDS).[171] It has also been demonstrated to be the case with steric stabilisation, as shown with poly(vinyl alcohol) (PVA).[172]

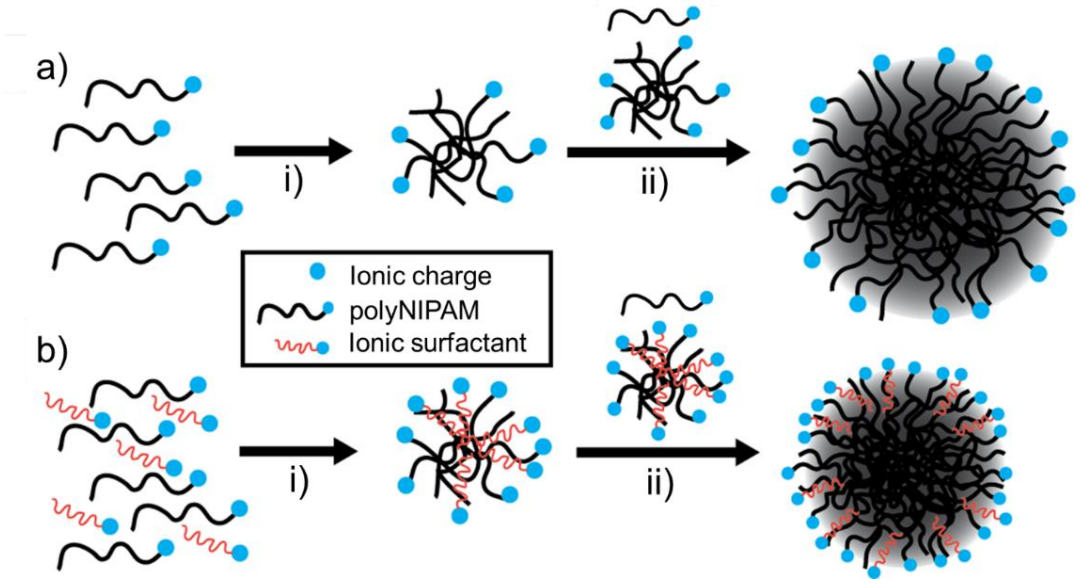

Figure 1.8 Illustration of a) precipitation and b) dispersion polymerisation to produce polyNIPAM nanogels, i) formation of precursor particle and ii) coagulation of precursor particles and oligomers to colloidally stable particle.

1.6.3. PolyNIPAM Nanogel Colloidal Stability

Although a polyNIPAM nanogel is colloidally stable at the point of synthesis above and below its VPTT, further changes to its environment may cause aggregation, such as a change in ionic strength. Below the VPTT polyNIPAM nanogel particles usually contain between 80 and 99% water in their swollen state.[127] Consequently the Van der Waals forces of attraction between particles are small, and chain ends extend from the particle to act as a steric stabiliser.[129] The particles are thus colloidally stable, and addition of salt to increase the ionic strength of the solvent has little effect.[173] However when the particles are heated at high ionic strength they aggregate above the VPTT.[160] This is because the particles contract and expel most of the water contained within them. Hence the Hamaker constant of the particle is no longer similar to the medium, and Van der Waals forces of attraction now exert a greater influence.[155] The chain ends are also now collapsed and so no longer provide steric stabilisation.[172] The surface charge density increases as the particles contract, and this provides electrostatic stabilisation to replace the loss of steric stabilisation and counter the increasing van der Walls forces in water (figure 1.9, a,i).[174] However, the presence of ions in the solution may potentially negate this electrostatic stabilisation and hence aggregation

of the particles now occurs above the LCST, (figure 1.9, a, ii).[175] This is important to consider in biomedical applications as a polyNIPAM nanogel will be in its collapsed state at body temperature and so the ionic strength of extracellular fluid (0.137 M) will cause aggregation if further stabilisation is not provided, such as steric stabilisation. Steric stabilisation with polyvinylpyrrolidone (PVP) or poly(vinyl alcohol) (PVA), has previously been demonstrated to prevent aggregation of polyNIPAM nanogels.[172,176] Hence these the nanogels can be heated above there VPTT in the presence of higher ionic strength, (figure 1.9, b).

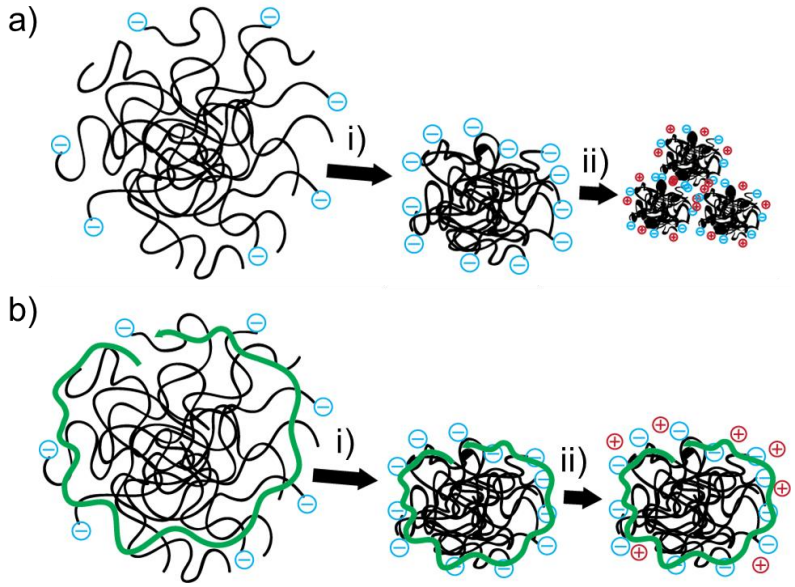

Figure 1.9 Illustration of colloidal stability of a) polyNIPAM nanogels and b) polyNIPAM nanogels with a steric stabiliser when i) the temperature rises above the VPTT and ii) the ionic strength increases whilst a temperature above the VPTT is maintained.

1.7. Thesis Overview and Research Objectives

It can be concluded that medication adherence is an issue of great importance, especially when taking into consideration the future rise in chronic conditions as the size of the global population, and average age, both increases. Whilst a range of solutions has been explored, no one particular solution has been shown to give a dramatic effect across the multitude of chronic conditions and types of patient which exist. Implants have been shown to have some success at removing the burden of administering doses by the patient. ISFIs have improved upon this by creating an implant which can be implanted with a minimally invasive procedure. However, drawback of ISFIs include the fact that they often suffer from a large burst release. A

few examples of nanogels ISFIs have been explored which aim to improve upon current ISFIs by being easier to formulate and administer, however these systems also suffer from a large burst release.

The main objective of the research presented in this thesis is to develop polyNIPAM nanogels for use as an ISFI. These nanogels will be formulated into a dispersion which is shear thinning to allow injection into a depot site, and then utilise the smart response of the nanogels to undergo triggered solidification under physiological conditions. As in section 1.6, only polyNIPAM-co-acrylamide and polyNIPAM-co-acrylic acid nanogels have previously been demonstrated to gelate and provide release of a drug payload, however the systems suffered from a large burst release and could not be degraded into small polymer fragments for excretion from the body. This work seeks to develop nanogels which avoid burst release and can be degraded into smaller polymer fragments, as well as other advantages such as the ability to control the release rate through the chemistry of the nanogel. A novel method of solidification which has not previously been investigated will also be explored using aggregation of nanogels triggered by physiological temperature and ionic strength.

The development of a polyNIPAM nanogel based ISFI will first involve the exploration of triggering solidification under physiological conditions using three different solidification concepts enabled by altering the chemistry of the nanogel. The most suitable concept will be taken forward to undergo further development and investigation. This will include pursuing further aims to produce an ISFI which is potentially commercially and clinically viable, whilst exploring further novelty in the system. These objectives include the following (and are shown schematically in figure 1.10):

a) Drug release which can be maintained over an extended period of time from the ISFI.
b) A drug release rate which can be tuned via a change in the nanogel chemistry by incorporating a comonomer in the synthesis.
c) A minimal burst release of drug during and shortly after solidification of the ISFI to form a drug depot.
d) Study into how nanogel size effects rheology and drug release rate from an ISFI.

e) An ISFI with minimal cytotoxicity.

f) Ability to deliver hydrophobic drugs.

g) An understanding into the underlying structure of the nanogel depot.

h) A fully biodegradable depot where the polymer structure of the nanogel is transformed into small polymer fragments.

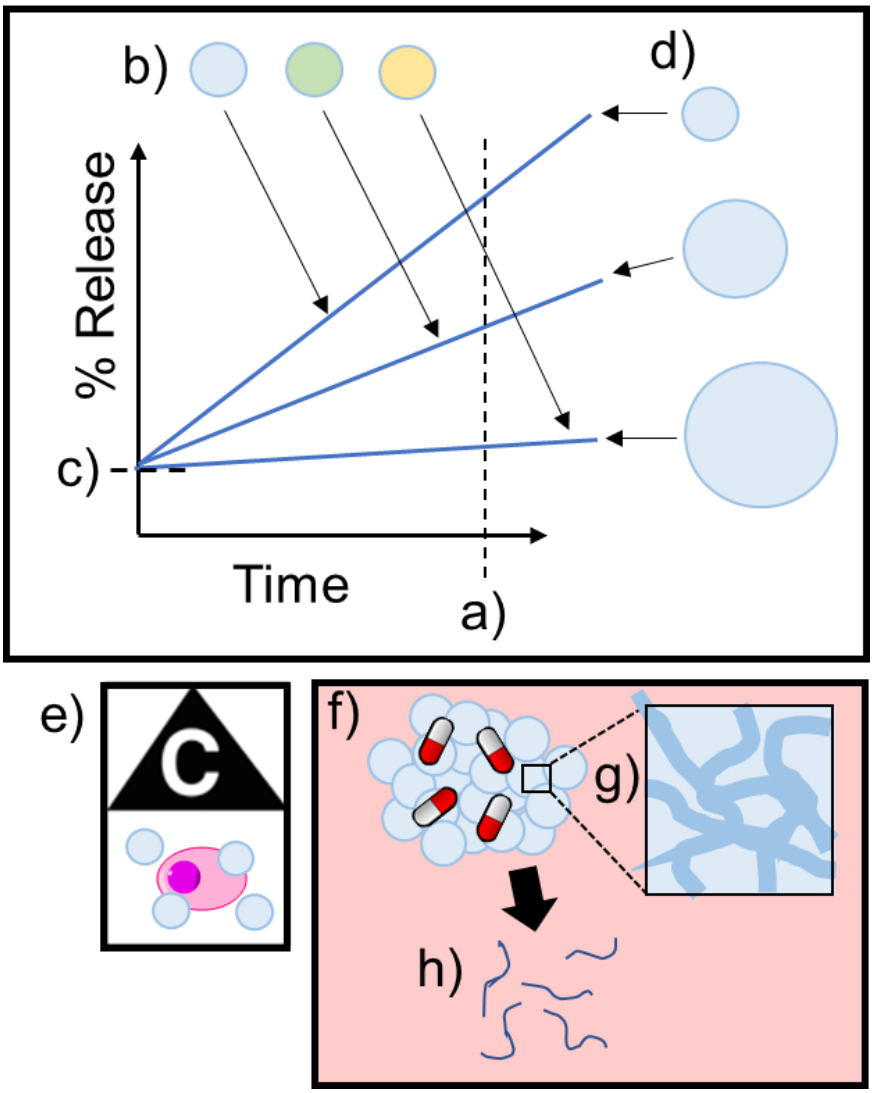

Figure 1.10 Visual representation of the research objectives of a polyNIPAM nanogel based ISFI which will be explored in this thesis. Objectives: a-d) illustrated with graph of release rate of drug from an ISFI over time, a) sustained release over time b) altering nanogel chemistry to tune release rate, c) achieving low burst release of drug, d) altering nanogel size to tune release rate, e) illustration of cell interacting with nanogels; synthesising nanogels with low cytotoxicity, f-h) illustration of depot site f) achieving hydrophobic drug delivery, g) depot structure investigation and h) biodegradability of nanogel polymer network into short polymer fragments.

The thesis is structured into the following chapters:

Chapter 2

- Exploration of triggering solidification using physiological conditions and three different solidification concepts, with the selection of the most promising concept for further exploration and development.

Chapter 3

- Development of an in situ forming implant in which the aggregation of nanogels is triggered by physiological temperature and ionic strength. This includes studying the depot structure, *in vitro* release of drug, cytotoxicity studies and tuning drug release based on nanogel composition.

Chapter 4

- Exploration into the influence of nanogel size on the in situ forming nanogel implant properties. This includes studying the phase and rheological properties of the nanogels, and effect on drug release rate.

Chapter 5

- Developing a degradable version of the nanogels, whilst maintaining the nanogel aggregation response to physiological temperature and ionic strength. The degradation process of the nanogels is also explored, and effects such as temperature on degradation rate.

1.8. References

1 J. Oeppen and W. Vaupel, *Science (80-.).*, 2002, **296**, 1029–1031.

2 V. Kontis, J. E. Bennett, C. D. Mathers, G. Li, K. Foreman and M. Ezzati, *Lancet*, 2017, **389**, 1323–1335.

3 R. McGlone and A. Bodenham, *Arch Emerg Med*, 1990, **7**, 65–68.

4 K. Barnett, S. W. Mercer, M. Norbury, G. Watt, S. Wyke and B. Guthrie, *Lancet*, 2012, **380**, 37–43.

5 W. Lutz, W. Sanderson and S. Scherbov, *Nature*, 2008, **451**, 716–719.

6 J. Cleland, *Environ. Resour. Econ.*, 2013, **55**, 543–554.

7 S. K. Bardal, J. E. Waechter and D. S. Martin, in *Applied Pharmacology*, eds. K. Dimock, M. Hyde and B. Cicalese, Elsevier Inc., St. Louis, 1st edn., 2011, pp. 17–34.

8 J. F. Steiner and M. A. Earnest, *Ann. Intern. Med.*, 2000, **132**, 926–930.

9 B. Jimmy and J. Jose, *Oman Med. J.*, 2011, **26**, 155–159.

10 S. De Geest and E. Sabaté, *Eur. J. Cardiovasc. Nurs.*, 2003, **2**, 323.

11 M. R. DiMatteo, *Med. Care*, 2004, **42**, 200–209.

12 A. Liebl, A. Neiss, A. Spannheimer, U. Reitberger, T. Wagner and A. Görtz, *Dtsch. medizinische Wochenschrift*, 2001, **126**, 585–589.

13 R. Haynes, P. Montague, T. Oliver, K. McKibbon, M. Brouwers and R. Kanani, *Cochrane Database Syst. Rev.*, 2001, CD000011.

14 H. Anglada-Martinez, G. Riu-Viladoms, M. Martin-Conde, M. Rovira-Illamola, J. M. Sotoca-Momblona and C. Codina-Jane, *Int. J. Clin. Pract.*, 2015, **69**, 9–32.

15 T. Mathes, D. Pieper, S. L. Antoine and M. Eikermann, *Ger. Med. Sci.*, 2012, **10**, 4–7.

16 J. Leider and G. Kalkut, *Ann. Intern. Med.*, 2000, **132**, 418.

17 W. H. Polonsky and R. R. Henry, *Patient Prefer. Adherence*, 2016, **10**, 1299–1307.

18 B. Waeber, G. Leonetti, R. Kolloch and G. T. McInnes, *J. Hypertens.*, 1999, **17**, 1041–1045.

19 C. A. Jackevicius, M. Mamdani and J. V Tu, *JAMA*, 2002, **288**, 462–467.

20 A. J. Claxton, J. Cramer and C. Pierce, *Clin. Ther.*, 2001, **23**, 1296–1310.

21 N. D. N. Berkman, S. S. L. Sheridan, K. E. K. Donahue, D. D. J. Halpern and K. Crotty, *Ann. Intern. Med.*, 2011, **155**, 97–107.

22 A. O. Iuga and M. J. McGuire, *Risk Manag. Healthc. Policy*, 2014, **7**, 35–44.

23 D. Juarez, C. Tan, D. J and M. Mau, *J Pharm Heal. Serv Res.*, 2013, **4**, 89–94.

24 M. Sokol, L. McGuigan, R. Verbrugge and R. Epstein, *Med Care*, 2005, **43**, 521–530.

25 R. M. Benjamin, *Public Health Rep.*, 2012, **127**, 2–3.

26 A. J. Atkinson, in *Principles of Clinical Pharmacology*, eds. A. J. Atkinson, D. R. Abernethy, C. E. Daniels, R. Dedrick and S. P. Markey, Elsevier Science & Technology, Burlington, USA, 3rd edn., 2006, pp. 13–26.

27 A. J. Atkinson, in *Principles of Clinical Pharmacology*, eds. A. J. Atkinson, D. R. Abernethy, C. E. Daniels, R. Dedrick and S. P. Markey, Elsevier Science & Technology, Burlington, USA, 3rd edn., 2006, pp. 41–53.

28 A. J. Atkinson, in *Principles of Clinical Pharmacology*, eds. A. J. Atkinson, D. R. Abernethy, C. E. Daniels, R. Dedrick and S. P. Markey, Elsevier Science & Technology, Burlington, USA, 3rd edn., 2006, pp. 27–40.

29 R. Jelliffe and M. Neely, in *Individualized Drug Therapy for Patients*, eds. R. W. Jelliffe and M. Neely, Academic Press, Boston, USA, 2017, pp. 3–18.

30 P. Y. Muller and M. N. Milton, *Nat. Rev. Drug Discov.*, 2012, **11**, 751–761.

31 R. K. Rajoli, D. Back, S. Rannard, C. Meyers, C. Flexner, A. Owen and M. Siccardi, *Clin Pharmacokinet.*, 2015, **54**, 639–650.

32 M. Siccardi, R. K. R. Rajoli, P. Curley, A. Olagunju, D. Moss and A. Owen, *Future Virol.*, 2013, **8**, 871–890.

33 T. Loftsson, in *Essential Pharmacokinetics*, eds. M. Haley, K. Jones, M. McLaughlin, C. Johnson and G. Harris, Elsevier, London, 1st edn., 2015, pp. 9–84.

34 M. Boyd, R. Aarnoutse, K. Ruxrungtham, M. Stek, R. van Heeswijk, J. Lange, D. Cooper, P. Phanuphak and D. Burger, *J. Acquir. Immune Defic. Syndr.*, 2003, **34**, 134–139.

35 N. Mehrotra, M. Gupta, A. Kovar and B. Meibohm, *Int. J. Impot. Res.*, 2007, **19**, 253–264.

36 H. S. Blix, K. K. Viktil, T. A. Moger and A. Reikvam, *Pharm. Pract. (Granada).*, 2010, **8**, 50–55.

37 J. R. Ickovics, A. Cameron, R. Zackin, R. Basset, M. Chesney, V. A. Johnson and D. R. Kuritzkes, *Antivir. Ther.*, 2002, **7**, 185–193.

38 M. Chesney, *AIDS Patient Care STDS*, 2003, **17**, 169–177.

39 B. Spilker, *IRB Ethics Hum. Res.*, 1992, **14**, 1–6.

40 M. Schulz and A. Schmoldt, *Pharmazie*, 2003, **58**, 447–474.

41 B. DS, N. Shehab, K. SR and R. CL, *Ann. Intern. Med.*, 2007, **147**, 755–765.

42 M. Vervloet, L. Van Dijk, J. Santen-Reestman, B. Van Vlijmen, M. L. Bouvy and D. H. De Bakker, *BMC Health Serv. Res.*, 2011, **11**, 1–8.

43 H. Rb, E. Ackloo, N. Sahota, M. Hp, X. Yao, R. B. Haynes, E. Ackloo, N. Sahota, H. P. Mcdonald and X. Yao, *Cochrane database Syst. Rev.*, 2008, 2–4.

44 R. Horwitz and S. Horwitz, *Arch. Intern. Med.*, 1993, **153**, 1863–1868.

45 N. M. Albert, *Critial Care Nurse*, 2008, **28**, 54–64.

46 E. Costa, A. Giardini, M. Savin, E. Menditto, E. Lehane, O. Laosa, S. Pecorelli, A. Monaco and A. Marengoni, *Patient Prefer. Adherence*, 2015, **9**, 1303–1314.

47 K. C. Ferdinand, F. F. Senatore, H. Clayton-Jeter, D. R. Cryer, J. C. Lewin, S. A. Nasser, M. Fiuzat and R. M. Califf, *J. Am. Coll. Cardiol.*, 2017, **69**, 437–451.

48 G. J. Treharne, A. C. Lyons and G. D. Kitas, *N. Engl. J. Med.*, 2005, **353**, 1972-4; author reply 1972-4.

49 D. V. Dimitrov, *Healthc. Inform. Res.*, 2016, **22**, 156–163.

50 M. Hunckler, *ScriptDrop Leverages Blockchain To Combat $300 Billion Cost of Prescription Drug Abandonment, https://www.forbes.com/sites/matthunckler/2017/10/09/scriptdrop-leverages-blockchain-to-combat-300-billion-cost-of-prescription-drug-abandonment/#2b373ff614da*, 2017.

51 B. Winner, J. F. Peipert, Q. Zhao, C. Buckel, T. Madden, J. E. Allsworth and G. M. Secura, *N. Engl. J. Med.*, 2012, **366**, 1998–2007.

52 G. Rossi, S. Frediani, R. Rossi and A. Rossi, *BMC Psychiatry*, 2012, **12**, 122.

53 N. Graham, *Br. Polym. J.*, 1978, **10**, 260–266.

54 J. C. Wright and D. J. Burgess, *Long Acting Injections and Implants*, Springer-Verlag, Berlin, 2012.

55 A. K. Bajpai, S. K. Shukla, S. Bhanu and S. Kankane, *Prog. Polym. Sci.*, 2008, **33**, 1088–1118.

56 A. K. Dash and G. C. Cudworth II, *J. Pharmacol. Toxicol. Methods*, 1998, **40**, 1–12.

57 A. S. Hoffman, *J. Control. Release*, 2008, **132**, 153–163.

58 J. F. Remenar, *Mol. Pharm.*, 2014, **11**, 1739–1749.

59 J. Wright and D. Burgess, in *Long Acting Injections and Implants*, 2012, pp. 11–24.

60 S. Freiberg and X. X. Zhu, *Int. J. Pharm.*, 2004, **282**, 1–18.

61 E. A. Yapar, Ö. Inal, Y. Özkan and T. Baykara, *Trop. J. Pharm. Res.*, 2012, **11**, 307–318.

62 L. Yu and J. Ding, *Chem. Soc. Rev.*, 2008, **37**, 1473.

63 T. Smith, P. Pearson, D. Blandford, J. Brown, K. Goins, J. Hollins, E. Schmeisser, P. Glavinos, L. Baldwin and P. Ashton, *Arch Ophthalmol*, 1992, **110**, 255–258.

64 V. G and S. Whitcup, *Br. J. Ophthalmol.*, 1999, **83**, 1225–1229.

65 D. C. Musch, D. F. Martin, J. F. Gordon, M. D. Davis and B. D. Kuppermann, *N. Engl. J. Med.*, 1997, **337**, 83–90.

66 J. Kent, D. Lewis, L. Sanders and T. Tice, *Microencapsul. water soluble Act. Polypept.*, **US Patent**, 4675189.

67 A. C. Anselmo and S. Mitragotri, *J. Control. Release*, 2014, **28**, 15–28.

68 S. Rietveld and J. M. Koomen, *Dis Manag. Heal. Outcomes*, 2002, **10**, 621–630.

69 C. M. Negrín, A. Delgado, M. Llabrés and C. Évora, *Biomaterials*, 2001, **22**, 563–570.

70 A. L. Kjøniksen, M. T. Calejo, K. Zhu, A. M. S. Cardoso, M. C. P. De Lima, A. S. Jurado, B. Nyström and S. A. Sande, *J. Pharm. Sci.*, 2014, **103**, 227–234.

71 J. Jin, L. Zhu, M. Chen, H. Xu, H. Wang, X. Feng, X. Zhu and Q. Zhou, *Patient Prefer. Adherence*, 2015, **9**, 923–942.

72 N. A. Peppas and A. R. Khare, *Adv. Drug Deliv. Rev.*, 1993, **11**, 1–35.

73 K. Modi, M. Modi, D. Mishra, P. Mittal, U. Sorathiya and P. Shelat, *Int. Res. J. Pharm.*, 2013, **4**, 70–76.

74 S. Davis, J. Hardy and J. Fara, *Gut*, 1986, **27**, 886–892.

75 R. Gref, Y. Minamitake, M. Peracchia, V. Trubetskoy, V. Torchilin and R. Langer, *Science (80-.).*, 1994, **263**, 1600–1603.

76 J. M. Metselaar and E. M. and G. Storm, *Mini-Reviews Med. Chem.*, 2002, **2**, 319–329.

77 D. J. Burgess and J. C. Wright, in *Long Acting Injections and Implants*, eds. J. C. Wright and D. J. Burgess, Springer-Verlag, Berlin, 2012, pp. 1–10.

78 M. Kastellorizios and D. J. Burgess, in *Long Acting Injections and Implants*, eds. J. C. Wright and D. J. Burgess, Springer-Verlag, Berlin, 2012, pp. 475–504.

79 M. Danckwerts and A. Fassihi, *Drug Dev. Ind. Pharm.*, 1991, **17**, 1465–1502.

80 H. Park and K. Park, *Pharm. Res.*, 1996, **13**, 1770–1776.

81 L. Olanoff and J. M. Anderson, *J. Pharm. Sci.*, 1979, **68**, 1151–1155.

82 L. S. Olanoff and J. M. Anderson, *J. Pharmacokinet. Biopharm.*, 1980, **8**, 599–620.

83 R. B. Patel, L. Solorio, H. Wu, T. Krupka and A. A. Exner, *J. Control. Release*, 2010, **147**, 350–358.

84 J. C. Wright, M. Sekar, W. van Osdol, H. C. Su and A. R. Miksztal, in *Long Acting Injections and Implants*, eds. J. C. Wright and D. J. Burgess, Springer-Verlag, Berlin, 2012, pp. 153–166.

85 A. McDowell and N. J. Medlicott, in *Long Acting Injections and Implants*, eds. J. C. Wright and D. J. Burgess, Springer-Verlag, Berlin, 2012, pp. 57–72.

86 N. Washington, C. Washington and C. G. Wilson, in *Physiological Pharmaceutics Barriers to drug absorption*, eds. N. Washington, C. Washington and C. G. Wilson, Taylor and Francis, New York, 2nd edn., 2001, pp. 19–34.

87 R. Langer and N. Peppas, *J. Macromol. Sci. Part C*, 1983, **23**, 61–126.

88 K. Park, *J. Control. Release*, 2015, **190**, 3–8.

89 A. Fakhari and J. Anand Subramony, *J. Control. Release*, 2015, **220**, 465–475.

90 C. S. Brazel and X. Huang, in *Carrier-Based Drug Delivery*, ed. S. Svenson, American Chemical Society, Washinton, DC, 2004, vol. 879, pp. 267–282.

91 K. Hirano, T. Ichihashi and H. Yamada, *Chem. Pharm. Bull. (Tokyo).*, 1981, **29**, 519–531.

92 J. R. Howard and J. Hadgraft, *Int. J. Pharm.*, 1983, **16**, 31–39.

93 W. Chen, A. Palazzo, W. E. Hennink and R. J. Kok, *Mol. Pharm.*, 2017, **14**, 459–467.

94 M. F. Butler, A. H. Clark and S. Adams, *Biomacromolecules*, 2006, **7**, 2961–2970.

95 F. Plourde, A. Motulsky, A. C. Couffin-Hoarau, D. Hoarau, H. Ong and J. C. Leroux, *J. Control. Release*, 2005, **108**, 433–441.

96 A. W. Bridges, R. E. Whitmire, N. Singh, K. L. Templeman, E. Babensee, L. A. Lyon and A. J. García, *J Biomed Mater Res A*, 2010, **94**, 252–258.

97 Samir Mitragotri, P. A. Burke and R. Langer, *Nat. Rev. Drug Discov.*, 2014, **13**, 655–672.

98 S. Kempe and K. Mäder, *J. Control. Release*, 2012, **161**, 668–679.

99 C. B. Packhaeuser, J. Schnieders, C. G. Oster and T. Kissel, *Eur. J. Pharm. Biopharm.*, 2004, **58**, 445–455.

100 Y. M. Kang, S. H. Lee, J. Y. Lee, J. S. Son, B. S. Kim, B. Lee, H. J. Chun, B. H. Min, J. H. Kim and M. S. Kim, *Biomaterials*, 2010, **31**, 2453–2460.

101 U. W. Tunn, *BMC Urol.*, 2011, **11**, 15.

102 D. Y. Kim, D. Y. Kwon, J. S. Kwon, J. H. Kim, B. H. Min and M. S. Kim, *Polym. Rev.*, 2015, **55**, 407–452.

103 M. Amiram, K. M. Luginbuhl, X. Li, M. N. Feinglos and A. Chilkoti, *J. Control. Release*, 2013, **172**, 144–151.

104 R. R. S. Thakur, H. L. McMillan and D. S. Jones, *J. Control. Release*, 2014, **176**, 8–23.

105 M. Kilicarslan, M. Koerber and R. Bodmeier, *Drug Dev. Ind. Pharm.*, 2014, **40**, 619–624.

106 H. Kranz and R. Bodmeier, *Int. J. Pharm.*, 2007, **332**, 107–114.

107 E. Ruel-Gariépy and J. C. Leroux, *Eur. J. Pharm. Biopharm.*, 2004, **58**, 409–

426.

108 D. Y. Ko, U. P. Shinde, B. Yeon and B. Jeong, *Prog. Polym. Sci.*, 2013, **38**, 672–701.

109 A. Shikanov, B. Vaisman, M. Y. Krasko, A. Nyska and A. J. Domb, *J. Biomed. Mater. Res. A*, 2004, **69**, 47–54.

110 A. Hatefi and B. Amsden, *J. Control. Release*, 2002, **80**, 9–28.

111 A. Vintiloiu and J. C. Leroux, *J. Control. Release*, 2008, **125**, 179–192.

112 B. Balakrishnan and A. Jayakrishnan, *Biomaterials*, 2005, **26**, 3941–3951.

113 M. Mekhail, J. Daoud, G. Almazan and M. Tabrizian, *Adv. Healthc. Mater.*, 2013, **2**, 1126–1130.

114 T. Wang, M. Turhan and S. Gunasekaran, *Polym. Int.*, 2004, **53**, 911–918.

115 M. Timmer, C. Ambrose and A. Mikos, *J. Biomed. Mater. Res. Part A*, 2003, **66A**, 811–818.

116 A. L. Kraus, I. C. Munro, R. L. Orr, J.C. Binder, R. A. Leboeuf and G. M. Williams, *Regul. Toxicol. Pharmacol.*, 1995, **21**, 87–107.

117 K. Ono, Y. Saito, H. Yura, K. Ishikawa, A. Kurita, T. Akaike and M. Ishihara, *J. Biomed. Mater. Res.*, 2000, **49**, 289–295.

118 M. Ishihara, K. Obara, S. Nakamura, M. Fujita, K. Masuoka, Y. Kanatani, B. Takase, H. Hattori, Y. Morimoto, M. Ishihara, T. Maehara and M. Kikuchi, *J. Artif. Organs*, 2006, **9**, 8–16.

119 M. Martignac, S. Balayssac, V. Gilard and F. Benoit-Marquié, *J. Phys. Chem. A*, 2015, **119**, 6215–6222.

120 A. Vintiloiu, M. Lafleur, G. Bastiat and J. C. Leroux, *Pharm. Res.*, 2008, **25**, 845–852.

121 A. Chenite, C. Chaput, D. Wang, C. Combes, M. . Buschmann, C. . Hoemann, J. . Leroux, B. . Atkinson, F. Binette and A. Selmani, *Biomaterials*, 2000, **21**, 2155–2161.

122 F. Mottu, A. Laurent, D. a Rufenacht and E. Doelker, *PDA J. Pharm. Sci. Technol.*, 2000, **54**, 456–469.

123 R. L. Dunn, J. P. English, D. R. Cowsar, D. P. Vanderbelt, US Patent 4,938,763, 1990.

124 A. Mashak, H. Mobedi, F. Ziaee and M. Nekoomanesh, *Polym. Bull.*, 2011, **66**, 1063–1073.

125 B. Jeong, Y. K. Choi, Y. H. Bae, G. Zentner and S. W. Kim, *J. Control. Release*, 1999, **62**, 109–114.

126 M. A. Pulickal, S. Uthaman, C.-S. Cho and I.-K. Park, in *Nanogels for Biomedical Applications*, eds. A. Vashist, A. K. Kaushik, S. Ahmad and M. Nair, The Royal Society of Chemistry, London, 2018, pp. 181–203.

127 B. R. Saunders and B. Vincent, *Adv. Colloid Interface Sci.*, 1999, **80**, 1–25.

128 M. J. Murray and M. J. Snowden, *Adv. Colloid Interface Sci.*, 1995, **54**, 73–91.

129 R. Pelton, *Adv. Colloid Interface Sci.*, 2000, **85**, 1–33.

130 W. O. Baker, *Rubber Chem. Technol.*, 1949, **41**, 511–520.

131 H. Staudinger and E. Husemann, *Berichte Der Dtsch. Chem. Gesellschaft*, 1935, **68**, 1618–1635.

132 F. Sultana, Manirujjaman, Imran-Ul-Haque, M. Arafat and S. Sharmin, *J. Appl. Pharm. Sci.*, 2013, **3**, 95–105.

133 K. Ogawa, A. Nakayama and E. Kokufuta, *Langmuir*, 2003, **19**, 3178–3184.

134 J. K. Oh, R. Drumright, D. J. Siegwart and K. Matyjaszewski, *Prog. Polym. Sci.*, 2008, **33**, 448–477.

135 G. Zhou, Y. Zhao, J. Hu, L. Shen, W. Liu and X. Yang, *React. Funct. Polym.*, 2013, **73**, 1537–1543.

136 K. Raemdonck, J. Demeester and S. De Smedt, *Soft Matter*, 2009, **5**, 707–715.

137 J. H. Lee, I. J. Gomez, V. B. Sitterle and J. C. Meredith, *J. Colloid Interface*

Sci., 2011, **363**, 137–144.

138 M. Das, H. Zhang and E. Kumacheva, *Annu. Rev. Mater. Res.*, 2006, **36**, 117–142.

139 D. M. Öle Kiminta and P. F. Luckham, *Polymer (Guildf).*, 1995, **36**, 4827–4831.

140 H. Wang, M. B. Hansen, D. W. P. M. Löwik, J. C. M. Van Hest, Y. Li, J. a. Jansen and S. C. G. Leeuwenburgh, *Adv. Mater.*, 2011, **23**, 119–124.

141 Q. Wang, L. Wang, M. S. Detamore and C. Berkland, *Adv. Mater.*, 2008, **20**, 236–239.

142 T. Gan, Y. Zhang and Y. Guan, *Biomacromolecules*, 2009, **10**, 1410–5.

143 T. R. Hoare and D. S. Kohane, *Polymer (Guildf).*, 2008, **49**, 1993–2007.

144 N. a. Peppas, J. Z. Hilt, A. Khademhosseini and R. Langer, *Adv. Mater.*, 2006, **18**, 1345–1360.

145 W. JC, *J. Long. Term. Eff. Med. Implants*, 1996, **6**, 207–217.

146 Y. Qiu and K. Park, *Adv. Drug Deliv. Rev.*, 2012, **64**, 49–60.

147 Y. Qiu and K. Park, *Adv. Drug Deliv. Rev.*, 2001, **53**, 321–39.

148 J. F. Gilchrist, A. T. Chan, E. R. Weeks and J. a Lewis, *Langmuir*, 2005, **21**, 11040–11047.

149 Z. Gu, A. a Aimetti, Q. Wang, T. T. Dang, Y. Zhang, O. Veiseh, H. Cheng, R. S. Langer and D. G. Anderson, *ACS Nano*, 2013, **7**, 4194–201.

150 Y. Wang, J. L. Robertson, W. B. Spillman and R. O. Claus, *Pharm. Res.*, 2004, **21**, 1362–1373.

151 M. H. Hsiao, M. Larsson, A. Larsson, H. Evenbratt, Y. Y. Chen, Y. Y. Chen and D. M. Liu, *J. Control. Release*, 2012, **161**, 942–948.

152 H. S. Chou, M. Larsson, M. H. Hsiao, Y. C. Chen, M. Röding, M. Nydén and D. M. Liu, *J. Control. Release*, 2016, **224**, 33–42.

153 D. Chen, H. Yu, K. Sun, W. Liu and H. Wang, *Drug Deliv.*, 2014, **21**, 258–

264.

154 T. Nakai, T. Hirakura, Y. Sakurai, T. Shimoboji, M. Ishigai and K. Akiyoshi, *Macromol. Biosci.*, 2012, **12**, 475–483.

155 M. Rasmusson and B. Vincent, *React. Funct. Polym.*, 2004, **58**, 203–211.

156 G. Huang, J. Gao, Z. Hu, J. V St. John, B. C. Ponder and D. Moro, *J. Control. Release*, 2004, **94**, 303–311.

157 Q. Wang, Y. Zhao, Y. Yang and H. Xu, *Colloid Polym. Sci.*, 2007, **285**, 515–521.

158 Q. Wang, H. Xu, X. Yang and Y. Yang, *Int. J. Pharm.*, 2008, **361**, 189–193.

159 W. Xiong, X. Gao, Y. Zhao, H. Xu and X. Yang, *Colloids Surf. B. Biointerfaces*, 2011, **84**, 103–10.

160 R. H. Pelton and P. Chibante, *Colloids and Surfaces*, 1986, **20**, 247–256.

161 K. Kratz, A. Lapp, W. Eimer and T. Hellweg, *Colloids Surfaces A Physicochem. Eng. Asp.*, 2002, **197**, 55–67.

162 C. Obeso-Vera, J. M. Cornejo-Bravo, A. Serrano-Medina and A. Licea-Claverie, *Polym. Bull.*, 2013, **70**, 653–664.

163 R. Mohsen, G. J. Vine, N. Majcen, B. D. Alexander and M. J. Snowden, *Colloids Surfaces A Physicochem. Eng. Asp.*, 2013, **428**, 53–59.

164 C. Wu and X. Wang, *Phys. Rev. Lett.*, 1998, **80**, 4092–4094.

165 S. Chen, J. Long and Y. Dan, *J. Appl. Polym. Sci.*, 2011, **121**, 3322–3331.

166 A. L. Kjøniksen, M. T. Calejo, K. Zhu, A. M. S. Cardoso, M. C. P. De Lima, A. S. Jurado, B. Nyström and S. A. Sande, *J. Pharm. Sci.*, 2014, **103**, 227–234.

167 R. Arshady, *Colloid Polym. Sci.*, 1992, **270**, 717–732.

168 X. Wu, R. H. Pelton, a. E. Hamielec, D. R. Woods and W. McPhee, *Colloid Polym. Sci.*, 1994, **272**, 467–477.

169 W. D. Snyder and I. M. Klotz, *J. Am. Chem. Soc.*, 1975, **97**, 4999–5003.

170 Y. Chen, N. Ballard, O. D. Coleman, I. J. Hands-Portman and S. a. F. Bon, *J. Polym. Sci. Part A Polym. Chem.*, 2014, **52**, 1745–1754.

171 W. McPhee, K. C. Tam and R. Pelton, *J. Colloid Interface Sci.*, 1993, **156**, 24–30.

172 A. Lee, H.-Y. Tsai and M. Z. Yates, *Langmuir*, 2010, **26**, 18055–18060.

173 R. H. Pelton, H. M. Pelton, a. Morphesis and R. L. Rowell, *Langmuir*, 1989, **5**, 816–818.

174 N. Al-manasir, S. Fanaian, K. Zhu, B. Nyström, G. Karlsson and A. Kjøniksen, *J. Phys. Chem. B*, 2009, **113**, 11115–11123.

175 M. Rasmusson, A. Routh and B. Vincent, *Langmuir*, 2004, **20**, 3536–3542.

176 K. M. Koczkur, S. Mourdikoudis, L. Polavarapu and S. E. Skrabalak, *Dalt. Trans.*, 2015, **44**, 17883–17905.

Chapter 2

Exploration of In Situ Forming Implant Concepts Based on Poly(N-isopropylacrylamide) Nanogels

2.1. Introduction

Whilst a wide array of in situ forming implant (ISFI) systems are available,[1] there are very few examples of nanogels being employed as ISFIs, with many of the advances in this area being made very recently.[2–4] This is despite the potential advantages they offer over bulk hydrogel based ISFIs. These include the easier administration of low viscosity nanogel dispersions, to reduce invasiveness and discomfort, and fast response to stimuli, to reduce burst release of drug from slower depot formation.[5] Of particular interest are poly(N-isopropylacrylamide) (polyNIPAM) nanogels, which are inert, biocompatible, and exhibit physiologically relevant responsive behaviour.[6–9] This can include a response to temperature, pH and ionic strength. Finally, the properties of nanogels can also be tuned through the inclusion of comonomers in the nanogel synthesis, potentially allowing a tuneable controlled release rate from a polyNIPAM nanogel depot. This chapter will investigate three possible concepts in which polyNIPAM nanogels can be utilised as an ISFI. These concepts are 1) pH enhanced thermally triggered gelation 2) charge-based assembly into a colloidal gel network and 3) triggered aggregation through the dual stimuli of temperature and ionic strength. The following sections will briefly outline the background to these concepts for ISFIs based on polyNIPAM nanogels.

2.1.1. pH Enhanced Thermally Triggered Gelation Concept

The incorporation of comonomers such as acrylic acid into the synthesis of polyNIPAM nanogels creates nanogels which are able to respond to pH.[10] In the case of acrylic acid, the monomer has a pKa of 4.25.[11] If the pH of a dispersion containing polyNIPAM-co-acrylic acid nanogels is raised above the pKa of the carboxylic acid functional group of the acrylic acid then the comonomer becomes increasingly deprotonated, leading to a greater anionic charge density. These charges cause greater intra-particle repulsion, causing the nanogel to expand.[12] The pH response can also influence the phases present in a polyNIPAM nanogel dispersion at different pH values.[9,13] Phosphate buffered saline (PBS) is often used in literature to mimic the ionic strength and range of salts present in the extracellular environment of the human body, and has been used previously in phase studies.[14,15] In PBS, a dispersion of concentrated polyNIPAM nanogels presents different phases depending on the temperature of the

dispersion. At a low temperature the nanogels exist as a self-supporting swollen gel (i.e. a gel which is able to remain suspended in a sample vial when inverted), (Scheme 2.1, a).[16,17] The swollen gel phase arises due the volume blocking mechanism of hard sphere theory, in which the nanogel spheres become close packed.[18,19] Upon heating the particles deswell resulting in a phase transition to a liquid,[16] which is accompanied by an increase in turbidity. (Scheme 2.1, b).[20] This change in turbidity arises from the increased difference between the refractive index of the nanogel particles and the surrounding liquid as they deswell.[21] In PBS, further heating above the VPTT of the nanogels causes a phase separated macroscopic aggregate phase to form, due to the lack of colloidal stability at the ionic strength of PBS (> 0.1M NaCl) (Scheme 2.1, c).[22] The addition of acrylic acid into the polymerisation yields a dispersion of polyNIPAM-co-acrylic acid nanogels with different phase behaviour. Below ~ pH 4, the acrylic acid becomes predominantly protonated, and the nanogels are hence less swollen. This also reduces the overlapping of electrical double layers, which reduces the viscosity of a concentrated dispersion.[23] Hence protonation of the acrylic acid comonomer allows a lower viscosity liquid instead of a gel, (Scheme 2.1, d).[9] This difference allows easier injection. As with the polyNIPAM nanogels, the acrylic acid containing nanogels deswell as they are heated, (Scheme 2.1, e).[12] However, the third aggregate phase is replaced with a shrunken gel phase under physiological ionic strength, pH and temperature, (Scheme 2.1, f).[13,24] This shrunken gel is also self-supporting (able to remain suspended in an inverted vial), but with high turbidity and a small volume excess of water expelled upon formation. As with the aggregate phase, there is an increasing tendency of the nanogels to become more hydrophobic with polymer-polymer interactions dominating polymer-water interactions as the temperature increases. This behaviour favours aggregation through attractive interactions,[25,26] however this is opposed by an increased electrostatic repulsion from the inclusion of acrylic acid preventing this aggregation occuring.[17,27] Hence polyNIPAM-co-acrylic acid nanogels are injectable at low pH, where they will exist as a liquid, and then become more charged at higher pH, to allow formation of a shrunken gel depot at the injection site, as demonstrated in previous work.[9] These nanogels can therefore be used as an ISFI in which gelation is triggered thermally and enhanced by a change in pH at physiological temperature and ionic strength.

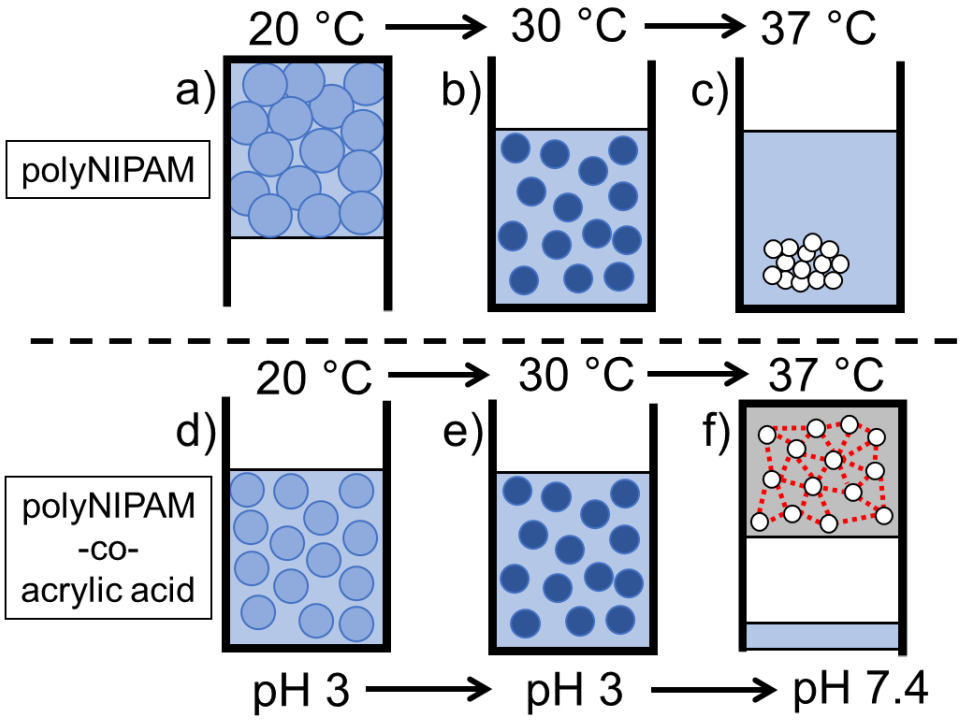

Scheme 2.1 Illustration of phase behaviour under different conditions of polyNIPAM (a,b,c) and polyNIPAM-co-acrylic acid (d,e,f) nanogels dispersed as a concentrated dispersion in phosphate buffer saline (a,b,c,f), or pH 3 aqueous dispersion (d,e) : a) self-supporting swollen gel at 20 °C, b) liquid at 30 °C, c) phase separated aggregate at 37 °C, d) liquid at 20 °C and pH 3, e) liquid at 30 °C and pH 3, f) shrunken gel at 37 °C and pH 7.4.

2.1.2. Charge Based Colloidal Gel Network Concept

Previous work has shown that when two populations of nanoparticles, one with a cationic charge, and one with an anionic charge are combined, they can form a colloidal gel network through electrostatic attraction between the particles.[28–30] These charges can be introduced by coating the particle surface with polyelectrolyte,[28] or achieving an intrinsic charge during the synthesis.[29,30] With polyNIPAM nanogels, as discussed above, anionic charge can be introduced with the addition of acrylic acid as a comonomer in the synthesis. Likewise, cationic charge can be introduced with a comonomer such as allylamine in the synthesis in polyNIPAM-co-allylamine nanogels.[31,32] The conjugate acid of this comonomer has a pKa of 9.49.[33] Hence at a physiological pH of 7.4, the carboxylic acid groups in polyNIPAM-co-acrylic acid nanogels are fully deprotonated, and the amine groups of polyNIPAM-co-allylamine

are fully protonated, (scheme 2.2), giving two species of oppositely charged nanogels potentially able to interact and form a colloidal gel at a physiologically relevant pH.

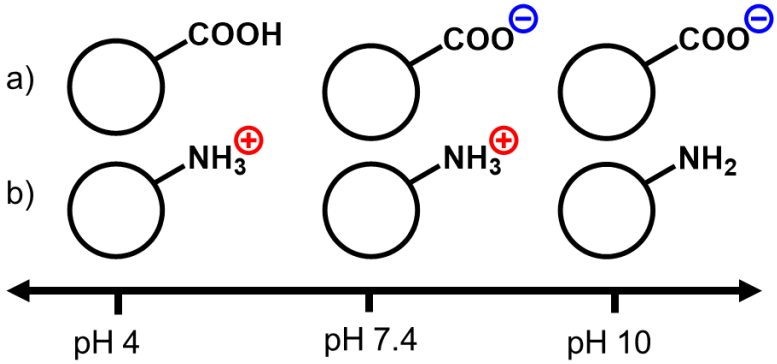

Scheme 2.2 Predominate surface charge at different pH values for polyNIPAM nanogels with pH responsive comonomer incorporated, a) polyNIPAM-co-acrylic acid and b) polyNIPAM-co-allylamine.

PolyNIPAM-co-acrylic acid and polyNIPAM-co-allylamine nanogels have previously been synthesised and used together in drug delivery.[34] However the nanogels were covalently cross-linked to each other to form a three-dimensional gel network, rather than relying on electrostatic attraction to form a gel after injection, and so could not be used as an injectable ISFI.[34] When not covalently linked together, polyNIPAM nanogels are both nano-sized and shear thinning, giving an injectable dispersion.[9,19] Oppositely charged hydrogel particles were previously demonstrated to be injectable; the shear force of the injection syringe destroys the colloidal gel network, which then reforms after injection.[30] Hence it is reasonable to assume that polyNIPAM-co-acrylic acid and polyNIPAM-co-allylamine nanogels can be synthesised and used together as an ISFI. Implant formation would take place through the assembly of a colloidal gel network through electrostatic interactions, after the shear force of injection through a hypodermic needle, (scheme 2.3). The strongest network cohesion is achieved when the overall charge of particles is balanced.[28]

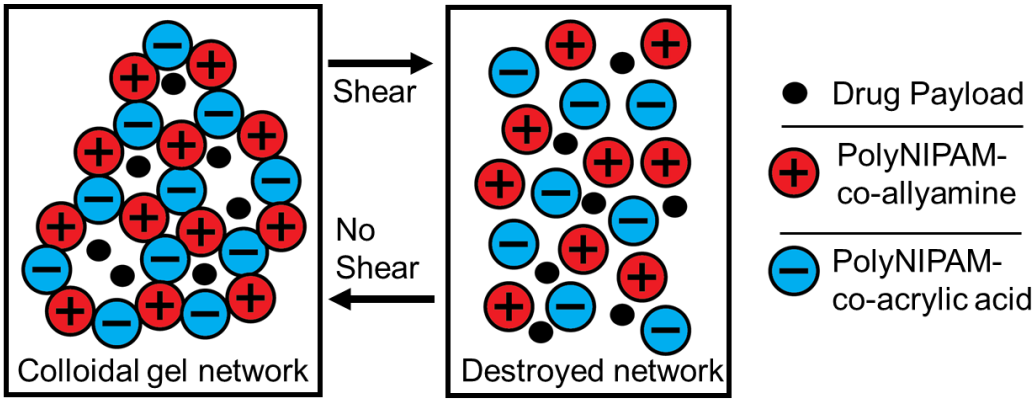

Scheme 2.3 Reversible formation of a colloidal gel network after application of shear force to nanogels passing through an injection needle.

2.1.3. Triggered Aggregation through the Dual Stimuli of Temperature and Ionic Strength Concept

It is well known in literature that insufficient stabilisation of nanogels will cause them to flocculate or aggregate completely above the VPTT. However, Few studies have focused on purposefully achieving this, as nanogels are usually required to be colloidally stable, particularly for biomedical applications.[35] In forming a drug depot in situ from aggregated nanogels, a nanogel dispersion at room temperature, (Scheme 2.4, a), which is colloidally stable above the VPTT in water, (Scheme 2.4, b), but then aggregates only in physiological ionic strength medium, (Scheme 2.4, c) is required. This approach avoids potential issues of premature gelation when injected into a subcutaneous site; as the nanogel dispersion is injected from a syringe (Scheme 2.4, d), if the particles were purely temperature responsive they may prematurely aggregate, causing a needle blockage as they heat up travelling along the hypodermic needle into the body (Scheme 2.4, e). Additionally, the aggregation response of the nanogels once in the tissue and in contact with a higher ionic strength is likely to be rapid, so that they aggregate to entrap their payload to avoid a burst release of drug into the body, (Scheme 2.4, f). Hence the need for the nanogels to be dual responsive, i.e. they aggregate when both above their VPTT, and in the presence of physiological ionic strength. There are a few limited examples in which the triggered flocculation of polyNIPAM nanogels into larger microscopic flocs has previously been used to block both membrane pores,[36,37] and release drug,[38] however there are currently no examples that use triggered aggregation on a macroscopic scale to form a drug depot.

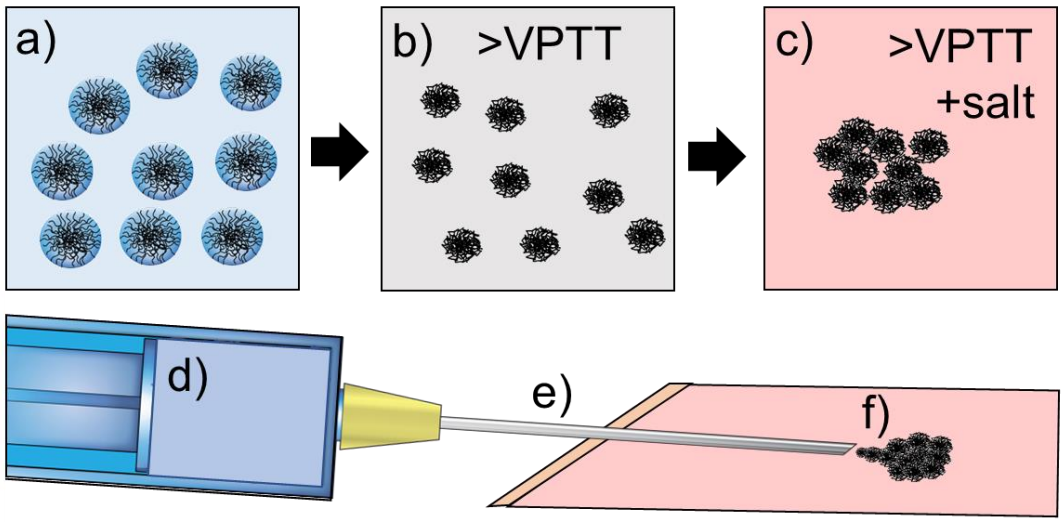

Scheme 2.4 Illustration of ISFI based on dual triggered aggregation of polyNIPAM nanogels: a) swollen nanogels at room temperature in aqueous dispersion form, b) collapsed nanogels above VPTT, c) aggregated nanogels above VPTT and in contact with salt, d) aqueous dispersion in syringe, e) injection of dispersion through hypodermic needle inserted into subcutaneous site f) aggregation of dispersion upon arrival at subcutaneous site.

In designing an ISFI using temperature and ionic strength as dual triggers to induce nanogel aggregation there are two main aspects to consider. Firstly, the size of the nanogel, and secondly, surfactant or stabiliser used in the synthesis; both of these factors could have an effect on depot formation behaviour. This could include the porosity of the depot, influencing the drug release rate.[38] The uniformity and mechanical strength of the depot could also vary, giving potentially unwanted fluctuation or variation in drug release rate.[39] There may also be flocculation on a microscopic scale, rather than complete macroscopic aggregation, and differences in the degree of aggregation at different dispersion concentrations. Finally the optimal system must undergo fast aggregation to avoid burst release of its payload,[40] and only display aggregation behaviour selectively at physiological ionic strength and temperature, rather than at a temperature above the VPTT of the nanogels alone.

Control over the size of the nanogels can be achieved by varying the concentration of surfactant, as demonstrated previously with sodium dodecyl sulphate (SDS), a surfactant which provides electrostatic stabilisation.[41] Polymerisation with surfactants such as SDS has been shown to allows greater control over the polymerisation;

producing particles with lower dispersity. Polyvinylpyrrolidone (PVP) (scheme 2.5), a steric stabiliser, may also have an effect on particle size with concentration, as shown previously for poly(vinyl alcohol), which is another steric stabiliser.[35]

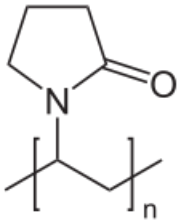

Scheme 2.5 Chemical structure of Polyvinylpyrrolidone (PVP).

2.1.4. Polyvinylpyrrolidone Aided Nanogel Synthesis and Dispersion

More generally, polyNIPAM nanogel ISFIs for all three solidification concepts could also be enhanced with the inclusion of PVP. This is because PVP is a stabiliser which complexes with many drugs to increase dissolution rate, as well as acting as a dispersing agent for nanoparticles.[42] With nanogels usually stored in lyophilised form before use, PVP physical absorption would potentially aid in the dispersion process of both the nanogels and drug payload, aiding the preparation of the ISFI before injection. PVP also exhibits minimal cytotoxicity and immunogenicity in parenteral usage,[43] and can aid colloidal nanoparticle synthesis and colloidal stability.[44] PVP has already been incorporated in the synthesis of polyNIPAM nanogels,[45] and although it was suggested that the PVP is chemically grafted to the surface of nanoparticles in free radical polymerisation through the generation of PVP macroradicals,[46,47] this is unlikely and physical absorption of PVP is instead suggested to take place. This could give greater control of particle size and dispersity, as shown to be the case in the synthesis of other nanoparticles.[44,48] For the charge based colloidal gel network concept, the relative size of the two nanogel species likely also has an effect on the cohesion strength of the network. Hence PVP could be used to control nanoparticle size through the usage of different average molecular weight (M_w) PVP. In the formation of poly(glycidyl methacrylate) particles, higher M_w PVP created smaller particles. This behaviour was attributed to the higher M_w PVP being able to absorb faster and stabilise a larger surface area in the dispersion polymerisation process before the particles have

time to agglomerate into larger particles.[48] Hence a similar effect should be seen when PVP is used in the synthesis of polyNIPAM nanogels to control particle size.

2.1.5. Chapter Aims

The aims of this chapter are to determine the feasibility of three different ISFI formation concepts which are all based on polyNIPAM nanogels. Generally, the aim for each of the three concepts is to alter the chemistry of the nanogels to create nanogels that match a set of criteria required to become a good candidate for an in situ forming implant. Criteria to be met: a) liquid or injectable gel at room temperature b) rapid solidification at 37 °C in PBS* (Phosphate Buffered Saline, 1X strength, pH 7.4) c) intended colloidal stability/instability under different conditions. To meet this criteria, properties such as surface charge density, size, and colloidal stability will be modified through the use of different co-monomers and stabiliser compositions.

The aims of each concept are as follows:

1. pH enhanced thermally triggered gelation to form a shrunken gel

Main objective:

- Incorporate PVP into a polyNIPAM-co-acrylic acid nanogel, to improve its function as an ISFI in terms preventing nanogel aggregation under physiological conditions and control over nanogel size and dispersity during synthesis.

Other objectives:

- Synthesis of PVP and non PVP polyNIPAM-co-acrylic acid nanogels (scheme 2.5), to compare the effect of PVP on the synthesis of these nanogels.
- Study effect of pH and PBS (1X strength, pH 7.4) on colloidal stability of polyNIPAM-co-acrylic acid nanogels across a temperature range.
- Vary nanogel acrylic acid content and find relationship to nanogel surface charge density and pH based swelling.
- Study effect of nanogel dispersion concentration on phase behaviour.

* For the remainder of the thesis 'PBS' refers to (Phosphate Buffered Saline, 1X strength, pH 7.4)

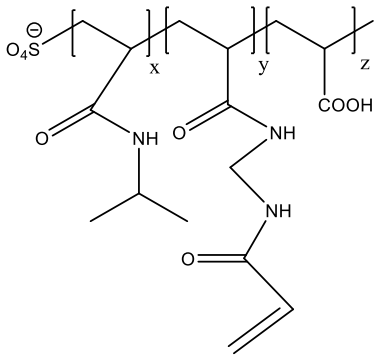

Scheme 2.6 Chemical structure of polyNIPAM-co-acrylic acid nanogels formed from free radical precipitation polymerisation. x = polyNIPAM, y = BIS, z = poly(acrylic acid).

2. Charge based colloidal gel network formation

Main objective:

- Demonstrate the formation of a gel via charge interactions between polyNIPAM-co-acrylic acid and polyNIPAM-co-allylamine nanogels at 37 °C in PBS.

Other objectives:

- Synthesis of polyNIPAM-co-allylamine nanogels (scheme 2.6) with different sizes and charge densities.
- Study effect of pH and PBS (1X strength, pH 7.4) on colloidal stability of polyNIPAM-co-allylamine nanogels across a temperature range.
- Compare surface charge density of polyNIPAM-co-allylamine and polyNIPAM-co-acrylic acid nanogels across a pH range.

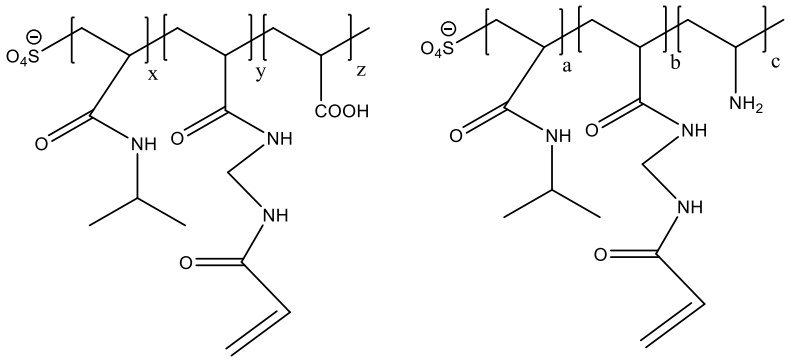

Scheme 2.7 Chemical structure of polyNIPAM-co-acrylic acid and polyNIPAM-co-allylamine nanogels formed from free radical precipitation polymerisation. x = polyNIPAM, y = BIS, z = poly(acrylic acid), a = polyNIPAM, b = BIS, c = allylamine.

3. Triggered aggregation through the dual stimuli of temperature and ionic strength

Main objective:

- Create a nanogel which as a dispersion can selectively aggregate when both at 37 °C and in PBS rather than water.

Other objectives:

- Determine how SDS and PVP concentration used in the synthesis effects the size and dispersity of the polyNIPAM nanogels formed.
- Investigate the colloidal stability of nanogels synthesised with no surfactant, PVP or SDS in water and PBS across a temperature range.
- Determine how dilute behaviour of nanogels compares with a concentrated dispersion in terms of aggregation behaviour.

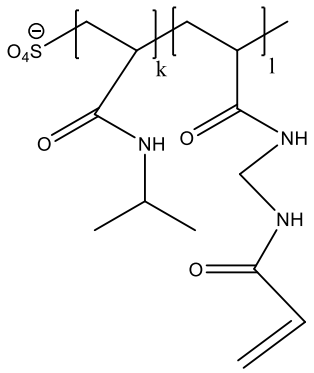

Scheme 2.8 Chemical structure of polyNIPAM nanogels formed from free radical precipitation polymerisation. k = polyNIPAM, l = BIS.

2.2. Results and Discussion

2.2.1. pH Enhanced Thermally Triggered Gelation to give an In Situ Implant

PolyNIPAM-co-acrylic acid nanogels were synthesised using 5.0 and 15.0 wt% acrylic acid as a comonomer via precipitation polymerisation (figure 1.8, a) (AcA-5.0, AcA-15.0), (table 2.1). See methods section 2.4.2, for full synthesis details. It was previously found that surfactant free polymerisation of NIPAM (N-isopropylacrylamide) gave large particles with a broad dispersity above a reactant concentration of 0.5% w/v as the charge conferred on the particles from the initiator was considered too low.[49] This synthesis was improved with the addition of a surfactant (dispersion polymerisation), to give much better control over particle size, stability, and polydispersity.[41,49] The reactant concentration for AcA-5.0 and AcA-15.0 was 0.7% w/v. It was anticipated that the extra charge provided by the acrylic acid comonomer would be great enough to electrostatically stabilise the particles during synthesis, however, AcA-5.0 and AcA-15.0 particles were still large compared to the usual size of polyNIPAM nanogels (hydrodynamic diameters of 1025 and 1328 nm respectively),[35] and have a broad dispersity (PdI values of 0.51 and 0.43 respectively). However, they showed a swelling in response to pH change, with a significant reduction in particle hydrodynamic diameter when the pH was reduced from pH 7 to pH 2, (table 2.1). With the introduction of the steric stabilizer PVP 55K (where 55K refers to an average molecular weight of 55,000) in the synthesis of samples with increasing wt% of acrylic acid comonomer (AcA-0.0-55K, AcA1.5-55K, AcA2.0-55K and AcA5.0-55K), the dispersity was narrower than AcA-5.0 and AcA-15.0 ($\leq$0.29 for the four samples compared to $\geq$0.43), owing to the steric stabilisation provided by PVP to the precursor particles during synthesis, despite an increase to a reactant concentration of 1.9% w/v. The hydrodynamic diameter was also correspondingly smaller for the four samples ($\leq$ 688 nm compared to $\geq$1025 nm); this is an indication the precursor particles were stabilised by PVP in the initial stage of synthesis, allowing them to grow at the same rate to maintain a lower dispersity, rather than coalescence into larger particles with broader dispersity at a later stage of the synthesis.[48,50,51] The presence of PVP after synthesis and workup was confirmed with 1H NMR, substantiating previous claims that PVP remains physically absorbed to the nanogel surface after synthesis, as any non-associated PVP is likely to have been removed in the dialysis and centrifugation steps after synthesis (table A.1, figure A.1, Appendix).[46,47]

Table 2.1 Properties of polyNIPAM-co-acrylic acid nanogels, with and without PVP.

Sample	Reactant concentration[a] (w/v %)	Acrylic acid[b] (wt%)	PVP (M_w)	H_d[c] (nm) pH 2	H_d[c] (nm) pH 7	PdI
AcA-5.0	0.7	5.0	-	637	1025	0.51
AcA-15.0	0.7	15.0	-	846	1328	0.43
AcA-0.0-55K	1.9	0.0	55K	442	474	0.21
AcA-1.5-55K	1.9	1.5	55K	418	424	0.29
AcA-2.0-55K	1.9	2.0	55K	419	391	0.20
AcA-5.0-55K	1.9	5.0	55K	426	688	0.28

[a] percentage mass of NIPAM, BIS and acrylic acid in reaction solvent volume.
[b] wt% of acrylic acid used in the synthesis of the nanogel (wt% of NIPAM and acrylic acid mass).
[c] Hydrodynamic diameter (H_d) measurements performed at 1mg ml^{-1}, 25 °C using DLS with the mean value of triplicate measurements used.

Lower wt% acrylic acid additions were used in the PVP nanogels (0.0, 1.5, 2.0, 5.0 wt% in PVP nanogels vs 5.0 and 15.0 in non PVP nanogels), and from this it can be seen that a minimum of 5.0 wt% of acrylic acid is required to give a great enough charge density for a pH swelling response to be seen in nanogels on increasing from pH 2 to pH 7 with or without PVP (there is no significant change in particle hydrodynamic diameter at pH 2 and pH 7 with <5 wt% acrylic acid nanogels, table 2.1).

Firstly, the colloidal stability of the non PVP nanogels was investigated. This was done by probing the AcA-15.0 nanogels at different pH values. This was of interest as in previous work, polyNIPAM-co-acrylic acid nanogels used in ISFIs were only stabilised electrostatically rather than sterically (e.g. with PVP) above the VPTT.[9] As mentioned previously, at a pH < 4.25, the carboxylic acid functionality of the acrylic acid comonomer is predominantly protonated, due to its pKa value of 4.25, greatly reducing electrostatic stabilisation. Hence if polyNIPAM-co-acrylic acid nanogels are heated above their VPTT at low pH, there is the potential for the nanogels to flocculate or aggregate as electrostatic stabilisation is minimised. In use as an ISFI, the nanogels are injected at lower pH to give a less viscous, more easily injectable liquid. However, if the nanogels experience a temperature rise during the injection before the pH of their

dispersion increases, they could potentially aggregate prematurely and become difficult to inject into the body. The stability of polyNIPAM-co-acrylic acid nanogels above the VPTT at low pH was tested with AcA-15.0. This sample was heated at pH 4, pH 3 and pH 2 and analysed by dynamic light scattering (DLS) to observe the colloidal stability of the nanogels above the VPTT with decreased electrostatic stabilisation of lower pH values, (figure 2.1). Using the pKa value of 4.25 for acrylic acid, the percentage of carboxylic acid groups in carboxylate anion form at pH 4, 3 and 2 can be estimated as 36.0, 5.3 and 0.5% respectively, by using a form of the Henderson-Hasselbalch equation previously used to determine the degree of ionisation of comonomers at a given pH in polyNIPAM nanogels.[10,52] When heated at pH 4 the hydrodynamic diameter of the AcA-15.0 nanogels decreased with increasing temperature as the particles deswelled from 1330 nm at 25 °C to 630 nm at 35 °C. Hence it can be concluded that they remained colloidally stable above the VPTT, owing to the electrostatic stabilisation provided by the acrylic acid, with an estimated 36% in ionised form, (figure 2.1, a). At pH 3 a decreasing fraction of the acrylic acid is ionised (c.a. 5.3%), reducing electrostatic stabilisation. Again, the particles began to reduce in diameter as they deswelled with increasing temperature, however, above the VPTT the particles now began to flocculate, indicated by a rise in hydrodynamic diameter to ~2750 nm, which likely represents the average hydrodynamic diameter of multiple particles contained in flocs (figure 2.1, b). At pH 2 the electrostatic stabilisation is very low, essentially provided only by potassium persulfate initiator (c.a. 0.5% of acrylic acid in ionised form), and consequently the particles completely aggregated above the VPTT, with a rapid increase in hydrodynamic diameter to > 4000 nm as macroscopic aggregates form (figure 2.1, c). If these particles are injected at < pH 4 there is the potential for them to flocculate or macroscopically aggregate and cause difficulties in injection, or complete needle blockage.

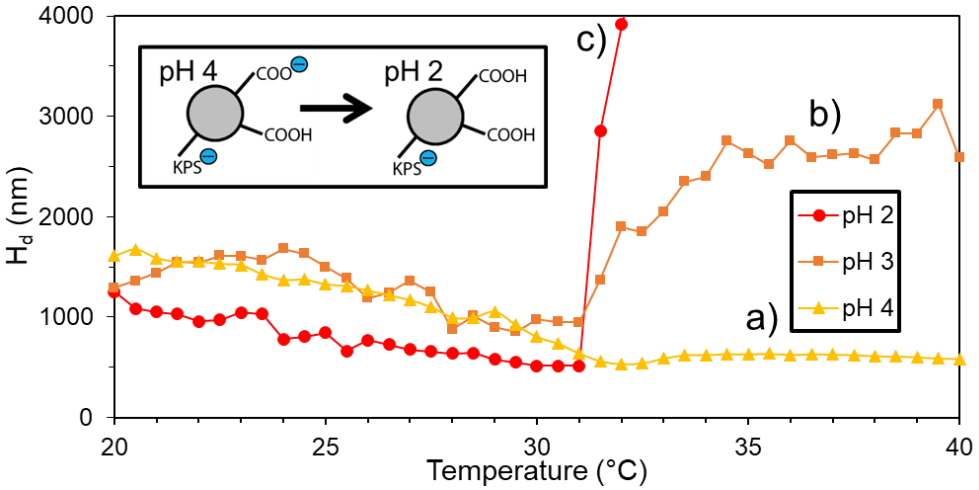

Figure 2.1 Colloidal stability of AcA-15.0 when heated from 20 °C to 40 °C at different pH values as a 1 mg ml^{-1} dispersion. Top left inset: Graphical representation of charge density at different pH values, KPS = potassium persulphate initiator fragment, COOH = carboxylic acid functional group of acrylic acid comonomer. Samples measured using DLS with the mean value of triplicate measurements used.

Interestingly, this temperature triggered aggregation behaviour above the VPTT, specifically in deionised water, is most likely only possible when acrylic acid or other pH responsive comonomers are incorporated into the nanogel and the pH is then lowered. This is because a lower charge density is required to give lower electrostatic stabilisation, allowing aggregation above the VPTT in water. Particles cannot simply be synthesised with lower charge density to allow their aggregation above the VPTT, as the synthesis is also conducted above the VPTT. Hence particles would keep growing in size until a higher charge density is reached, or synthesis fails with the creation of bulk aggregated material. To summarise, some of the charge density in the particle synthesis must be provided by a pH responsive comonomer, so charge density can be reduced post synthesis, via a change in pH, to allow temperature triggered aggregation in deionised water. As aggregation occurs when the temperature is > 31 °C and pH is <4, this provides us with nanogels which are able to undergo triggered aggregation at low pH and physiological temperature, which may find future usage. Examples would be in the potential application to release drug or adhere to tissue in an acidic environment,[53,54] or to protect drug as it transits through the stomach for delivery to the intestine.[55]

It is well known that polyNIPAM nanogels and particles with a polyNIPAM shell used for biomedical applications often become colloidal unstable in physiological ionic strength medium (e.g. PBS) if sufficient colloidal stabilisation is not provided. This is because electrostatic stabilisation is reduced by the screening of surface charge in the

high ionic strength media.[56] Previous examples show the result of this is that aggregation can occur at physiological temperature and ionic strength.[57,58] When PVP is physically absorbed to the nanogels, it provides steric stabilisation of the nanogels above the VPTT to prevent aggregation.[35,45] A sample containing 55K PVP, and no acrylic acid comonomer, AcA-0.0-55K, was heated in water and PBS to assess the colloidal stability of these nanogels above the VPTT in ionic strength medium. The sample without acrylic acid was selected, as this then determines colloidal stability provided only by the steric stabilisation of PVP, avoiding any extra contribution to colloidal stability from the electrostatic stabilisation provided by acrylic acid. It can be seen that with PVP physically absorbed to the nanogel, the particle deswelled to a smaller particle diameter in both water and PBS with increasing temperature, suggesting the sample remained colloidally stable when heated both in water and PBS, (figure 2.2). This can be compared to electrostatically stabilised polyNIPAM nanogels, which are often not colloidally stable when heated above the VPTT in physiological ionic strength medium.[59] PBS can also be seen to shift the VPTT of AcA-0.0-55K to lower temperature compared to water. The electrolyte concentration of PBS is 0.15 M, and similar VPTT shifts were seen for polyNIPAM nanogels when the electrolyte concentration reached > 0.1 M,[6,60] as well as the LCST of linear polyNIPAM.[61]

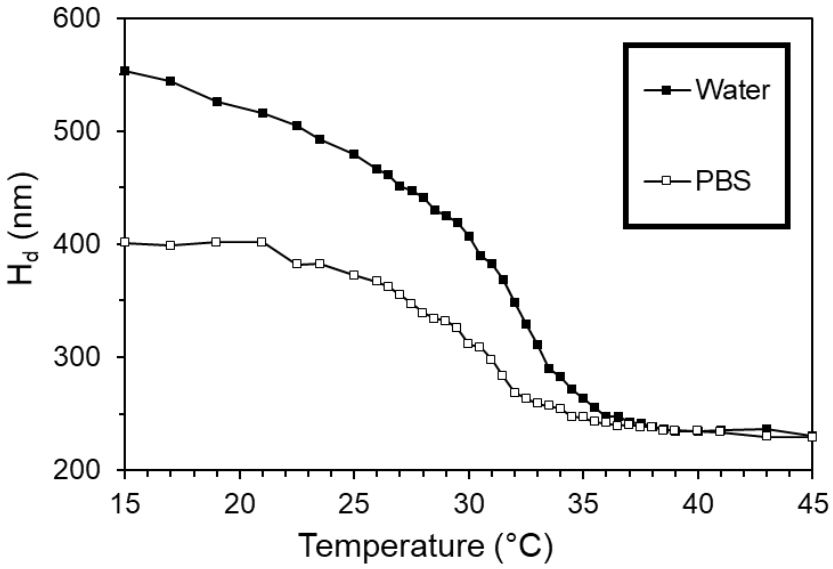

Figure 2.2 Colloidal stability of AcA-0.0-55K when heated from 15 °C to 45 °C in water and PBS as a 1 mg ml^{-1} dispersion. Samples measured using DLS with the mean value of triplicate measurements used.

The hydrodynamic diameter and zeta potential of the 55K PVP nanogels which were synthesised with acrylic acid comonomer were then measured at different pH values

to ascertain the pH at which swelling of the nanogels occurs, (figure 2.3). As the pH increased, the zeta potential of each nanogel sample decreased from an initial value of -2 mV, except for AcA-0.0-PVP, which does not contain any pH responsive acrylic acid comonomer. The zeta potential reached a maximum value of -4.5, -8.4 and -22.8 mV for 1.5, 2.0 and 5.0 wt% of acrylic acid used in the particle synthesis respectively when a pH of 7 was reached. The onset of increasing negative zeta potential occurred at pH 3.5 for all the nanogel samples containing acrylic acid. The hydrodynamic diameter of the particles however remained constant with increasing pH, at ~420 nm. Only the sample with 5 wt% of acrylic acid (AcA-5.0-55K) showed a change in hydrodynamic diameter with pH. These particles started to swell at pH 5, by which point they had reached a corresponding negative zeta potential value of -13 mV. Therefore it seems likely that swelling of the particles only occurs once a sufficient negative zeta potential value is reached, where there is a great enough density of ionised acrylic acid groups to cause internal repulsion and hence particle swelling. The other acrylic acid nanogels (AcA-1.5-55K, AcA-2.0-55K) did not show swelling as pH increased, as the maximum value of zeta potential they reach is below the zeta potential value at which the onset of swelling in AcA-5.0-55K (-13 mV) occurred.

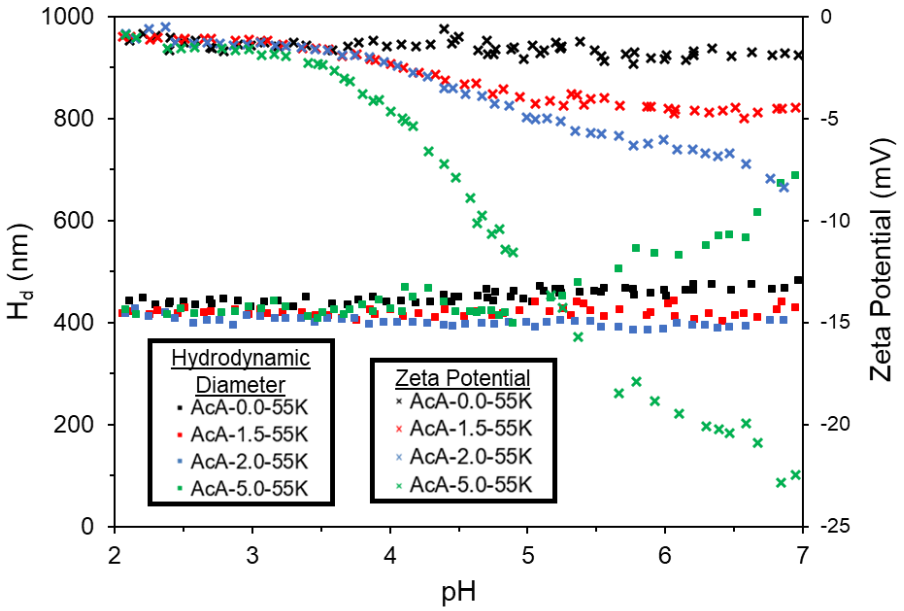

Figure 2.3 pH responsive change in hydrodynamic diameter (■) and zeta potential (✕) of 55K PVP polyNIPAM nanogels containing varying amounts of acrylic acid comonomer in the pH range 2-7 of nanogels dispersed as a 1 mg ml^{-1} dispersion with 10 mM NaCl at 25 °C. Samples measured using DLS and laser doppler electrophoresis (LDE) with the mean value of triplicate measurements used.

The increase in zeta potential magnitude with pH can be related to the increasing proportion of deprotonated carboxylic acid groups providing greater surface charge, as zeta potential reflects the electrostatic potential at the outer boundary of a nanogel, which is effected by a change in charge density.[29,62] The α-value, as derived previously,[10] gives the fraction of deprotonated carboxylic acid groups for a given pKa value, can be determined with a derivative of the Henderson-Hasselbalch equation:[10,52]

$$\alpha = \left(\frac{1}{1+10^{(pKa-pH)}}\right) \quad (1)$$

The pKa of poly(acrylic acid) is 4.5.[63] This is higher than the respective monomer pKa of 4.25,[11] due to the polyelectrolyte effect. This effect is caused by a high density of deprotonated carboxylic acid groups in the polymer chain opposing the formation of more deprotonated groups, due to the increased electrostatic repulsion this would cause, increasing the pKa value.[10] We can assume the density of carboxylic acid groups in polyNIPAM-co-acrylic acid particles is similar to poly(acrylic acid), as the hydrophilicity of the comonomer will concentrate it towards the surface of the particle. Hence the negative value of α (when pKa = 4.5), representing the fraction of deprotonated carboxylic acid groups, mirrors the increase in zeta potential of the AcA-5.0-55K particles with pH, due to the change in charge density of the particles (figure 2.4). The increase in zeta potential of the particles occurred at an even higher pKa value than is accounted for with the polyelectrolyte effect, (figure 2.4), which was previously attributed to factors such as the hydrophobic microenvironment of the nanogels hindering formation of deprotonated carboxylic acid groups.[10,64]

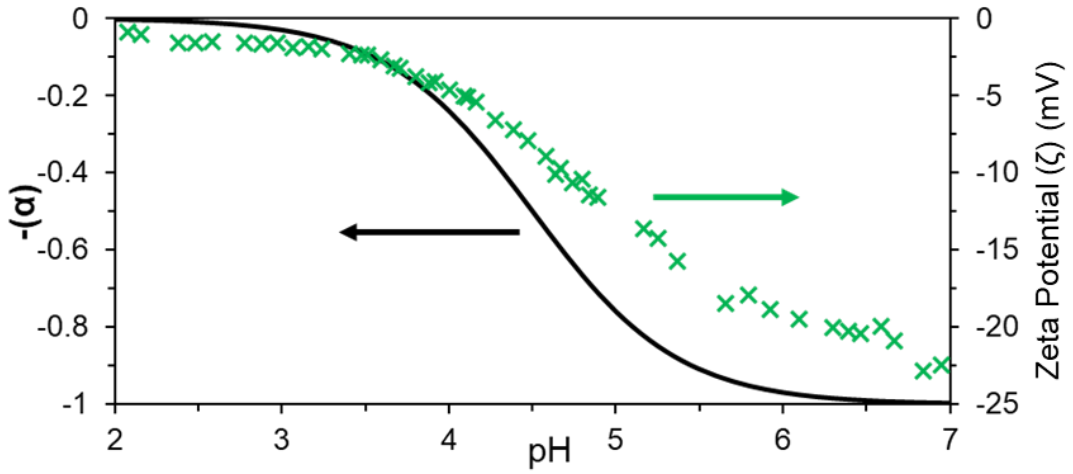

Figure 2.4 Comparison of fraction of deprotonated carboxylic acid groups (α) based on a pKa value of 4.5 with zeta potential (✕) of AcA-5.0-55K at different pH values. Samples measured using LDE with the mean value of triplicate measurements used.

AcA-5.0-55K particles showed pH responsive swelling, and colloidal stability at physiological ionic strength and temperature. These properties are desirable in a system which undergoes pH triggered gelation to form an implant. Hence this sample was selected to conduct a phase study. Concentrated dispersions were formed in PBS (1X strength, pH 7.4) at 37 °C to ascertain whether a shrunken gel phase could be formed, (table 2.2). In previous work, a shrunken gel was found to form in a 4 wt% and 3.5 wt% dispersion of polyNIPAM nanogels at 37 °C.[16,17] The viscosity of the liquid dispersion formed by AcA-5.0-55K increased with increasing concentration, but only became a gel at a concentration of 350 mg ml^{-1} (25.9% w/w). There was also no expulsion of any solvent from the gel as occurs upon shrunken gel formation. These results suggest that PVP physically absorbed to the surface of the nanogels disrupts the particles from forming a shrunken gel. Instead a swollen gel was formed due to a volume blocking mechanism of hard sphere theory in which the nanogel spheres become close packed at high enough concentration.[18,19]

Table 2.2 AcA-5.0-55K phase behaviour with concentration.

Concentration (mg ml^{-1})	Phase[a]
100	Liquid
200	Liquid
300	Liquid
350	Gel

[a] Phase behaviour in PBS (1X strength, pH 7.4) dispersion at 37 °C

Upon cooling the 350 mg ml^{-1} dispersion a gel remained with a reduction in turbidity, (table 2.3). Further heating of the sample resulted in aggregation at 60 °C, see images in table A.2, Appendix. This further suggests the formation of a swollen gel of close packed particle, as a shrunken gel would be expected to change phases into a liquid as it cooled,[16,17] whereas a swollen gel would remain in the gel phase. This finding means PVP nanogel samples are not suitable for an ISFI, as a very high concentration of the sample is required to form a depot and injectability of this gel would potentially present issues. Hence other alternative methods of forming an ISFI were explored.

Table 2.3 AcA-5.0-55K phase behaviour with temperature.

Temperature (°C)	Phase[a]
5	Gel
18	Gel
25	Gel
37	Gel
45	Gel
60	Aggregate

[a] Phase behaviour in PBS dispersion at 350 mg ml^{-1}

To conclude, it was found that pH 4.5 was the optimal pH to inject polyNIPAM-co-acrylic acid nanogels without steric stabilisation, which are intended for use in an ISFI. This is because pH 4.5 lies above the pH 4 limit of colloidal stability, but below the onset of particle swelling at pH 5. However, injection at this pH may causes discomfort for a patient.[65] These nanogels could also potentially be used for triggered aggregation at low pH and physiological temperature. When PVP is physically absorbed to the surface of the nanogels, they remain colloidally stable under physiological conditions, and at least 5.0 wt% of acrylic acid is required to give a swelling response, however the PVP appears to disrupt the ability of the nanogels to form a shrunken gel.

2.2.2. Charge Based Assembly to form a Colloidal Gel Network Implant

PolyNIPAM-co-allylamine nanogels with increasing PVP M_w were synthesised, with moles of PVP and allylamine used kept constant in samples AlA-2.6-10K, AlA-2.6-25K, AlA-2.6-40K and AlA-2.6-55K, (table 2.4), whilst average molecular weight (M_w) of PVP increased.

Table 2.4 Properties of polyNIPAM-co-allylamine nanogels.

Sample	Allylamine[a] (wt%)	PVP (M_w)	H_d (nm)[b]	PdI	Zeta Potential (ζ) (mV)[c]	
					pH 5	pH 10
AlA-2.6-10K	2.6	10K	1600	0.45	-	-
AlA-2.6-25K	2.6	25K	487	0.18	-	-
AlA-2.6-40K	2.6	40K	385	0.18	-	-
AlA-2.6-55K	2.6	55K	218	0.13	0.5*	-4.6*
AlA-5.0-10K	5.0	10K	475	0.06	10.3	-6.4*
AlA-10.0-10K	10.0	10K	390	0.22	14.1	-5.0*
AlA-15.0-10K	15.0	10K	392	0.07	15.4	-5.4*

[a] wt% of allylamine used in the synthesis of the nanogel (wt% of NIPAM and allylamine mass).
[b] Hydrodynamic diameter (H_d) measurements performed at pH 7, 1 mg mL^{-1} in water at 25 °C using the mean of three DLS measurements.
[c] Zeta Potential measured at pH 5 and pH 10, 1mg ml^{-1}, 25 °C, in 10 mM NaCl, samples measured using LDE with the mean value of triplicate measurements used.
*Zeta potential value negligible (< ±10mV)

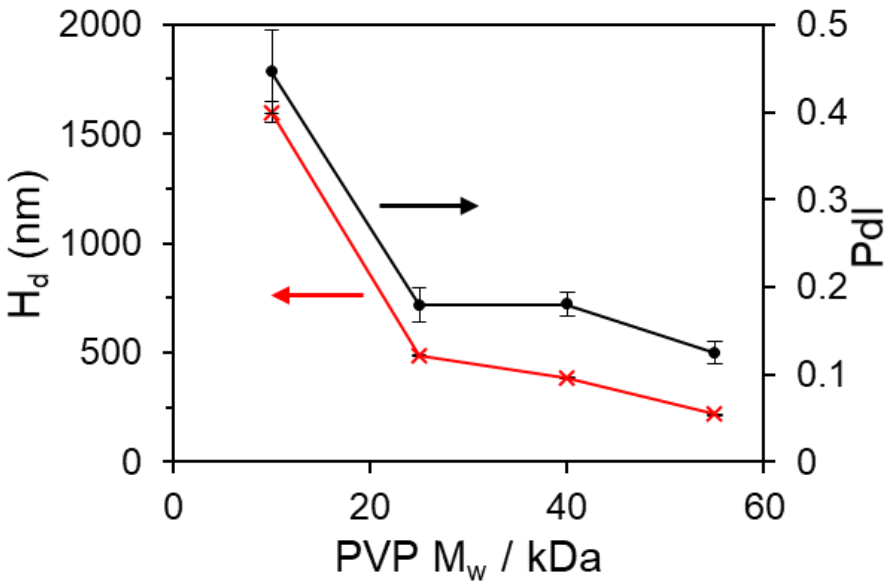

Figure 2.5 Hydrodynamic diameter (H_d) and Polydispersity index (PdI) of polyNIPAM-co-allylamine nanogels with 2.6 wt% allylamine comonomer and varying M_w PVP. Samples measured using DLS with the mean value of triplicate measurements used.

It can be seen that larger M_w PVP leads to smaller particles, (figure 2.5). There was a big decrease in particle hydrodynamic diameter (from 1600 to 487 nm) and PdI (from

0.45 to 0.18) on increasing PVP M_w from 10K to 25K respectively. This was followed by a much more gradual decrease on increasing PVP M_w from 25K, to 40K and then 55K (487, 385, 218 nm and 0.18, 0.18, 0.13 for 25K, 40K, 55K stabilisation respectively). The zeta potential of the AlA-2.6-55K particles was measured, but was found to be negligible (< ±10mV), suggesting the positive charge from the allylamine comonomer at 2.6 wt% counters the negative charge of the persulfate initiator chain end fragment, leaving an overall neutral surface charge, (table 2.4). This suggests that with the loss of electrostatic stabilisation, the particle synthesis relied on steric stabilisation. 10K PVP did not appear to be adequate to provide full stabilisation during the dispersion polymerisation, leading to large particles with broad dispersity. From 25K to 55K PVP, the particles become gradually smaller, and can be attributed to the greater surface area of a precursor particle which can be stabilised by a longer PVP chain, and greater rate of PVP absorption to the particle surface.[48] To determine whether electrostatic stabilisation was able to produce particles of small size and low dispersity, 10K PVP was used in conjunction with higher allylamine wt%, where increasing allylamine should provide greater electrostatic stabilisation, without the influence of steric stabilisation from PVP with a M_w higher than 10K. In the synthesis of AlA-5.0-10K, AlA-10.0-10K and AlA-15.0-10K, 5.0, 10.0 and 15.0 wt% of allylamine respectively were used. This lead to a measurable positive zeta potential at pH 5, as the charge contributed by allylamine comonomer outweighed that of the persulfate initiator, (table 2.4). At pH 10 the zeta potential is negligible as the amine groups become predominantly deprotonated (allylamine has a pKa of 9.49). When we compare these samples to AlA-2.6-10K, smaller particles of low dispersity are achievable, (figure 2.6). This time, despite the 10K PVP not being able to provide significant enough steric stabilisation, the greater allylamine content allows electrostatic stabilisation of the precursor particles in the polymerisation process. It can be concluded that stabilisation during synthesis was provided sterically by PVP with a M_w of 25K or greater, or by a sufficient charge density for electrostatic stabilisation. In the case of allylamine nanogels, a greater than expected comonomer addition was required to achieve electrostatic stabilisation, as some of the charge is effectively neutralised by using a negatively charged persulfate initiator.

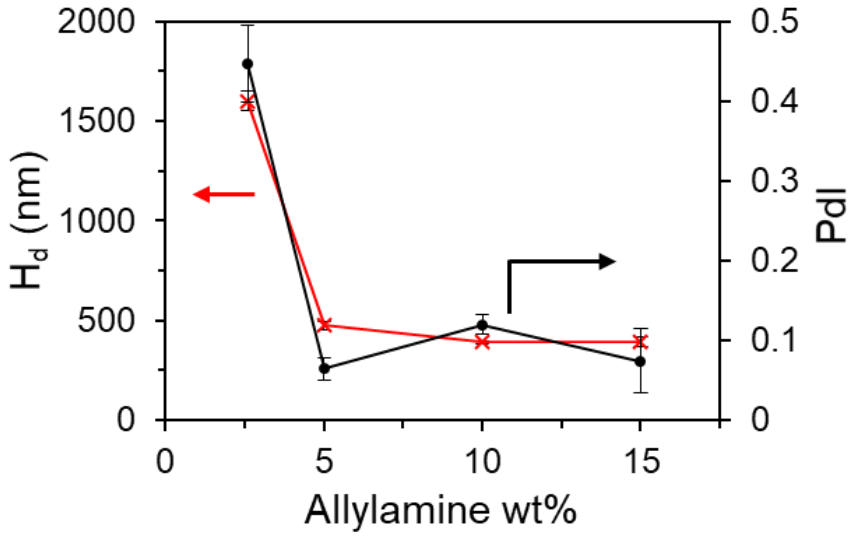

Figure 2.6 Hydrodynamic diameter (H_d) and Polydispersity index (PdI) of polyNIPAM-co-allylamine nanogels with 10K PVP and varying wt% of allylamine comonomer. Samples measured using DLS with the mean value of triplicate measurements used.

With an understanding of the effect of precursor particle stability with increasing PVP M_w and allylamine wt%, the stability provided by these steric or electrostatic contributions on the nanogel above its VPTT and in the presence of PBS was determined. AlA-10.0-10K was heated in water at different pH values and in PBS. In water, at pH 7.4 we can see that the electrostatic stabilisation provided by the allylamine prevents the nanogels from flocculating or aggregating, (figure 2.7, a). When conducted at pH 10, the particles aggregated as electrostatic stabilisation was removed with the deprotonation of the amine groups, and 10K PVP again, was unable to provide the steric stabilisation required, (figure 2.7, b). In pH 7.4 PBS, the electrostatic stabilisation was also screened to a great enough extent that the particles aggregate above the VPTT, (figure 2.7, c). The particle deswelling and aggregation takes place at a lower temperature in PBS than at pH 10. As mentioned previously, the higher electrolyte content of PBS (1X strength, pH 7.4) shifts the VPTT to lower temperature.[6,60] This effect is especially prominent with Cl^- ions, (which along with Na^+) are the highest concentration ions in PBS. In a range of ions, these were found to have the largest effect on the disruption of water molecules in the hydration shell around polyNIPAM.[66]

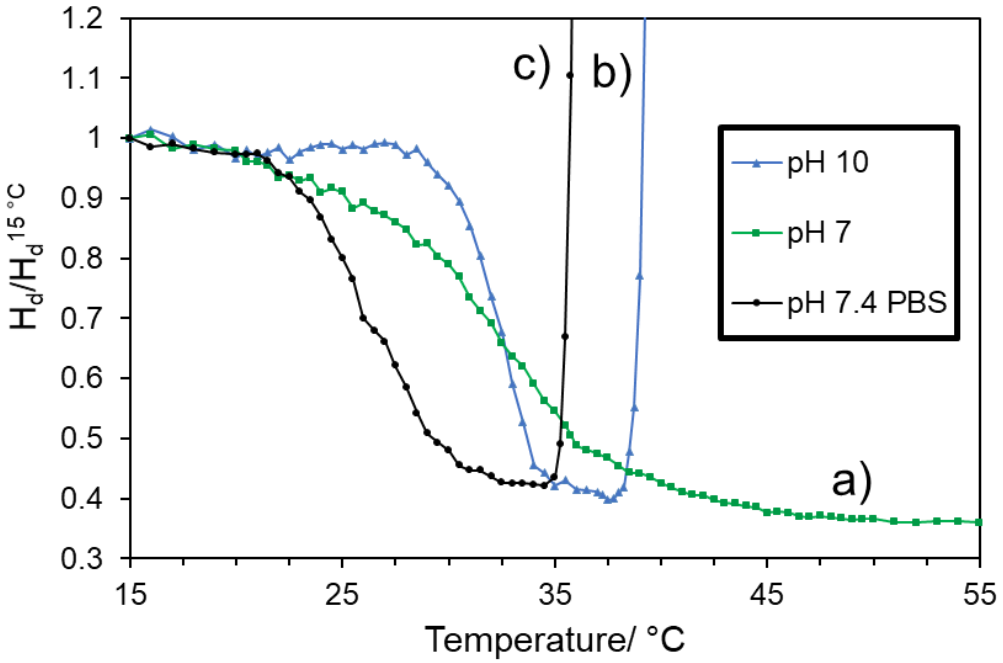

Figure 2.7 Hydrodynamic diameter (H_d) as a fraction of hydrodynamic diameter at 15 °C ($H_d^{15\ °C}$) of polyNIPAM-co-allylamine nanogels with 10K PVP and 10 wt% of allylamine comonomer (AlA-10.0-10K) in water at a) pH 7 and b) pH 10 and c) PBS at pH 7.4. Samples measured using DLS with the mean value of triplicate measurements used.

The zeta potential of AlA-10.0-10K with changing pH was measured and compared with AcA-5.0-55K to observe the pH value at which both polyNIPAM-co-allylamine and polyNIPAM-co-acrylic acid nanogels reside at maximum zeta potential. This value was found to be pH 6.5, (figure 2.8), however extracellular pH lies at pH 7.4. At this pH the polyNIPAM-co-allylamine nanogel would be at 70% of its maximum zeta potential. The two nanogels were dispersed separately in water at pH 7, where they behaved as a flowable liquid at 25 °C. The two species have a significant magnitude of zeta potential at pH 7, (table 2.5). When these two liquid dispersions were combined in an equal mass ratio to form a 7 wt% aqueous dispersion, a self-supporting gel was formed in water when at room temperature (25 °C), (figure 2.9). However upon heating, this turned into a liquid. Upon heating the nanogels deswell as the PNIPAM reduces contact with water. It is likely that the PVP physically absorbed to the surface of the nanogel, remains extended into solution. This would create a greater separation of the charges which are contained in the receded PNIPAM chains, so that they can no longer interact strongly enough to form a colloidal gel network. As in section 2.2, the PVP appears to disrupt the phase behaviour of the nanogels. In this case it prevents the formation of a colloidal gel network to form an in-situ drug delivery depot.

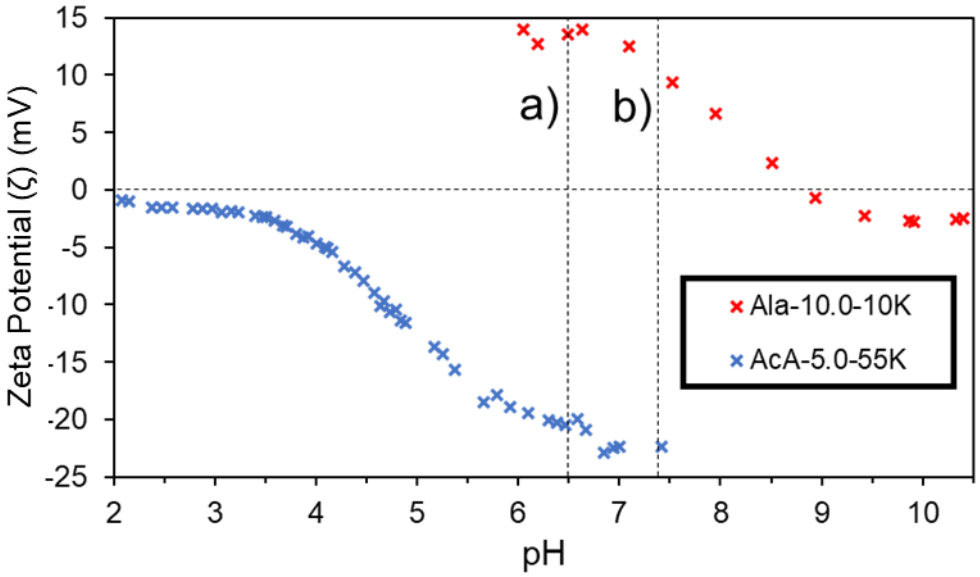

Figure 2.8 Zeta potential of AlA-10.0-10K and AcA-5.0-55K with change in pH, a) pH 6.5, b) pH 7.4. Samples measured at 25 °C using LDE with the mean value of triplicate measurements used.

Table 2.5 Properties of nanogels used to form a colloidal gel network. Samples measured using LDE and DLS in triplicate and mean value used.

Sample	Zeta Potential (ζ)[a] (mV)	H_d[b] (nm)	PVP (M_w)
AlA-10.0-10K	+14	390	10K
AcA-5.0-55K	-22	688	55K

[a] Zeta Potential measured at pH 7, 1mg ml-1, 25 °C, in 10 mM NaCl.
[b] Hydrodynamic diameter (H_d) measurements performed at pH 7, 1mg ml^{-1}, 25 °C. Samples measured using DLS with the mean value of triplicate measurements used.

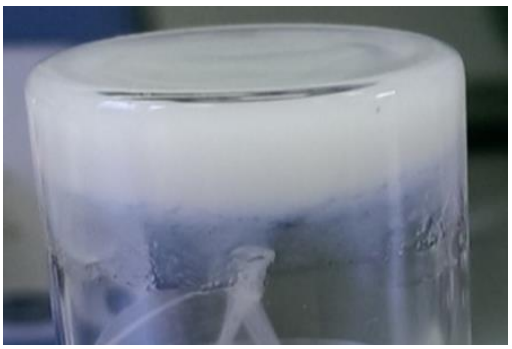

Figure 2.9 Photograph (digital image) of self-supporting gel formed from AlA-10.0-10K and AcA-5.0-55K in an equal mass ratio as a 7 wt% dispersion. The respective starting nanogels were liquid dispersions which formed a self-supporting gel when combined.

2.2.3. In Situ Implant Formation Triggered by Temperature and Ionic Strength

PolyNIPAM nanogels were synthesised in the presence of SDS, PVP, or without surfactant and the hydrodynamic diameter and PdI of the particles were measured (table 2.6). The samples AcA-5.0 and AcA-15.0 in section 2.2.1 and nanogels previously synthesised without surfactant or stabiliser showed that often large nanogels with high dispersity are produced without surfactant present,[41,49] however particles with lower dispersity have also previously been produced, with the concentration of monomer, initiator and cross-linking agent amongst factors which affect the quality of the nanogels produced.[67,68] Nanogels without added surfactant or stabiliser were considered a good candidate for a depot which forms through aggregation, as the relatively small amount of electrostatic stabilisation from the persulfate initiator may allow rapid aggregation of the nanogels in PBS at 37 °C to entrap a payload without a burst release. Hence nanogels with a NIPAM monomer concentration of 6 mg ml^{-1} and BIS cross-linking agent concentration of 0.6 mg ml^{-1} where synthesised in a series of five repeats, PNA-00, PNA-00-2, PNA-00-3, PNA-00-4, PNA-00-5. These concentrations lie well below the maximum concentration at which Pelton and Chibante found 'good' nanogels were no longer formed.[67] It can be seen that whilst a reasonably low dispersity is achieved in all samples, there is some variation in the size of the nanogels formed, (figure 2.10), likely because a surfactant is required in the synthesis for complete control over particle size.[41,49]

Table 2.6 Properties of polyNIPAM nanogels.

Sample	10K PVP (mg ml^{-1})	SDS (mg ml^{-1})	Z-Ave[a] (nm)	PdI
PNA-00	-	-	581	0.10
PNA-00-2	-	-	879	0.13
PNA-00-3	-	-	776	0.07
PNA-00-4	-	-	605	0.10
PNA-00-5	-	-	884	0.11
PVP-0.3	0.3	-	604	0.06
PVP-0.9	0.9	-	629	0.15
SDS-0.015	-	0.015	573	0.01
SDS-0.030	-	0.030	496	0.03
SDS-0.060	-	0.060	370	0.01

[a] Hydrodynamic diameter (H_d) measurements performed at 1mg ml^{-1}, 25 °C. Samples measured using DLS with the mean value of triplicate measurements used.

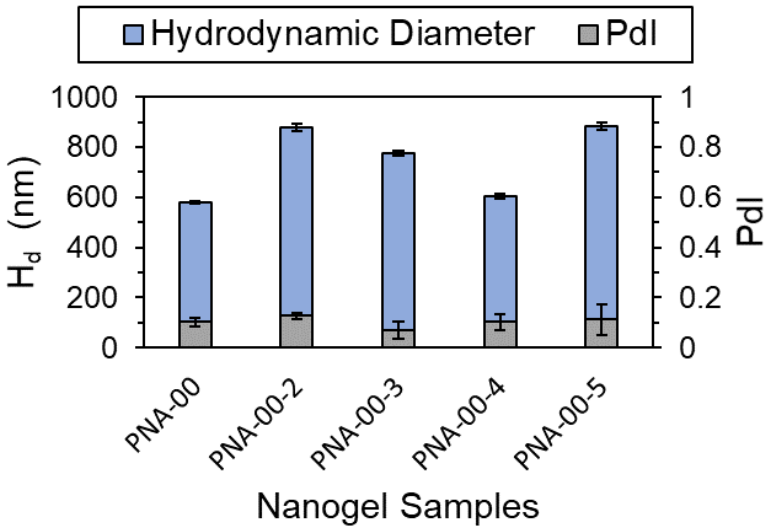

Figure 2.10 Hydrodynamic diameter (H_d) and Polydispersity index (PdI) of surfactant/stabiliser free polyNIPAM nanogels with an identical repeat synthesis. Samples measured using DLS with the mean value of triplicate measurements used.

Samples were also synthesised with different concentrations of 10K PVP, (PVP-0.3 and PVP-0.9), which contained 0.3 and 0.9 mg ml^{-1} PVP respectively. These samples are similar in size and dispersity to the non-PVP samples, as the 10K PVP was previously demonstrated to not provide steric stabilisation in the nanogel synthesis, and hence any significant effect on the resulting nanogel size and dispersity. Finally an increasing concentration of SDS was used in the synthesis of SDS-0.015, SDS-0.030 and SDS-0.060 of 0.015, 0.030 and 0.060 mg ml^{-1} respectively. Increasing amounts of SDS reduce the particle size, (figure 2.11), as shown previously.[41] The dispersity of these samples was also very low (≤0.03).

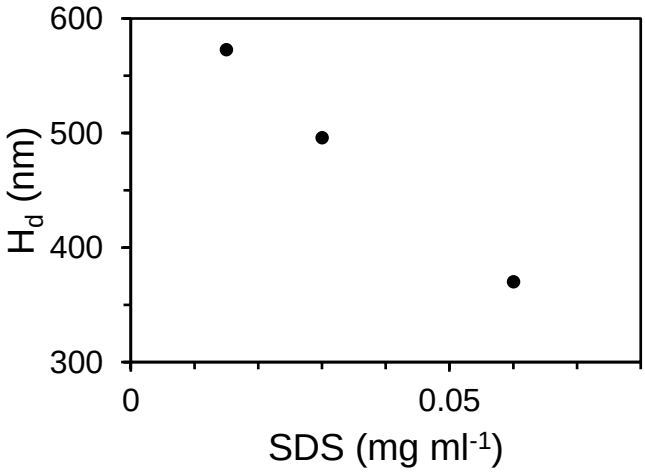

Figure 2.11 Decrease in hydrodynamic diameter (H_d) with increasing SDS concentration used in particle synthesis. Samples measured using DLS with the mean value of triplicate measurements used.

To assess the aggregation behaviour of the nanogels they were heated as a dilute dispersions (1 mg ml^{-1}) to monitor changes in the dispersion properties using DLS, and as a concentrated dispersion (175 mg ml^{-1}) to visually observe aggregation in water and PBS. Ideally the samples should remain colloidally stable as an aqueous dispersion as both a dilute and concentrated dispersion at elevated temperatures, where a concentrated dispersion should exist as a liquid phase rather than aggregating. In PBS the samples should aggregate, and a concentrated dispersion should phase separate when heated to act as a suitable ISFI. This aggregation should be into a single uniform depot material, as opposed to irregular fragments of fractured or varying sized aggregates. Sample PNA-00 (no surfactant or stabiliser) remained stable as a dilute dispersion (1 mg ml^{-1}) when heated in water, and aggregated completely in a narrow temperature range (32.5 °C ±0.5) in PBS, as indicated by monitoring the hydrodynamic diameter of the dispersion over a temperature range (figure 2.12, a). As a concentrated dispersion the same behaviour was reflected in the visual phase behaviour; a swollen gel at 25 °C transitions to a liquid when the nanogels are dispersed in water, (figure 2.12, b). In PBS this swollen gel phase separates when heated, rapidly forming a single piece of aggregate which expels excess solvent and retains the uniform shape of the cylindrical vial.

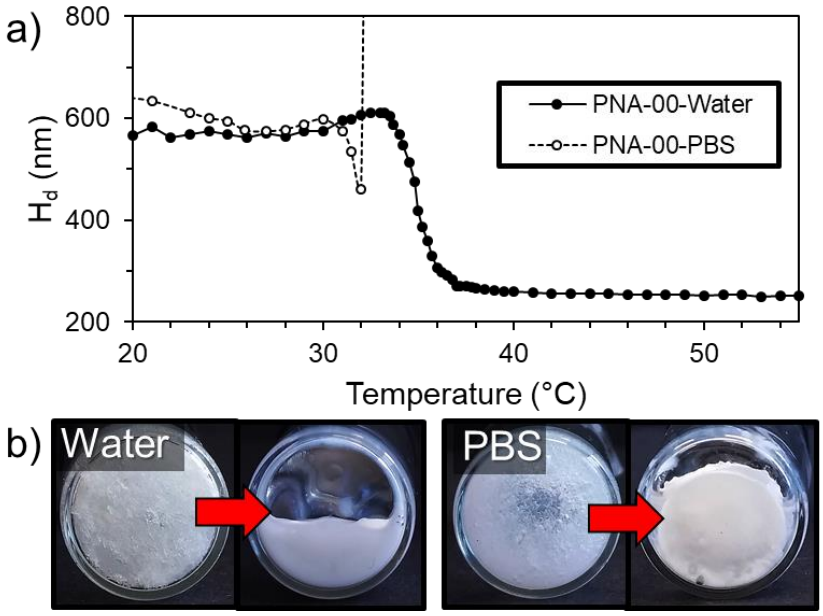

Figure 2.12 Dilute and concentrated nanogel dispersion behaviour of sample PNA-00, a) dilute dispersion colloidal stability in water and PBS measured using DLS, samples measured using DLS with the mean value of triplicate measurements used, b) Photographs (digital images) of concentrated dispersion phase behaviour in water (left) and PBS (right), arrows show transition from 25 °C to 37 °C.

With the PVP nanogels, the same dilute dispersion behaviour as PNA-00 can be seen for PVP-0.3, with aggregation at (32.5 °C ±0.5), however with greater PVP content, PVP-0.9 only flocculates to a diameter of 930 nm above 40 °C, resisting complete aggregation in PBS (figure 2.13, a). This was most likely due to the greater steric stabilisation provided by a large amount of PVP physically absorbed to the nanogel.[44] Unlike PNA-00, the PVP based nanogels show varying degrees of aggregation in water as a concentrated dispersion. PVP-0.3 partially aggregates at 37 °C, and PVP-0.9 completely aggregates. This suggests that whilst PVP provides colloidal stability in a dilute dispersion, it induces aggregation in a concentrated dispersion, (figure 2.13, b). This behaviour may be due to an attractive depletion force existing between the nanogels at higher concentration, where the separation distance of the particles is much smaller.[69] At higher colloidal particle concentration, PVP has been shown to first bridge particles, followed by depletion phase separation as the concentration is further increased.[70] The flocculation rate through bridging was also found not to be effected by the existence of double layer repulsion in negatively charge colloids,[71] hence the negatively charged polyNIPAM nanogels created with persulfate initiator are unable to resist the PVP flocculation at higher concentration. PVP flocculation at high concentration also explains why PVP-0.9 is more completely aggregated than PVP-0.3, as it contains a higher proportion of PVP to enable the aggregation to occur. The PVP-0.9 sample also forms a less uniform aggregate, with the aggregate having a visibly rough surface, and imperfections in the cylindrical shape formed, especially in PBS.

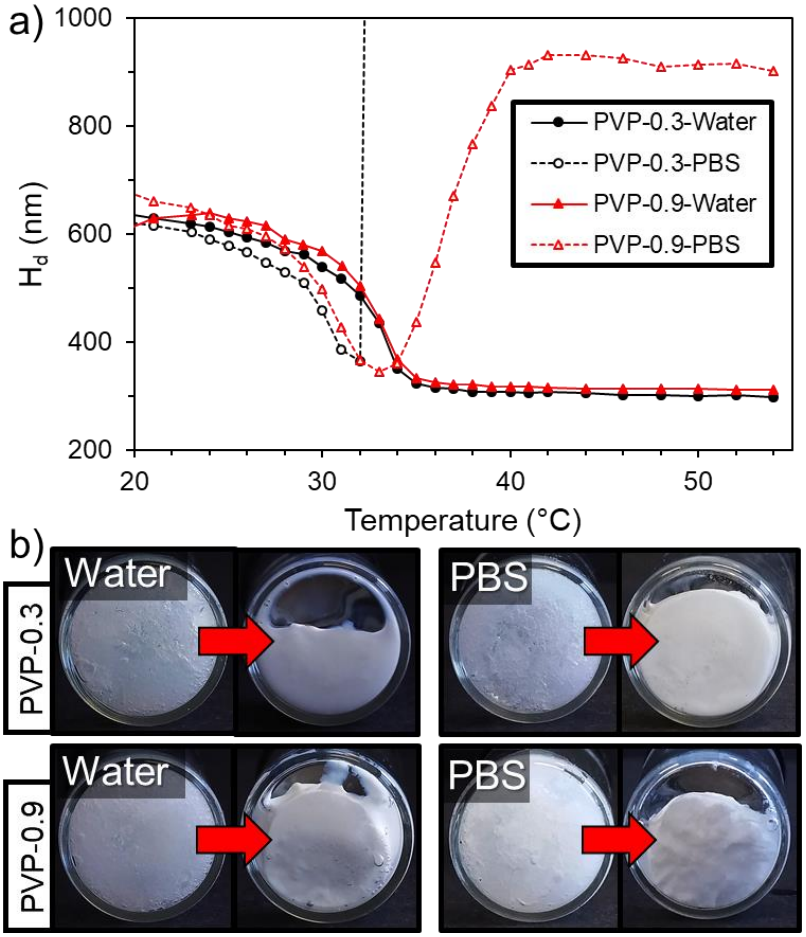

Figure 2.13 Dilute and concentrated nanogel dispersion behaviour of PVP-0.3 and PVP-0.9, a) dilute dispersion colloidal stability in water and PBS, measured using DLS, samples measured using DLS with the mean value of triplicate measurements used, b) Photographs (digital images) of concentrated dispersion phase behaviour in water (left) and PBS (right), PVP-0.3 (top), and PVP-0.9 (bottom), arrows show transition from 25 °C to 37 °C.

Finally, with nanogels synthesised in the presence of SDS, the colloidal stability and phase behaviour were almost identical to the PNA-00 nanogel, (figure 2.14). As a dilute dispersion the aggregation temperature is 1 °C lower than PNA-00 at 31.5 °C ±0.5. This aggregation temperature was the same for the three samples, despite different concentrations of SDS being used to create particles of different sizes. In a concentrated dispersion highly uniform aggregates were formed in PBS.

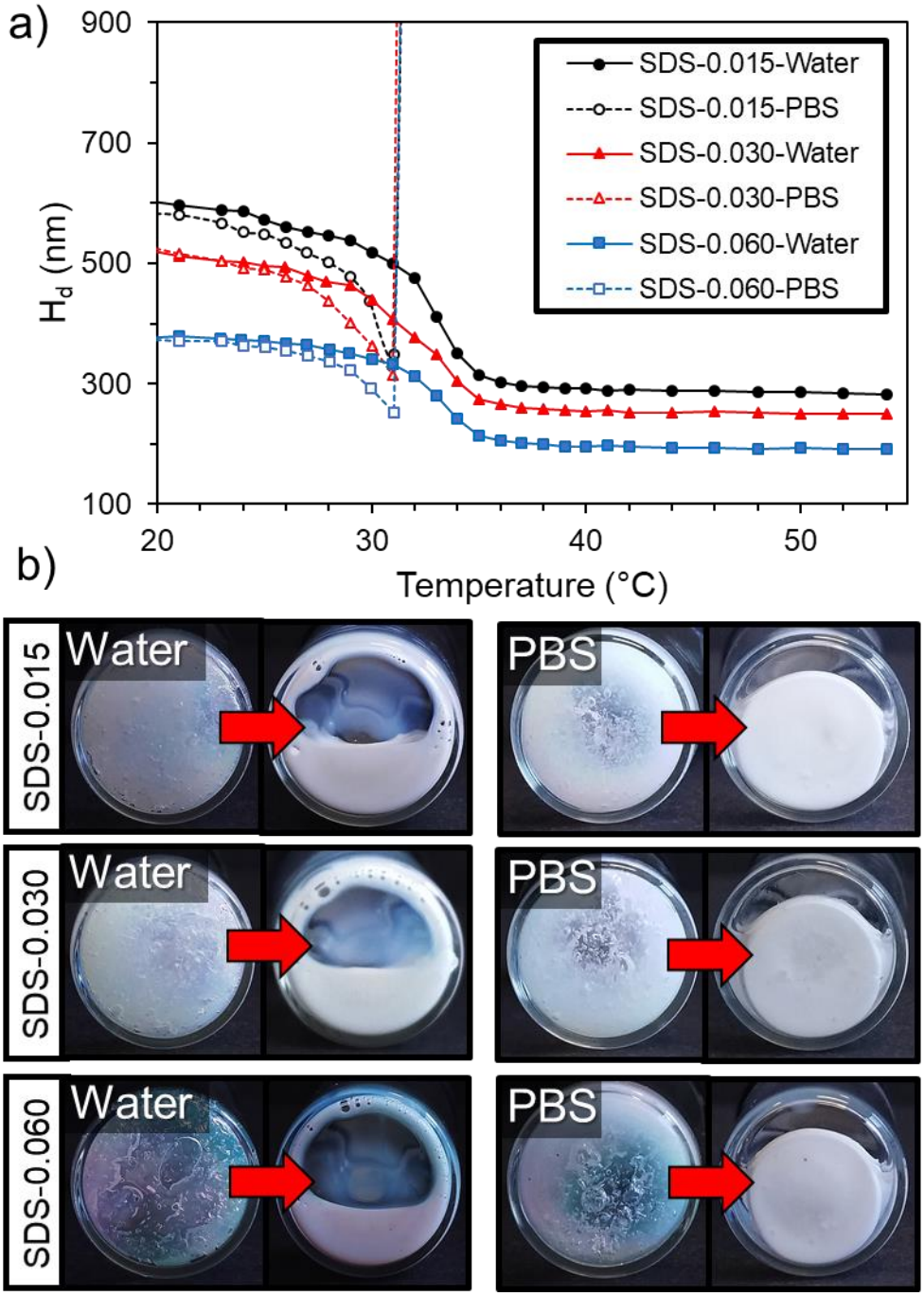

Figure 2.14 Dilute and concentrated nanogel dispersion behaviour of SDS-0.015, SDS-0.030 and SDS-0.060, a) dilute dispersion colloidal stability in water and PBS, samples measured using DLS with the mean value of triplicate measurements used, b) Photographs (digital images) of concentrated dispersion phase behaviour in water (left) and PBS (right), SDS-0.015 (top), SDS-0.030 (middle), and SDS-0.060 (bottom), arrows show transition from 25 °C to 37 °C.

In summary, PNA-00 and SDS based nanogels remain a liquid when heated in water, and aggregate below 37 °C in PBS, over a wide concentration range of 1-175 mg ml^{-1}. This makes them suitable candidates for an ISFI. PVP based nanogels unfortunately aggregate at a higher concentration in water, and form less uniform aggregates in PBS, suggesting they are not as suitable, as the injection needle could become blocked, and the variation in the shape of the aggregate could lead to a variation in the release rate of drug.[1]

2.3. Conclusions

For an ISFI to function, a solidification must occur in situ. Three different approaches were investigated in order to find ways to trigger this solidification in response to physiological pH, ionic strength and temperature. PVP was physically absorbed to the nanogels for the two concepts which used pH to trigger the formation of a shrunken gel, and the formation of a self-assembled gel through charge interactions. This aided the synthesis process, producing nanogels with a lower dispersity and controlled size, as well as providing the nanogels with colloidal stability under physiological conditions to prevent aggregation. However, in both cases the PVP appeared to disrupt the formation of a gel under physiological conditions, and solidification under physiological conditions is a vital aspect required of an ISFI. This led to the elimination of these systems from further development. This was because the preliminary study into nanogels which selectively aggregate under physiological conditions was more promising as an ISFI, due to the rapid and complete aggregation under physiological conditions. Using PVP, SDS, and no stabiliser or surfactant, nanogels could be synthesised which were a liquid at room temperature and 37 °C in water, and aggregated when heated to 37 °C in PBS. However as a concentrated dispersion PVP based nanogels aggregated when heated in water, and so were eliminated as a potential candidate. The nanogels created with SDS, and without surfactant both remains liquid in water, and formed a macroscopic aggregate in PBS when heated as a concentrated dispersion, as desired. However, SDS gave the added advantage that nanogel size could also be tuned, with no impact of their phase behaviour, and the formation of the most uniform aggregates. SDS and surfactant free nanogels are therefore likely able to be injected and then solidify in situ when used as

a dispersion for an ISFI. These nanogels were taken forward for further development and testing. Although the nanogels form an aggregate rapidly, the ability of the nanogels to entrap a payload, and avoid a large burst release needs to be assessed, as well as the ability of the aggregate matrix which forms to allow sustained release over time.

2.4. Materials and Methods

2.4.1. Materials

N-Isopropylacrylamide (NIPAM, ≥99%), allylamine (AlA, ≥99%), acrylic acid (AcA, 99%), N,N-methylenebis(acrylamide) (BIS, 99%), potassium persulfate (KPS, ≥99%), sodium chloride (NaCl, ≥99.5%), anhydrous sodium hydroxide pellets (NaOH, analysis grade), sodium dodecyl sulphate (SDS, ≥99%), polyvinylpyrrolidone, average mol wt 10,000 (PVP 10K), polyvinylpyrrolidone, average mol wt 25,000 (PVP 25K), polyvinylpyrrolidone, average mol wt 40,000 (PVP 40K), polyvinylpyrrolidone, average mol wt 55,000 (PVP 55K), were purchased from Sigma-Aldrich Company Ltd, Gillingham (Dorset) UK, a subsidiary of Merck KGaA, Darmstadt, Germany. Phosphate buffered saline tablets (Bioreagent), hydrochloric acid 37% (HCl, analytical grade), were purchased from Fischer Scientific UK, Loughborough, UK, a part of Thermo Fisher Scientific. Type I distilled water obtained from a water purification system with a resistivity of >18 MΩ cm^{-1} (PURELAB option R, Veolia). Spectra/Por 2 Dialysis Tubing (MWCO = 12-14 kDa) was purchased from Spectrum Europe B.V., Breda, The Netherlands. All materials were used as received.

2.4.2. PolyNIPAM Nanogel Synthesis

The polyNIPAM nanogels were synthesised by precipitation polymerisation, or dispersion polymerisation where SDS or PVP was included in the synthesis. A summary of the formulation which was used for each nanogel species can be found in Table M.2.1. In a typical synthesis, the NIPAM monomer and N,N′-methylenebis(acrylamide) (BIS) cross-linking agent were dissolved in distilled water in a 250 ml two-neck round bottom flask equipped with a reflux condenser, along with any additional comonomers (acrylic acid or allylamine), surfactants (SDS) or stabilisers (PVP). This was then sealed, and nitrogen was bubbled through the aqueous solution for 1 hour whilst stirring (400 rpm) to remove dissolved oxygen. The solution was then heated to 60 °C. Separately potassium persulfate (KPS) initiator was dissolved in distilled water (25 mg ml^{-1}) and degassed with N_2 for 1 hour before being transferred to the flask containing the monomers. The reaction was maintained under a N_2 atmosphere for 4 hours at 60 °C before being cooled down to room temperature. To remove unreacted impurities, the nanogel suspension was dialysed for 5 days using

12-14 kDa MWCO dialysis tubing, replacing the distilled water every 12 hours. Nanogels containing PVP were also further purified by centrifugation (Thermo Scientific Heraeus Megafuge 8R centrifuge) at a relative centrifugal force (RCF) of 10,900 in 50 mL centrifuge tubes for 1 hour, and washed with distilled water (ca. 50 mL), this process was repeated four times. The purified suspension was then lyophilised (Virtis Benchtop K with ultra-low temperature condenser) and sealed for storage.

Table M.2.1 The composition of reactants used in nanogel synthesis

Sample	NIPAM mg	AcA mg	AlA mg	BIS mg	SDS mg	PVP[a] M_w	PVP mg	KPS mg	Water[b] ml
AcA-5.0	712.5	37.5	-	75.0	-	-	-	75.0	130
AcA-15.0	637.5	112.5	-	75.0	-	-	-	75.0	130
AcA-0.0-55K	750.0	-	-	75.0	-	55	750.0	75.0	85
AcA-1.5-55K	738.6	11.4	-	75.0	-	55	750.0	75.0	85
AcA-2.0-55K	734.8	15.2	-	75.0	-	55	750.0	75.0	85
AcA-5.0-55K	712.0	38.0	-	75.0	-	55	750.0	75.0	85
AlA-2.6-10K	2000.0	-	53.0	80.0	-	10	363.6	60.0	85
AlA-2.6-25K	2000.0	-	53.0	80.0	-	25	909.0	60.0	85
AlA-2.6-40K	2000.0	-	53.0	80.0	-	40	1454.5	60.0	85
AlA-2.6-55K	2000.0	-	53.0	80.0	-	55	2000.0	60.0	85
AlA-5.0-10K	2000.0	-	105.3	80.0	-	10	363.6	60.0	85
AlA-10.0-10K	2000.0	-	222.2	80.0	-	10	363.6	60.0	85
AlA-15.0-10K	2000.0	-	352.9	80.0	-	10	363.6	60.0	85
PNA-00	750	-	-	75.0	-	-	-	75.0	130
PNA-00-2	750	-	-	75.0	-	-	-	75.0	130
PNA-00-3	750	-	-	75.0	-	-	-	75.0	130
PNA-00-4	750	-	-	75.0	-	-	-	75.0	130
PNA-00-5	750	-	-	75.0	-	-	-	75.0	130
PVP-0.3	750	-	-	75.0	-	10	50	75.0	130
PVP-0.9	750	-	-	75.0	-	20	150	75.0	130
SDS-0.015	750	-	-	75.0	2.5	-	-	75.0	130
SDS-0.030	750	-	-	75.0	5.1	-	-	75.0	130
SDS-0.060	750	-	-	75.0	10.0	-	-	75.0	130

[a] M_w of PVP used, e.g. average molecular weight of 10,000 = 10 (K)

[b]Total volume of water, including addition of KPS dissolved in water.

2.4.3. Characterisation

Dynamic light scattering (DLS) measurements were performed at 25 °C with a 1 mg mL^{-1} nanogel dispersion using an equilibration time of 600 seconds, unless otherwise stated, with a Malvern Zetasizer Nano ZS (running Malvern Zetasizer software V7.12) (Malvern Instruments, Malvern, UK) with 633 nm He–Ne laser and the detector positioned at 173°. 1 cm path length disposable polystyrene cuvettes were used for measurements. Measurements were repeated in triplicate to give a mean Z-average diameter and polydispersity index (PdI) value. Adjustments of dispersion pH were made with NaOH and HCl solutions, and dispersion pH measurements were made with a HI-11310 pH Edge Electrode (HANNA Instruments, Bedfordshire, UK). Zeta potential measurements were performed using DTS1070 folded capillary cells (Malvern, UK). The pH of the sample was measured before performing zeta potential measurements. Capillary cells were flushed with ethanol and water prior to usage. The zeta potential measurement was made with a minimum of 10 and maximum of 40 runs, and the voltage applied was automatically selected by the software. The Smoluchowski approximation f(Ka) = 1.5 was used, and dispersions contained 10 mM NaCl and were measured at 25 °C. Hydrodynamic diameter and zeta potential measurements across a pH range were measured using an MPT-2 multipurpose autotitrator (Malvern Instruments, Malvern, UK) equipped with HCl and NaOH solutions, and connected to a Malvern Zetasizer Nano ZS, with measurements made using a DTS1070 folded capillary cell. ^{1}H nuclear magnetic resonance (NMR) spectra were recorded in D_2O using a Bruker Avance spectrometer operating at 400 MHz. Chemical shifts (δ) are reported in parts per million (ppm) and TMS (Tetramethylsilane) was used as an internal standard. Lyophilised microgel sample was dissolved in D_2O at 30 mg mL^{-1}.

2.4.4. Phase Studies

To form nanogels at different wt% in water and PBS the lyophilised nanogels were first packed at the bottom of glass sample vials. Water or PBS (1X strength, pH 7.4) was then added to the sample vials and the samples were held at 20 °C for 30 minutes to allow the solvent to soak into the lyophilized nanogel material. The samples were then held at 27 °C for 24 hours to allow the nanogels to completely disperse. The samples were then added to a sonication bath (S 100/H, Elmasonic) for 30 minutes to

remove any trapped air bubbles formed in the high concentration dispersions. This was repeated up to three times and the temperature of the bath was kept below 25 °C. For phase studies the sample was allowed to equilibrate for 5 minutes at each temperature. The phase of each sample was then observed by visual inspection and the vial inversion method:[72] A liquid flowed down to the bottom of the vial; a swollen gel remained self-supporting and did not flow over 10 seconds; a shrunken gel remained self-supporting and adhered to the sides of the vial over 10 seconds with a small excess of water phase separating; an aggregate formed a pellet which was not self-supporting and with a large excess of water phase separated.

2.5. Appendix

Table A.1 NMR Chemical shifts in polyNIPAM, poly(acrylic acid) and PVP.

Assignment in NMR Spectra	H1	H2	H3	H4	H5	a	b	c	d	e	f	g	D_2O	TSP
Chemical shift (ppm)	3.67	3.33	2.33	2.04	1.75	*	*	3.90	7.78	1.15	*	*	4.84	0.00

* NMR peak masked by polyvinylpyrrolidone peaks

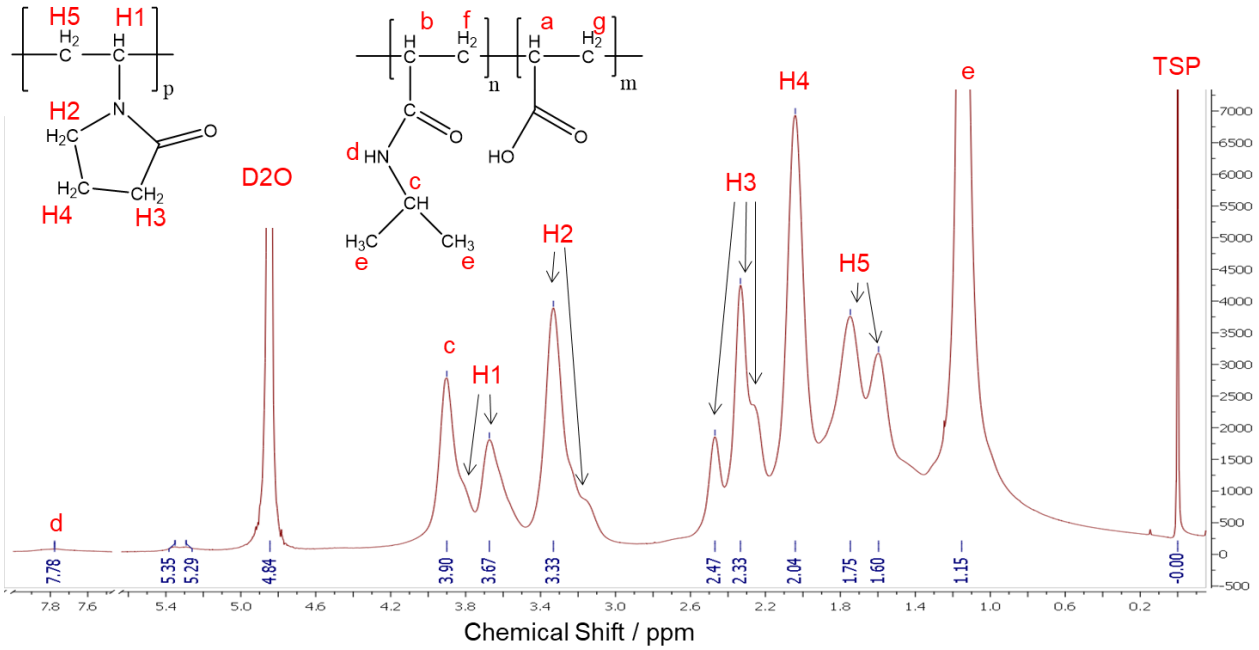

Figure A.1 Assignment of NMR chemical shifts of polyNIPAM-co-acrylic acid nanogels stabilised with 55K PVP. AcA-1.5-55K dispersed at 30 mg ml^{-1} in D_20 containing TSP (Trimethylsilylpropanoic acid) as an internal reference.

Table A.2 Photographs (digital images) of AcA-5.0-55K dispersed at 350 mg ml^{-1} in phosphate buffered saline at different temperatures.

Temperature		
25 °C	35 °C	60 °C
Phase		
Gel	Gel	Aggregate
		

2.6. References

1 S. Kempe and K. Mäder, *J. Control. Release*, 2012, **161**, 668–679.

2 Z. Gu, A. a Aimetti, Q. Wang, T. T. Dang, Y. Zhang, O. Veiseh, H. Cheng, R. S. Langer and D. G. Anderson, *ACS Nano*, 2013, **7**, 4194–201.

3 D. R. Griffin, W. M. Weaver, P. O. Scumpia, D. Di Carlo and T. Segura, *Nat. Mater.*, 2015, **14**.

4 M. A. Pulickal, S. Uthaman, C.-S. Cho and I.-K. Park, in *Nanogels for Biomedical Applications*, eds. A. Vashist, A. K. Kaushik, S. Ahmad and M. Nair, The Royal Society of Chemistry, London, 2018, pp. 181–203.

5 E. Sharmin, in *Nanogels for Biomedical Applications*, eds. A. Vashist, A. K. Kaushik, S. Ahmad and M. Nair, The Royal Society of Chemistry, London, 1st edn., 2018, pp. 29–49.

6 R. Pelton, *Adv. Colloid Interface Sci.*, 2000, **85**, 1–33.

7 P. C. Naha, K. Bhattacharya, T. Tenuta, K. A. Dawson, I. Lynch, A. Gracia, F. M. Lyng and H. J. Byrne, *Toxicol. Lett.*, 2010, **198**, 134–143.

8 M. A. Cooperstein and H. E. Canavan, *Biointerphases*, 2013, **8**, 19.

9 W. Xiong, X. Gao, Y. Zhao, H. Xu and X. Yang, *Colloids Surf. B.*

Biointerfaces, 2011, **84**, 103–10.

10 B. R. Saunders, N. Laajam, E. Daly, S. Teow, X. Hu and R. Stepto, *Adv. Colloid Interface Sci.*, 2009, **147**–**148**, 251–262.

11 J. F. J. Dippy, S. R. . Hughes and A. Rozanski, *J. Chem. Soc.*, 1959, 2492–2498.

12 N. Al-manasir, S. Fanaian, K. Zhu, B. Nyström, G. Karlsson and A. Kjøniksen, *J. Phys. Chem. B*, 2009, **113**, 11115–11123.

13 J. Zhou, G. Wang, L. Zou, L. Tang, M. Marquez and Z. Hu, *Biomacromolecules*, 2008, **9**, 142–148.

14 E. Ruel-Gariépy and J. C. Leroux, *Eur. J. Pharm. Biopharm.*, 2004, **58**, 409–426.

15 C. K. Han and Y. H. Bae, *Polymer (Guildf).*, 1998, **39**, 2809–2814.

16 Q. Wang, Y. Zhao, Y. Yang and H. Xu, *Colloid Polym. Sci.*, 2007, **285**, 515–521.

17 G. Zhou, Y. Zhao, J. Hu, L. Shen, W. Liu and X. Yang, *React. Funct. Polym.*, 2013, **73**, 1537–1543.

18 C. G. de Kruif, E. M. F. van Iersel, A. Vrij and B. W. Russel, *J. Chem. Phys.*, 1985, **83**, 4717–4725.

19 D. M. Öle Kiminta and P. F. Luckham, *Polymer (Guildf).*, 1995, **36**, 4827–4831.

20 V. Wintgens and C. Amiel, *Macromol. Chem. Phys.*, 2008, **209**, 1553–1563.

21 L. Wu, H. Zhou, H.-J. Sun, Y. Zhao, X. Yang, S. Z. D. Cheng and G. Yang, *Biomacromolecules*, 2013, **14**, 1078–1084.

22 M. Rasmusson, A. Routh and B. Vincent, *Langmuir*, 2004, **20**, 3536–3542.

23 D. Saville, W. Russel and W. Schowalter, *Colloidal Dispersions*, Cambridge University Press, 1991.

24 Q. Wang, H. Xu, X. Yang and Y. Yang, *Int. J. Pharm.*, 2008, **361**, 189–193.

25 B. R. Saunders and B. Vincent, *Adv. Colloid Interface Sci.*, 1999, **80**, 1–25.

26 S. Chen, J. Long and Y. Dan, *J. Appl. Polym. Sci.*, 2011, **121**, 3322–3331.

27 S. Minami, T. Watanabe, D. Suzuki and K. Urayama, *Polym. J.*, 2016, **48**, 1079–1086.

28 Q. Wang, L. Wang, M. S. Detamore and C. Berkland, *Adv. Mater.*, 2008, **20**, 236–239.

29 D. Go, T. E. Kodger, J. Sprakel and A. Kuehne, *Soft Matter*, 2014, **10**, 8060–8065.

30 H. Wang, M. B. Hansen, D. W. P. M. Löwik, J. C. M. Van Hest, Y. Li, J. a. Jansen and S. C. G. Leeuwenburgh, *Adv. Mater.*, 2011, **23**, 119–124.

31 E. C. Cho, J. Kim, A. Ferna and D. A. Weitz, *Nano Lett.*, 2008, **8**, 168–172.

32 H. Hathaway, D. R. Alves, J. Bean, P. P. Esteban, K. Ouadi, J. Mark Sutton and A. T. A. Jenkins, *Eur. J. Pharm. Biopharm.*, 2015, **96**, 437–441.

33 H. K. Hall, *J. Am. Chem. Soc.*, 1957, **79**, 5441–5444.

34 G. Huang, J. Gao, Z. Hu, J. V St. John, B. C. Ponder and D. Moro, *J. Control. Release*, 2004, **94**, 303–311.

35 A. Lee, H.-Y. Tsai and M. Z. Yates, *Langmuir*, 2010, **26**, 18055–18060.

36 R. Mohsen, G. J. Vine, N. Majcen, B. D. Alexander and M. J. Snowden, *Colloids Surfaces A Physicochem. Eng. Asp.*, 2013, **428**, 53–59.

37 M. Snowden, J. Morgan, B. Vincent, UK Patent No. GB2262117A, 1993.

38 A. L. Kjøniksen, M. T. Calejo, K. Zhu, A. M. S. Cardoso, M. C. P. De Lima, A. S. Jurado, B. Nyström and S. A. Sande, *J. Pharm. Sci.*, 2014, **103**, 227–234.

39 B. Jeong and A. Gutowska, *Trends Biotechnol.*, 2002, **20**, 305–311.

40 H. Kranz and R. Bodmeier, *Int. J. Pharm.*, 2007, **332**, 107–114.

41 W. McPhee, K. C. Tam and R. Pelton, *J. Colloid Interface Sci.*, 1993, **156**, 24–30.

42 V. Bühler, *Polyvinylpyrrolidone excipients for pharmaceuticals: povidone, crospovidone and copovidone.*, Springer Berlin Heidelberg Ne, Wachenheim, 1st edn., 2005.

43 B. Nair, *Int. J. Toxicol.*, 1998, **17**, 95–130.

44 K. M. Koczkur, S. Mourdikoudis, L. Polavarapu and S. E. Skrabalak, *Dalt. Trans.*, 2015, **44**, 17883–17905.

45 H. Tsai, PhD Thesis, University of Rochester, 2013.

46 A. J. Paine, W. Luymes and J. McNulty, *Macromolecules*, 1990, **23**, 3104–3109.

47 S. Tsuneyuki, *J. Macromol. Sci. Part A*, 1979, **13**, 751–766.

48 D. Horák and P. Shapoval, *J. Polym. Sci. Part A Polym. Chem.*, 2000, **38**, 3855–3863.

49 M. J. Murray and M. J. Snowden, *Adv. Colloid Interface Sci.*, 1995, **54**, 73–91.

50 S. Kawaguchi and K. Ito, in *Advances in Polymer Science*, Springer-Verlag Berlin Heidelberg, 2005, vol. 175, pp. 299–328.

51 S. Shen, E. Sudol and M. El-Aasser, *J. Polym. Sci. Part A Polym. Chem.*, 1993, **31**, 1393–1402.

52 H. Dalmont, O. Pinprayoon and B. R. Saunders, *Langmuir*, 2008, **24**, 2834–2840.

53 K. S. Soppimath, D. C. W. Tan and Y. Y. Yang, *Adv. Mater.*, 2005, **17**, 318–323.

54 J. Li, P. Angsantikul, W. Liu, B. Esteban-Fernández de Ávila, S. Thamphiwatana, M. Xu, E. Sandraz, X. Wang, J. Delezuk, W. Gao, L. Zhang and J. Wang, *Angew. Chemie - Int. Ed.*, 2017, **56**, 2156–2161.

55 C. Ramkissoon-Ganorkar, F. Liu, M. Baudys and S. W. Kim, *J. Control. Release*, 1999, **59**, 287–298.

56 W. Liu, H. Chen, Y. Zhou, Y. Huang, H. Liu and Y. Hu, *J. Dispers. Sci.*

Technol., 2009, **30**, 1281–1287.

57 S. I. Yusa, K. Fukuda, T. Yamamoto, Y. Iwasaki, A. Watanabe, K. Akiyoshi and Y. Morishima, *Langmuir*, 2007, **23**, 12842–12848.

58 Z. Zhang, S. Maji, A. B. D. F. Antunes, R. De Rycke, Q. Zhang, R. Hoogenboom and B. G. De Geest, *Chem. Mater.*, 2013, **25**, 4297–4303.

59 S. Nayak, H. Lee, J. Chmielewski and L. A. Lyon, *J. Am. Chem. Soc.*, 2004, **126**, 10258–10259.

60 R. H. Pelton, H. M. Pelton, a. Morphesis and R. L. Rowell, *Langmuir*, 1989, **5**, 816–818.

61 C. Scherzinger, A. Schwarz, A. Bardow, K. Leonhard and W. Richtering, *Curr. Opin. Colloid Interface Sci.*, 2014, **19**, 84–94.

62 S. Bhattacharjee, *J. Control. Release*, 2016, **235**, 337–351.

63 K. F. Tjipangandjara and P. Somasundaran, *Adv. Powder Technol.*, 1992, **3**, 119–127.

64 S. E. Creager and J. Clarke, *Langmuir*, 1994, **10**, 3675–3683.

65 R. McGlone and A. Bodenham, *Arch Emerg Med*, 1990, **7**, 65–68.

66 M. Annaka, K. Motokawa, S. Sasaki, T. Nakahira, H. Kawasaki, H. Maeda and Y. Tominaga, *J. Chem. Phys.*, 2000, **113**, 5980–5985.

67 R. H. Pelton and P. Chibante, *Colloids and Surfaces*, 1986, **20**, 247–256.

68 S. Chen, X. Jiang and L. Sun, *J. Appl. Polym. Sci.*, 2013, **130**, 1164–1171.

69 B. Götzelmann, R. Evans and S. Dietrich, *Phys. Rev. E - Stat. Physics, Plasmas, Fluids, Relat. Interdiscip. Top.*, 1998, **57**, 6785–6800.

70 N. L. McFarlane, N. J. Wagner, E. W. Kaler and M. L. Lynch, *Langmuir*, 2010, **26**, 13823–13830.

71 F. Csempesz and S. Rohrsetzer, *Colloids and Surfaces*, 1988, **31**, 215–230.

72 B. Jeong, Y. H. Bae and S. W. Kim, *Macromolecules*, 1999, **32**, 7064–7069.

Chapter 3

Dual-Stimuli Responsive Injectable Nanogel Based In Situ Forming Implant Development

Publications arising from this chapter:

"Dual-stimuli responsive injectable microgel/solid drug nanoparticle nanocomposites for release of poorly soluble drugs."

A. R. Town, M. Giardiello, R. Gurjar, M. Siccardi, M. E. Briggs, R. Akhtar, T. O. McDonald

Nanoscale, 2017, **9**, 6302–6314

3.1. Introduction

Chapter 2 demonstrated that polyNIPAM nanogels in the form of a concentrated dispersion displayed dual-stimuli responsive behaviour. These dispersions formed shape persistent bulk aggregates in the presence of both salt (at physiological ionic strength) and at body temperature (above the lower critical solution temperature of the polymer); such materials could potentially act as a controlled drug delivery depot. This responsive property of the nanogels represented an attractive opportunity for use as an ISFI.

3.1.1. *In Vitro* Release Experiments

In order to assess the drug release behaviour of a depot, in terms of whether burst release occurs, and sustained release is achieved, the amount of drug released from the depot over time must be quantified to obtain a drug release profile. Drug release is usually studied *in vitro* before progressing to *in vivo* studies. '*In vitro'* refers to drug release testing of a parental formulation into a release medium.[1] There are currently no regulatory guidelines for measuring drug release from parenteral controlled drug delivery systems,[2] with different experimental techniques suiting different materials and formulations of ISFI's. In terms of *in vitro* release, this can include pumps, agitation and stirring, release through a dialysis membrane, complete or partial replacement of the release media, and release into agarose gel.[3–6] *In vitro* drug release experiments can be broadly categorised into sample and separate, continuous flow, and dialysis based methods.[7] For implant based drug delivery systems, implants are usually placed in glass vials, and the surrounding release media is sampled,[8] falling into the sample and separate methodology category. One downside of this *in vitro* method is the lack of accountability for tissue inflammation response at the implant site on the drug release rate,[9] and so variation can exist between *in vitro* and *in vivo* drug release rate. Olanoff and Anderson showed that an implant can be surrounded by a fibrous capsule of collagen fibrils,[10] and so an *in vivo* release rate study was required to develop a pharmacokinetic model to describe plasma concentration of drug.[11] As polyNIPAM nanogels have previously been shown to be susceptible to protein absorption on their surface, this could be a factor which influences the drug release *in-vitro-in-vivo* correlation.[12] However, generally, if an *in vitro* experiment is designed

suitably there should be an *in-vitro-in-vivo* correlation.[8] Using a typical example of a release experiment, by Hyun *et al*., depot material was incubated at 37 °C for 1 hr to form solid depot material, and then release media was sampled from the vial over time.[13] This sampling technique is appropriate to the behaviour of the polyNIPAM nanogels in Chapter 2, which formed a single shape persistent aggregate in a glass vial when incubated at 37 °C. In this variation of the sample and separate methodology, release media could easily be sampled from around a cylindrical shape persistent polyNIPAM aggregate depot, and the technique is hence the most suitable for *in vitro* drug release quantification from this material.

3.1.2. Quantification of Drug Release Using High Performance Liquid Chromatography

To quantify the amount of drug release from a parenteral formulation into release media in an *in vitro* release experiment high performance liquid chromatography (HPLC) is widely used.[4,14,15] This technique can separate the analyte of interest (the drug payload) from any other material released by the depot, to quantify the drug release.[16] It is also able to accurately quantify low concentrations of drug.[17] This gives HPLC important advantages over another quantification technique, UV-Vis spectrophotometry, despite being more time consuming and less economical to perform.[18]

HPLC analysis also has other benefits. In some depots, the drug may not be fully stable. This could simply be due to the drug degrading when held in an aqueous environment at 37 °C for an extended period of time,[19] or due to the modification of the drug by the depot materials.[2] For example, in certain implantable gels, degradation of the gel in the drug release time frame causes a drop in pH which can degrade the drug payload.[20] This degradation can be monitored using HPLC. Where a drug starts to degrade, the degradation product will often appear as a new chromatogram peak at different retention times specific to the drug under analysis and HPLC methodology employed.[21]

3.1.3. Drug Release Profile

Through sampling release media at appropriate intervals, and quantifying release with HPLC, a drug release profile can be created. The drug release profile provides insight into drug release from a depot. First of all it can be used to assess the performance of the ISFI, for example by indicating if a burst release occurs.[22] The 'burst release' from an implant is when a significant percentage of total drug is released over a short time period at the start of the release period (c.a. 24 hrs), and is often seen in drug implants, preventing them from being safe to use.[23,24] The drug release profile also reveals whether sustained release of drug over a long period is achieved, and allow the determination of the rate of this release.[25] Also if a depot fails structurally, for example breaking into smaller fragments of larger surface area, fluctuations in the release profile are seen.[26] Mathematical release models have been fitted to release profiles to determine the kinetics of release, and the mechanism by which release occurs, to gain a deeper understanding of the way drug release occurs from the depot.[27,28]

3.1.4. Mathematically Modelling Drug Release

In order to understand the drug release profile from polyNIPAM nanogels, the models of drug release from other drug depots must be considered. When a drug delivery depot consists of a drug which is dispersed through a polymer network, this network is referred to as a matrix. The main mechanism for drug release from a matrix is via diffusion of the drug through this polymer network, assuming this rather than partitioning into the surrounding aqueous environment it the limiting factor.[27] Drug diffusion occurs as there is random movement of drug from high concentration in the depot to low concentration at the surface of the depot where drug partitioning into the surrounding medium occurs.[29] Many physical and chemical phenomena can affect the drug release kinetics, and provide alternative mechanisms to diffusion for release through a matrix type system, giving a complex model for drug release.[26] In the case of aggregated polyNIPAM nanogels, a non-biodegradable and non swellable matrix is formed. Hence the physical properties and dimensions of the matrix are likely to remain constant over time, and so the release rate can be simplified to a diffusion controlled model, based on Fick's second law of diffusion, as erosion, degradation and swelling based release will not occur.[28] The Higuchi mathematical model was

developed to describe this drug release, based on Fick's second law of diffusion, where drug is dispersed through a matrix.[30,31] This describes the amount of drug released in time (t) per unit area (Q) in relation to unit area (A), the diffusivity of the drug molecules in the matrix (D), initial drug concentration (C), drug solubility in the matrix media (Cs) in equation (1).

$$\boldsymbol{Q = A\sqrt{D(2C - 2Cs)Cs.t}} \qquad (\mathbf{1})$$

A very simple equation (2) was later derived from the Ritger-Peppas mathematical model.[32]

$$\boldsymbol{F_t = kt^n} \qquad (\mathbf{2})$$

The fraction of total drug released (F_t), is given by the diffusional exponent (n) and the constant (k), at time (t). The constant (k) is dependent on the characteristics of the matrix and drug. When n = 0.5, the release is Fickian, giving a simplified equation to represent the mathematics of Higuchi release. The equation accurately models release from non-swellable matrix devices, including cylinders, for the first 60% of the release curve, and even when near-perfect sink conditions are not obtained.[33] Equation (1) was previously applied to drug release from a depot formed through thermo gelation of chitosan nanoparticles, demonstrating Fickian diffusion based release to occur.[34] Fickian diffusion was also shown to control the release from a swollen gel consisting of polyNIPAM nanogels.[35] As such, this equation should be well suited to modelling the drug release behaviour of the cylindrical polyNIPAM nanogel aggregates, and give insight into how drug is released from polyNIPAM nanogel aggregates.

3.1.5. Drug Payload

With over 60% of new drug candidates estimated to be poorly water soluble,[36] there is a need for an ISFI that can deliver poorly soluble drugs over an extended period of time at a greater rate of dissolution than is permitted by the very low solubility of hydrophobic drugs, which are often crystalline in nature.[12,37] One way to increase the rate of dissolution of poorly water soluble drugs is to nanoformulate the drug into solid drug nanoparticles (SDNs).[38–42] SDN's have an increased surface area,[43] and amorphous nature,[44] aiding the rate of dissolution. They are also able to form a nanosuspension, where drug can exist at a much higher concentration in a liquid than in the free drug from.[45]

Poorly water soluble drugs have also been shown to have a slower release rate from a hydrophobic matrix than more water soluble drug.[46] Poorly water soluble drugs also favour the hydrophobic environment of polyNIPAM nanogels at physiological temperature.[47] Hence, by varying the hydrophobicity of a drug release matrix the rate of release of a drug is likely tuneable. PolyNIPAM becomes less hydrated and more hydrophobic in character above its LCST, expelling water from its polymer network in nanogel form, which has been shown to encourage the absorption (and hence retention) of hydrophobic species.[12,48] A comonomer which remains hydrophilic at 37 °C such as allylamine,[49] would give a polyNIPAM nanogel with a less hydrophobic character above it's LCST,[50] therefore a greater release rate of hydrophobic drug would be expected.

3.1.6. Cytotoxicity

PolyNIPAM has been widely used as a potential biomaterial for drug delivery and has been shown not to display cytotoxic properties in numerous studies including polyNIPAM in nanogel form.[51–53] Additionally, Kjøniksen *et al* have revealed that even at a high concentration polyNIPAM nanogels are not cytotoxic,[54] which is important when they are used in aggregated form. One important consideration for polyNIPAM nanogels is the incorporation of charged comonomers and their potential cytotoxicity. Surface charge can have a cytotoxic effect, depending on charge type and density,[55] and so cytotoxicity of nanogels should be studied where charged comonomers are included, by assessing if charge has an effect on cell plasma-membrane integrity or causes mitochondrial damage.[56]

3.1.7. Chapter Aims

In order to progress the polyNIPAM nanogel ISFI concept further, research can be grouped into three key areas; (i) understanding the aggregation process and formation of an implant, (ii) characterising the structure of the aggregate and (iii) investigating the relationship between the structure of the aggregate and drug release behaviour. It is also important to acknowledge that during development, ISFIs developed previously in other studies have suffered from a number of issues. For example a large burst release of drug is very prevalent in ISFI's.[57] There are also others issues which have been encountered which should also be accounted for and investigated; these include

the long-term stability of drug within the implant,[20] mechanical stability of the implant,[58] injectability issues,[59,60] variation in the shape of the implant formed, which leads to a variation in the amount of drug released,[2] as well as potential cytotoxicity of the depot.[9,61] All of these potential issues can be tested as part of the development of the polyNIPAM nanogel responsive aggregation ISFI concept.

The main aim of this chapter is to demonstrate the suitability of polyNIPAM nanogels to act as a dual stimuli responsive ISFI for the delivery of poorly water soluble drug loaded in the from solid drug nanoparticles (SDNs), (scheme 3.1).

In doing so the following five objectives will be achieved:

- Synthesise and characterise two species of nanogels to act as ISFI depot biomaterials, one of which will include allylamine comonomer.
- Test the aggregation behaviour, injectability, and depot formation and structure.
- Demonstrate the tuneable release rate of drug when different ratios of the two nanogel species are used to tune the hydrophilicity of the depot.
- Investigate and explain release rates and burst release from depots containing free drug in powdered crystalline form and its solid drug nanoparticle form. This will include the application of a drug release model to the drug release data to explain the mechanism of release, and probing burst release with polystyrene particles.
- Perform initial cytotoxicity study on the nanogels, to indicate any cytotoxicity issues which may need further investigation.

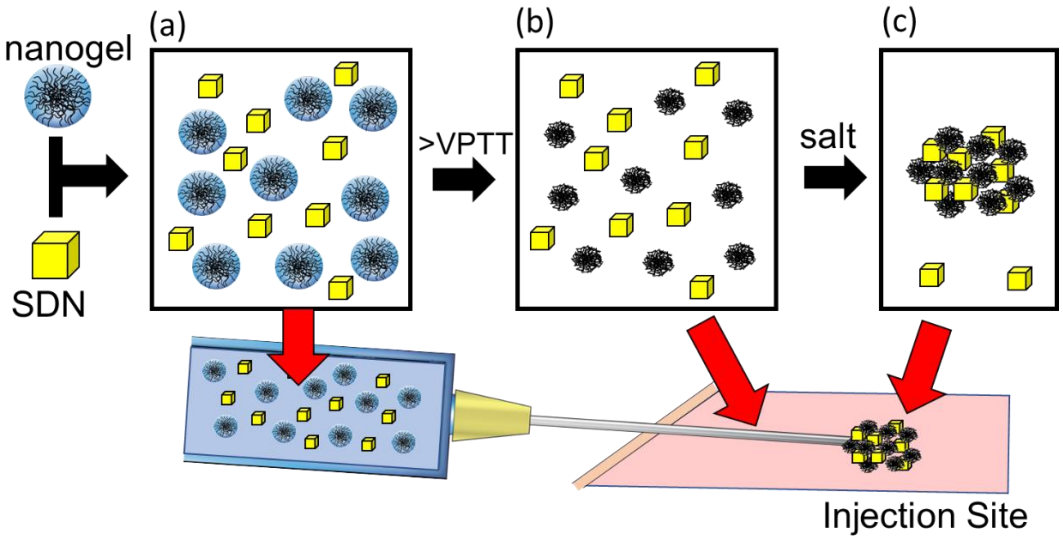

Scheme 3.1 Nanogel/solid drug nanoparticle composite ISFI system (a) Nanogel/SDN solution loaded into syringe (b) De-swelling of nanogel particles in hypodermic needle above VPTT (c) Aggregation of nanogel particles entrapping SDNs at depot site, due to contact with salt.

3.2. Results and Discussion

3.2.1. Nanogel Synthesis and Characterisation

Two species of polyNIPAM nanogels were synthesised using precipitation polymerisation (surfactant/stabiliser free). In chapter 2 nanogels synthesised with and without SDS both proved adequate for triggered aggregation. Therefore SDS was not used in the synthesis of these nanogels as unbound SDS is potentially cytotoxic, and so functional nanogels synthesised without SDS have less potential to be cytotoxic. These consisted of a polyNIPAM (PNA-00), and polyNIPAM-co-allylamine (PNA-25) samples, in which 25 mol% allylamine comonomer as a mol% of all reactants was used in the synthesis, (table M.3.1, methods section). These nanogels were then characterised using dynamic light scattering (DLS), scanning electron microscopy (SEM), Fourier transform infrared spectroscopy (FTIR), ^{1}H NMR and potentiometric titration. As in section 2.4, chapter 2, PNA-00 nanogels were synthesised using a concentration at the limit which allows the production of surfactant free polyNIPAM nanogels with a narrow dispersity to be produced (~0.5% w/v);[62] in this case 5.8 mg ml^{-1}. Reasonably narrow polydispersity particles, (mean hydrodynamic diameter = 567 nm, PdI = 0.24 at 25 °C) were produced, (figure 3.1 a)). When the charged comonomer allylamine was introduced at 25 mol% the concentration of NIPAM in the synthesis could be increased to 25.0 mg ml^{-1} whilst

still obtaining monodisperse particles of a similar size, as in PNA-25 (mean hydrodynamic diameter = 547 nm, PdI = 0.11 at 25 °C) (figure 3.1, b). This was attributed to the amount of allylamine comonomer used in the synthesis being able to provide electrostatic stabilisation of the precursor particles, preventing aggregation when the concentration of particles during synthesis is increased, as explored in Chapter 2, section 2.3, (25 mol% PNA-25 equals 15 wt% of allylamine for comparison). SEM images show that discrete monodisperse particles were formed for both nanogel samples PNA-00 and PNA-25, with a diameter corresponding to the hydrodynamic diameter of the particles above the VPTT measured via DLS (approximately 250 nm).

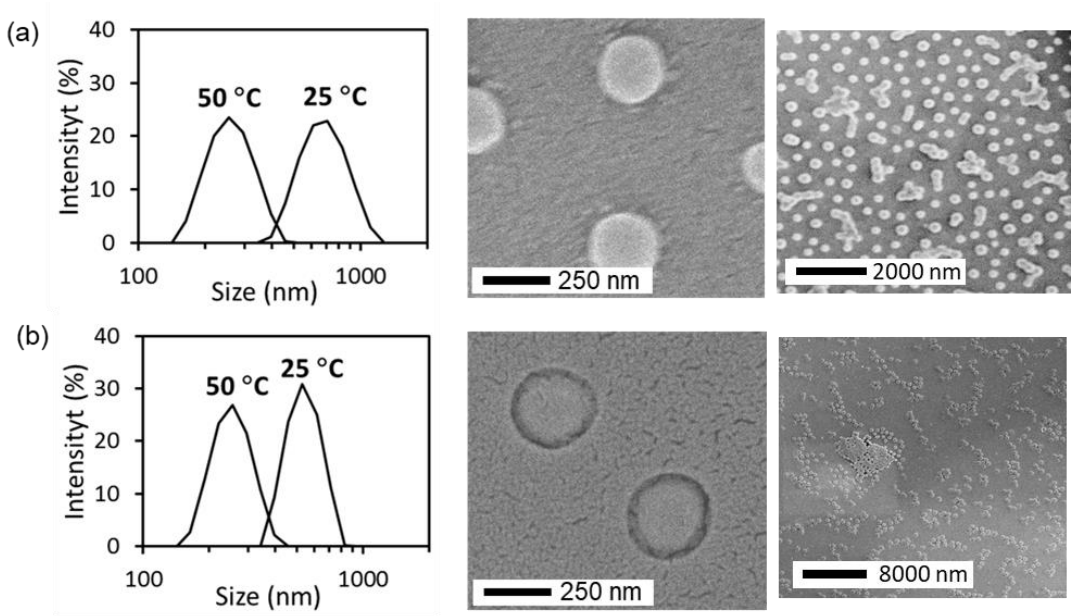

Figure 3.1 Characterisation of (a) PNA-00 and (b) PNA-25 nanogels by SEM, and DLS. (left column) DLS size distribution by intensity at 25 °C and 50 °C, samples measured using DLS with the mean value of triplicate measurements used and (middle and right column) SEM images of the dried nanogel particles with a beam intensity of 3.0 kV. All SEM images created using back scattered electrons with the exception of PNA-25 image with 250 nm scale bar, created with low angle back scattered electrons. Nanogels prepared as a 0.01 mg mL^{-1} aqueous dispersion for SEM imaging.

^{1}H NMR and FTIR spectra was consistent with previous nanogel characterisations, with all proton signals of polyNIPAM accounted for in PNA-00 and PNA-25, (figure 3.2), with a weak signal detected at 2.81 ppm for the CH_2 in the side group of the poly(allylamine) repeat unit in PNA-25.[63–65] NMR analysis also demonstrated that all unreacted monomers were removed during workup of the nanogels as no vinyl

peaks can be seen in the range 5.5-6.5 ppm. The FTIR spectra for the nanogels were found to match that of previously studied polyNIPAM nanogels, however there was no noticeable difference between the IR spectra for PNA-00 and PNA-25. This was likely because the mol% of comonomer allylamine incorporation was low, or due to overlap between the signals for the primary amines of the poly(allylamine) repeat unit with the signal from the amides contained in poly(N-isopropylacrylamide), (figure A.1, Appendix).[66] Due to the lack of clear signals to prove allylamine inclusion, potentiometric titration was used to quantify the number of ionisable amines present in the sample, as used in previous studies. Two equivalence points can be seen (figure 3.3, a).[67–69] The difference in volume of 0.1M NaOH between the equivalence points for HCl (140 µL) and allylamine (280 µL) was used to calculate the moles of allylamine contained in PNA-25, (figure 3.3, b). This suggests only 3.1 mol% allylamine was incorporated into the nanogel, concluding with FTIR and NMR results that only a low percentage of allylamine used in the synthesis is incorporated into PNA-25.

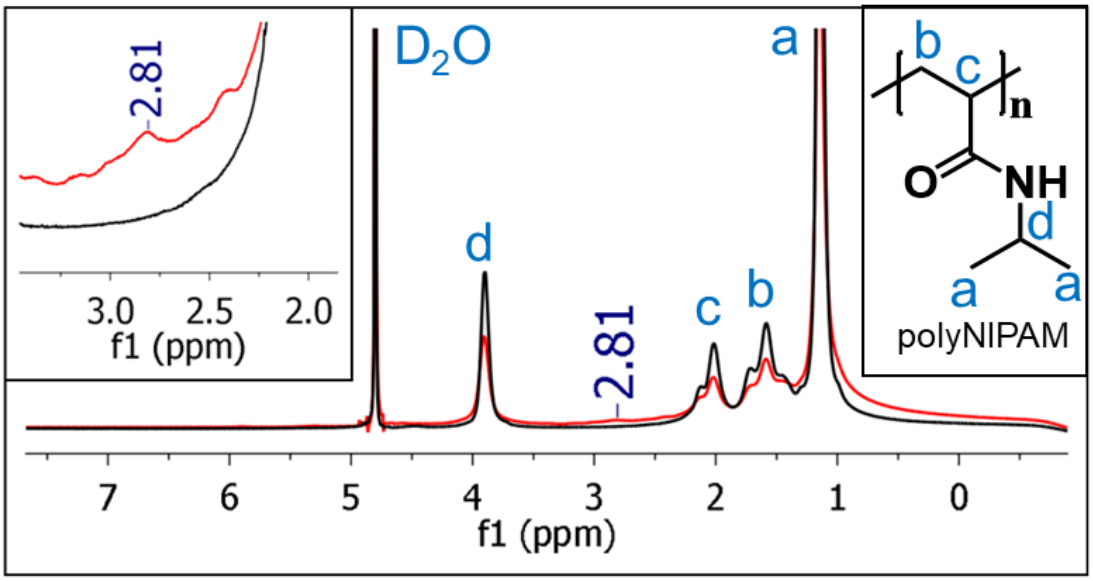

Figure 3.2 ^{1}H NMR Spectra of PNA-00 (black) and PNA-25 (red). Identification of polyNIPAM peaks in ^{1}H NMR spectra of PNA-00. Peak at 2.81 ppm indicates presence of allylamine comonomer due to NH_2 protons.

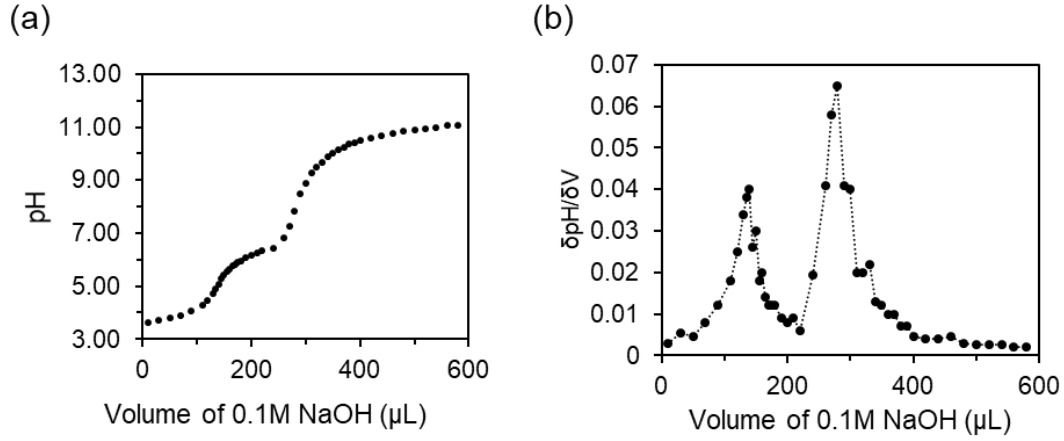

Figure 3.3 a) Potentiometric titration curve of PNA-25. Sample solution prepared by dispersing 50 mg of lyophilized nanogel into 50 mL of distilled water, followed by lowering sample pH to <pH4 with HCl. Sample titrated with 0.1M NaOH at 25 °C +/- 0.5 °C under a nitrogen atmosphere. b) Differential of titration curve, difference between two equivalence points used to calculate allylamine content in nanogel.

In order to investigate the dual-stimuli responsive properties of the nanogel samples, the hydrodynamic diameter of the nanogels were measured at intervals over the temperature range 15 to 55 °C for both PNA-00 and PNA-25. As PNA-00 was heated in water the particles de-swelled but remain colloidally stable, resulting in the dramatic decrease in hydrodynamic diameter at the VPTT, (figure 3.4, a), as first shown by Pelton *et al.*[70] In the presence of salts at physiological concentrations (PBS, 1X strength, pH 7.4) the particles flocculated as they reached the VPTT, indicated by the dramatic increase in hydrodynamic diameter beyond 32 °C.[71] The sample containing 25 mol% allylamine, (PNA-25), showed the same colloidal stability in water and triggered flocculation in PBS, (figure 3.4, b). The salt-responsive flocculation of the nanogels was also investigated with a range of NaCl concentrations. Previous work by Rasmusson *et al* has shown that polyNIPAM nanogels synthesised with BIS and a sulphate initiator flocculate in NaCl above a concentration of 0.025M when raising the temperature.[72] At a low NaCl concentration the interparticle electrostatic repulsion was great enough to prevent flocculation. At a higher concentration this electrostatic repulsion was weakened enough to allow flocculation. They also found that with increasing NaCl concentration the temperature of flocculation decreases as the higher ionic strength creates a poorer solvent environment for the polyNIPAM. PNA-00 and PNA-25 displayed a similar response in both respects, (table 3.1). The higher aggregation temperature of PNA-25 compared

to PNA-00 in 0.1 M NaCl suggests the extra electrostatic stabilisation from allylamine is able to resists aggregation to a greater extent. Analysis of the zeta potential of PNA-00 with increasing temperature in water displayed an initial negative zeta_potential of -12 mV up to 25 °C (figure 3.4, a), attributed to the KPS initiator providing a negative surface charge on the nanogels through its incorporation at the polymer chain ends. As the temperature increases above the VPTT the zeta potential shows a corresponding decrease to > -40 mV as the surface charge density increases with the decrease in particle surface area, and the chains ends collapse onto the surface. For sample PNA-25 the zeta potential was positive (figure 3.4, b), indicating successful incorporation of allylamine comonomer to give a cationic charge that counters the anionic charge of the chain ends. When the particles were heated above their VPTT the zeta potential increased as the reduction in size resulted in an increase in charge density.

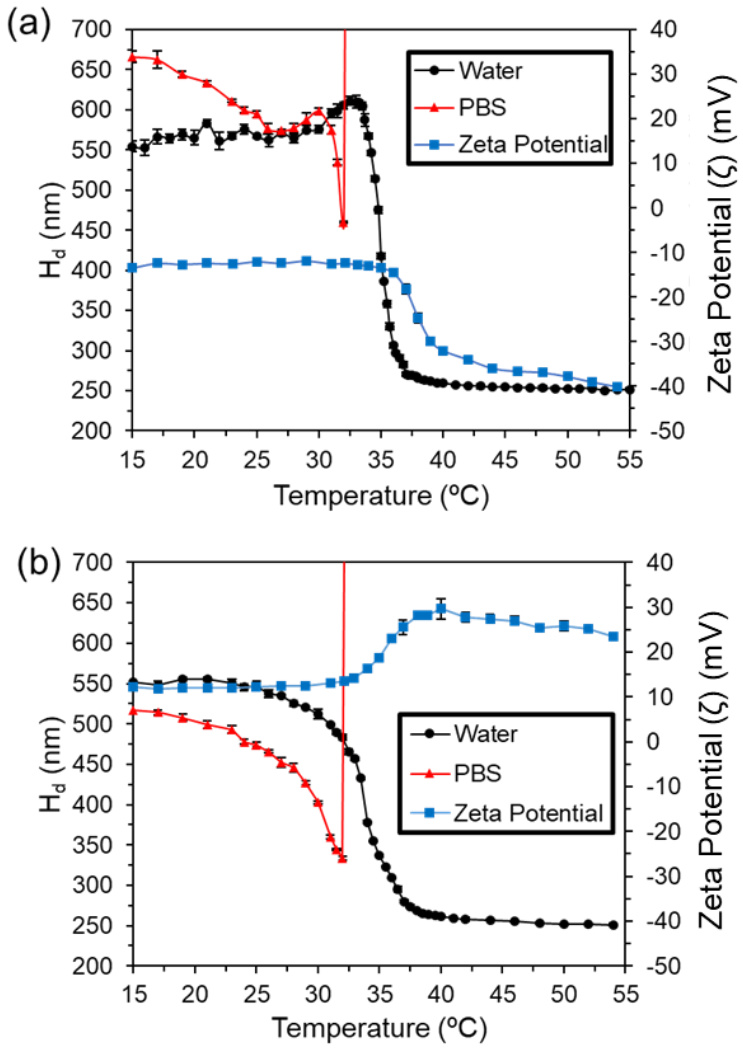

Figure 3.4 Temperature responsive behaviour of (a) PNA-00 and (b) PNA-25 nanogels by DLS and laser Doppler electrophoresis. DLS measurements performed on nanogels as 1 mg ml^{-1} nanogels dispersions in water and PBS. Zeta potential measurements performed on aqueous dispersion only at pH 7. Samples measured using DLS and LDE with the mean value of triplicate measurements used.

Table 3.1 Nanogel flocculation in NaCl

[NaCl] (M)	Aggregation Temperature (°C)[a]	
	PNA-00	PNA-25
0.001	-	-
0.010	-	-
0.100	34	42
1.000	24	24

[a]Samples heated in 1°C intervals from 15 to 55 °C. Flocculation temperature indicated by large increase in hydrodynamic diameter, as shown in Figure 3.3.

The two nanogels show temperature and salt responsive behaviour, with flocculation only occurring when both the temperature is above the VPTT and the ionic strength was equivalent to 0.1 M NaCl or greater. This is ideal for triggered aggregation in response to physiological conditions in an ISFI system.

3.2.2. PolyNIPAM Nanogel Aggregate Studies

Given the propensity for the nanogels to flocculate in a dilute dispersion, the concentration of the dispersion was increased to confirm that bulk aggregation on a macroscopic scale was possible, as demonstrated in chapter 2, section 2.4. The concentration (% (w/w)) of PNA-00 and PNA-25 in PBS at 25 °C was increased and studied *via* the tube inversion method until a gel was formed. The concentration required for a self-supporting gel was 6.24% (w/w) for PNA-25 and 14.90% (w/w) for PNA-00. These values were used to form swollen gels at 25 °C for aggregation studies. The lower % (w/w) of material required to form a gel with PNA-25 is postulated to be due to the polyampholytic nature of PNA-25. These nanogels contain both positive charge from allylamine, and negative charge from persulfate initiator, and so inter-particle electrostatic attraction could occur, in a similar manner to the electrostatic interactions which allow the formation of a colloidal gel network.[73,74] Hence a lower (% w/w) of PNA-25 was required to form a self-supporting gel in PBS than PNA-00. Upon heating to 37 °C both gels aggregate and expel solvent in the process. The nanogels formed a phase separated disc shape of aggregated material, due to the cylindrical shape of the vial used, (figure 3.5). The aggregated form of the nanogels was observed as the surface charge of the nanogel was not great enough to form a shrunken gel.[75]

The formation of aggregate over time was also studied, with samples contained in a glass vial slowly heated by being placed in an incubator at 37 °C, (figure 3.6), with both samples forming dense aggregates in approximately 90 minutes. This process was reversible, after being held at 37 °C for 1 hour and cooling, the aggregate returned to a self-supporting gel that re-adsorbed the expelled solvent within 1 hour.

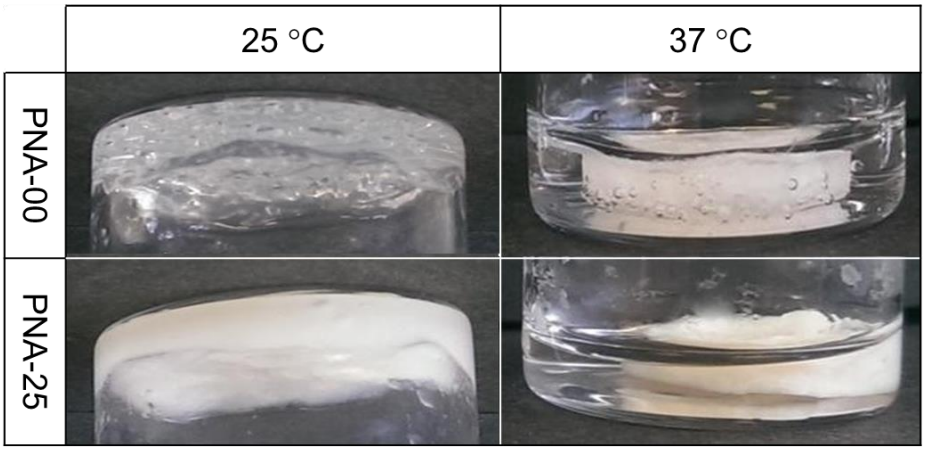

Figure 3.5 Images of dual-responsive transition of the nanogels in PBS (1X strength, pH 7.4); from swollen self-supporting gels to bulk aggregates. Nanogel samples as swollen gel (left) and bulk aggregate (right). PNA-00, 14.90% (w/w) (top) and PNA-25, 6.24% (w/w) (bottom).

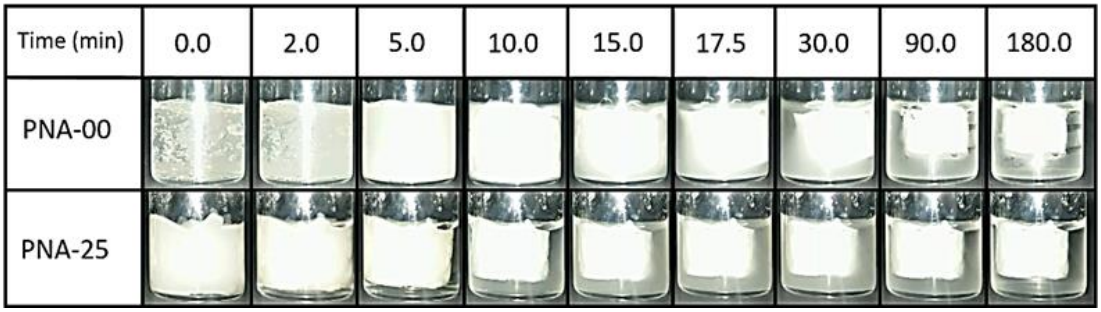

Figure 3.6 Images of nanogel aggregate formation from swollen gel over time. The swollen gel was formed in PBS using 14.90% (w/w) PNA-00 and 6.24% (w/w) PNA-25, and placed in an incubator at 37 °C. This meant the time taken to aggregate is in relation to the rate of heat transfer from the incubator, and so aggregation is more rapid when in direct contact with a heated fluid environment such as in figure 3.8.

The aggregate formed by PNA-25 has visibly larger dimensions than PNA-00, despite being formed from a swollen gel consisting of a lower mass of nanogel, (figure 3.6). This suggested the aggregate was less dense, as the PNA-25 sample contains hydrophilic allylamine comonomer which will resists complete expulsion of water above the VPTT as the aggregate forms. Hence the water content of PNA-00 and PNA-25 were measured both above and below the VPTT to confirm this, (table 3.2). Below the VPTT the water content of the samples were 85.1% and 93.8% for PNA-00 and PNA-25 respectively. The hydrophilic nature of allylamine is independent of temperature,[49] hence the sample containing allylamine, PNA-25, remained much more hydrophilic above the VPTT (at 37 °C) containing 76.8% w/w water while PNA-00 contained only 34.3% water. This difference in the water content of the aggregates was

reflected in the reduction in volume when the swollen gel forms an aggregate. As swollen gels at 25 °C PNA-00 and PNA-25 had the same initial starting volume, however, the volume of PNA-00 on forming an aggregate was smaller than PNA-25. This is reflected in a larger percentage reduction in volume than PNA-25 upon forming an aggregate. It's important to remember that PNA-00 also contains a higher % (w/w) of nanogel despite shrinking in volume by a greater percentage. This suggests the aggregate of PNA-25 contains a much greater volume of free space between aggregated nanogel particles.

Table 3.2 Water content of the nanogels at 25 °C and 37 °C and change in volume.

Sample	% (w/w) of water contained within the sample		% reduction in volume upon forming aggregate[a]
	25 °C	37 °C	
PNA-00	85.1	34.5	76
PNA-25	93.8	76.8	66

[a]The height and diameter of the cylindrical swollen gel and corresponding aggregate were used to calculate the change in volume (see figure 3.5 for images of the samples).

To give more insight into the difference in structure and porosity between the aggregates of PNA-00 and PNA-25 the aggregates were dried and imaged by SEM and are shown in (figure 3.7, A-B) respectively. SEM has previously been used to study the porosity of biomaterials,[74] and hence describe the greater burst release of a payload with increasing porosity.[23,76] The PNA-00 aggregate displayed a dense structure with a tendency to film-form while the PNA-25 aggregate presented a looser, fibrous structure in which individual particles could easily be distinguished. AFM analysis was then utilised to assess the topography of the samples, (figure 3.7, C and D for PNA-00 and PNA-25 respectively) these images revealed that PNA-25 presented a fibrous structure compared to the irregular structure of PNA-00. The differences in the topography of the samples are clearly shown in the 3D representation of the AFM characterisation, (figure 3.7, E) for PNA-00 and (figure 3.7, F) for PNA-25. The surface of the PNA-25 aggregate was much rougher than PNA-00 and revealed potential pores between the fibres. This fibrous structure of the PNA-25 aggregates was not expected and is an aspect for further investigation in the future.

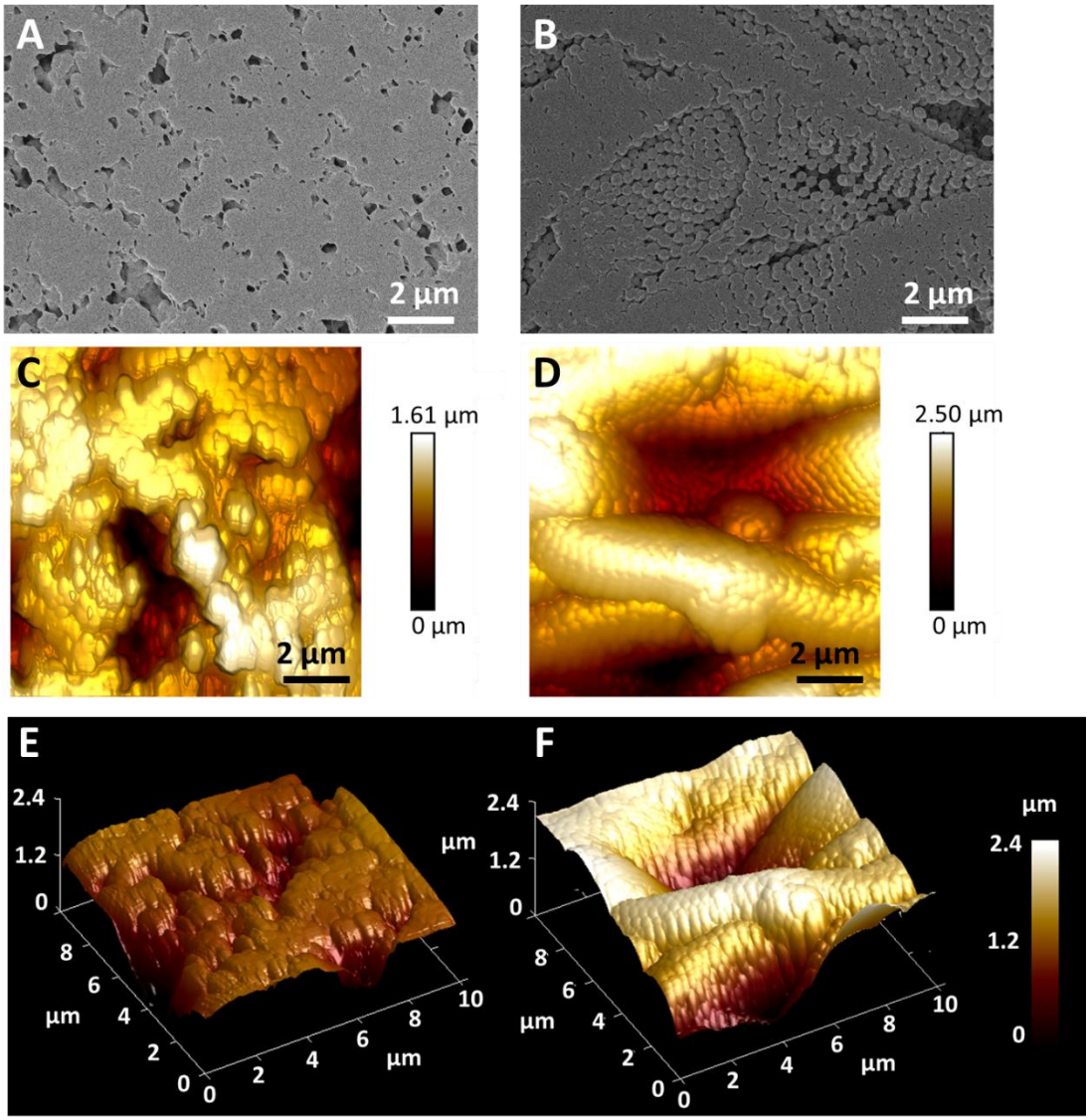

Figure 3.7 Characterisation of nanogel aggregates. (A,B) SEM images, (C,D) AFM images and (E,F) 3D representations of (C,D) respectively. PNA-00 shown in (A,C,E) and PNA-25 in (B,D,F). Aggregates formed at 14.90% (w/w) PNA-00 and 6.24% (w/w) PNA-25 in 1x strength PBS for imaging.[‡]

[‡] AFM imaging of samples (figure 3.6, E-F) was performed by Dr. Riaz Akhtar (Department of Mechanical, Materials and Aerospace Engineering, School of Engineering University of Liverpool, George Holt Building, Brownlow Hill, Liverpool, L69 3GH, UK).

The differences between the two aggregates explains the higher water content of PNA-25 due to its greater porosity and may alter the rate of drug release from the aggregates. The propensity for the nanogels to flocculate in response to both temperature and salt could be utilised to give a macroscopic aggregate at high nanogel concentrations. Potentially the porosity and relative hydrophilicity of an aggregate can also be tuned by mixing PNA-00 and PNA-25 due to their different water content and apparent structural differences in aggregated form.

We must also consider the fact that upon injection as an ISFI the swollen gel will be in contact with interstitial fluid, which contains the metal ions magnesium and calcium as part of a complex mixture of inorganic salts.[77] This inorganic salt composition can be simulated by Hank's balanced salt solution (HBSS). On moving from PBS to HBSS there is a slight decrease in ions with a more chaotropic nature (weakly hydrated) (i.e. K^+, Na^+), and the introduction of more kosmotropic ions (strongly hydrated) (i.e. Mg^{2+}, Ca^{2+}). Chaotropic ions accumulate at the polyNIPAM/water interface to increase the zeta potential of the nanogel,[78] and above the VPTT colloidal stability is dictated by electrostatic stabilisation in PNA-00 and PNA-25. Hence aggregation behaviour may change in different ion compositions. Therefore the aggregation of the nanogels was assessed in HBSS instead of PBS. Aggregation was found to occur in HBSS (figure A.2, Appendix) in a similar manner to the PBS studies and hence the different metal ions present in HBSS were not found to greatly affect the aggregation process.

3.2.3. Injection Studies

With the demonstration of the formation of an aggregate from a concentrated nanogel dispersion upon exposing it to physiological conditions, the suitability of injection into tissue was assessed. For this purpose agarose gel was utilised as a matrix which acts as a subcutaneous tissue mimic at 37 °C. Agarose gel has previously been utilised in UV imaging of drug diffusion as its transparency allows visual observations of drug diffusion through the agarose matrix.[79] Hence the depot shape and formation can be

easily observed. Agarose gel also resembles the macromolecular properties, rheological behaviour and water content of extracellular matrix.[80–83] Hence, it was employed in the injection studies of nanogel dispersions. The concentrated nanogel dispersion at ambient temperature was injected through a hypodermic needle into agarose gel formed using PBS at 37 °C. PolyNIPAM nanogels show shear thinning behaviour,[84] and so even at the concentration at which PNA-00 and PNA-25 form a swollen gel they could be injected through a 18G needle (0.84 mm internal diameter). This was 14.90% (w/w) for PNA-00 and 6.24% (w/w) for PNA-25. This was then followed by rapid aggregation of the particles into an aggregate depot. Additionally, depot formation was also possible with lower nanogel concentrations; PNA-00 was injected at 9.1% (w/w) and PNA-25 was injected as a liquid at 2.0% (w/w) and displayed the same aggregation behaviour as higher nanogel concentrations, (figure 3.8, a,b). The ability to obtain depot formation at lower concentrations is beneficial as a liquid is more desirable for ease of formulation with drug and loading into a syringe for as an ISFI.[61] The nanogel aggregate formed a planar depot that is most likely due to the fracturing of the agarose gel by the hypodermic needle, and the subsequent filling of the void by the nanogel outwards along the fault line.

The injection of the nanogel dispersion was further studied *ex vivo* into tissue to determine how this would affect depot shape. Intravitreal injection of drug is often used to treat the growing prevalence of conditions such as diabetic retinopathy[85] and age-related macular degeneration,[86] which effects 30% of individuals with diabetes,[87] and 25% of people over 75 respectively.[88] These intravital injections are performed by injecting drug in to the vitreous humour of the eye, which is a gel network of collagen fibres and glycoprotein. With the potential for this ISFI system to reduce injection frequency into the eye by providing long term release, porcine vitreous humour was used to demonstrate nanogel injection *ex vivo*. Vitreous also has the benefit of being optically transparent, to allows visual observation of the aggregation formation and shape. A 9.1% (w/w) dispersion of PNA-00 combined with Ponceau Red dye was injected into porcine vitreous at 37 °C, which led to the formation of a globular aggregate depot (figure 3.8, c). It is acknowledged that further exploration of injections

ex vivo in subcutaneous tissue is required to understand what shape an aggregate would form in at this type of injection site, and how much variation in this shape would exist.

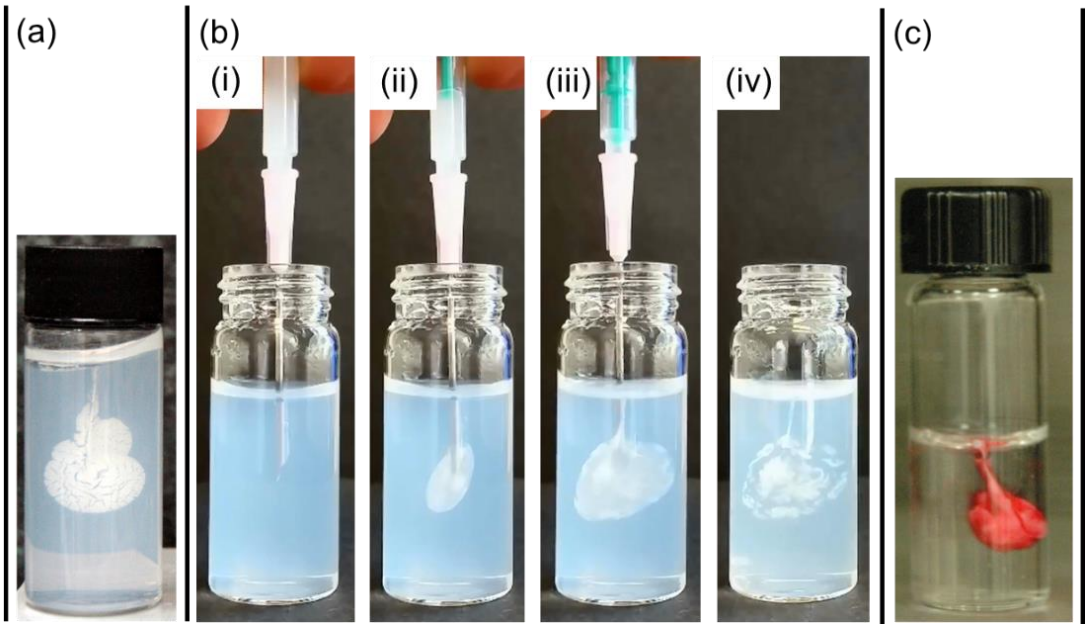

Figure 3.8 Digital images showing injection of PNA-25 and PNA-00 through 18G hypodermic needle: (a) PNA-00 at 9.1% (w/w) injection into 37 °C agarose gel. (b) PNA-25 at 2.0% (w/w) injection into 37 °C agarose gel, timepoints: (i) 0 (ii) 5 (iii) 12 and (iv) 19 seconds. (c) PNA-00 at 9.1% (w/w) combined with ponceau red dye injection into 37 °C porcine vitreous humour.[‡]

3.2.4. Model Payload Entrapment Study

An ISFI will ideally display no initial burst release, in our system as the nanogels come into contact with physiological strength medium and aggregate they should be able to rapidly entrap a payload of drug containing nanoparticles with high entrapment efficiency.[2] To probe this ability, Oil Red O dye-containing polystyrene (PS) nanoparticles were synthesised as a model payload which mimics the entrapment of solid drug nanoparticles. Like solid drug nanoparticles, Oil Red O dye-containing PS nanoparticles can form a suspension in water, and are a similar size, however the Oil

[‡] Porcine vitreous experimental work, (figure 3.7, c), was performed by Dr. Dinos Caserides (Eye and Vision Science, Institute of Ageing and Chronic Disease, William Henry Duncan Building, 6 West Derby Street, Liverpool, L7 8TX, UK).

Red O which is contained within the PS particles allows quantification of the amount of particles released using UV-Vis spectroscopy. Firstly, the PS particles were synthesised using adaptations from a previously published dispersion polymerisation method.[47] The PS nanoparticles were then dyed with the hydrophobic dye Oil Red O (OR), using adaptations from a previously published PS particle dying method which uses the solvent tetrahydrofuran to swell the particles and load dye.[48] Release could then be quantified at a wavelength of 580 nm, where there is negligible absorbance by any potential polyNIPAM fragments lost from the aggregate. These dye containing particles will be denoted as PS-OR. The PS colloids were characterised using DLS after synthesis and when dispersed into PBS as PS-OR after dying and lyophilisation (table 3.3). The slightly larger hydrodynamic diameter after dying can be accounted for by entrapment of dye. SEM images revealed that monodisperse particles with spherical morphology were synthesised, along with a second population of much smaller particles (Figure A.3, Appendix). The absorbance spectra of PS-OR particles was deconvoluted to form a calibration curve based on the Oil Red dye peak of the PS-OR particles, (Figure A.4, Appendix).[89] Nanocomposites containing PS-OR nanoparticles and PNA-25 nanogel were then prepared. With PNA-25 showing a less dense more porous structure in aggregate studies, this nanogel was considered more likely to fail to entrap a payload and show burst release, hence this nanogel was selected to form nanocomposites. PNA-25 was dispersed at 6.24% (w/w) in PBS to give a swollen gel and then PS-OR nanoparticles were mixed into the gel at 10, 20 and 40% (w/w) of the total mass of PS-OR nanoparticles and lyophilised mass of PNA-25. These samples remained as swollen self-supporting gels even with 40% (w/w) PS-OR nanoparticles loaded, (figure 3.9, a (i)). Upon heating to 37 °C to induce aggregation, the expelled solvent was visibly colourless, suggesting that PS-OR particles remained entrapped as a nanocomposite with the nanogel (figure 3.9, a (ii)). This burst release behaviour was quantified by UV-Vis to determine the concentration of PS-OR particles in the expelled liquid. This analysis showed low burst release (<13%) for all samples, but that increasing the concentration of PS-OR nanoparticles led to greater burst release, particularly from 20 to 40 % w/w loading, (figure 3.9, b). These data indicate the nanogels are able to retain the majority of a nanoscale payload distributed through the nanocomposite as it aggregates from a swollen gel. This is despite a

substantial volume of PBS being expelled from the polymer network of the contracting nanogel particles.

Table 3.3 Polystyrene nanoparticle properties

PS after synthesis		PS-OR dispersed in PBS	
H_d (nm)	PdI	H_d (nm)	PdI
802 ± 14	0.05 ± 0.03	821 ± 25	0.05 ± 0.04

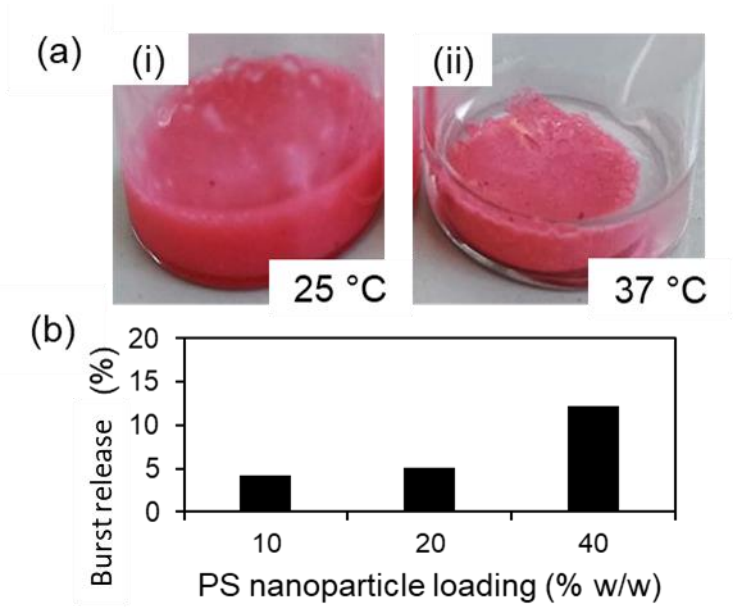

Figure 3.9 (a) (i) Swollen gel composite of 40% (w/w) PS-OR nanoparticle loaded into PNA-25 at 25 °C and (ii) Aggregation of composite at 37 °C with entrapment of PS-OR nanoparticles. (b) Percentage of total PS particles released 1 hour after aggregation of composite.

3.2.5. *In Vitro* Release Study

To test the release rate of a drug from the nanogel aggregates *in vitro*, formulations were created from the mixing of poorly water-soluble antiretroviral drug lopinavir (LPV) in its powder form, or solid drug nanoparticle (SDN) form, into swollen gels, (table 3.4).

Table 3.4 Formulations of nanogel-drug for ISFI's

Formulation	LPV (mg)	LPV SDN[a] (mg)	PNA-00 (mg)	PNA-25 (mg)	% (w/w) water[b]
Free SDN	-	44.4	-	-	-
PNA-25-SDN	-	44.4	-	66.6	76.8
PNA-00/25-SDN	-	44.4	87.5	33.3	56.4[c]
PNA-00-SDN	-	44.4	175.0	-	34.5
PNA-25-LPV	22.2	-	-	66.6	76.8

[a] LPV SDNs consist of 50% (w/w) LPV the remainder is 40% PVA and 10% Kolliphor TPGS.

[b] % (w/w) of water in aggregate at 37 °C.

[c] Calculated from: total amount of water contained in mass of each nanogel, and total mass of nanogel in formulation.

LPV is a potent HIV-specific protease inhibitor which is administered in combination with ritonavir as a booster and requires daily oral dosing for life.[90,91] We selected LPV as the model hydrophobic drug in our study given its very low aqueous solubility (predicted to be 0.00192 mg mL^{-1}) and on-going evaluation of LPV SDNs in clinical trial (clinicaltrials.gov reference NCT02631473) identifying it as a potentially commercially relevant payload. LPV also shows no degradation in an aqueous environment at 80 °C over extended periods, making it suitable for quantification via HPLC in our drug release study.[92] The LPV SDNs used had a hydrodynamic diameter of 330 nm and PdI of 0.18 (figure A.5, Appendix). The SDNs were composed of 50% (w/w) LPV, 40% PVA and 10% Kolliphor TPGS.[§]

An LPV drug calibration curve was created from the LPV HPLC chromatograms, which contained a single elution peak at a retention time of 7.1 minutes, allowing quantification of drug release within a linear working range of 0.24-15 μg ml^{-1} (figure A.6, Appendix). It was anticipated in the release study that LPV drug could be released into the release media in dissolved form, or still in the form of an SDN,

[§] LPV SDNs were synthesised in conjunction with Dr. Marco Giardiello, Department of Chemistry, University of Liverpool, Crown Street, Liverpool, L69 7ZD,UK.

especially in the case of burst release. Hence a known concentration of 50% (w/w) LPV SDN was analysed alongside a known concentration of LPV drug to verify LPV SDNs fully dissolved in the HPLC mobile phase (30% v/v aqueous acetonitrile) to ensure accurate quantification of the drug still in its SDN form was possible. No variation in the HPLC chromatograms of the two samples can be seen, and single LPV peak can be seen for both LPV and LPV SDN samples, (figure A.7, Appendix). As the concentration of LPV was made to the same value in LPV and LPV SDN samples, the ratio of the area under the SDN LPV HPLC elution peak ($\mathbf{I}_{SDN}$) to LPV drug standard ($\mathbf{I}_{LPV}$) should equate to 1 assuming LPV SDN completely dissolved in the mobile phase of the HPLC. The value determined from HPLC samples was 1.002 (i.e. 0.2% difference) confirming the SDNs fully dissolve in the mobile phase, (table A.1, Appendix). No degradation products were seen for LPV or LPV SDN in the HPLC chromatograms. This is expected as degradation peaks existed at lower retention time in previous studies which used a C18 column only when LPV underwent a forced degradation under strongly acidic and alkali conditions.[92,93]

In the ISFI formulations, nanogels were used at a concentration at which they formed a swollen gel, so that aggregated disk shaped samples formed upon heating, to simplify sampling release media in the release experiment, and eliminate the variation of aggregate shape having an effect on drug release rate (figure A.8., Appendix). Utilising the large difference in the water content and porosity of the PNA-00 and PNA-25 aggregated nanogel materials at 37 °C, (table 3.2), allows the two nanogel samples to be mixed in different ratios to tune the water content of the aggregate. We expected the water content and structure of the different aggregates to control the rate of release of drug. PNA-00 and PNA-25 were used together with a mass of each that gave a self-supporting gel at room temperature in 1 mL of PBS, and 56.4% (w/w) water in the aggregated form (denoted as PNA-00/25-SDN), giving an intermediate water content between that of the two nanogels when used separately. The release of drug into the PBS surrounding the nanogel/SDN nanocomposites was then measured over time, using HPLC. Due to the low saturation concentration of the drug, the release media was completely removed and replaced during the release experiment at each sample interval.[9] The nanocomposites showed excellent mechanical stability, remaining in their original shape over the complete release period. Comparing the release of LPV from the formulations PNA-25-SDN, PNA-00/25-SDN and PNA-00-SDN it can be seen that if the depot has a higher % (w/w) water content the release rate is enhanced, with PNA-25-SDN having the highest % (w/w) water content, and hence the greatest release rate and largest total cumulative release after 120 days,

(figure 3.10, a-b). The release rate and total cumulative release is reduced for PNA-00/25-SDN, and lowest for PNA-00-SDN, which has the lowest water content. This effectively allows us to tune the release rate from the depot. Based on the characterisation of the aggregate with SEM and AFM it is speculated that this could be due to the formation of a more porous structure containing more water, which has been linked with faster drug release.[54] We applied the Ritger-Peppas equation (equation (1), section 3.1.4) assuming Fickan release, (figure 3.10, c).[94] This suggests that for PNA-25-SDN and PNA-00/ 25-SDN there are two phases of release (**I** and **II**). In phase **I** the porosity introduced by PNA-25 could allow SDNs to be released from the aggregate, giving a much larger dissolution constant than the other formulations, (table 3.5). This early release was followed by phase **II** where it appears that the remainder of the SDNs are unable to diffuse out of the aggregate and instead are released as drug molecules which then diffuse with a dissolution constant similar to the other formulations. PNA-00-SDN and PNA-25-LPV only displayed one release phase. PNA-00-SDN only contains PNA-00 nanogel which forms a much less porous structure, suggesting there was only release of drug molecules rather than SDNs.

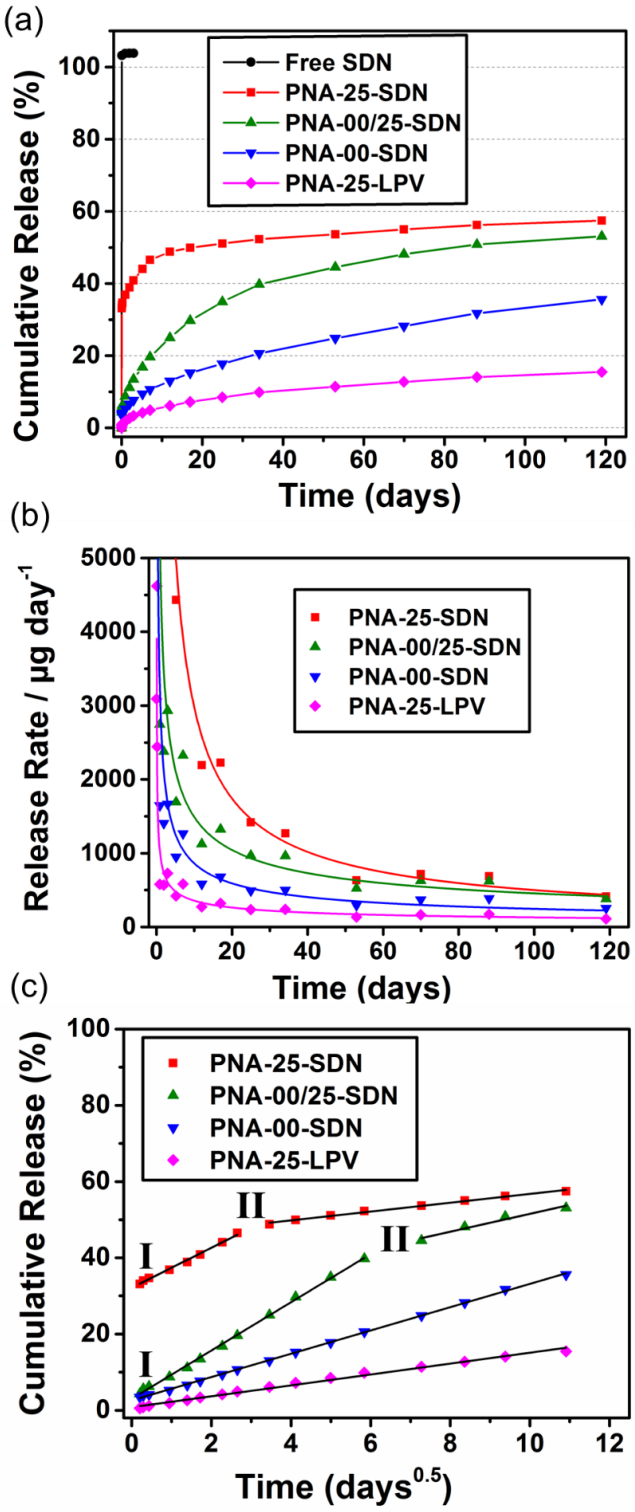

Figure 3.10 Release of LPV drug from aggregated nanogel discs over 120 days; quantified by HPLC analysis, measurements made in duplicate with mean value used. An SDN control without nanogel, 'Free SDN', was performed. After 120 days the depot was dissolved in acetonitrile for HPLC analysis to check remaining drug + amount released = 100% (a) cumulative release (b) release rate, lines are guides for the eye (c) application of the Ritger-Peppas equation to the LPV release over 120 days giving two phases of release (**I**, **II**) in PNA-25-SDN and PNA-00/25-SDN.

Table 3.5 Correlation coefficient (R_c) and dissolution constant (k).

	Phase I		Phase II	
Formulation	R_c	k	R_c	k
PNA-25	0.994	5.25	0.993	1.16
PNA-00/25-SDN	0.999	6.33	0.966	2.34
PNA-00-SDN	0.999	3.05	-	-
PNA-25-LPV	0.992	1.43	-	-

In PNA-25-LPV the lopinavir drug was in the form of a micrometer sized powder (figure A.9, Appendix), not as SDNs. Hence no two stage release is seen, as the large powder particles are not able to diffuse through the aggregate and instead only dissolved drug molecules are released. This rate of release is slower due to the reduced surface area and crystallinity of these larger particles of drug compared to amorphous SDNs.

The burst release from the initial aggregation of the nanocomposites was only 4.3% and 3.4% for PNA-00/25-SDN and PNA-00-SDN respectively. The PNA-25-SDN nanocomposite was the only sample to show appreciable burst release of 33.1%. As seen in the SEM/AFM analysis, (figure 3.7), the PNA-25 nanogel aggregate was the most porous, therefore it is possible that the SDNs near the surface of the aggregate were squeezed out rapidly through the pores during the initial aggregation, leading to a burst release. This theory is also supported by the concentration of LPV obtained during the burst release, much higher than the solubility of the hydrophobic drug lopinavir which would only be possible if the drug was released in SDN form. However, the water content of PNA-00/25-SDN nanocomposite was also reasonably high at 56.4% (w/w) and may have presented porosity and yet very little burst release was found. This difference could also be attributed to different particle packing; the opposite surface charges in PNA-00/25-SDN may lead to attractive interactions between nanogel particles reducing the porosity of the material. Also of note, a maximum of 13% burst release was seen with PS-OR particles in a PNA-25 depot (compared to 33.1% for the SDNs), however these particles had a hydrodynamic diameter of 821 nm compared to 330 nm for the SDNs, implying larger particles are more effectively entrapped by the more porous PNA-25 nanogel aggregate.

The formulation PNA-25-LPV, which contains the drug in powdered form, rather than as an SDN, displayed the slowest release rate with total release lower than all the SDN formulations, despite being loaded into the most porous depot formed from PNA-25. Hence, loading of the drug in SDN form allows the release rate from the depot to be enhanced, likely due to the much greater surface area of the SDNs assisting dissolution;[43] or their amorphous nature,[44] which aids in dissolution rate of drugs compared to the crystalline drug form.[37] This behaviour potentially offers an additional mechanism of controlling the rate of drug release from the nanocomposite. In powdered drug form the burst release was also minimal at 0.5%, despite the SDNs having a 33.1% burst release from the same PNA-25 nanogel. This reinforces the idea of porosity being linked to water content of the aggregates, with smaller nanoparticles releasing at a greater rate than the powdered form of the drug.

The minimum effective concentration for LPV has been shown to be 3000 ng ml^{-1}.[95] Based on the assumption of 5 litres of blood in the human body, then 16 g of the PNA-00/25 LPV SDN nanocomposite (which displayed sustained release of over 1000 μg day^{-1} over 20 days), would potentially provide LPV concentrations exceeding the minimum effective concentration. However, this does not take into account the clearance rate of the drug. Furthermore, dosing 16 g of the nanocomposite by subcutaneous/intramuscular injection would not be feasible. Although the release rate was not clinically relevant for LPV, we have used the drug as a model to demonstrate sustained release and the potential for the rate of release to be tuneable for the drug and it's SDN form. Hence, this system should be applicable to other more potent poorly water-soluble drugs. These release studies showed that the rate of release of dissolved drug molecules can be tuned by blending nanogels with different polymer composition, and by varying the form of the drug.

3.2.6. Cytotoxicity Study

With primary amine groups showing moderate cytotoxicity effects in some studies,[96] cytotoxicity studies were conducted on the nanogels, particularly to determine whether the nanogels containing poly(allylamine) exhibited any cytotoxicity. ATP, (figure 3.11), and MTT (figure A.10, Appendix) assays[97] were conducted on PNA-00 and PNA-25 nanogels. These assays detect the viability of cells when exposed to the nanogels compared to a negative control of cells without exposure, and a positive

control of cells exposed to rotenone which greatly reduces cell viability. These assays showed that when Madin-Darby canine kidney (MDCK-II) cells were incubated with PNA-00 and PNA-25 for 72 hours, at concentrations ranging from 0.04 mg ml^{-1} to 10 mg ml^{-1}, no sign of cell toxicity could be detected. It can be concluded that the MTT assay appears to show no reduction of cell mitochondrial activity in the presence of PNA-00 and PNA-25. The ATP assay could measure the cell viability by measuring the luminescent signal given out when beetle luciferin is oxidised to oxyluciferin in the presence of ATP obtained from the cells after lysis, and again showed no reduction in the presence of nanogel. The positive control rotenone was characterised by reduced cell viability compared to the control at all tested concentrations (from 0.19 µM to 100 µM), (figure A.11, Appendix). Considering the nature of the MTT and ATP assay, other cytotoxic effects cannot be dismissed; consequently, future investigations to support the development of PNA-00 and PNA-25 clinical applications should include a comprehensive evaluation of cellular, immunological and tissue toxicities.

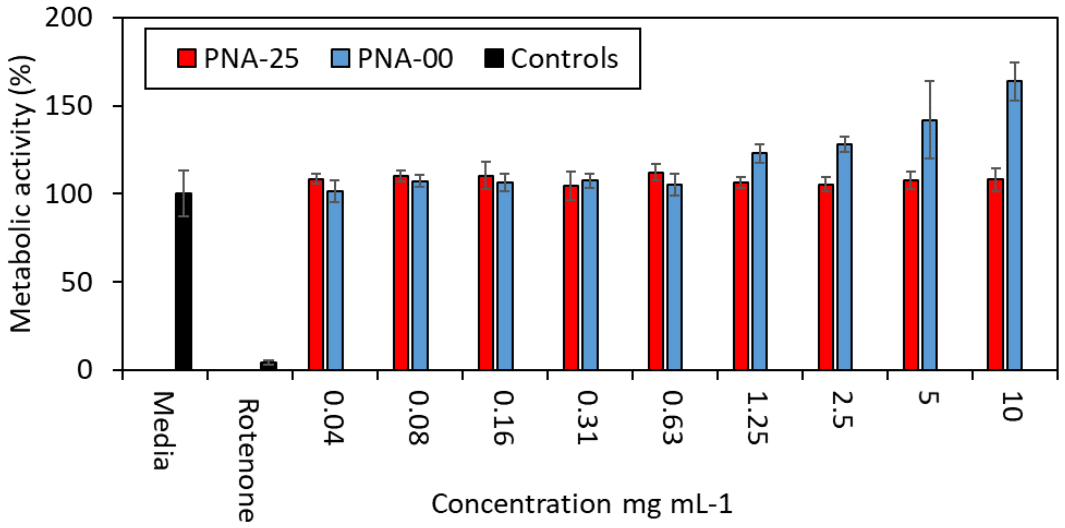

Figure 3.11 Cytotoxicity of nanogels towards cells in ATP assay, samples measured in quadruplet. Rotanone control = 0.19 µM, full range of rotanone control concentrations found in figure A.11.**

** All cytotoxicity assay experimental work was conducted by Rohan Gurjar, Department of Molecular and Clinical Pharmacology, University of Liverpool, Block H, 70 Pembroke Place, Liverpool, L69 3GF, UK.

3.3. Conclusions

After the initial investigation of an ISFI based on the aggregation of nanogels in Chapter 2, further investigation in this chapter has proved more thoroughly that these nanogels have very promising potential for use in an ISFI system. The polyNIPAM (PNA-00) and polyNIPAM-co-allylamine (PNA-25) nanogels were found to provide a long term sustained release of the hydrophobic drug LPV and its SDN form. PolyNIPAM nanogels could be formulated to contain a nanoparticulate payload to form an injectable nanocomposite material which rapidly aggregated in response to a dual stimulus of temperature and salt. The system also overcomes some of the common problems associated with ISFIs that have previously been developed. For example, the formulation with drug was simple to perform, it was easily injectable through a minimally invasive hypodermic needle, showed minimal burst release, and mechanical stability throughout the release. Sustained release of drug from the material was also maintained for a period of at least 120 days. The potential to easily tune the release rate from the system by adjusting the ratio of the two nanogel species PNA-00 and PNA-25, or enhance the release rate of the drug by using the form of SDNs was also demonstrated, and explained by investigating the structure of the aggregate depots. It was also shown through mathematical modelling that drug release occurred through Fickian diffusion of drug through the matrix. This drug delivery system should be applicable to other hydrophobic drugs and nanoparticulate payloads, and cytotoxicity was not an issue. This makes the system a suitable candidate as an ISFI for hydrophobic drugs and SDNs, where injections could possibly be given as infrequently as twice a year to improve adherence rates in the treatment of long term and particularly chronic conditions. The inflammation response at the depot site still requires investigation. There is also the potential to release multiple drugs as a combination therapy. There are also further opportunities to develop and understand the ISFI system, for example in terms of nanogel size and how this affects rheological and release rate behaviour, Chapter 4. Also a major drawback of this system is its lack of degradability, with the possibility to incorporate degradability explored in Chapter 5.

3.4. Materials and Methods

3.4.1. Materials

N-Isopropylacrylamide (NIPAM, ≥99%), allylamine (≥99%), N,N-methylenebis(acrylamide) (BIS, 99%), potassium persulfate (KPS, ≥99%), Oil Red O (OR), agarose (BioReagent, for molecular biology), sodium chloride (NaCl, ≥99.5%), styrene (≥99%), 50% (w/v) aqueous poly(acrylic acid) (P(AcA), M_n = 2000), dichloromethane (DCM, analytical grade), polyvinyl alcohol (PVA grade 4–88, MW 57–77 000), sodium phosphate dibasic dihydrate (Na_2HPO_4, ≥99%) potassium phosphate monobasic ($KH2PO_4$, ≥99%), sodium phosphate dibasic dihydrate ($Na_2HPO_4 \cdot 2H_2O$, ≥99%), (orthophosphoric acid solution 50% (H_3PO_4, HPLC Grade), anhydrous sodium hydroxide pellets (NaOH, analysis grade), 3-(4,5-dimethylthiazol-2-yl)-2,5-diphenyltetrazolium bromide (MTT, 98%), dulbecco's modified eagle's medium (DMEM, suitable for cell culture), rotenone (>95%), Hank's balanced salt solution (HBSS), MDCK-II cell lines, N,N-dimethylformamide (DMF, 99.8%), sodium dodecyl sulphate (SDS, ≥99%) were purchased from Sigma-Aldrich Company Ltd, Gillingham (Dorset) UK, a subsidiary of Merck KGaA, Darmstadt, Germany. Lopinavir (ABT-378) (LPV) was purchased from WuXi PharmaTech, Shanghai, China. Kolliphor TPGS was purchased from BASF, Ludwigshafen, Germany. CellTiter-Glo® substrate and CellTiter-Glo® buffer were purchased from Promega UK, Southhampton UK. Phosphate buffered saline tablets (Bioreagent), tetrahydrofuran (THF, HPLC grade), ethanol (EtOH, analytical grade), Acetonitrile (MeCN, HPLC grade), hydrochloric acid 37% (HCl, analytical grade), were purchased from Fischer Scientific UK, Loughborough, UK, a part of Thermo Fisher Scientific. Type I distilled water obtained from a water purification system with a resistivity of >18 MΩ cm−1 (PURELAB option R, Veolia). Spectra/Por 2 (MWCO = 12-14 kDa) dialysis tubing was purchased from Spectrum Europe B.V., Breda, The Netherlands. Chromafil Xtra PET 0.45 µm syringe filters were purchased from Hicrom Ltd. Theale, UK. All materials were used as received.

3.4.2. Synthesis of PolyNIPAM Nanogels

The polyNIPAM nanogels were synthesised by precipitation polymerisation. A summary of the formulation which was used for each nanogel species can be found in Table M.3.1. In a typical synthesis, the NIPAM monomer, allylamine comonomer and BIS cross-linking agent were dissolved in distilled water (130 mL for PNA-00 and 160 mL for PNA-25) in a 250 ml two-neck round bottom flask equipped with a reflux condenser. This was then sealed and nitrogen was bubbled through the aqueous solution for 1 hour whilst stirring (400 rpm) to remove dissolved oxygen. The solution was then heated to 60 °C. Separately KPS initiator was dissolved in distilled water (3.75 mL for PNA-00 and 10.5 mL for PNA-25) and degassed with N_2 for 1 hour before being transferred to the flask containing the monomers. The reaction was maintained under a N_2 atmosphere for 4 hours at 60 °C before being cooled down to room temperature. To remove unreacted impurities, the nanogel suspension was dialysed for 5 days using 12–14 kDa MWCO dialysis tubing, replacing the distilled water every 12 hours. The purified suspension was then lyophilised (Virtis Benchtop K with ultra-low temperature condenser) and sealed for storage.

Table M.3.1 The composition used in nanogel synthesis.

Sample	NIPAM (mol%)	allylamine (mol%)	BIS (mol%)	KPS[a] (mol%)	[NIPAM] (mg ml^{-1})
PNA-00	94.3	-	3.6	2.1	5.8
PNA-25	70.9	24.8	2.7	1.6	25.0

[a] KPS dissolved at 20 mg ml^{-1} in distilled water.

3.4.3. Characterisation of PolyNIPAM Nanogels and Aggregate Material

Characterisation of the nanogel dispersions and aggregates was carried out using dynamic light scattering (DLS), laser Doppler electrophoresis (LDE), scanning electron microscopy (SEM), 1H nuclear magnetic resonance (NMR), potentiometric titration, atomic force microscopy (AFM) and Fourier transform infrared spectroscopy (FTIR). DLS and LDE was performed using a Malvern Zetasizer Nano ZS (running Malvern Zetasizer software V7.11) (Malvern Instruments, Malvern, UK) with 633 nm He–Ne laser and the detector positioned at 173°. Dialysed samples were diluted to

1 mg mL^{-1}. The hydrodynamic diameter was recorded in the range (20–50 °C) using a thermal equilibration time of 600 seconds in 1 cm path length disposable cuvettes. Measurements were repeated in triplicate to give a mean hydrodynamic diameter and polydispersity index (PdI). Zeta potential measurements were performed using DTS1070 folded capillary cells (Malvern, UK). The pH of the sample was measured before performing zeta potential measurements, and for both samples fell in the range pH 7 ± 0.5. DTS1070 folded capillary cells were flushed with ethanol and water prior to usage. The zeta potential measurement was made with a minimum of 10 and maximum of 40 runs, and the voltage applied was automatically selected by the software. The Smoluchowski approximation where f(Ka) = 1.5 was used, and dispersions contained 10 mM NaCl and were measured at 25 °C. To prepare the nanogel dispersions for SEM imaging, the samples were diluted to 0.01 mg mL^{-1} in distilled water. 50 μL of solution was pipetted onto a circular cover glass (10 mm diameter) attached to a carbon adhesive disc on an aluminium SEM specimen stub (12.5 mm diameter). For SEM images of the aggregated material, swollen gel (14.90% (w/w) PNA-00 and 6.24% (w/w) PNA-25) was formed in PBS (1X strength, pH 7.4) and then adhered to a coverslip on an SEM stub. This was heated to 37 °C to induce aggregation. The samples were left to air-dry for 24 hours, followed by sputter coating with gold (EMITECH K550X) with a deposition current of 25 mA for 100 seconds before imaging. SEM images of the nanogel morphology were then obtained using a Hitachi S-4800 FE-SEM at 3 kV. To record 1H NMR spectra lyophilised nanogel sample was dissolved in D_2O at 20 mg mL^{-1} and analysed on a Bruker 400 MHz spectrometer (Bruker, MA, USA). The potentiometric titration of PNA-25 was conducted with a 50 mL aqueous dispersion of PNA-25 at 1 mg mL^{-1}. The sample pH was then lowered below pH 4 using 0.1 M HCl. The sample was then titrated with 0.1 M NaOH at 25 °C ± 0.5 °C under a nitrogen atmosphere. A Hanna Instruments HI-11310 pH electrode (Hanna Instruments, Bedfordshire, UK) was used to record the change in pH. To record FTIR spectra a blank background scan was performed, followed by a recording of the spectra of lyophilised nanogel ca. 5 mg, which was clamped onto the ATR crystal of a Bruker alpha platinum ATR (Bruker, Santa Barbara, CA, USA). Atomic force microscopy (AFM) was carried out using a Bruker Multimode 8 system (Bruker, Santa Barbara, CA, USA) operated with ScanAsyst Mode in ambient conditions. All testing was conducted using a Bruker RTESPA-150 probe with a nominal radius of 8 nm and a spring constant of 5 N m^{-1}. Each scan was conducted with a resolution of 256 pixels per line and with a scan rate of 0.799 Hz.

The samples were prepared by placing a thin layer of swollen gel formed in PBS (1X strength, pH 7.4) (14.90% (w/w) PNA-00 and 6.24% (w/w) PNA-25) onto glass coverslips, which were then incubated at 37 °C in a water saturated atmosphere for 72 hours. The coverslips were then adhered to 15 mm diameter metal stubs for mounting in the AFM. The AFM images were analysed off-line using Bruker Nanoscope Analysis 1.7 software

3.4.4. PolyNIPAM Nanogel Gelation and Aggregation Studies

The concentration at which the nanogel samples formed a self-supporting gel was found by first adding 10 mg of material to 1 mL of phosphate buffered saline (1X strength, pH 7.4) in a glass vial with an internal diameter of 20 mm. Using the tube inversion method, the mass of nanogel was increased in increments until the nanogel no longer flowed upon inversion of the vial for 30 seconds. The percentage (w/w) of water contained in the nanogel at 25 °C was calculated from the mass of freeze dried nanogel and water in the swollen nanogel formed from the tube inversion method. After heating to 37 °C the aggregate was separated from the eluted solvent to determine its mass. The mass of nanogel remains constant, so the difference in mass is due to any solvent remaining in the aggregate, allowing the % (w/w) of water at 37 °C to be calculated.

3.4.5. Tissue Injection Simulation

Agarose powder (0.5% (w/w)) was slowly added to a beaker of PBS (1X strength, pH 7.4) whilst stirring, and then weighed, before covering the beaker with plastic wrap with a hole for ventilation, and heating to 95 °C for 10 minutes. Hot water was then added to bring the contents to the original weight. This was then cooled to 55 °C and cast into pre-warmed vials with an internal diameter of 20 mm. These were then left for 12 hours at 37 °C before use. PNA-25 at 6.2% and 2.0% (w/w) and PNA-00 at 14.9% and 5.7% (w/w) in distilled water were injected through a 18G hypodermic needle into 0.5% (w/w) agarose gel at 37 °C. For injection into tissue *ex vivo*, a 9.1% (w/w) dispersion of PNA-00 combined with ponceau red dye (1 mg ml^{-1}) was injected into porcine vitreous at 37 °C.

3.4.6. Polystyrene Nanoparticle Synthesis and Oil Red Dye (OR) Encapsulation

Polystyrene (PS) nanoparticles were prepared using modifications of a dispersion polymerisation method in which colloidal stability was provided by poly(acrylic acid).[98] Briefly, styrene monomer (15.35 mL) was dissolved in ethanol (26.23 mL) and

distilled water (101.05 mL) in a 250 mL two-neck round bottom flask equipped with a reflux condenser. 50% (w/v) aqueous poly(acrylic acid) (2.92 mL) was then added along with KPS (234 mg) in distilled water (3.32 mL). This was then sealed and nitrogen was bubbled through the aqueous solution for 1 hour whilst stirring (400 rpm), to remove dissolved oxygen. The solution was then heated to 70 °C. The reaction was maintained under a N_2 atmosphere for 24 hours before being cooled to room temperature. The PS nanoparticle suspension was purified by centrifugation (Thermo Scientific Heraeus Megafuge 8R centrifuge) at a relative centrifugal force (RCF) of 10,900 in 50 mL centrifuge tubes for 1 hour, and washed with distilled water (ca. 50 mL), this process was repeated twice. Oil Red O (OR) was encapsulated into the particles by modifying a previous swelling-diffusion technique.[99] Firstly, the aqueous PS suspension (32 mg mL^{-1}, 25 mL) and aqueous Pluronic F127 (72 mg mL^{-1}, 8.3 mL) were added to a 50 ml centrifuge tube. This was vortexed at 3000 rpm for 60 seconds and then left for 24 hours on a tube roller (33 rpm). Tetrahydrofuran (THF) (16.66 mL, 33% (v/v)) containing OR (14.7 mg) was added to the suspension, and then vortexed at 3000 rpm for 600 seconds, followed by 0.5 hours on a tube roller (33 rpm). The colloid was then washed five times with distilled water using a centrifuge (RCF = 10 900, 1 hour) between washes and then lyophilised (Virtis Benchtop K with ultra-low temperature condenser). A sample of the PS nanoparticles with encapsulated OR was prepared at a concentration of 0.1 mg mL^{-1} and was analysed with DLS after synthesis and after lyophilisation.

3.4.7. Polystyrene Nanoparticle Entrapment Study

In a glass vial with internal diameter 20 mm, 66.6 mg of PNA-25 was mixed with lyophilised PS nanoparticles of 10, 20 and 40% (w/w) relative to the nanogel. After adding 1 mL of PBS (1X strength, pH 7.4) the dispersion was left for 10 min to allow the lyophilised nanogel to swell. The samples were then vortexed at 300 rpm to mix the PS nanoparticles through the swollen nanogel dispersion. These samples were then heated (in a water bath) to 37 °C for 1 hour to form shrunken discs of aggregated nanogel, with excess PBS (1X strength, pH 7.4) expelled from the discs in the heating process. A negative control of nanogel alone and positive control of PS particles alone were conducted alongside the samples. 0.2 mL of solution was removed for UV-visible spectrophotometric analysis (Thermo Scientific NanoDrop 2000c) with a 1 cm path length quartz cuvette at a wavelength of 565 nm (λmax for OR). To determine the concentration of PS nanoparticles a stock solution of 1 mg mL^{-1} dispersed in PBS

(1X strength, pH 7.4) was serially diluted to form a linear calibration curve of absorbance at 565 nm against concentration in the range 1–100 μg mL^{-1}.

3.4.8. Lopinavir (LPV) Solid Drug Nanoparticle (SDN) Synthesis

The LPV SDNs were prepared by emulsion-spray-drying as described by Giardiello *et al*.[44] Briefly, a stock solution of LPV (200 mg mL^{-1} in dichloromethane (DCM)), polyvinyl alcohol (PVA grade 4–88, MW 57–77 000) (50 mg mL^{-1} in water), Kolliphor TPGS (50 mg mL^{-1} in water) were prepared. Three stock solutions were mixed in the LPV: PVA : Kolliphor TPGS ratio of 60 : 192 : 48 (mL) in a 1 : 4 DCM to water mixture. Emulsification was conducted using a Hielscher UP400S ultrasonic processor equipped with a H14 Probe at 100% output (140 W) for 180 seconds, with immediate spray-drying using a benchtop spray-dryer (BUCHI Mini-290) with an air-atomizing nozzle and compressed air as the drying gas. Spray-drying process conditions: 7 mL min^{-1} solution flow rate; 65 °C outlet temperature; 110 °C inlet temperature. Resultant powders were further dried under vacuum for 48 hours to remove residual DCM. SDN dispersions result from subsequent powder dispersion in water; for DLS characterisation, powders were dispersed in distilled water at 2 mg mL^{-1} (1 mg mL^{-1} cf. LPV).

3.4.9. Drug Release in Phosphate Buffered Saline (PBS)

The *in vitro* drug release was performed using adaptations of the sample and separate method,[8] as performed in previous work.[13] The required amount of each lyophilised nanogel, 6.24% (w/w) for PNA-25, and 14.90% (w/w) for PNA-00, was dispersed to form a swollen self-supporting gel in 1 mL of PBS (pH 7.4, 0.137 M NaCl and 0.0027 M KCl) in a glass vial of internal diameter 20 mm. To this 22.2 mg of LPV or 44.4 mg of LPV SDNs (50% (w/w) loading of LPV) were vortexed to give 22.2 mg of LPV per formulation. These were then heated to 37 °C for 1 hour to form shrunken discs with excess PBS expelled from the discs in the heating process, this was removed and used as the first release time point. These discs were transferred to larger 250 mL glass sample jars with 100 mL of fresh PBS. Subsequent release samples were taken at pre-determined intervals by removing 100 mL from the vessel and replacing with 100 mL of fresh PBS at 37 °C to prevent a saturation limit with a large excess of solvent. Release vessels were kept at 37 °C ± 0.5 °C in a water bath. The amount of LPV released was quantified by HPLC analysis.

3.4.10. HPLC Procedure

The HPLC method is adapted from the method published by Giovanni Di Perri *et al.*[100] Briefly, HPLC grade acetonitrile (MeCN) (1.8 mL) was added to each release sample (4.2 mL) to create 30% (v/v) MeCN samples, followed by filtering through a 0.45 μm PTFE syringe filter. 40 μL of the solution was injected into a HPLC-PDA system (PerkinElmer Series 200). The mobile phase was composed of solvent A (KH_2PO_4 50 mM dissolved in HPLC grade water then pH adjusted with H3PO4 to reach pH 3.23) and solvent B (MeCN) with the gradient reported in Table M.2. Chromatographic separation was performed with an Agilent ZORBAX Eclipse Plus 3.5 μm C18 column (100 × 4.6 mm ID, Santa Clara, CA) maintained at 25 °C in a column oven with a solvent flow rate of 0.5 mL min^{-1} giving a retention time of LPV of 9.6 ± 0.2 min. The PDA detector was set to 210 nm with a bandwidth of 2 nm. The concentration of LPV in the samples was calculated against known standards using the area under the chromatogram peaks. Three standards covering the concentration range of the HPLC method were used to verify the results, and samples were analysed in duplicate.

Table M.2 The solvent gradient used in the HPLC method

Time (min)	Solvent A % (v/v)	Solvent B % (v/v)	Flow (mL min^{-1})
0.0	70	30	0.5
1.0	70	30	0.5
3.0	30	70	0.5
11.5	30	70	0.5
12.0	70	30	0.5
12.5	70	30	0.5

3.4.11. *In Vitro* Nanogel Cytotoxicity Study

Cytotoxicity experiments were carried out on MDCK-II cell lines by MTT and ATP assay (Promega CellTiter-Glo® Luminescent Cell Viability Assay, Madison, WI). In both assays cells were seeded on 96-well plates at a density 2×10^4 cells per well in 100 μL of Dulbecco's Modified Eagle Medium (DMEM) and incubated for 24 hours. Ten different concentrations of the nanogels were prepared by ten-fold serial dilution with the media, starting at 10 mg mL^{-1}. A ten-fold serial dilution of rotenone from 100 μM acted as a positive control, and cells alone in media as a negative control.

Cells were incubated for 72 hours at 37 °C. In the ATP assay the wells were then equilibrated at room temperature for 30 minutes. 100 µL of Beetle Luciferin (CellTiter-Glo® Reagent) was added and mixed on an orbital shaker for 2 minutes to induce cell lysis. After incubation for 10 minutes at room temperature the luminescent signal was measured using a GENios microplate reader (TECAN). Samples were repeated in quadruplicate. The background luminescence of DMEM was subtracted from the sample luminescence. In the MTT assay after the 72 hour incubation period, 5 mg of MTT was dissolved in 1 mL of hank's balanced salt solution (HBSS). 20 µL was added to each well and incubated for 2 hours, followed by 100 µL of lysis buffer (50% DMF in water containing 20% SDS) for 12 hours. The absorbance of each well was measured at a wavelength of 560 nm using a GENios microplate reader (TECAN). Samples were repeated in quadruplicate. The absorbance of DMEM, and the absorbance of nanogel interaction with MTT without cells present, was subtracted from the sample absorption.

3.5. Appendix

Table A.1 Comparison of area under LPV HPLC elution peak to validate quantification of LPV in LPV SDNs.

[LPV]	[SDN][a]	Area under LPV elution peak		
µg ml^{-1}	µg ml^{-1}	$\mathbf{I}_{SDN}$	$\mathbf{I}_{LPV}$	$\mathbf{I}_{SDN}/\mathbf{I}_{LPV}$
14.0	28.0	2,067,615	2,071,892	1.002

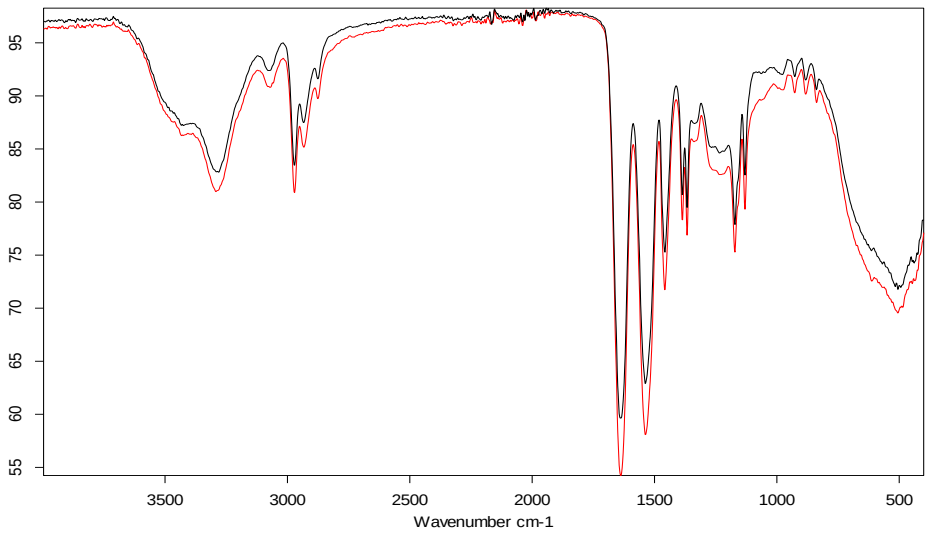

Figure A.1 FTIR Spectra of nanogels. PNA-00 (black) and PNA-25 (red). 910–665 cm^{-1} (s, b) N-H wag 1˚, 2˚ amines, 3400–3250 cm^{-1} (m) N–H stretch 1˚, 2˚ amines, amides, 1650–1580 cm^{-1} (m) N–H bend 1˚ amines, 1250–1020 cm^{-1} (m) C–N stretch aliphatic amine.

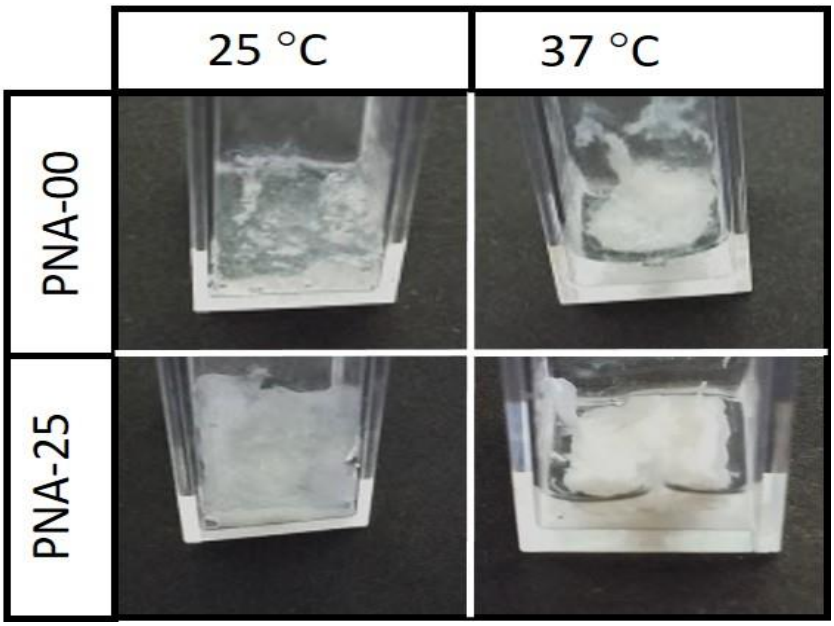

Figure A.2 Images of dual-responsive transition of the nanogels in HBSS; from swollen self-supporting gels to bulk aggregates. Nanogel samples as swollen gel (left) and bulk aggregate (right). PNA-00, 14.90% (w/w), (top) and PNA-25, 6.24% (w/w), (bottom).

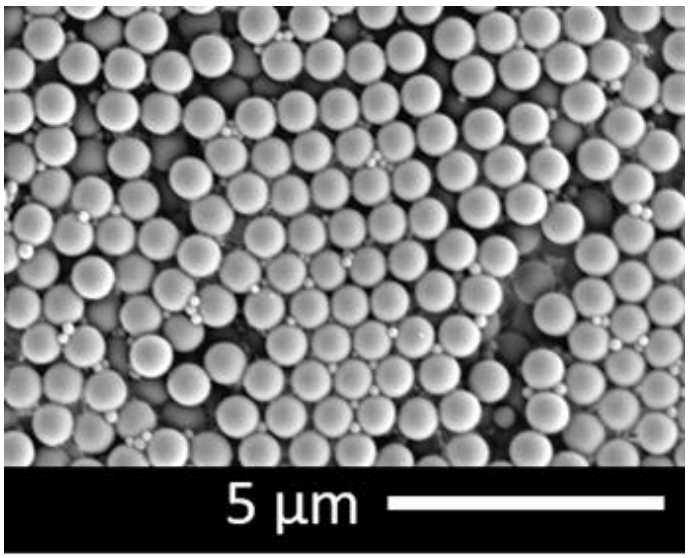

Figure A.3 SEM image of polystyrene particles. Sample diluted to 0.01 mg mL^{-1} in distilled water. Sputter coated with gold (EMITECH K550X) with a deposition current of 25 mA for 100 seconds before imaging. SEM images were then obtained using a Hitachi S-4800 FE-SEM at 3 kV.

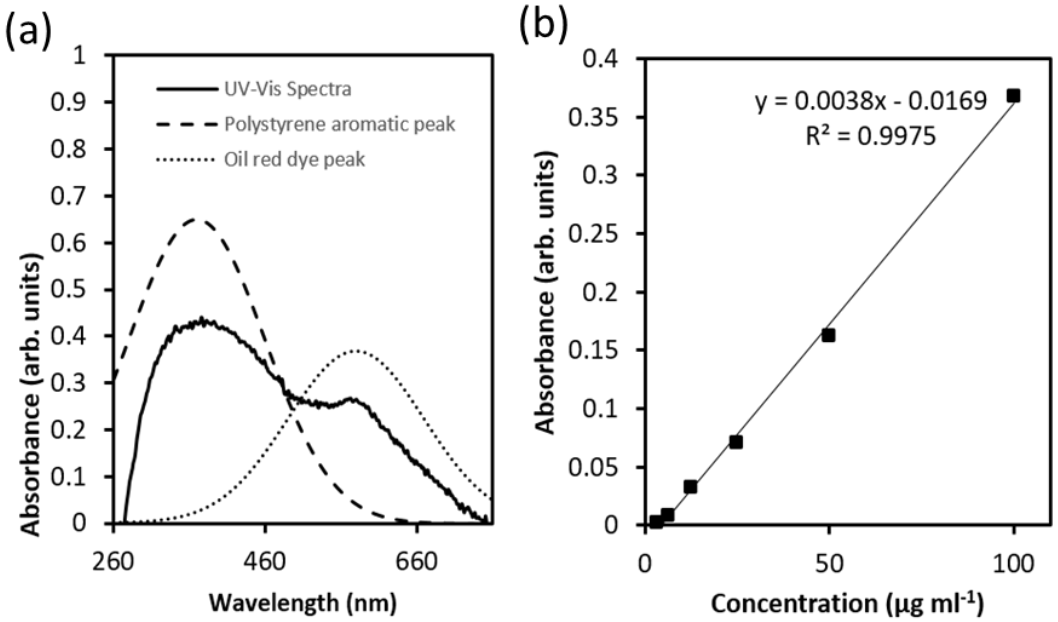

Figure A.4 (a) UV-vis absorbance spectrum of oil red dyed polystyrene nanoparticles, deconvoluted into two component peaks using Gaussian amplitude peak fitting with a Gaussian response width of 2 standard deviations using peakFIT®v4.11 software. (b) UV-Vis calibration data using absorbance of deconvoluted oil red dye peak, linear relationship between absorbance and concentration from 5-100 µg mL^{-1}.

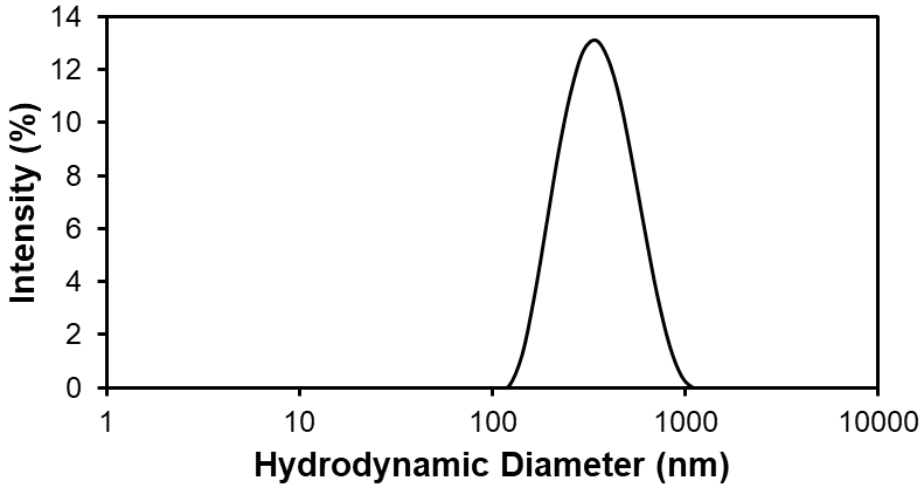

Figure A.5 DLS analysis of lopinavir solid drug nanoparticles. Size distribution by intensity at 25 °C. Z-average diameter = 330 nm, PdI = 0.18.

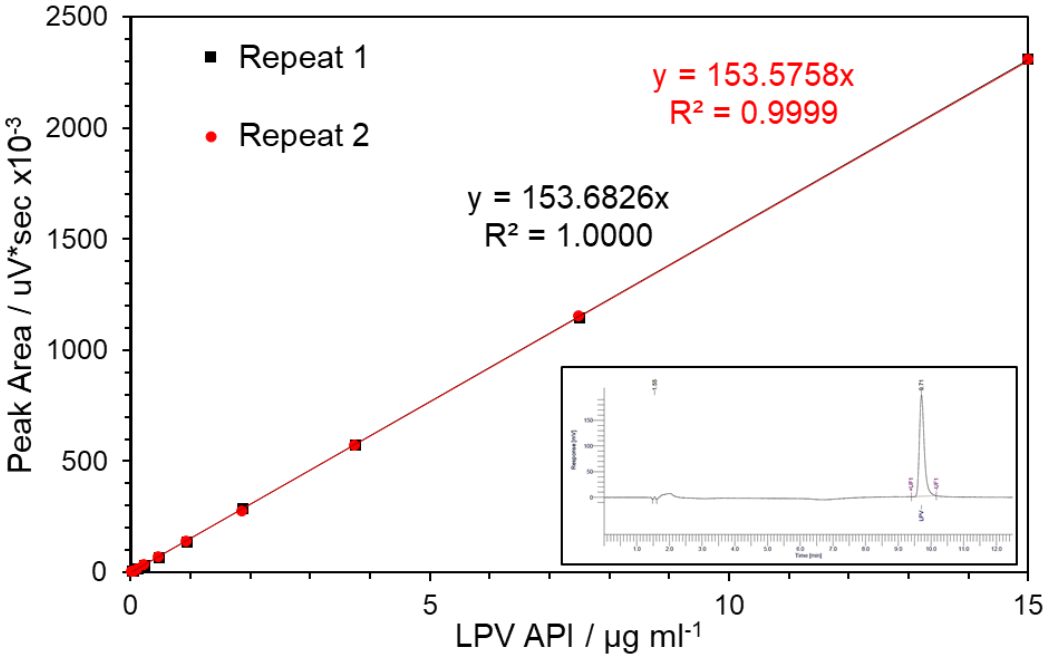

Figure A.6 Linear working range of LPV calibration curve (inset LPV HPLC chromatogram).

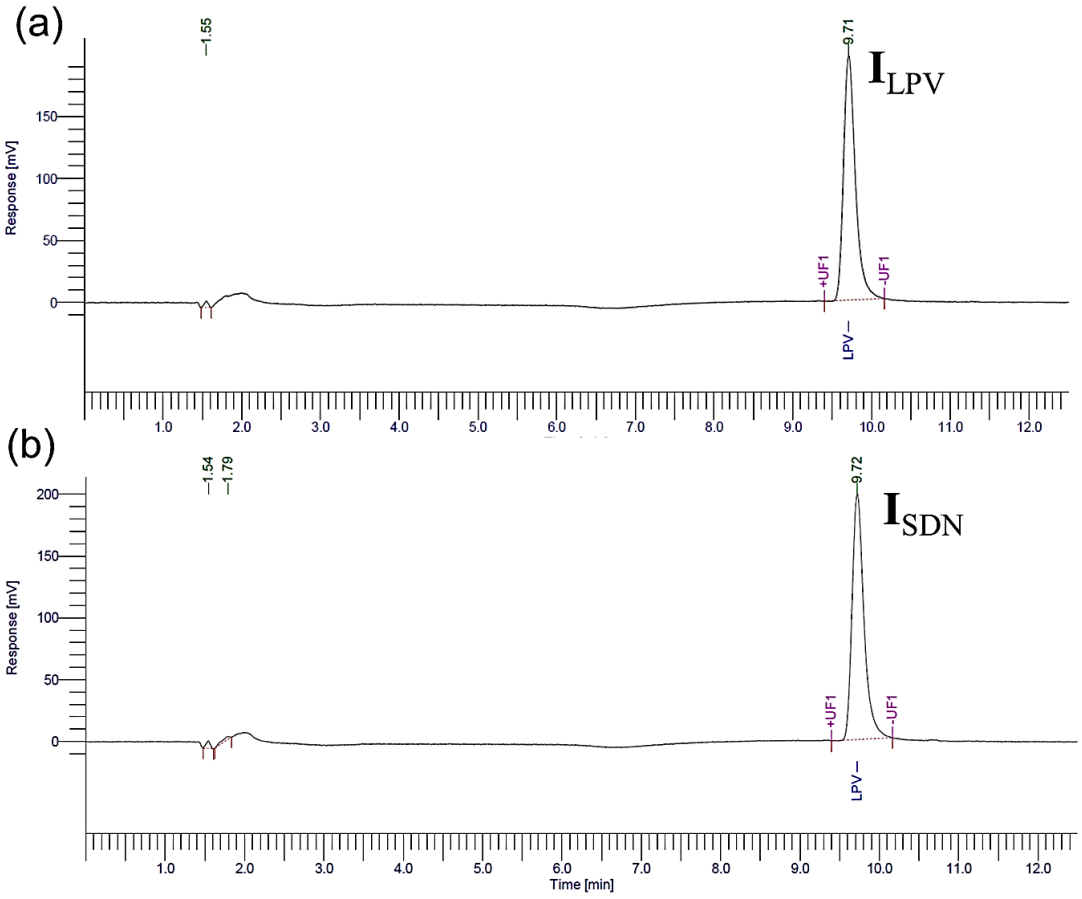

Figure A.7 HPLC Chromatograms of LPV elution peak at retention time of 9.7 minutes for (a) LPV drug, 14 µg ml^{-1} and (b) LPV SDNs, 28 µg ml^{-1}.

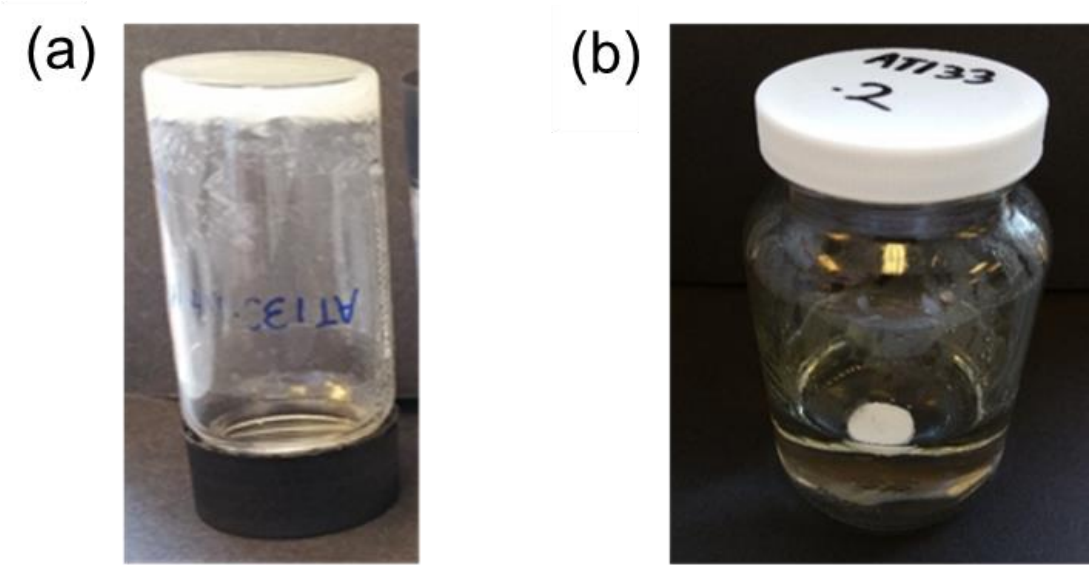

Figure A.8 LPV release experiment a) example of formulation of nanogel and LPV SDNs at room temperature b) formulation in shrunken disk form after heating to 37 °C and transferring to 100 mL of release medium (PBS).

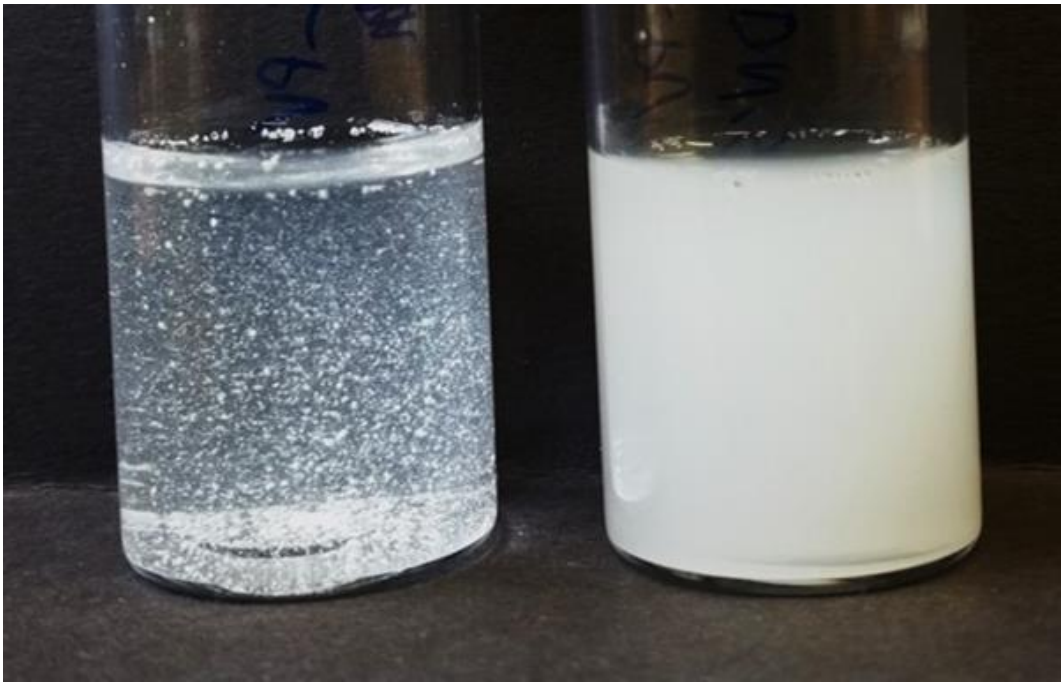

Figure A.9 (left) LPV drug particulates and (right) LPV SDN's. Both dispersed in water at 1mg ml^{-1}.

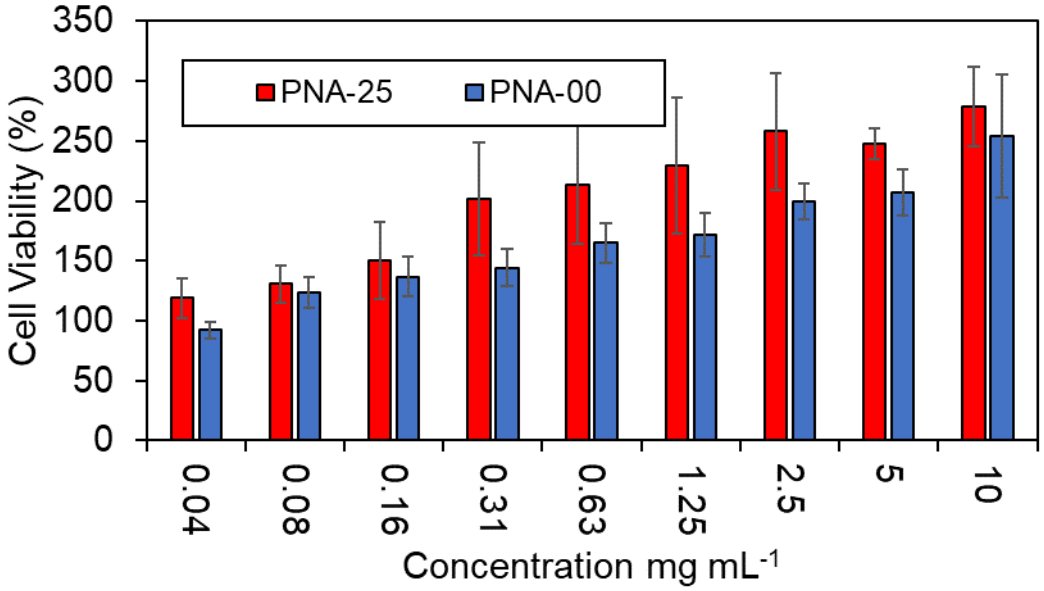

Figure A.10 Cytotoxicity of nanogels towards cells in MTT Assay.

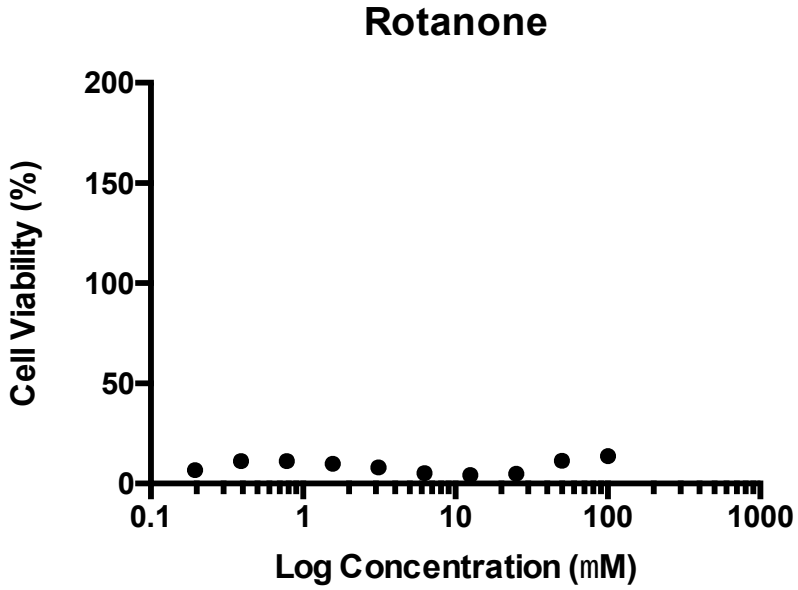

Figure A.11 ATP assay cell viability results of positive control (rotenone) at concentrations of 0.19 µM to 100 µM.

3.6. References

1 J. Aiache, N. Aoyagi, D. Bashaw, C. Brown, W. Brown, D. Burgess, P. Deluca, R. Djerki, J. Dressman, T. Foster, K. Gjellan, V. Gray, A. Hussain, T. Ingallinera, J. Klancke, J. Kraemer, H. Kristensen, K. Kumi, M. Mueller-zsigmondy, N. Okafo, L. Ouderkirk, S. Parsi and S. Qureshi, *AAPS PharmSciTech*, 2003, **4**, 1–10.

2 S. Kempe and K. Mäder, *J. Control. Release*, 2012, **161**, 668–679.

3 K. Qian, Y. Ma, J. Wan, S. Geng, H. Li, Q. Fu, X. Peng, X. Kan, G. Zhou, W. Liu, B. Xiong, Y. Zhao, C. Zheng, X. Yang and H. Xu, *J. Control. Release*, 2015, **212**, 41–49.

4 T. Hirakura, K. Yasugi, T. Nemoto, M. Sato, T. Shimoboji, Y. Aso, N. Morimoto and K. Akiyoshi, *J. Control. Release*, 2010, **142**, 483–489.

5 C. Yang, X. Wang, X. Yao, Y. Zhang, W. Wu and X. Jiang, *J. Control. Release*, 2015, **205**, 206–217.

6 X. Zhang, K. Achazi, D. Steinhilber, F. Kratz, J. Dernedde and R. Haag, *J. Control. Release*, 2014, **174**, 209–16.

7 C. Larsen, S. W. Larsen, H. Jensen, A. Yaghmur and J. Østergaard, *Expert Opin. Drug Deliv.*, 2009, **6**, 1283–1295.

8 J. Shen and D. J. Burgess, *J. Pharm. Pharmacol.*, 2012, **64**, 986–996.

9 J. C. Wright and D. J. Burgess, *Long Acting Injections and Implants*, Springer-Verlag, Berlin, 2012.

10 L. Olanoff and J. M. Anderson, *J. Pharm. Sci.*, 1979, **68**, 1151–1155.

11 L. S. Olanoff and J. M. Anderson, *J. Pharmacokinet. Biopharm.*, 1980, **8**, 599–620.

12 H. Kawaguchi, K. Fujimoto and Y. Mizuhara, *Colloid Polym. Sci.*, 1992, **270**, 53–57.

13 H. Hyun, Y. H. Kim, I. B. Song, J. W. Lee, M. S. Kim, G. Khang, K. Park and H. B. Lee, *Biomacromolecules*, 2007, **8**, 1093–1100.

14 S. Mangalathillam, N. S. Rejinold, A. Nair, V.-K. Lakshmanan, S. V Nair and R. Jayakumar, *Nanoscale*, 2012, **4**, 239–250.

15 W. Il Choi, J. H. Lee, J. Y. Kim, J. C. Kim, Y. H. Kim and G. Tae, *J. Control. Release*, 2012, **157**, 272–278.

16 S. C. Moldoveanu and V. David, in *Essentials in Modern HPLC Separations*, 2013, pp. 1–51.

17 N. L. Rezk, R. R. Tidwell and A. D. M. Kashuba, *J. Chromatogr. B Anal. Technol. Biomed. Life Sci.*, 2002, **774**, 79–88.

18 S. M. Dhole, P. B. Khedekar and N. D. Amnerkar, *Pharm. Methods*, 2012, **3**, 68–72.

19 K. C. Waterman and R. C. Adami, *Int. J. Pharm.*, 2005, **293**, 101–125.

20 D. Y. Ko, U. P. Shinde, B. Yeon and B. Jeong, *Prog. Polym. Sci.*, 2013, **38**, 672–701.

21 L. Gao, D. Zhang and M. Chen, *J. Nanoparticle Res.*, 2008, **10**, 845–862.

22 J. M. Schierholz, H. Steinhauser, A. F. E. Rump, R. Berkels and G. Pulverer, *Biomaterials*, 1997, **18**, 839–844.

23 X. Huang and C. S. Brazel, *J. Control. Release*, 2001, **73**, 121–136.

24 L. W. Kleiner, J. C. Wright and Y. Wang, *J. Control. Release*, 2014, **181**, 1–10.

25 L. Wang, A. Wang, X. Zhao, X. Liu, D. Wang, F. Sun and Y. Li, *Int. J. Pharm.*, 2012, **427**, 284–292.

26 R. Zarzycki, Z. Modrzejewska, K. Nawrotek and U. Lek, *Ecol. Chem. Eng. S*, 2010, **17**, 117–136.

27 L. E. Achenie and N. Pavurala, *Nov. Approaches Drug Des. Dev.*, 2017, **2**, 1–10.

28 Y. Fu and W. J. Kao, *Pharm. Res.*, 2009, **7**, 429–444.

29 D. Jones, in *Rapra Review Reports*, Volume 15., 2004.

30 T. Higuchi, *J. Pharm. Sci.*, 1961, **50**, 874–875.

31 T. Higuchi, *J. Pharm. Sci.*, 1963, **52**, 1145–1149.

32 P. L. Ritger and N. A. Peppas, *J. Control. Release*, 1987, **5**, 23–36.

33 P. L. Ritger and N. A. Peppas, *J. Control. Release*, 1987, **5**, 37–42.

34 M. H. Hsiao, M. Larsson, A. Larsson, H. Evenbratt, Y. Y. Chen, Y. Y. Chen and D. M. Liu, *J. Control. Release*, 2012, **161**, 942–948.

35 Q. Wang, Y. Zhao, Y. Yang and H. Xu, *Colloid Polym. Sci.*, 2007, **285**, 515–521.

36 S. Sareen, L. Joseph and G. Mathew, *Int. J. Pharm. Investig.*, 2012, **2**, 12.

37 M. Parks and B. C. Hancock, *Pharm Res*, 2000, **17**, 397–404.

38 B. E. Rabinow, *Nat. Rev. Drug Discov.*, 2004, **3**, 785–796.

39 S. Ranjita, *J. Pharm. Investig.*, 2013, **43**, 1–26.

40 T. O. Mcdonald, M. Siccardi, D. Moss, N. Liptrott, M. Giardiello, S. Rannard and A. Owen, in *The application of nanotechnology to drug delivery in Medicine.*, Elsevier Health Sciences, Toronto, 2015, pp. 173–223.

41 T. O. McDonald, L. M. Tatham, F. Y. Southworth, M. Giardiello, P. Martin, N. J. Liptrott, A. Owen and S. P. Rannard, *J. Mater. Chem. B*, 2013, **1**, 4455–4465.

42 T. O. McDonald, P. Martin, J. P. Patterson, D. Smith, M. Giardiello, M. Marcello, V. See, R. K. O'Reilly, A. Owen and S. Rannard, *Adv. Funct. Mater.*, 2012, **22**, 2469–2478.

43 E. Merisko-Liversidge and G. G. Liversidge, *Adv. Drug Deliv. Rev.*, 2011, **63**, 427–440.

44 M. Giardiello, N. J. Liptrott, T. O. McDonald, D. Moss, M. Siccardi, P. Martin, D. Smith, R. Gurjar, S. P. Rannard and A. Owen, *Nat. Commun.*, 2016, **7**, 13184.

45 V. R. Patel and Y. K. Agrawal, *J. Adv. Pharm. Technol. Res.*, 2011, **2**, 81–87.

46 S. Allababidi and J. C. Shah, *J. Pharm. Sci.*, 1998, **87**, 738–744.

47 T. Hoare and R. Pelton, *Langmuir*, 2008, **24**, 1005–1012.

48 R. Pelton, *J. Colloid Interface Sci.*, 2010, **348**, 673–674.

49 G. Huang, J. Gao, Z. Hu, J. V St. John, B. C. Ponder and D. Moro, *J. Control. Release*, 2004, **94**, 303–311.

50 J. Ramos, M. A. Peláez-Fernández, J. Forcada and A. Moncho-Jordá, in *Soft Nanoparticles for Biomedical Applications*, eds. J. Callejas-Fernández, J. Estelrich, M. Quesada-Pérez and J. Forcada, RSC publishing, Cambridge, 2014, pp. 133–156.

51 W. Xiong, X. Gao, Y. Zhao, H. Xu and X. Yang, *Colloids Surf. B. Biointerfaces*, 2011, **84**, 103–10.

52 P. C. Naha, K. Bhattacharya, T. Tenuta, K. A. Dawson, I. Lynch, A. Gracia, F. M. Lyng and H. J. Byrne, *Toxicol. Lett.*, 2010, **198**, 134–143.

53 M. A. Cooperstein and H. E. Canavan, *Biointerphases*, 2013, **8**, 19.

54 A. L. Kjøniksen, M. T. Calejo, K. Zhu, A. M. S. Cardoso, M. C. P. De Lima, A. S. Jurado, B. Nyström and S. A. Sande, *J. Pharm. Sci.*, 2014, **103**, 227–234.

55 Y. Wang, J. L. Robertson, W. B. Spillman and R. O. Claus, *Pharm. Res.*, 2004, **21**, 1362–1373.

56 E. Fröhlich, *Int. J. Nanomedicine*, 2012, 5577–5591.

57 H. Kranz and R. Bodmeier, *Int. J. Pharm.*, 2007, **332**, 107–114.

58 B. Jeong and A. Gutowska, *Trends Biotechnol.*, 2002, **20**, 305–311.

59 B. Jeong, Y. H. Bae, D. S. Lee and S. W. Kim, *Nature*, 1997, **388**, 860–862.

60 L. Pescosolido, PhD Thesis, Sapienza University of Rome, 2011.

61 E. Ruel-Gariépy and J. C. Leroux, *Eur. J. Pharm. Biopharm.*, 2004, **58**, 409–426.

62 R. H. Pelton and P. Chibante, *Colloids and Surfaces*, 1986, **20**, 247–256.

63 S. Chen, X. Jiang and L. Sun, *J. Appl. Polym. Sci.*, 2013, **130**, 1164–1171.

64 C. Hoskins, P. K. T. Lin, L. Tetley and W. P. Cheng, *Polym. Adv. Technol.*, 2012, **23**, 710–719.

65 X. Ma, Y. Cui, X. Zhao, S. Zheng and X. Tang, *J. Colloid Interface Sci.*, 2004, **276**, 53–9.

66 S. Chen, J. Long and Y. Dan, *J. Appl. Polym. Sci.*, 2011, **121**, 3322–3331.

67 K. Ogawa, A. Nakayama and E. Kokufuta, *Langmuir*, 2003, **19**, 3178–3184.

68 K. Kratz, T. Hellweg and W. Eimer, *Colloids Surfaces A Physicochem. Eng. Asp.*, 2000, **170**, 137–149.

69 S. Ito, K. Ogawa, H. Suzuki, B. Wang, R. Yoshida and E. Kokufuta, *Langmuir*, 1999, **15**, 4289–4294.

70 R. H. Pelton, H. M. Pelton, a. Morphesis and R. L. Rowell, *Langmuir*, 1989, **5**, 816–818.

71 R. Pelton, *Adv. Colloid Interface Sci.*, 2000, **85**, 1–33.

72 M. Rasmusson, A. Routh and B. Vincent, *Langmuir*, 2004, **20**, 3536–3542.

73 H. Wang, M. B. Hansen, D. W. P. M. Löwik, J. C. M. Van Hest, Y. Li, J. a. Jansen and S. C. G. Leeuwenburgh, *Adv. Mater.*, 2011, **23**, 119–124.

74 Q. Wang, L. Wang, M. S. Detamore and C. Berkland, *Adv. Mater.*, 2008, **20**, 236–239.

75 J. Zhou, G. Wang, L. Zou, L. Tang, M. Marquez and Z. Hu, *Biomacromolecules*, 2008, **9**, 142–148.

76 N. S. Patil, J. S. Dordick and D. G. Rethwisch, *Biomaterials*, 1996, **17**, 2343–2350.

77 N. Fogh-Andersen, B. M. Altura, B. T. Altura and O. Siggaard-Andersen, *Gen. Clin. Chem.*, 1995, **41**, 1522–1525.

78 T. López-León, A. Elaïssari, J. L. Ortega-Vinuesa and D. Bastos-González, *ChemPhysChem*, 2007, **8**, 148–156.

79 F. Ye, S. W. Larsen, A. Yaghmur, H. Jensen, C. Larsen and J. Østergaard, *Eur. J. Pharm. Sci.*, 2012, **46**, 72–8.

80 S. J. Lee, G. L. Pishko, G. W. Astary, T. H. Mareci and M. Sarntinoranont, *J. Appl. Polym. Sci.*, 2009, **114**, 1992–2002.

81 J. K. Francis Suh and H. W. T. Matthew, *Biomaterials*, 2000, **21**, 2589–2598.

82 J. L. Drury and D. J. Mooney, *Biomaterials*, 2003, **24**, 4337–4351.

83 H. Geckil, F. Xu, X. Zhang, S. Moon and U. Demirci, *Nanomedicine*, 2011, **5**, 469–484.

84 M. Stieger, P. Lindner and W. Richtering, *J. Phys. Condens. Matter*, 2004, **16**, 3861–3872.

85 T. Y. Wong, C. M. G. Cheung, M. Larsen, S. Sharma and R. Simó, in *Nature Reviews Disease Primers*, Macmillan Publishers Limited, 2016, vol. 2, p. 16012.

86 W. M. Al-Zamil and S. A. Yassin, *Clin. Interv. Aging*, 2017, **12**, 1313–1330.

87 T. Y. Wong, R. Klein, F. M. A. Islam, M. F. Cotch, A. R. Folsom, B. E. K. Klein, A. R. Sharrett and S. Shea, *Am. J. Ophthalmol.*, 2006, **141**, 446–455.

88 W. Smith, J. Assink, R. Klein, P. Mitchell, C. C. W. Klaver, B. E. K. Klein, A. Hofman, S. Jensen, J. J. Wang and P. T. V. M. de Jong, *Ophthalmology*, 2018, **108**, 697–704.

89 L. Antonov and D. Nedeltcheva, *Anal. Lett.*, 1996, **29**, 2055–2069.

90 H. L. Sham, D. J. Kempf, A. Molla, K. C. Marsh, G. N. Kumar, C. M. Chen, W. Kati, K. Stewart, R. Lal, A. Hsu, D. Betebenner, M. Korneyeva, S. Vasavanonda, E. McDonald, A. Saldivar, N. Wideburg, X. Chen, P. Niu, C. Park, V. Jayanti, B. Grabowski, G. R. Granneman, E. Sun, A. J. Japour, J. M. Leonard, J. J. Plattner and D. W. Norbeck, *Antimicrob Agents Chemother*, 1998, **42**, 3218–3224.

91 V. Oldfield and G. L. Plosker, *Drugs*, 2006, **66**, 1275–1299.

92 E. M. Donato, C. L. Dias, R. C. Rossi, R. S. Valente, P. E. Fröehlich and a.

M. Bergold, *Chromatographia*, 2006, **63**, 437–443.

93 S. N. Hiremath and C. H. Bhirud, *J. Taibah Univ. Med. Sci.*, 2015, **10**, 271–277.

94 D. Samaha, R. Shehayeb and S. Kyriacos, *Dissolution Technol.*, 2009, **16**, 41–46.

95 C. Solas, I. Poizot-Martin, M. Drogoul, I. Ravaux, C. Dhiver, A. Lafeuillade, T. Allegre, M. Mokhtari, J. Moreau, G. Lepeu, N. Petit, A. Durand and B. Lacarelle, *Br. J. Clin. Pharmacol.*, 2003, **57**, 436–40.

96 D. Fischer, Y. Li, B. Ahlemeyer, J. Krieglstein and T. Kissel, *Biomaterials*, 2003, **24**, 1121–31.

97 T. L. Riss, R. A. Moravec, A. L. Niles, S. Duellman, H. A. Benink, T. J. Worzella and L. Minor, in *Assay Guidance Manual*, eds. G. S. Sittampalam, N. P. Coussens, K. Austin, A. Grossman, M. Arkin, D. Auld, C. Dahlin, J. Bael, B. Bejcek, T. D. Y. Chung, J. Glicksman, V. Devanaryan, T. L. Foley, M. Iversen, M. D. Hall, J. V Hass, J. Inglese, P. W. Li, S. D. Kahl, S. C. Kales, M. Lal-Nag, Z. Li, J. McGee, O. McManus, T. Riss, O. J. Trask, J. R. Weidner, M. Xia and X. Xin, Eli Lilly & Company and the National Center for Advancing Translational Sciences, Bethesda, MD, 2004, pp. 355–386.

98 H. Zhang, J. Y. Lee, A. Ahmed, I. Hussain and A. I. Cooper, *Angew. Chemie*, 2008, **47**, 4573–4576.

99 J. H. Lee, I. J. Gomez, V. B. Sitterle and J. C. Meredith, *J. Colloid Interface Sci.*, 2011, **363**, 137–144.

100 A. D'Avolio, L. Baietto, M. Siccardi, M. Sciandra, M. Simiele, V. Oddone, S. Bonora and G. Di Perri, *Ther. Drug Monit.*, 2008, **30**, 662–669.

Chapter 4

Investigation into the Effect of Nanogel Size on Phase Behaviour, Rheological Properties and Release Behaviour

Publications arising from this chapter:

"Tuning HIV drug release from a nanogel-based in situ forming implant by changing nanogel size"

A. R. Town, J. Taylor, K. Dawson, E. Niezabitowska, N. M. Elbaz, A. Corker, E. Garcia-Tuñón and T. O. McDonald

Journal of Materials Chemistry B, 2019, **7**, 373–383

4.1. Introduction

An in situ forming implant (ISFI) based on the aggregation of dual responsive behaviour of polyNIPAM nanogels was discovered in Chapter 2 and developed in Chapter 3. It was anticipated that the size of the nanogel used in this ISFI would have an impact on the ISFI behaviour, in terms of phase behaviour, rheological properties, drug payload entrapment and drug release rate. Hence a range of four different sized polyNIPAM nanogels were synthesised and studied to demonstrate how size modifies this set of properties. Alongside nanogel size, the effect of temperature, dispersion concentration and ionic strength on the phase transition and rheological behaviour of the nanogel dispersions was also studied.

4.1.1. Nanogel Size Effect on Internal Structure

Less than a decade after the discovery of polyNIPAM nanogels in 1986 by Pelton and Chibante,[1] studies began to probe the internal structure of nanogels. It was found that heterogeneous cross-linking density existed within the nanogel particles under investigation,[2] with Pelton speculating that a zone of relatively high cross-linking density existed within the particles, due to the commonly employed N,N′-methylenebis(acrylamide) (BIS) cross-linking agent reacting faster than the NIPAM monomer.[3] Other studies concluded that a higher cross-link density core and lower cross-link density shell exists within polyNIPAM nanogels,[4] known as a core-shell structure.[5] Some variation in the nature of this structure was found depending on the synthesis conditions of the nanogels studied, with examples including the proposal of a uniform cross-link density core, and shell with graduated decrease in cross-link density,[6] and the existence of a thin shell (20 nm) which is polyelectrolyte rich.[7] It was also found that the core-shell structure could be influenced by different factors, such as the amount of cross-linking agent used.[6] A homogeneous cross-link density can also be achieved if the feed of monomer and cross-linking agent into the polymerisation reaction are regulated. This produces optically clear particles, as a highly cross-linked core is avoided.[8] Sodium dodecyl sulphate (SDS) is commonly employed to synthesise nanogels of different sizes.[9] Importantly, whilst controlling the size of the nanogel, SDS concentration also appears to have an effect on nanogel internal structure. The ratio of radius of gyration to hydrodynamic radius (R_g/R_h) describes the distribution of mass within a sphere, sometimes referred to as the shape

factor, ρ. Homogeneous radial density spheres have a ρ value of 0.775, and a swollen nanogel with a denser core typically has a ρ value of ~0.6.[10] Arleth *et al.* used a high concentration of SDS to create nanogels below 100 nm in size. These nanogels had a homogeneous cross-link density instead of a core-shell structure with a ρ value close to that of a sphere of homogeneous radial density (0.775).[11] It was suggested that high SDS concentration prevents the formation of permanent solid particles by creating a better solvent environment in the polymerisation to give more homogeneous particles.[12] As the SDS concentration was lowered to create larger particles, an increasing degree of core-shell internal structure was presented, with a correspondingly lower ρ value of 0.73 at 25 °C measured for nanogels of 116 nm in diameter.[13] Similar results are seen in other work.[10,14] To summarise, if nanogels are synthesised at low SDS concentration, large nanogels with a core-shell structure will form (figure 4.1, a), and a high SDS concentration will give small nanogels with a uniform radial density (figure 4.1, b). In between high and low SDS concentration, an intermediate structure exists, which contains some core-shell character. It is likely that not only nanogel size, but the variation in internal nanogel structure that accompanies different sized nanogels will alter the nanogel phase behaviour, rheological properties, and drug payload entrapment and release rate.

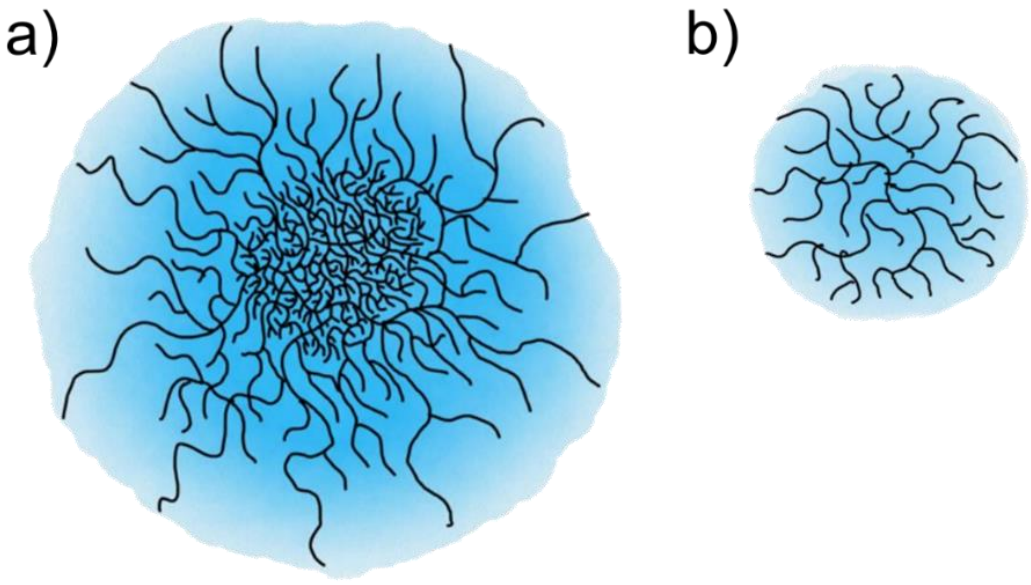

Figure 4.1 Illustration of polyNIPAM nanogel structure in terms of cross-linking density when synthesised using SDS a) low SDS concentration; large nanogel (>100 nm) with highly cross-linked core, and shell of decreasing cross-link density, b) high SDS concentration; small nanogel (<100 nm) with uniform cross-linking density.

4.1.2. Phase Studies

In using polyNIPAM nanogels as an ISFI, it would be of great benefit to understand the phase behaviour and rheological properties of the nanogels under the various conditions experienced by the nanogels when used as an ISFI. Although the macroscopic phase changes from ambient to body temperature was shown visually in Chapter 3 (figure 3.4), it would be useful to study the phase behaviour in more detail. An understanding of how the phase behaviour occurs over a range of concentrations, nanogel sizes and associated internal structure, and temperatures, would be very useful when designing the optimal conditions for an ISFI based on nanogels.

The aggregation of polyNIPAM nanogels above the VPTT temperature and at sufficient ionic strength, which was demonstrated in chapter 2 and 3, is a phase separation, which is just one of many possible rich phase change behaviour that can occur in a polyNIPAM dispersion.[15] Interestingly, unlike other nanogel dispersions, polyNIPAM nanogels are able to undergo thermoreversible gelation, transitioning from a liquid to a shrunken gel as the temperature increases.[16] Other phase changes such as a swollen gel transition at low temperature and high concentration, and colloidal crystal fluids have also been observed in polyNIPAM based nanogels.[16–19] Xiong *et al.* found the existence of at least four phases for polyNIPAM-co-acrylic acid nanogels.[18] For inter-penetrating polymer networks of polyNIPAM and poly(acrylic acid) nanogels, six phases were observed.[17] These phases are possible because of the many different combinations of colloidal interactions between the nanogels under specific conditions.[5] Below the VPTT colloidal interactions between nanogels include the steric stabilisation by polymer chain ends extending out from the particle into solution.[20] This steric stabilisation is lost above the VPTT, however, as the nanogels deswell, the charges introduced from the initiator on the polymer chain ends are concentrated more closely together giving an enhanced electrostatic repulsion between the nanogels. Above the VPTT the attractive dispersion interaction is also much greater.[21] PolyNIPAM nanogel dispersion phases have been studied previously using techniques such as visual observations, rheology[16,19,22–25], microscopy,[23] static and dynamic light scattering[26–28], SANS[26], DSC and turbidimetry.[29] Rheology is a useful and widely used technique for studying the phase behaviour of nanogel dispersions, as the shear storage (G') and shear loss (G'') modulus' of oscillatory rheometry often

change dramatically between different phases,[16,22,24,30,31] allowing the supplementation of visual observations of phase transitions more accurately with rheological measurements.

There are a number of reasons why it is important to study and understand how these phases occur with different nanogel size, concentration, temperature and ionic strength. First of all, phase changes may occur very close to ambient or body temperature. This could be an issue, for example, if a solidification phase change occurs just above 25 °C. If the ambient temperature of an environment is not well regulated, then an increase in temperature could cause nanogels to solidify in storage, or in the syringe before being injected. This problematic solidification would also be enhanced if heat was transferred to the syringe as it was handled during injection preparation. Alternatively, if macroscopic aggregation at physiological salt strength only occurs just below mean body temperature, then solidification could be very slow or unsuccessful, as body temperature fluctuations occur at different sites in the body and across different patients.[32,33] Therefore, any solidification phase change behaviour should ideally lie well above the upper limit of recommended temperature for storage of essential medicines (25 °C),[34] and aggregation should lie well below core body temperature (37 °C).[35] Phase changes and rheological properties of a nanogel dispersion are also likely to be dependent on their concentration. A dispersion which is too concentrated may be too viscous to inject. A lower concentration would give a liquid a room temperature, which is easier to formulate and inject, however, if the concentration is too low then the dispersion may not macroscopically aggregate until a higher temperature is reached. Hence a concentration range of a nanogel dispersions at different temperatures could be studied to build a two-dimensional understanding of phase behaviour. A further factor for consideration is how the size and internal structure of a nanogel used will also likely influence the temperature dependence of phase behaviour and the rheological properties of the different phases. Nanogels of a certain size may provide optimum performance in regards to their use as an ISFI. To summarise, under certain combination of nanogel size, concentration and temperature, unexpected phases and rheological properties may exist which hinder the performance of the nanogels as an ISFI, these variables need to be identified.

4.1.3. Drug Release

The size and internal structure of nanogels used is also likely to affect the maximum drug loading and release rate from a polyNIPAM nanogel and SDN loaded ISFI. The maximum payload of solid drug nanoparticles that can be successfully loaded into a polyNIPAM nanogel ISFI is also not yet known. This is an important factor to understand, as the larger the payload, the less depot material is required to be injected to obtain the same therapeutic effect. It is anticipated that as wt% of payload is increased there will eventually become a point at which burst release occurs, as there is no longer enough aggregate material to form a mechanically stable depot which can contain the payload. Many matrix controlled drug delivery systems contain a large burst release (~30 to 80%) regardless of the size of the payload,[36,37] and so if high loading can be achieved without burst release occurring, this gives the nanogel system a very useful advantage.

Nanogel size and internal structure may also have an effect on drug release rate. Drug release rate from a matrix is dependent on many factors such as drug characteristics, formulations aspects, and polymer variables, which all influence the release constant.[38] However, by keeping all aspects fixed except for nanogel size, the variation in release rate is limited to potential changes to the structure of the matrix due to the usage of different sized nanogels. When drug release occurs in a hydrophobic polymer matrix, particularly for drug loaded at a concentration above its solubility limit, release of the drug occurs via diffusion through interconnected water-filled pores.[38–40] It is anticipated that nanogels of different size will create aggregates of different pore size and pore interconnectivity, and hence change the diffusion rate of drug through the matrix. In terms of pore size, the pores created between the packing of larger nanogels (and openings between these pores) are naturally likely to be larger and so allow greater permeability than those between smaller nanogel particles.[41] In terms of pore interconnectivity, polyNIPAM nanogels act as soft spheres,[42] which as a concentrated dispersion undergo compression, deformation, and possibly interpenetrate.[31,43,44] Hence it is important to understand the role of nanogel size and structure on release.

4.1.4. Aims

The main aim of this chapter is to investigate how different sized nanogels determine the phase behaviour, rheological properties and drug entrapment and release from a nanogel depot.

In doing so the following objectives will be achieved:

- The synthesis and characterisation of polyNIPAM nanogels across a range of four different nanogel sizes and internal structures.
- Determine how phase changes across different nanogel sizes, concentrations and temperatures in water occur. This will lead to the selection of a nanogel dispersion concentration with most interesting phase behaviour to study in PBS (1X strength, pH 7.4) to compare phase behaviour with water.
- Study of rheological changes in water and PBS (1X strength, pH 7.4) based dispersions of nanogels with a comparison to visual phase changes.
- Examination of how a) drug release rate and b) burst release is affected by aggregates formed from different sizes of nanogel, and with different wt% of payloads. This includes finding the maximum wt% of payload that can be successfully employed before a large burst release and mechanical failure of the depot occur, as well as an *in vitro* release study to determine drug release rates.

4.2. Results and Discussion

4.2.1. Nanogel Synthesis and Dilute (1 mg mL^{-1}) Dispersion Characterisation

Nanogels of four different sizes were synthesised by using different amounts of the surfactant sodium dodecyl sulphate (SDS) (table M.4.1, methods), following the relationship previously reported by Pelton *et al*.[9] The relationship between nanogel size and SDS concentration used can be seen in figure A.1, Appendix. These samples are denoted PNA65, PNA160, PNA310 and PNA450, corresponding to their hydrodynamic diameter in water at 25 °C, and should not be confused with allylamine content, as allylamine was not used in the synthesis of these nanogels as in the previous chapter. The mean hydrodynamic diameter and polydispersity index (PdI) of each nanogel as determined by three DLS measurments was: PNA65, 65 nm, 0.13;

PNA160, 160 nm, 0.02; PNA310, 310 nm, 0.01; PNA450, 450 nm, 0.03. The size distribution of the samples as determined by DLS can be seen in figure 4.2. a), and the clear relationship between particle size and scattering intensity can be seen in figure 4.2 b). Tyndall scattering was observed for PNA310, (figure A.2, Appendix), while samples with a larger diameter were completely turbid.

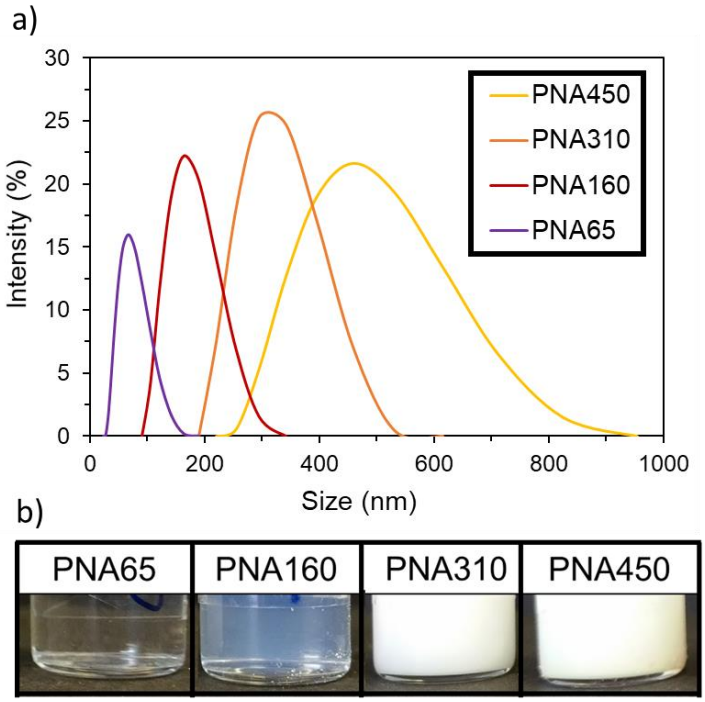

Figure 4.2. Nanogels synthesised in a range of sizes a) DLS size distribution by intensity at 25 °C for each nanogel as a 1 mg ml^{-1} aqueous dispersion, samples measured in triplicate and mean value used. b) Nanogel dispersion turbidity as a 15 mg ml^{-1} aqueous dispersion at 25 °C.

The change in hydrodynamic diameter of these nanogels in response to a rise in temperature when dispersed in water can be seen in figure 4.3. At the lowest temperature measured (15 °C), the nanogels were at their most swollen state, and hence at their maximum hydrodynamic diameter at this temperature. All samples then showed the characteristic thermoresponsive behaviour of polyNIPAM nanogels, with a dramatic decrease in hydrodynamic diameter at the VPTT of 34 °C, at which de-swelling occurs at a much greater rate with rise in temperature. As discussed in previous chapters, this occurs as the polymer-solvent hydrogen bonding becomes less

favourable and the polymer-polymer interactions dominate. The samples also all displayed similar swelling/deswelling behaviour, as was quantified by the swelling ratio (the ratio of the nanogel diameter at a given temperature to the diameter at 55 °C), (figure A.3, Appendix). All samples displayed values of 1.75-1.93 at 25°C. It can be noted that smaller nanogels PNA65 and PNA160 underwent greater deswelling upon heating with swelling ratios (at 25 °C) of 1.83 and 1.93 compared to the larger nanogels which had swelling ratios of 1.77 and 1.75 for PNA310 and PNA450 respectively, (table 4.1).

Table 4.1 Swelling ratio of nanogels diameter upon cooling from 55 to 25°C.

Sample	PNA65	PNA160	PNA310	PNA450
Swelling Ratio[a]	1.83	1.93	1.77	1.75

[a]Swelling ratio calculated from DLS measurement of hydrodynamic diameter (H_d) using 1 mg ml^{-1} aqueous dispersion, swelling ratio = H_d (25°C) / H_d (55°C)

This was likely due to differences in the internal structures of the nanogels, as discussed in section 4.1.1, it has previously been shown that using a higher concentration of SDS (c.a. 1.9 mg mL^{-1}) during the dispersion polymerisation route used for nanogels creates smaller more homogeneous partices.[12] While, using a lower concentration of SDS (c.a. 0.15 mg mL^{-1}) generates larger particles with a more heterogeneous structure which contains a dense gel particle core.[11] Therefore, it is likely that the larger particles contained a denser core which can be considered to have restricted swelling, surrounded by a less densely cross-linked polymer shell. PolyNIPAM nanogels have previously been shown to undergo less swelling when the particle is restrained by a highly cross-linked core, compared to greater swelling when cross-linking is homogeneous.[8] This core-shell type structure is likely to have caused restraint in the amount of swelling able to take place in the larger nanogels (PNA310 and PNA450), and hence the swelling ratio decreases with increasing nanogel particle size.

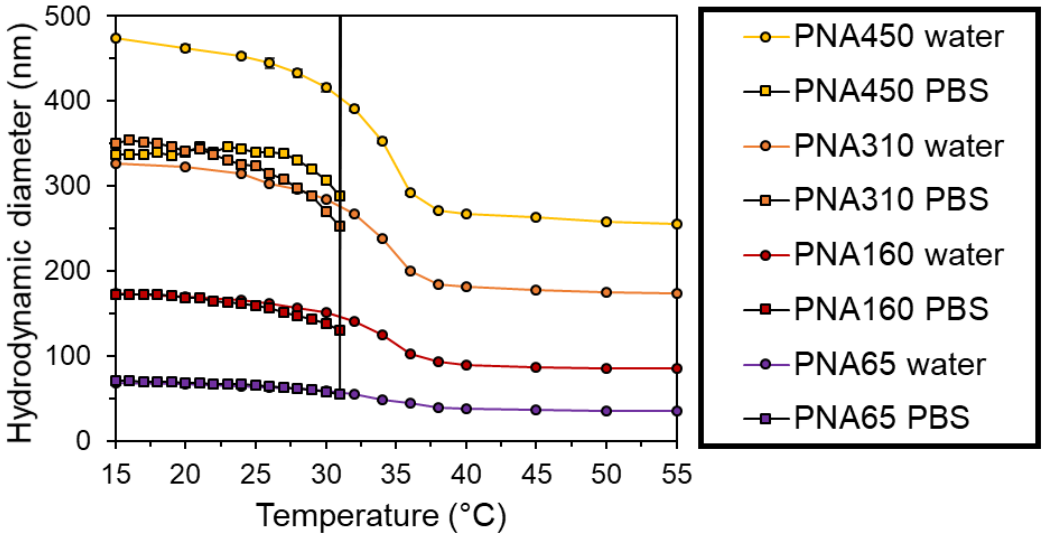

Figure 4.3. Hydrodynamic diameter of nanogels in Type I distilled water with a resistivity of >18 MΩ cm^{-1} water (circles) and PBS (1X strength, pH 7.4) (squares), samples measured using DLS with the mean value of triplicate measurements used.

The existence of a core-shell structure in the larger nanogels can also be seen in zeta potential and turbidity properties of the nanogel samples. The zeta potential was measured below (25 °C) and above (40 °C) the VPTT as shown in (figure 4.4). The zeta potential at 25 °C was similar for all the samples with the values ranging between -11.7 and -18.1 mV. When the nanogels were heated to a temperature of 40 °C all the samples become more charged with zeta potential values between -19.6 and -36.9, with a clear trend for samples with larger mean diameters having greater surface charge. The larger nanogels also have a much higher turbidity (figure 4.2, b). Andersson and Maunu showed that a similar substantial zeta potential increase and higher turbidity was seen for polyNIPAM nanogels with a hydrodynamic diameter of 194 and 400 nm, but not for smaller nanogels synthesised with a higher SDS concentration. Only the larger nanogels formed a highly cross-linked core, which gave rise to a higher turbidity and a polyelectrolyte rich shell.[12] Another study into core-shell nanogels also found that they contained a polyelectrolyte rich shell.[7] Based on swelling ratio, zeta potential and turbidity, it is reasonable to speculate that PNA450 and PNA310 have a core-shell like nature, whilst PNA65 effectively has a homogeneous internal structure, and PNA160 lies between the two structures.

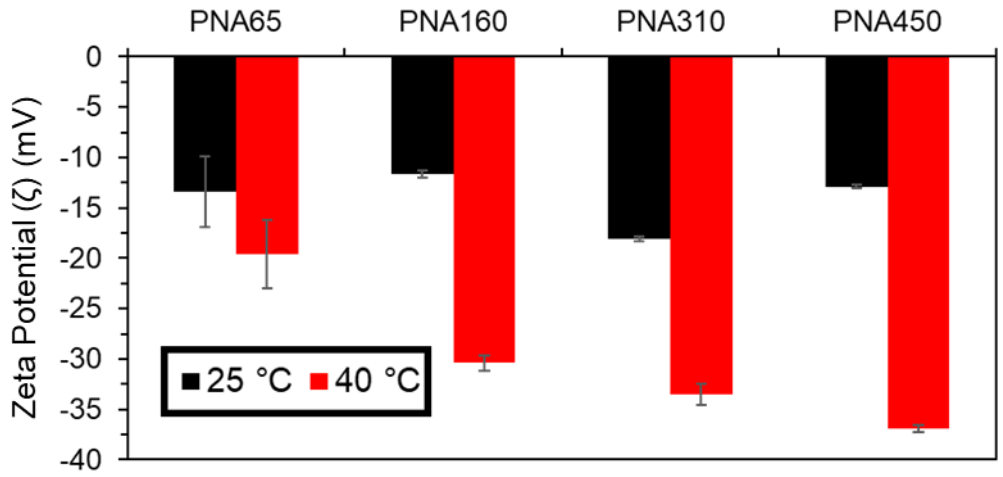

Figure 4.4. Zeta Potential measurements of nanogels at 25 °C and 40 °C, measured using Laser Doppler Electrophoresis with 1 mg ml^{-1} aqueous dispersions with 10 mM NaCl at pH 7 and taking the mean value of triplicate measurements.

When the nanogels were dispersed in PBS below their VPTT, (figure 4.3), generally each nanogel sample had approximately the same diameter in PBS as in water at the same temperature, however, the PNA450 nanogel had a significantly smaller diameter when dispersed in PBS compared to water, with a 24% reduction in diameter at 25 °C, giving it a diameter similar to PNA310 when dispersed in PBS. In water the sulphate groups from the initiator fragment located at the end of the polymer chains may provide some swelling due to the electrostatic repulsion within the particles, in the presence of PBS these charges will be screened by the increased concentration of ions and result in less swelling. Vincent and Rasmusson have shown that even a low NaCl concentration led to a reduction in the diameter of larger (700 nm) particles due to electrolyte screening of sulphate initiator fragments on the surface of the nanogel.[21] In the synthesis of nanogels, growth continues until a large enough charge density to achieve colloidal stability is achieved.[2,20] Hence, PNA450 is expected to contain the greatest amount of sulphate groups in each particle and the screening of these charged groups hence causes a pronounced shrinkage in diameter, as the swelling caused by a high amount of sulphate groups is reduced in PBS. Heating the nanogels in PBS resulted in the aggregation of the particles. It was seen that aggregation occurs at 33 °C for all samples, being completely independent of the particle size in a dilute dispersion. This aggregation was due to the loss of all colloidal stabilisation of the particles. Below the VPTT the nanogels were sterically stabilised by the solvated polymer chains on the surface of the particles,[20] and electrostatically stabilised by the

surface charge provided by the sulphate groups at the chain ends that were derived from the persulfate initiator.[9] Upon heating above the VPTT the steric stabilisation was likely lost as the solvated surface chains collapse and any colloidal stability was from the electrostatic repulsion between the particles.[45] However, in the presence of PBS the electrostatic repulsion was screened and the particles aggregated.[46] Increasing the ionic strength of the solvent has the effect of it becoming a poorer solvent for the nanogels. Hence, the aggregation occurs at lower temperature with increasing NaCl concentration, (table A.1, Appendix), as the polymer-polymer hydrogen bonding becomes more favourable than the polymer-solvent hydrogen bonding.[44] This result is similar to previous work by Vincent *et al*.[21]

4.2.2. Phase Behaviour

The samples were then prepared at a range of higher concentrations in order to draw a comparison between the data generated on the dilute dispersions and phase behaviour of the concentrated nanogels. In order to use nanogels at a higher concentration the nanogels were first lyophilised and then dispersed. To ensure complete dispersion of the nanogels the hydrodynamic diameter and PdI of the samples were measured before and after dispersal. It was found PNA65, PNA160 and PNA310 fully dispersed upon mechanical mixing, but PNA450 required a short period of sonication to fully disperse the sample (table A.2, Appendix).

In order to allow direct comparison between the different nanogel samples the phase behaviour of the samples dispersed in water was investigated in detail. The maximum concentration was limited by the amount of nanogel which could be dispersed to give a homogeneous dispersion, and so the nanogels were studied in increments of 2 wt% from 2 wt% up to a maximum value for each nanogel of: PNA65, 24 wt%; PNA160, 16 wt%; PNA310, 22 wt%; PNA450, 16 wt%. The samples were heated from 20 °C to 45 °C in 1 °C increments. The temperature responsive swelling of the nanogels resulted in a rich phase behaviour with swollen gel, liquid, shrunken gel and aggregate (phase separation) phases all observed under specific combinations of nanogel size, concentration and temperature, as seen in previous work.[47,48] Each of the four phases are shown using example combinations of nanogel size, concentration and temperature in figure 4.5.

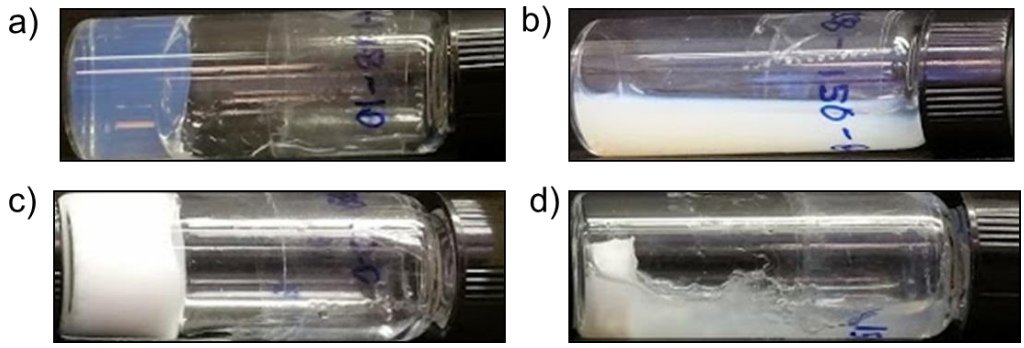

Figure 4.5 – Nanogel phases, a) swollen gel (PNA160, 10 wt%, 25 °C), b) liquid (PNA160, 10 wt%, 40 °C), c) shrunken gel (PNA65, 20 wt%, 40 °C), d) aggregate (phase separation) (PNA160, 16wt%, 40 °C).

The phase diagrams in figure 4.6, a) reveals the phase changes with temperature and concentration for each size of nanogel. At low temperature the three larger nanogel samples PNA160, PNA310 and PNA450 all showed a liquid to swollen gel transition above a certain concentration. At 20 °C swollen gels were observed at all concentrations above 7 wt% for PNA160 and 10 wt% for both PNA310 and PNA450. The swollen gels all had a low turbidity and were self-supporting. At higher temperatures an increased concentration of nanogel was required before a swollen gel was obtained, likely due to the smaller diameter of the particles as the temperature increases towards the VPTT. At temperatures below 30 °C nanoparticle interaction potential can be considered as purely repulsive,[23] with no significant change in the attractive part of the interaction potential. The swollen gel phase arises due to a volume blocking mechanism of hard sphere theory in which the nanogel spheres become close packed without significant deformation.[31,49] As the particles deswell upon heating this swollen gel transitioned into a turbid liquid, as seen in other polyNIPAM nanogels dispersions.[50] The deswollen particles were no longer large enough to form a gel through volume blocking, and hence a higher concentration is required to obtain a swollen gel at this temperature. Turbidity also increased with temperature due to the increased difference between the refractive index of the nanogel particles and the surrounding liquid.

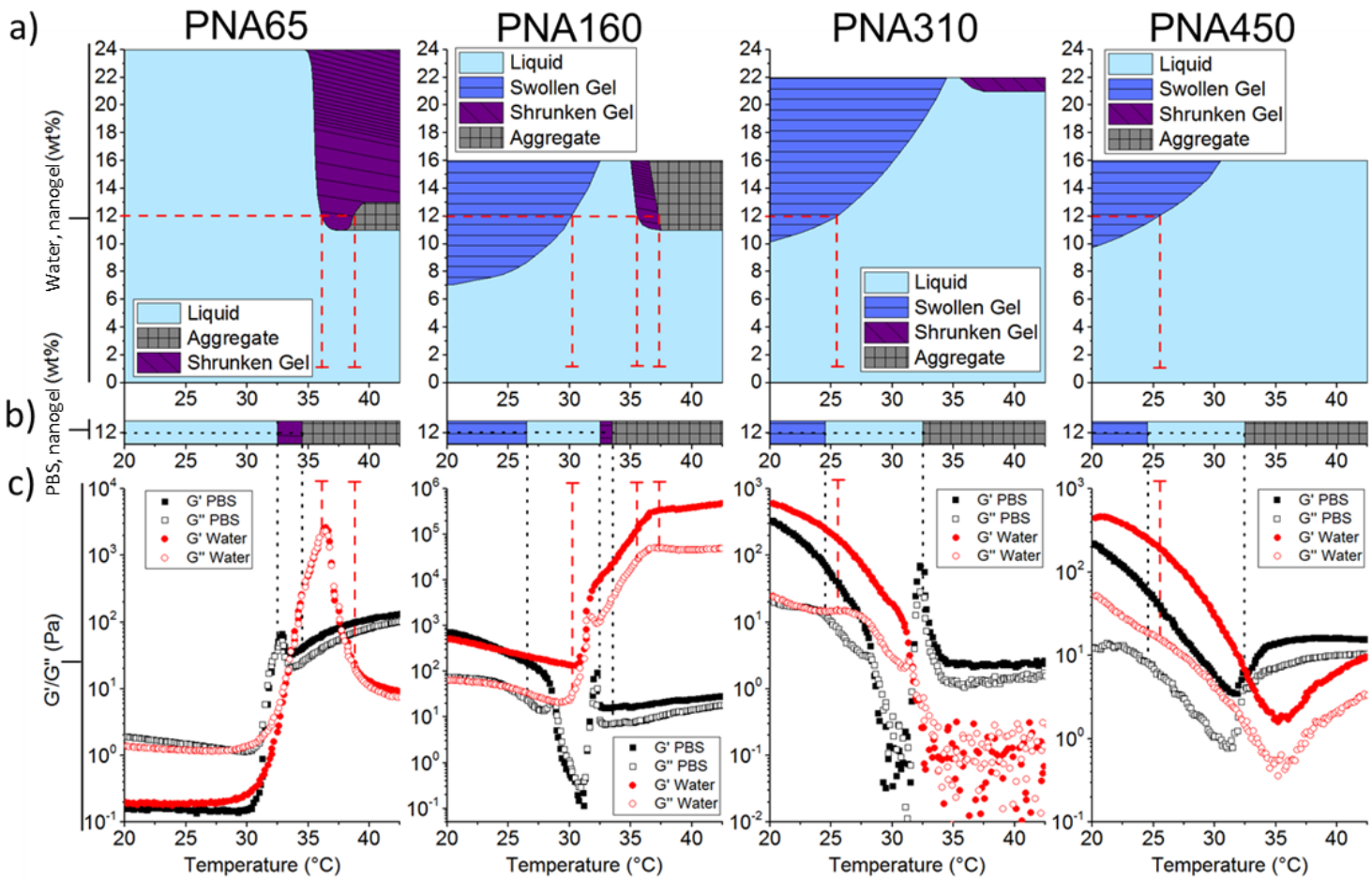

Figure 4.6 – Comparison of nanogel phase behaviour and rheological properties in water and PBS at temperatures between 20 °C and 45 °C with a heating rate of 1 °C min^{-1} for the different nanogel samples with mean diameters from smallest (left) to largest (right), 65 nm, 160 nm, 310 nm and 450 nm respectively. a) The phase diagrams of different nanogel samples dispersed in water at concentrations ranging from 2 wt% up to a maximum of 24 wt%. b) The phase diagrams of nanogel samples dispersed in PBS at 12 wt%. c) Rheological measurements of 12 wt% nanogels dispersions. Lines are a guide for the eye between the phase changes seen in the phase diagrams in water (dashed line) and PBS (dotted line) and the rheological data.

The temperature at which the swollen gel to liquid transition occurred can be explained when considering the effective volume fraction (φ_{eff}) of the different nanogels. The effective volume fraction gives a measure of the packing of the nanogels, and is both temperature and concentration dependent. An effective volume fraction of ~0.74 is the close packing limiting value for monodisperse hard spheres,[51] when the effective volume fraction is greater than this value the particles are restricted to volumes smaller than their dilute solution equilibrium swelling volumes.[23] Hence if the spheres are able to compress and deform a value greater than this can be achieved.[19] This is because the effective volume fraction does not take into account any effect of deformation, deswelling or interpenetration of particles on the volume fraction.[52] The effective volume fraction can be estimated using the viscosity of a dilute dispersion and the Batchelor equation (Figure 4.7, Equation (1).[53,54] Along with equation (2) and (3), this has been used to calculate the effective volume fraction of polyNIPAM nanogel dispersions in many previous studies.[19,23,24,28] If equation (2) is substituted into equation (1), the conversion constant (k) at a given temperature can be determined by fitting the Batchelor equation to measurements of viscosity at different dilute concentrations as a fixed temperature. The value of k can then be used in conjunction with the ratio of hydrodynamic diameters of a nanogel at different temperatures, equation (3), to obtain effective volume fraction at different temperatures for a given dispersion concentration.

$$(1)\quad \eta_{rel} = 5.9\varphi_{eff} + 2.5\varphi_{eff} + 1$$

$$(2)\quad \varphi_{eff} = kc$$

$$(3)\quad \varphi_{eff}(T) = kc(20\,^{\circ}\mathrm{C})\left[\frac{D_h(\mathrm{T})}{D_h(20\,^{\circ}\mathrm{C})}\right]^3$$

Figure 4.7 Equations used to calculate φ_{eff}. (1) Batchelor equation, η_{rel} = relative viscosity, c = concentration in w/w %, k = constant, φ_{eff} = effective volume fraction. (2) k = conversion constant. (3) D_h = hydrodynamic diameter, T= temperature (°C).

The relative viscosity (η_{rel}) of a range of dilute dispersions at different concentrations at 20 °C was measured, (figure 4.8, a), which gave a conversion constant (k) for each nanogel at this temperature (table A.3, Appendix). The value of k for each nanogel at 20 °C was then used to calculate the effective volume fraction at different temperatures, illustrated in figure 4.8, b) for a 12 wt% dispersion of each nanogel.

In the case of the nanogels, it was found that the smaller the nanogel the larger the effective volume fraction, and an increase in temperature causes the effective volume fraction for each nanogel to decrease. At the temperature of visual transition from swollen gel to liquid for a 12 wt% dispersion, the effective volume fraction for PNA160, PNA310 and PNA450 is 1.1, 1.1 and 1.0 respectively, see (*) and dashed line in figure 4.8 b). This suggests that the three larger nanogels are able to deform, deswell or interpenetrate slightly, as observed previously,[55] with the nanogels behaving as soft spheres below 30 °C.[56] This is most likely possible due to the existence of a lower cross-linking density shell.

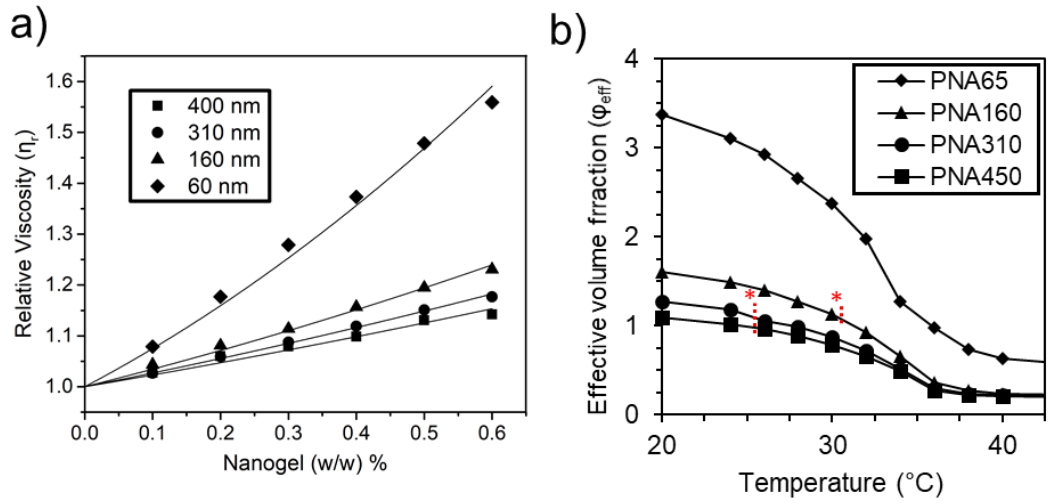

Figure 4.8 Determination of effective volume fraction (φ_{eff}) using the Batchelor equation and viscometry data. a) Relative viscosity data for nanogels measured at 20 °C fitted with Batchelor equation ($\eta_{rel}=5.9(kc)^2+2.5(kc)+1$, $\varphi_{eff}=kc$). b) φ_{eff} of 12 (w/w) % nanogel aqueous dispersion across a temperature range. PNA450, (squares) PNA310 (circles), PNA160 (triangles) and PNA65 (diamonds). Swollen gel to liquid visual phase transition occurs at dashed line (*).

The fact that the transition from swollen gel to liquid occurs at the same effective volume fraction for all three of the larger nanogels suggest they have a similar core shell structure, allowing the same degree of deformation, deswelling or interpenetration. Therefore any temperature induced deswelling of the particles (as shown in figure 4.3) that lowers the effective volume fraction below ~1 will lead to a swollen gel to liquid transition. Using this value the temperature this transition occurs at for other dispersion concentrations can be predicted with a good correlation with the actual temperature the phase transition was observed at for PNA160, PNA310 and

PNA450. This is demonstrated in table 4.2, where different nanogels and dispersion concentrations give a predicted transition temperature close to the transition temperature observed in figure 4.6.

Table 4.2 Comparison of predicted and visual swollen gel to liquid temperature transition for aqueous dispersions of different sized nanogels.

Nanogel	Dispersion wt%	Predicted transition temperature[a]	Visual transition temperature[b]
PNA450	16	30	30.5
PNA310	16	31	30
PNA310	22	33.5	34
PNA160	16	33	32.5

[a]Based on temperature at which φ_{eff}=1.1 for a given wt% dispersion concentration.
[b]As observed in visual phase transition (figure 4.6).

Interestingly, the smallest nanogel PNA65 did not display a swollen gel phase under the conditions tested, even at concentrations exceeding 12 wt% at 20°C, and despite this sample having an effective volume fraction well over 1. The viscosity of PNA65 was found to be considerably higher than the other three nanogel samples. Tan *et al* and Wolfe have previously shown that the viscosity of nanogels increases with decreasing cross-linking density,[57,58] and Senff and Richtering determined polyNIPAM nanogels of lower cross-linking density to act as softer particles.[42] Therefore, it is likely that PNA65 was composed of a lower cross-linking density without a dense gel core, and so the particles contained more lightly cross-linked chains with linear polymer character, and hence were able to have more hydrodynamic corona overlap,[24] reducing the mobility of the particles and giving a larger calculated effective volume fraction.[22,29] Despite an apparently high volume fraction the PNA65 nanogel cross-linking density was not of sufficient density to be able to form a swollen gel phase even at a high wt%. Instead, we propose that the nanogels are soft spheres which able to undergo large deformations to remain fluid as they behave more like lightly cross-linked polymers with linear polymer characteristics than hard spheres.[19] This is likely due to their perceived lack of core-shell structure, in which heterogenous cross-linking leads to a more highly cross-linked core which resists deformation. Bae and Han previously showed that no swollen gel phase was observable for linear polymers as a high concentration dispersion.[59]

The PNA65 sample did however form a shrunken gel at concentrations above 11 wt% and above 35 °C. The shrunken gel was also self-supporting but with high turbidity and a small excess of water expelled upon formation. Shrunken gel formation was observed for the PNA160 sample at the same temperature and concentration. The PNA310 sample only formed a shrunken gel above 21 wt% and 36 °C. While the largest nanogel sample PNA450 displayed no shrunken gel phase. It is clear that as the nanogel samples increased in diameter then a greater concentration was required for shrunken gel to be observed, it is most likely that this was not observed for PNA450 due to it occurring at a higher wt% than could be successfully dispersed and studied. This shrunken gel was formed due to the increasing tendency of the nanogels to become more hydrophobic and favour polymer-polymer instead of polymer-water hydrogen bonds as the temperature increases, favouring aggregation,[44,60] as well as an increasing electrostatic repulsion to prevent this aggregation occuring.[30] This balance of interactions results in a network structure forming throughout the continuous phase. The larger zeta potential of the larger nanogels at higher temperature appears to resist the formation of a shrunken gel unlike the smaller, lower zeta potential nanogels. Further heating of PNA65 and PNA160 resulted in complete phase separation resulting in aggregate formation for PNA65 above 38 °C when at 12 wt%, and for PNA160 above approximately 37 °C for any concentration above 11 wt%. This morphology is likely due to the complete aggregation of the nanogel particles. As aggregates were only observable in PNA65 and PNA160, it may be due to these nanogels having the smallest zeta potential at elevated temperature (figure 4.3), which was not sufficient to overcome the driving force for the nanogels to aggregate.

The phase behaviour of the four nanogel samples were then tested in PBS at 12 wt%, a concentration selected that showed phase changes for all four of the samples, allowing the effect of the PBS on the these phase changes to be observed, (figure 4.6, b). In the presence of PBS all samples exhibited at least 3 different phases. Samples PNA65 and PNA160 exhibited the same transitions as observed for the sample in water at 12 wt% but with lower transition temperatures. The larger nanogels PNA310 and PNA450 also displayed the liquid to swollen gel transition at lower temperatures in PBS compared to when dispersed in water, with the transition dropping from 25.5 to 24.5 °C for both samples. Additionally, these nanogel samples displayed an additional phase transition that was not observed in water at 12 wt%, the formation of aggregates

at 32.5 °C. The difference in phase transitions of the nanogels in PBS was likely driven by two main factors: Firstly, the increased polarity of the solvent when PBS was used instead of water will reduce the temperature at which polymer-polymer interactions dominate. Secondly, the ions in the PBS will screen the charges of the sulphate groups which provided electrostatic repulsion of the nanogels when they were dispersed in water. Therefore, the transition from a liquid to a shrunken gel phase occurred at a lower temperature in PBS. As the temperature was increased further the shrunken gel formed a phase-separated aggregate, likely due to the lack of either steric or electrostatic stabilisation. This behaviour is similar to that shown by Hu *et al*. where a shrunken gel was formed, but if the electrostatic repulsion was removed the sample would phase separate and form an aggregate.[16] In PBS the shrunken gel phase was found over a narrow temperature range, and only for PNA65 and PNA160. It is likely that when electrostatic repulsion has been heavily reduced in PBS, a shrunken gel can only occur when the particles still retain some supporting steric stabilisation below the LCST. Hence there is a transition to an aggregate when this is lost. When PNA310 and PNA450 were dispersed in PBS, the electrostatic repulsion between the particles was screened, and so all samples formed an aggregate as a 12 wt% PBS based dispersion.

4.2.3. Rheology Studies

Oscillatory rheology was also performed on the concentrated nanogel dispersions at 12 wt% in water and PBS, (figure 4.6 c),[‡‡] to compare the rheological properties of the dispersion with the visual phase behaviour in water, (figure 4.6 a), and PBS, (figure 4.6 b). The G' (storage modulus) and G'' (loss modulus) values were investigated as these values are the most relevant for studying the phase behaviour of the concentrated nanogel dispersions. A frequency of 1 Hz (6.28 rad s^{-1}) was used for all measurements as used previously in literature for similar nanogel dispersions and rheological experimental setup,[24,30] whilst an amplitude sweep was performed on each dispersion to find a suitable strain value within the linear viscoelastic range of each sample (figure A.4, Appendix) to perform a dynamic temperature sweep on each dispersion.

[‡‡] Figure 4.6 duplicated on next page.

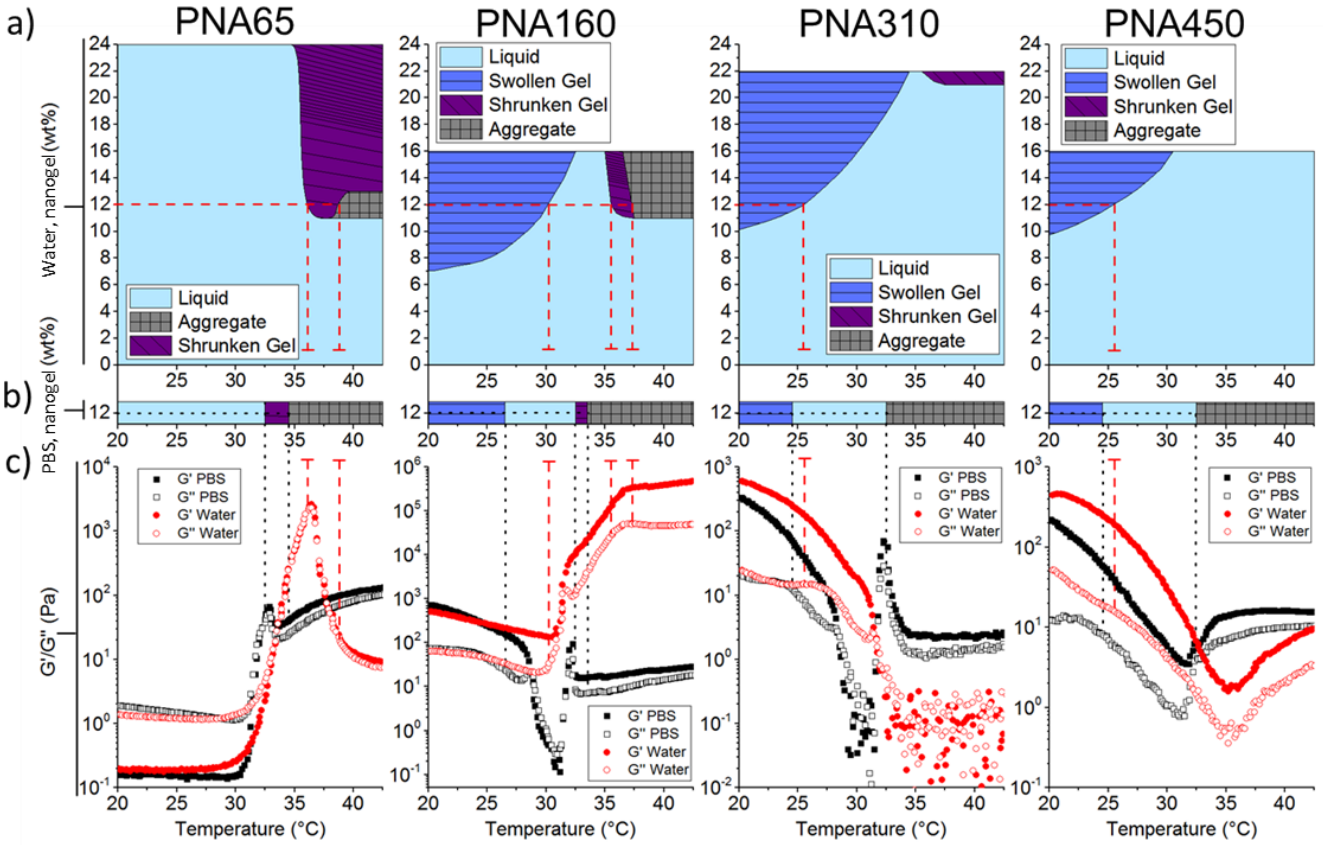

Figure 4.6 (Duplicate figure) – Comparison of nanogel phase behaviour and rheological properties in water and PBS at temperatures between 20 °C and 45 °C with a heating rate of 1 °C min^{-1} for the different nanogel samples with mean diameters from smallest (left) to largest (right), 65 nm, 160 nm, 310 nm and 450 nm respectively. a) The phase diagrams of different nanogel samples dispersed in water at concentrations ranging from 2 wt% up to a maximum of 24 wt%. b) The phase diagrams of nanogel samples dispersed in PBS at 12 wt%. c) Rheological measurements of 12 wt% nanogels dispersions. Lines are a guide for the eye between the phase changes seen in the phase diagrams in water (dashed line) and PBS (dotted line) and the rheological data.

Characterising the nanogels by rheology provides information on the mechanical properties of the different phases. The temperature at which transitions were observed by the vial inversion test were generally accompanied by changes in the rheological data, with the four nanogel samples displaying differing rheological properties. In PNA65, G'' is an order of magnitude larger than G' below 30 °C (c.a. 1 and 0.1 respectively) in both water and PBS, and has a tan δ >> 1, (figure A.5, Appendix), suggesting it existed as a viscous liquid, as seen in the phase study.[61] Conversely, The G' (storage modulus) is an order of magnitude greater than G'' (loss modulus) for PNA160, PNA310 and PNA450 at 20 °C (c.a. 10^3 and 10^2) suggesting the formation of a gel in water and PBS,[30] as seen in the phase study where a swollen gel was present for these nanogels dispersed at 12 wt%. As the temperature was increased G' and G'' gradually decrease, and the separation between G' and G'' reduces, corresponding to the decrease in size of the nanogel, (figure 4.3), resulting in nanogels less closely packing, as they begin to transition from a swollen gel to a liquid. The viscous properties of the material begin to dominate and so the material becomes more liquid-like. For PNA160, PNA310 and PNA450, before the swollen gel to liquid transition there was also a more gradual decrease of G' and G'' than after the transition where a slightly steeper gradient for G' and G'' can be observed, potentially providing a way to observe this transition rheologically. The exception to this is that in water, PNA160 behaves differently, with the moduli increasing after the transition at 30.5 °C. This is likely because a shrunken gel forms as the temperature continues to increase, as with PNA65 in water, which also shows an increase in moduli c.a. 5 °C before a shrunken gel was observed visually. Therefore the increase in moduli likely indicates the increasing interaction between nanogels which eventually leads to the formation of a shrunken gel network. The smallest nanogel, PNA65, had the properties of a viscous liquid until approximately 30 °C, while the three larger nanogels (PNA160, PNA310 and PNA450) displayed gel-like character between 20-25 °C, matching the data in the phase diagram where a swollen gel was observed by vial inversion. The initial values of G' and G'' are lower for PNA310 and PNA450 in PBS than water. This is likely due to PBS causing larger nanogels to deswell at low temperature.[21] The reduced diameter means the nanogels were less closely packed, so that the swollen gel exhibits as reduced stiffness.

As the temperature was increased above 30 °C in water and PBS, all samples displayed an abrupt increase in G' and G'' of at least two orders in magnitude for PNA65, PNA160 and PNA310 and one order of magnitude for PNA450 over a temperature

rise of less than 5 °C, when there is a corresponding formation of a shrunken gel or aggregate phase in the phase study. This was observed previously by Xu *et al.* in the formation of a shrunken gel,[62] as well as in other studies.[16,22,30] The rise in G' and G'' corresponds with the increasing attractive interaction between particles as they become more hydrophobic and transition from a liquid to either a shrunken gel or aggregate phase. In the case of PNA310 as an aqueous dispersion the sample remains a liquid at higher temperature. The dispersion is no longer viscoelastic and hence G' and G'' were not measurable above 35 °C (values < 0.1 Pa) and don't show the dramatic rise in G' and G'' values. In PNA450 there is a less significant and more gradual increase in G' and G'' at high temperature for the aqueous dispersion, which was unexpected as no phase transition occurs. This may be due to shear induced aggregation of the largest particles.[63] After performing the dynamic temperature sweep small aggregates were observed in the aqueous dispersion of PNA450, but not PNA310, (figure A.6, Appendix). Hence short range network formation due to particle-particle aggregation may occur, which alters the rheological properties of the dispersion, but is not observable in a vial inversion test. PNA 65, PNA160 and PNA310 also show an anomalous jump in G' and G'' (and intrinsic viscosity, figure A.7, Appendix) around the VPTT. This is due to shear induced chain entanglement, as observed by Howe *et al.*[27]

From the rheology measurements of the samples, it can be concluded that it is possible to monitor the phase transitions of the concentrated nanogel dispersions by tracking the change in G' and G'' as temperature increases. Changes in phase behaviour are mirrored in the rheological moduli behaviour. In the temperature range of 20 to 30 °C, steric stabilisation dominates. Nanogels larger than c.a. 100 nm transition from a swollen gel to a liquid as G' and G'' values decrease, with G' being larger than G''. Nanogels less than c.a. 100 nm remain a viscous liquid in this temperature range with G'' larger than G', and no significant change in either value. Between 30 and 35 °C electrostatic stabilisation dominates. The moduli of small or large nanogels in PBS or water either rapidly increase if the dispersion solidifies, or decrease if a liquid is formed. Above 35 °C the moduli plateau for solidification, or is below the measurable range for a liquid. This is summarised in figure 4.9, where phase formation is dependent on temperature, as well as nanogel size (and hence structure) and ionic strength of the dispersion. The phases and phase transitions can be predicted by trends in how G' and G'' change with increasing temperature. It is apparent from the phase studies and rheological data that all four nanogels are potentially suitable candidates

for an ISFI, however the size of a nanogel effects the overall suitability as an ISFI. All four nanogels showed either no solidification, or solidification above a temperature of 35 °C at a sufficiently high concentration in water, well above the upper limit of room temperature (25 °C), avoiding premature solidification. Aggregation in PBS occurred at 32.5 °C for all four nanogels, sufficiently below body temperature to expect there to be no problem with non-aggregation at a depot site due to the deviations below core body temperature which are possible. PNA65 appears to be the most suitable nanogel for an ISFI, as at low temperature it was the only one of the three nanogels which remained a liquid at low temperature at a concentration of nanogel of 12 wt%, as reflected in its G' and G'' values at low temperature. This was most likely due to it homogeneous cross-linking leading to a much softer deformable particle than the other nanogels. This would make it much easier to formulate with drug and inject. PNA65 also has the lowest zeta potential at elevated temperature, which may be useful for preventing charge induced biocompatibility issues associated with a high surface charge.[64]

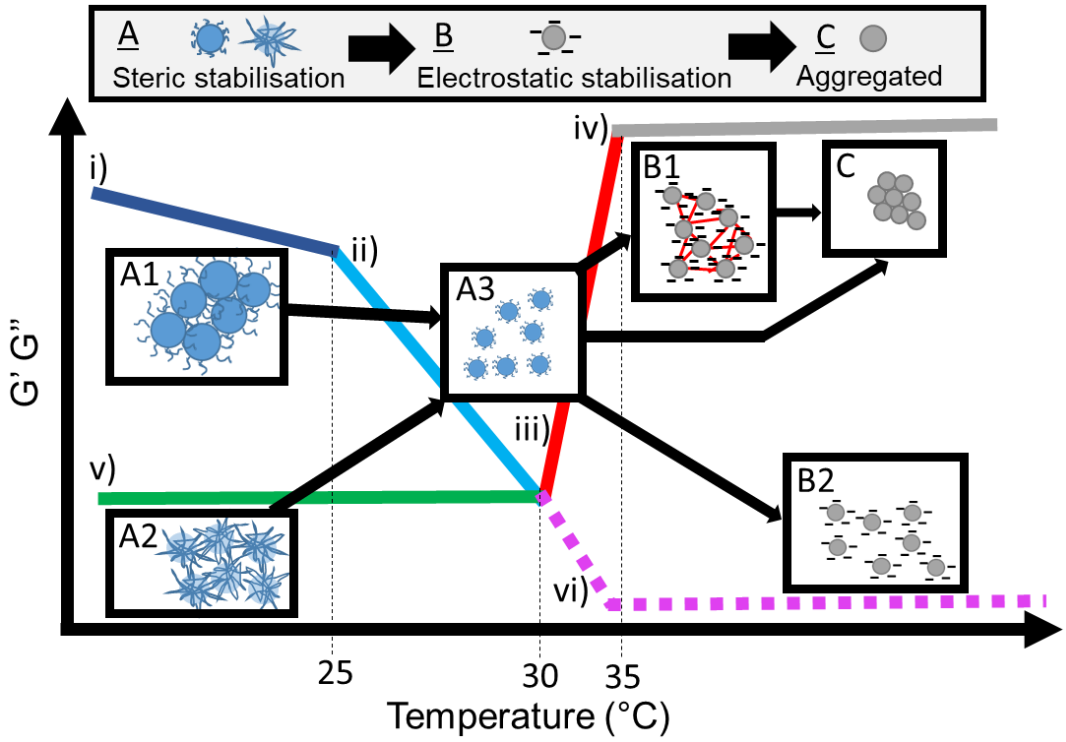

Figure 4.9 Schematic representation of the phase behaviour (A-C) and changes in rheological moduli (i-vi) of the concentrated nanogel dispersions. Stabilisation type shown in top box. Dependant on the nanogel size and ionic strength of the solvent, different pathways are taken through the phase data as the temperature increases. Phases: A1 - swollen gel, A2 – viscous liquid, A3 - liquid, B1 - shrunken gel B2 - low viscosity liquid, C - aggregate. Rheological moduli behaviour associated with each pathway: i) G' > 10G'' ii) G' < 10G'' iii) G'G''(35°C) > 10G'G''(30°C) iv) G'G'' (45°C) < 10G'G''(35°C) v) G'' > 10G' vi) G'G'' < 0.1 Pa.

4.2.4. *In Vitro* Study Release Formulations

Whilst PNA65 was the most appropriate nanogel for an ISFI from a phase transition and rheological perspective, there is also a need to know how nanogel size effects payload entrapment efficiency and drug release rate. In order to test this all four nanogels were loaded with varying amounts of 50% (w/w) lopinavir SDN payloads to conduct a sample and separate *in vitro* release experiment similar to the release experiment in Chapter 3. The release of drug from the aggregate into a surrounding PBS solution was quantified using HPLC, with release media completely replaced at each sample interval to avoid saturation of the release media by the poorly water soluble drug. Nanogel dispersions were prepared at 12 wt% for comparison with phase study and rheological data. Drug loading was tested at a nanogel:SDN ratio of 2:1, 1:1 and 1:2, which corresponds to 33, 50 and 66 wt% of loaded SDN mass vs nanogel mass. Formulations can be seen in table 4.3.

Table 4.3 Formulations of nanogel-drug for ISFI *in vitro* release study

Formulation	LPV SDN (mg)	SDN Loading wt%[a]	PNA65 (mg)	PNA160 (mg)	PNA310 (mg)	PNA450 (mg)
a) Saturation Study						
PNA450-66-S	136.4	66	-	-	-	68.2
b) *In vitro* release study						
Free SDN	68.2	100	-	-	-	-
PNA65-33	34.1	33	68.2	-	-	-
PNA65-50	68.2	50	68.2	-	-	-
PNA65-66	136.4	66	68.2	-	-	-
PNA160-33	34.1	33	-	68.2	-	-
PNA160-50	68.2	50	-	68.2	-	-
PNA160-66	136.4	66	-	68.2	-	-
PNA310-33	34.1	33	-	-	68.2	-
PNA310-50	68.2	50	-	-	68.2	-
PNA310-66	136.4	66	-	-	68.2	-
PNA450-33	34.1	33	-	-	-	68.2
PNA450-50	68.2	50	-	-	-	68.2
PNA450-66	136.4	66	-	-	-	68.2

[a] wt% based on dry nanogel mass, (mass of SDN/(mass of SDN + mass of nanogel)*100.

4.2.5. Saturation Study

To ensure the saturation limit of drug in release media was avoided, a saturation study was conducted on the nanogel predicted to give the greatest release rate, and at the highest SDN loading tested, PNA-450-66-S (table 4.3, a). PNA450 was expected to show the greatest permeability and hence drug release rate, owing to it being the largest

nanogel, and so containing the largest pores between nanogels. In the saturation study 1 ml of release media was removed from 200 ml of PBS at each sampling interval. It can be seen that the cumulative amount of drug released over time begins to plateau after approximately 30 hours, (figure 4.10). According to the European Pharmacopeia 8.0 (5.17.1) and United States Pharmacopeia (USP37/NF32),[65,66] sink conditions are reached when the volume of release media is at least three times saturation volume. Using the saturation study, a sampling interval of 24 hrs was selected for a 15 day *in vitro* study of drug release from aggregate depots, as a compromise between realistic experimental parameters, and avoiding a saturation limit on the rate of drug release.

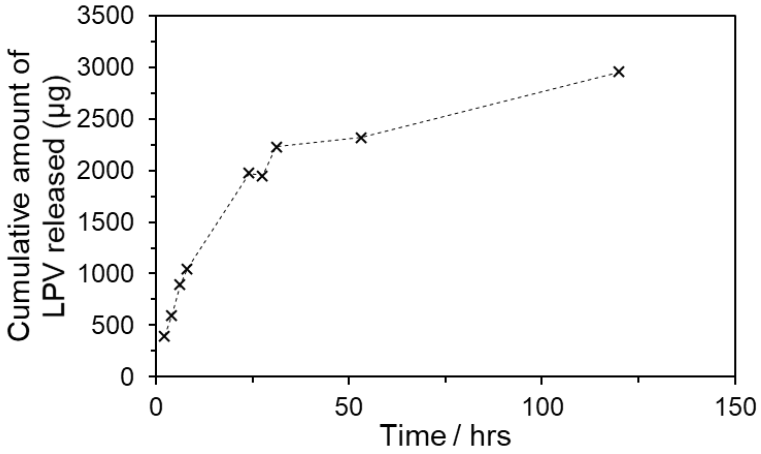

Figure 4.10 Cumulative release of Lopinavir drug from PNA450-66-S (table 4.3) into 200 ml of PBS, measured with HPLC in duplicate.

4.2.6. *In Vitro* Release from Different Sized Nanogels

With a greater SDN loading into the aggregates than chapter 3, it was expected that aggregate depots would be potentially more mechanically unstable and fracture upon or after formation. It is possible to retain fragments of depot matrix within a dialysis bag to prevent them from being lost in the sampling process, however a dialysis membrane can potentially hinder the diffusion of drug, with membrane permeation shown to control release rate.[67] For this reason aggregates were retained in 150 µm mesh containers suspended in the release media to prevent loss of aggregate upon replacement of release media, (figure A.8, Appendix). At the start of the release period in the *in vitro* release study, sampling was performed after the first 1,2, and 5 hours to completely remove burst release drug from the release media. It can be seen in the LPV SDN control sample 'Free SDN', (table 4.3), that 100% release occurred after the

first sample point at 1 hr, and so there is no limitation imposed by the mesh container on release of drug into the release medium, (figure 4.11, a). The depots composed of different sized nanogels and different amounts of SDN loading all showed controlled release after a prolonged period of time. After 360 hours (15 days), the percentage of drug released ranged from a minimum of 14.6% for PNA65-33 to a maximum of 67.8% for PNA160-66. This corresponds to a single order of magnitude difference in release rate of 4.9 and 40.3 μg hr^{-1} respectively, (figure 4.11, b). Applying the Ritger-Peppas equation,[68] (Chapter 3, section 3.1.3), to the release data with the assumption that drug release occurs via Fickian diffusion as observed previously (Chapter 3, figure 3.9, c), shows that a single phase of release occurs from all depots, with the equation showing a good linear fit to the data, (figure 4.11, c). The associated dissolution constant values (k), and correlation coefficients (R_c) can be found in table A.4, Appendix. This release behaviour concurs with the observation in chapter 3, that the polyNIPAM nanogels without allylamine comonomer form dense aggregates which completely entrap SDNs after any initial burst release during aggregate formation, so that drug is only released in dissolved form, rather than two release phases being present, where SDNs are released from the aggregate depot, followed by dissolved drug.

During the release experiment, certain depots of higher drug loading started to fail mechanically and fracture. This can be seen visually in figure 4.12. This instability was categorised into (**I**) a stable depot which retains its shape with no fracturing, (**II**) a low number of fractures occur, where c.a. < 10% of the depot volume may separate into a small number of fragments, (**III**) a high number of fractures occur so that the depot separates into many fragments (c.a. >10% of the depot volume). The instability of some of the depots was reflected in the greater than expected release rate of the depots. This can be seen by comparing the dissolution constant (k) of depots which were mechanically stable (**I**) and those which fractured (**III**). PNA65 showed excellent stability, with no depot fracturing even at high loading of 66% LPV SDNs. This is reflected in the linear increase in dissolution constant (k) with greater SDN loading % (figure 4.13).

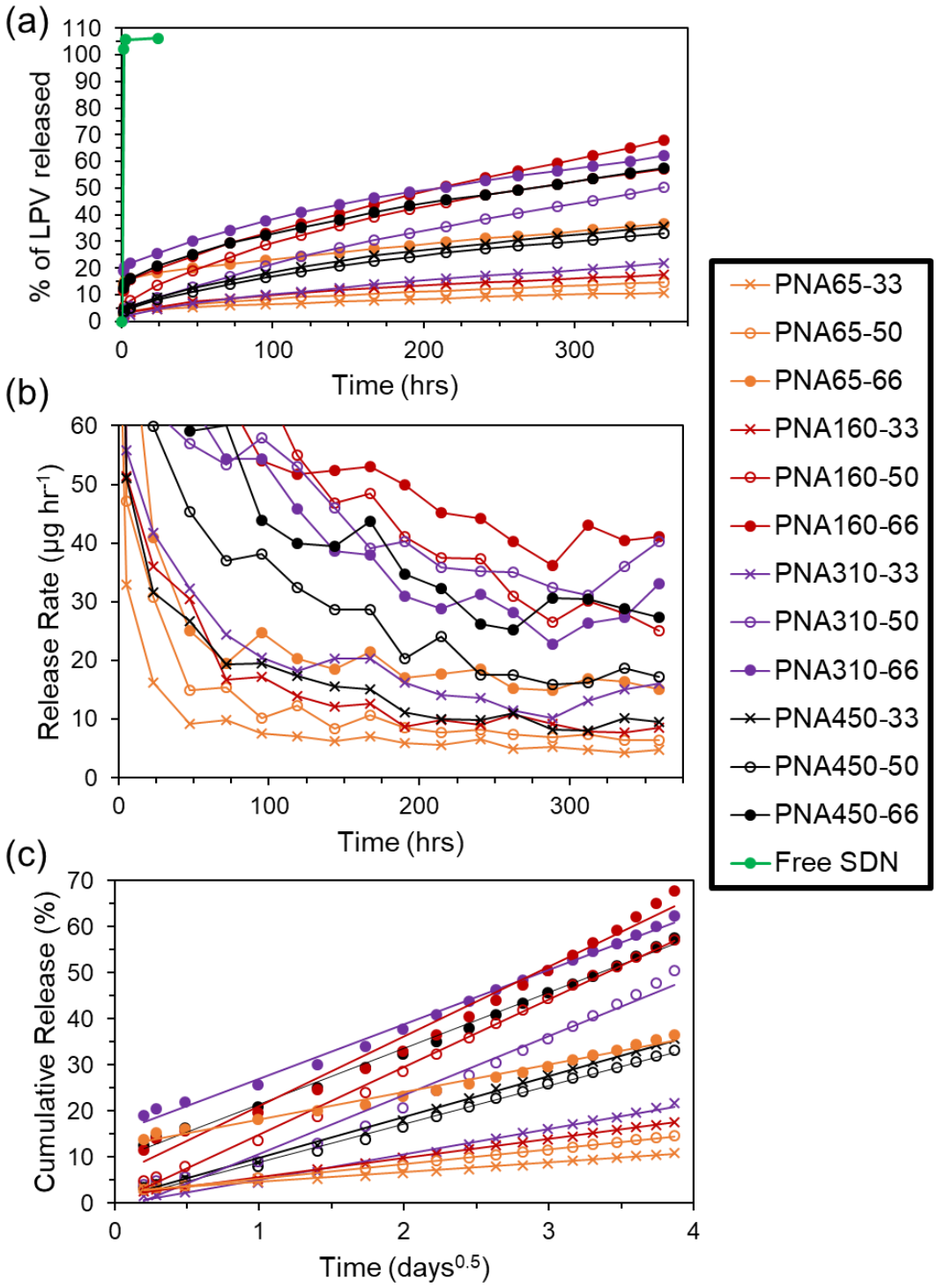

Figure 4.11 Release of LPV drug from aggregated nanogel discs over 360 hours; quantified by HPLC analysis, measurements performed in duplicate. An SDN control without nanogel, 'Free SDN', was performed. (a) cumulative release (b) release rate (c) application of the Ritger-Peppas equation to the LPV release over 360 hours.

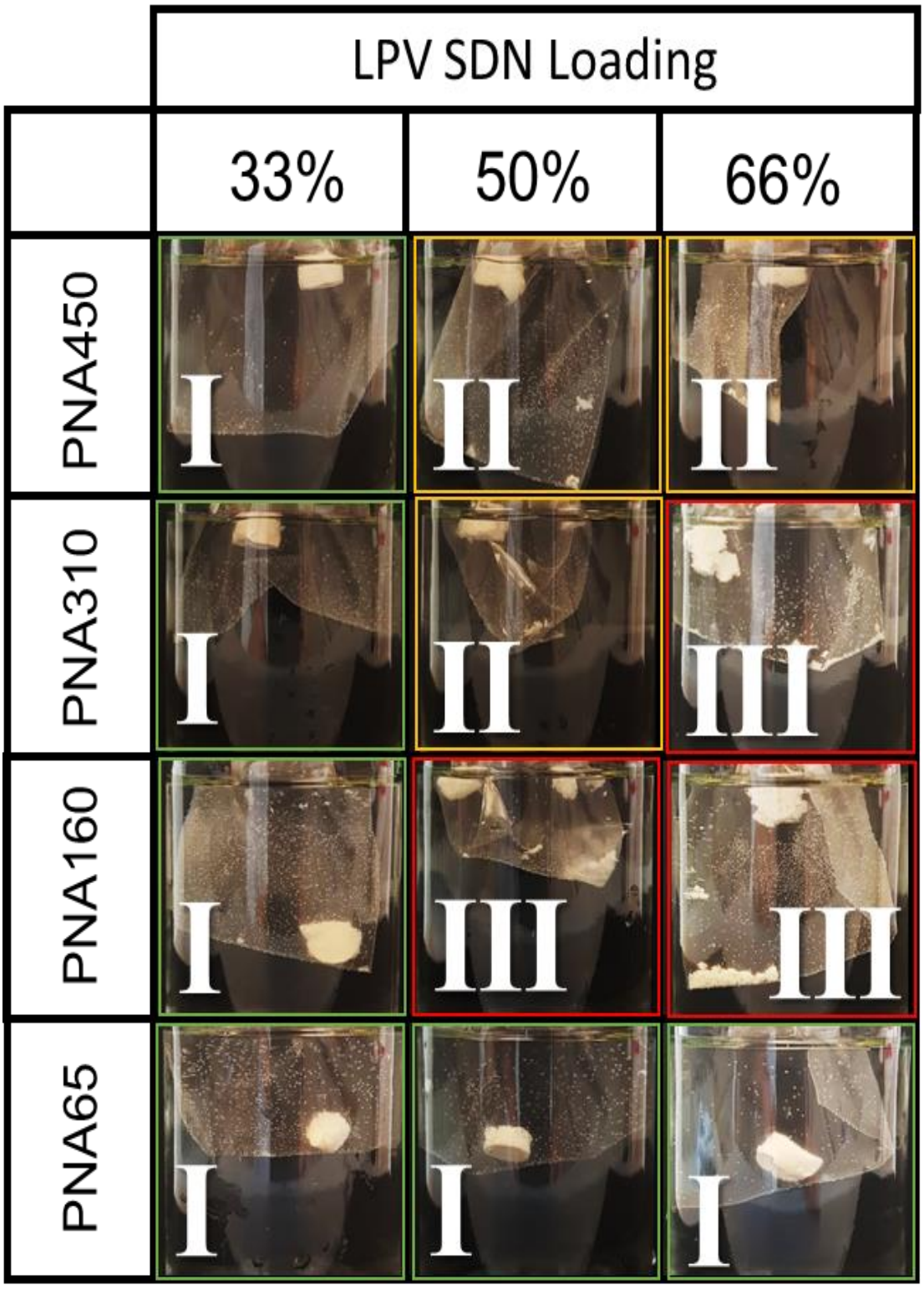

Figure 4.12 Images of *in vitro* release nanogel aggregate drug depots after 360 hours. The mechanical stability of the depots is categorised into (**I**) retains shape with no fracturing, (**II**) a low number of fractures into a small number of fragments, (**III**) a high number of fractures into many fragments.

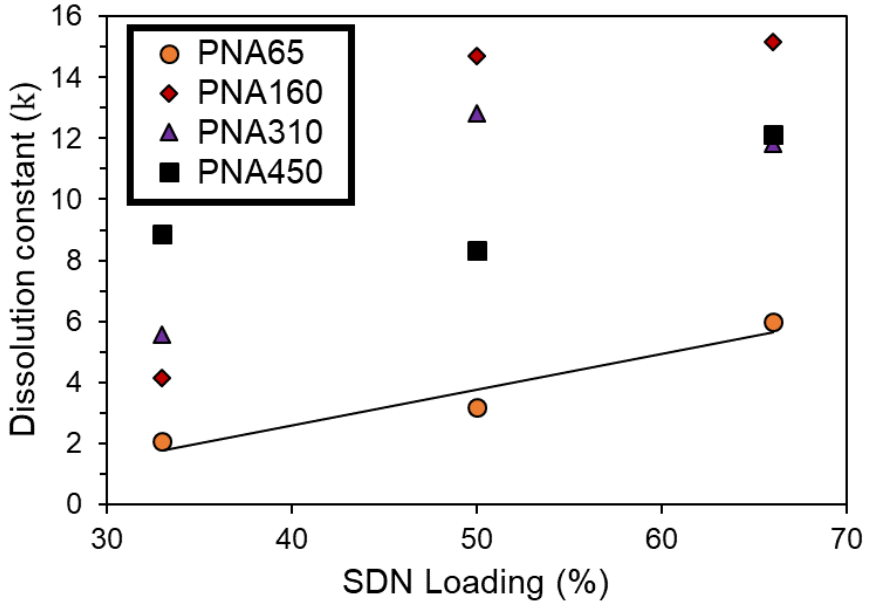

Figure 4.13 Comparison of dissolution constant (k) for mechanically stable depots (PNA65) and depots which fracture during release at increased loading % (PNA160, PNA310, PNA450). Determined from duplicate HPLC measurments.

The release rate can be tuned by changing the percentage of SDN loaded into the depot. Greater SDN loading is likely to introduce greater porosity into the release matrix, increasing the drug dissolution rate due to the increase in permeability of the depot. Theoretically as drug and excipient dissolves from the SDNs contained at the outer boundary of the depot over time, they are likely to be replaced with porous channels, to aid in the release of drug further within the depot, (figure 4.14). It is acknowledged that further detailed study into the structure of the aggregates is required to confirm this. In the case of PNA160, the depot only remained mechanically stable at 33% loading, with a great amount of fracturing (**III**) occurring with 50% and 66% loading. Hence a much greater increase in dissolution constant occurs for PNA160 at 50% and 66% loading compared to PNA65, (figure 4.13). Similar behaviour is seen for PNA310 and PNA450, which also became mechanically unstable above 33% loading. The dramatic increase in the diffusion constant can be explained by the fact that as the depot fractures into smaller fragments the drug has a shorter distance to diffuse, and greater surface area to diffuse from. The non-linear increase in dissolution constant for 50% and 66% loading for PNA160, PNA310 and PNA450 can be attributed to an increase in the porosity of the material with greater drug loading combined with a varying and unknown degree of fracturing of the aggregate to enhance release rate.

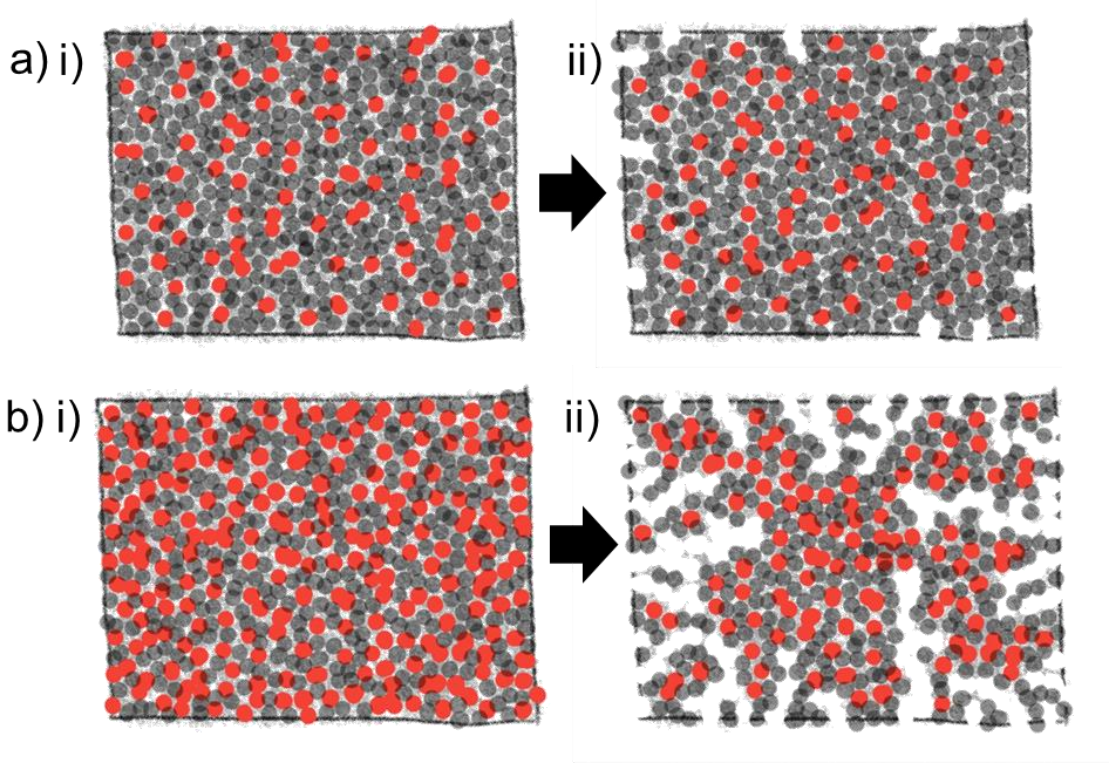

Figure 4.14 Illustration of the dissolution of SDNs loaded into nanogel aggregates to introduce different amounts of porous channels into the matrix depending on SDN loading %. SDNs represented by red circles and nanogels by grey circles. a) Low loading and b) high loading of SDNs, i) start of release period and ii) after a period of release, where surface drug has dissolved and released from the aggregate depot, leading to porous channels which aid further drug release in the interior of the depot.

With the indication that PNA65 nanogels were more deformable in section 4.2.2, the nanogels may have been able to deform around the payload or mesh together to form a more cohesive depot. Hence even with a high wt% of payload, the depot appeared to remain mechanically stable with no observed fracturing occurring. In regards to the larger nanogels, the likely existence of a highly cross-linked core,[28] gives less deformable spheres which are not as cohesive in the presence of greater SDN loading, and so fracturing of the aggregate depot occurs. Focussing on the lowest loading of 33%, where depots remained mechanically stable for all sizes of nanogel, it can be seen that the dissolution constant increase was linear with nanogel size when the dissolution constant was no longer affected by depot fracturing, (figure 4.15). Hence it is likely that smaller particles without a dense core underwent greater deformation upon packing to form an aggregate, reducing the inter-connectivity of pores in the aggregate, as well as containing smaller pores, lowering the permeability and hence

drug diffusion rate. Larger nanogels appear to form aggregates with greater porosity, providing another way to tune release rate from a nanogel release matrix by increasing the diffusion rate of drug from the depot.

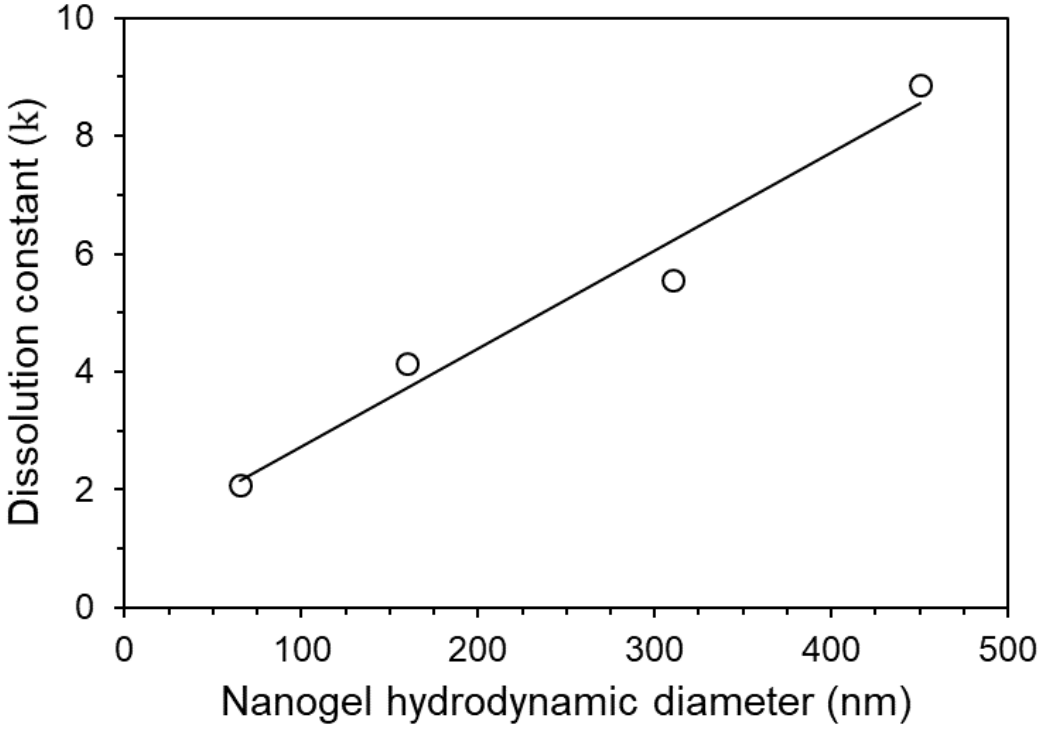

Figure 4.15 Comparison of dissolution constant (k) for mechanically stable (**I**) depots of different sized nanogels at a fixed SDN loading of 33%. Determined from duplicate HPLC measurments.

The nanogels depots generally showed excellent control over burst release, even with increasing SDN loading %, with values as low as 1.5% burst release achieved, (figure 4.16). The burst release period was deemed to occur within the first hour, due to the rapid aggregation of the nanogels, with no dramatic increase in the cumulative % of drug released after the first hour (figure A.9., Appendix). Regardless of nanogel size, burst release was generally 4.8% or less for ≤50% SDN loading. When loading was increased to 66%, all sizes of nanogel were no longer capable of fully retaining the SDN payload, with burst release now in the range of 11.6% to 18.9% got an SDN loading of 66%.

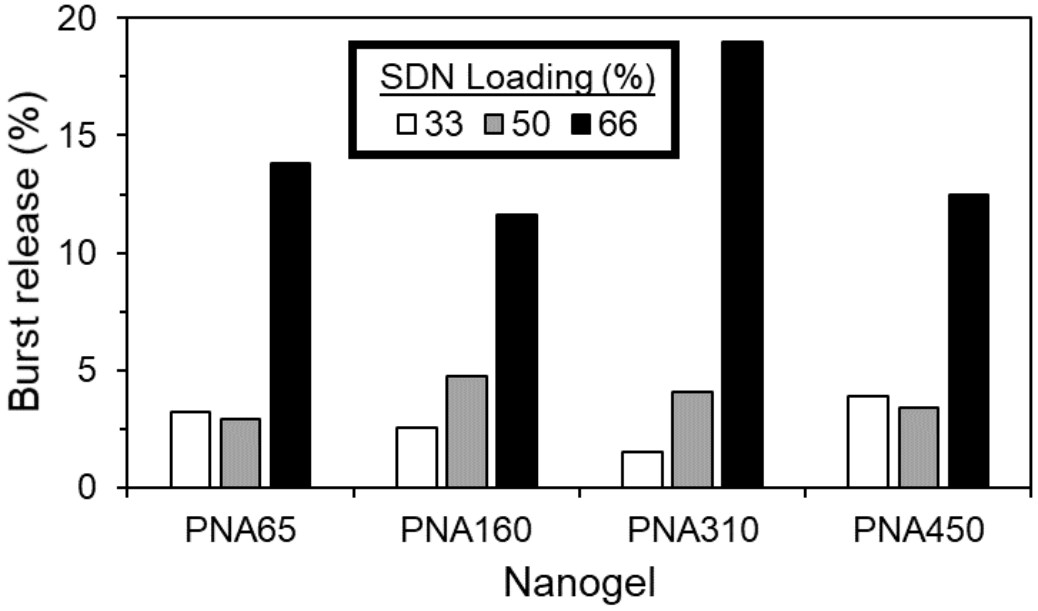

Figure 4.16 Burst release (first 1 hour of release) (%) from aggregate depots of different sized nanogels (PNA65, PNA160, PNA310, PNA450) with different SDN loading (%). Determined from duplicate HPLC measurments.

4.3. Conclusions

In using nanogels of four different sizes, it was shown that differences occurred in the phase and rheology behaviour of concentrated dispersions of nanogels, the release rate of drug from SDN loaded depots of different sized nanogels, and depot mechanical stability over time. Increasing the SDS concentration in the synthesis to create smaller nanogels is documented to have an effect on the internal structure of the nanogel, hence the differences seen were due to a combination of nanogel size and internal structure associated with different sizes of nanogel. PNA65 showed the greatest difference to the other nanogels, which is highly likely due to previous studies observing a homogeneous internal structure for nanogels of this size, compared to the increasing core-shell natured structure of the other nanogels with increasing size. The phase and rheological measurements of the concentrated nanogel dispersions were in good agreement. The phase transition of all nanogels were appropriate for use as an ISFI at all concentrations tested. Solidification in water was not an issue, as it only occurred for PNA65 and PNA130, at a temperature of 35 °C, well above the upper limit of room temperature (25 °C). Aggregation also occurred at 32.5 °C well below a mean body temperature of 37 °C. PNA65 was found to be the most suitable, as unlike the other nanogels it did not display a swollen gel phase behaviour at higher dispersion

concentration, due to its greater deformability and soft sphere nature. As it remained a liquid at < 35 °C, it would be easier to formulate with drug, and also inject than the other nanogels. In the *in vitro* drug release study, all nanogels proved suitable, with sustained release of drug over time, and low burst release when the SDN payload was as high as 50 % loading. The release rate of drug could also be tuned in a linear fashion by changing the % loading of SDN, or the size of the nanogel used to form the depot. Again, PNA65 showed the greatest performance, as unlike the larger nanogels at higher % loading, PNA65 depots remained stable over time regardless of SDN loading %, with no fracturing of the depot.

4.4. Materials and Methods

4.4.1. Materials

N-Isopropylacrylamide (NIPAM, ≥99%), N,N-methylenebis(acrylamide) (BIS, 99%), potassium persulfate (KPS, ≥99%), sodium chloride (NaCl, ≥99.5%), sodium phosphate dibasic dihydrate (Na_2HPO_4, ≥99%) potassium phosphate monobasic ($KH2PO_4$, ≥99%), sodium phosphate dibasic dihydrate ($Na_2HPO_4 \cdot 2H_2O$, ≥99%), (orthophosphoric acid solution 50% (H_3PO_4, HPLC Grade), anhydrous sodium hydroxide pellets (NaOH, analysis grade), sodium dodecyl sulphate (SDS, ≥99%) were purchased from Sigma-Aldrich Company Ltd, Gillingham (Dorset) UK, a subsidiary of Merck KGaA, Darmstadt, Germany. Lopinavir (ABT-378) (LPV) was purchased from WuXi PharmaTech, Shanghai, China. Kolliphor TPGS was purchased from BASF, Ludwigshafen, Germany. Phosphate buffered saline tablets (Bioreagent), Acetonitrile (MeCN, HPLC grade), hydrochloric acid 37% (HCl, analytical grade), were purchased from Fischer Scientific UK, Loughborough, UK, a part of Thermo Fisher Scientific. Type I distilled water obtained from a water purification system with a resistivity of >18 MΩ cm−1 (PURELAB option R, Veolia). Spectra/por 2 (MWCO = 12-14 kDa) and spectra/por 3 (MWCO = 3.5 kDa) dialysis tubing was purchased from Spectrum Europe B.V., Breda, The Netherlands. Chromafil Xtra PET 0.45 µm syringe filters were purchased from Hicrom Ltd. Theale, UK.

4.4.2. Synthesis of PolyNIPAM Nanogels

The polyNIPAM nanogels were synthesized by dispersion polymerisation. The composition used in the synthesis of each nanogel can be found in table M.4.1. The NIPAM monomer (7000 mg, 61.9 mmol), BIS cross-linker (700 mg, 4.5 mmol) and SDS surfactant (PNA450 = 30.0 mg, PNA310 = 78.8 mg, PNA160 = 260.2 mg,

PN60 = 939.1 mg) were dissolved in distilled water (470 mL) in a 1 L two-neck round bottom flask equipped with a stir bar and reflux condenser. This was then sealed and nitrogen was bubbled through the aqueous solution for 1 hour whilst stirring (400 rpm) to remove dissolved oxygen. The solution was then heated to 70 °C. Separately KPS initiator (280 mg) was dissolved in distilled water (30 mL) and degassed with N_2 for 1 hour before being transferred to the flask containing the monomers. The reaction was maintained under a N_2 atmosphere for 4 hours at 70 °C before being cooled down to room temperature. The solution was then filtered through glass wool. To remove unreacted impurities, the nanogel suspension was dialyzed for 5 days using regenerated cellulose dialysis tubing (12-14 kDa MWCO for PNA400, PNA310 and PNA160 and 3.5 kDa MWCO for PNA60), (Spectrum Labs), replacing the distilled water every 12 hours. The purified suspension was then lyophilized (Virtis Benchtop K with ultra-low temperature condenser) and stored in a desiccator.

Table M.4.1 The composition used in nanogel synthesis.

Sample	NIPAM (mg)	[SDS] (mg ml^{-1})	BIS (mg)	KPS[a] (mg)	Water[b] (ml)
PNA65	7000	1.88	700	280	500
PNA160	7000	0.52	700	280	500
PNA310	7000	0.16	700	280	500
PNA450	7000	0.06	700	280	500

[a] KPS dissolved at 9.3 mg ml^{-1} in distilled water.

[b]Total volume of water, including addition of KPS dissolved in water.

4.4.3. Characterisation of PolyNIPAM Nanogels

Characterisation of the nanogels was carried out using dynamic light scattering (DLS) and laser Doppler electrophoresis (LDE). DLS and LDE was performed using a Malvern Zetasizer Nano ZS (running Malvern Zetasizer software V7.12) with 633 nm He-Ne laser and the detector positioned at 173°. Dialysed samples were diluted to 1 mg mL^{-1}. The hydrodynamic diameter was recorded in the range (15-55 °C) using a thermal equilibration time of 600 seconds in 1 cm path length disposable polystyrene cuvettes. Measurements were repeated in triplicate to give a mean hydrodynamic diameter and polydispersity index (PdI). Zeta Potential measurements were performed

using DTS1070 folded capillary cells (Malvern, UK). The pH of the sample was measured before performing zeta potential measurements, and for all samples fell in the range pH 7 +/- 0.5. Capillary cells were flushed with ethanol and water prior to usage. The zeta potential measurement was made with a minimum of 10 and maximum of 40 runs, with a voltage of 150 V. The Smoluchowski approximation where f(Ka) = 1.5 was used. Due to the tendency of the nanogels to aggregate with increasing ionic strength solution when above 32°C, the measurements were conducted in the highest stable concentration of 0.001 M NaCl. This is despite the ISO 13099-2:2012 and ASTM E2865-12 standard recommendation of 0.01 M NaCl to avoid potentially inducing electrode polarization, which causes voltage irregularities if solution conductivity is too low. Hence the zeta values give a relative qualitative comparison of zeta potential trends between the samples measured under the same conditions, rather than a quantitative value.

4.4.4. Viscometery Measurements

Lyophilized nanogels were dissolved in water for 24 hours on a sample tube roller. PNA450 required 30 minutes sonication in a sonication bath (S 100/H, Elmasonic) for complete dispersal. DLS was used to check complete dispersal of lyophilized nanogel was achieved, with particle size and PdI values equivalent to those before lyophilization during the nanogel synthesis, see table A.2. A Poulten Self U-Tube Ostwald Viscometer (V1618/02) was used to determine the relative viscosity of the dilute aqueous nanogel samples. All viscometry measurements were conducted at 20 +/- 0.5 °C and performed in triplicate.

4.4.5. Phase and Rheological Studies

To form nanogels at different wt% in water and PBS (1X strength, pH 7.4) the lyophilized nanogels were first packed at the bottom of glass sample vials. Water or PBS was then added to the sample vials and the samples were held at 20 °C for 30 minutes to allow the solvent to soak into the lyophilized nanogel material. The samples were then held at 27 °C for 24 hours to allow the nanogels to completely disperse. The samples were then added to a sonication bath (S 100/H, Elmasonic) for 30 minutes to remove any trapped air bubbles formed in the high concentration dispersions. This was repeated up to three times and the temperature of the bath was kept below 25 °C.

For phase studies the sample increasing in 2 wt % intervals from 2 wt % up to the maximum wt % at which each nanogel sample could be homogeneously dispersed were heated in 1 °C intervals and allowed to equilibrate for 5 minutes at each temperature. The phase of each sample was then observed by visual inspection and the vial inversion method:[69] A liquid flowed down to the bottom of the vial; a swollen gel remained self-supporting and did not flow over 10 seconds; a shrunken gel remained self-supporting and adhered to the sides of the vial over 10 seconds with a small excess of water phase separating; an aggregate formed a pellet which was not self-supporting and with a large excess of water phase separated. When a phase transition occurred between two consecutive temperatures or wt % values the intermediate value was used. For example a phase transition between 10 wt % and 12 wt % is stated as occurring at 11 wt %. For rheological studies a Thermo Fischer Haake MARS III rotational rheometer was used with a 35 mm parallel-plate head geometry to perform oscillatory rheology, A sample cover and solvent trap were used to prevent water evaporation from the sample. 12 wt% samples were loaded into syringes at 33 °C for placement on the rheology geometry as a liquid. The parallel-plate geometry was lowered onto the sample (0.5 mL) and cooled down to 20 °C for 10 minutes before commencing measurements to erase any loading and stress history. Amplitude sweeps were performed in the range of 0.1 to 100 % strain to find the linear viscoelastic range (LVE) for each sample, (figure A.4, Appendix) A strain in the LVE of each sample was selected for the proceeding measurements. This was 1 % for PNA450, PNA310 and PNA160, and 20 % for PNA65. A time sweep was then conducted for 600 seconds at the fixed strain values to ensure G' and G'' remained constant over time, to confirm that the sample remained stable under measurement conditions. A dynamic temperature sweep was then performed with a heating rate of 1 °C min^{-1} in the range of 20 °C to 45 °C. A frequency of 1 Hz (6.28 rad s^{-1}) was used for all measurements as used previously in literature.[24,30]

4.4.6. Lopinavir (LPV) Solid Drug Nanoparticle (SDN) Synthesis

The LPV SDNs were prepared by emulsion-spray-drying as described by Giardiello *et al.*[70] Briefly, a stock solution of LPV (200 mg mL^{-1} in dichloromethane (DCM)), polyvinyl alcohol (PVA grade 4–88, MW 57–77 000) (50 mg mL^{-1} in water), Kolliphor TPGS (50 mg mL^{-1} in water) were prepared. Three stock solutions were

mixed in the LPV: PVA : Kolliphor TPGS ratio of 60 : 192 : 48 (mL) in a 1 : 4 DCM to water mixture. Emulsification was conducted using a Hielscher UP400S ultrasonic processor equipped with a H14 Probe at 100% output (140 W) for 180 seconds, with immediate spray-drying using a benchtop spray-dryer (BUCHI Mini-290) with an air-atomizing nozzle and compressed air as the drying gas. Spray-drying process conditions: 7 mL min^{-1} solution flow rate; 65 °C outlet temperature; 110 °C inlet temperature. Resultant powders were further dried under vacuum for 48 hours to remove residual DCM. SDN dispersions result from subsequent powder dispersion in water; for DLS characterisation, powders were dispersed in distilled water at 2 mg mL^{-1} (1 mg mL^{-1} cf. LPV).

4.4.7. *In Vitro* Release Study

The in vitro drug release was performed using adaptations of the sample and separate method,[71] as performed in previous work.[72] A mass of 12 wt% (68.2 mg) of each lyophilised nanogel was dispersed to form a swollen self-supporting gel in 0.5 mL of PBS (pH 7.4, 0.137 M NaCl and 0.0027 M KCl) in a glass vial of internal diameter 14 mm. To this 33, 50 or 66 wt% (34.1, 68.2 or 136.4 mg) of LPV SDNs (50% (w/w) loading of LPV) were vortexed. These were then heated to 37 °C for 1 hour to form shrunken discs with excess PBS expelled from the discs in the heating process, this was removed and used as the first release time point. These discs were transferred to 150 μm mesh containers suspended in the release media in 250 mL glass sample jars with 200 mL of fresh PBS. Subsequent release samples were taken at pre-determined intervals by removing 200 mL from the vessel and replacing with 200 mL of fresh PBS at 37 °C to prevent a saturation limit with a large excess of solvent. Release vessels were kept at 37 °C ± 0.5 °C in a water bath. The amount of LPV released was quantified by HPLC analysis. A similar setup was used for the saturation study with PNA-450-66-S (table 4.3, a). However only 1 mL of release media was removed from 200 ml of PBS at each sampling interval.

4.4.8. HPLC Procedure

The HPLC method is adapted from the method published by Giovanni Di Perri *et al.*[73] Briefly, HPLC grade acetonitrile (MeCN) (1.8 mL) was added to each release sample (4.2 mL) to create 30% (v/v) MeCN samples, followed by filtering through a 0.45 μm

PTFE syringe filter. 40 μL of the solution was injected into a HPLC-PDA system (PerkinElmer Series 200). The mobile phase was composed of solvent A (KH2PO4 50 mM dissolved in HPLC grade water then pH adjusted with H3PO4 to reach pH 3.23) and solvent B (MeCN) with the gradient reported in Table M.2. Chromatographic separation was performed with an Agilent ZORBAX Eclipse Plus 3.5 μm C18 column (100 × 4.6 mm ID, Santa Clara, CA) maintained at 25 °C in a column oven with a solvent flow rate of 0.5 mL min^{-1} giving a retention time of LPV of 9.6 ± 0.2 min. The PDA detector was set to 210 nm with a bandwidth of 2 nm. The concentration of LPV in the samples was calculated against known standards using the area under the chromatogram peaks. Three standards covering the concentration range of the HPLC method were used to verify the results, and samples were analysed in duplicate.

Table M.2 The solvent gradient used in the HPLC method

Time (min)	Solvent A % (v/v)	Solvent B % (v/v)	Flow (mL min^{-1})
0.0	70	30	0.5
1.0	70	30	0.5
3.0	30	70	0.5
11.5	30	70	0.5
12.0	70	30	0.5
12.5	70	30	0.5

4.5. Appendix

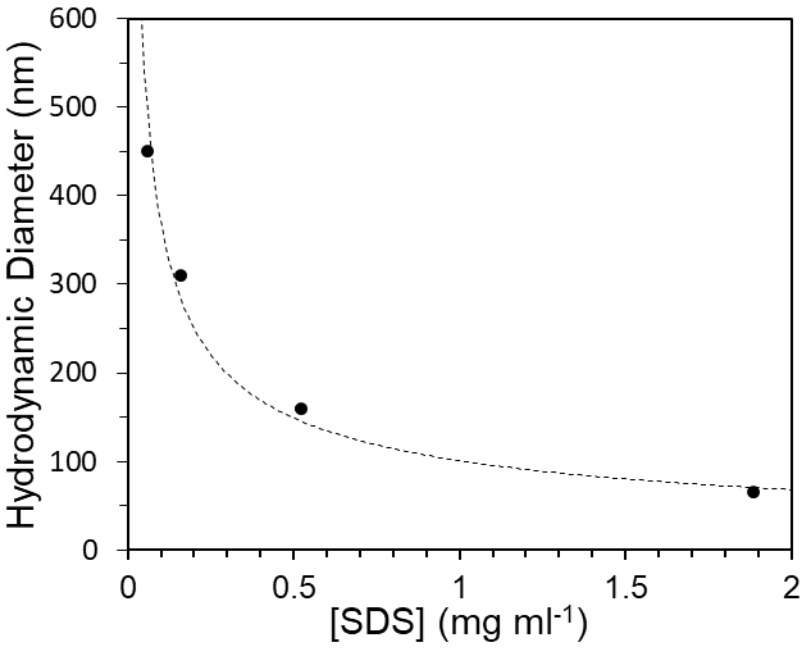

Figure A.1 PolyNIPAM nanogel hydrodynamic diameter vs concentration of sodium dodecyl sulphate (SDS) used in synthesis. Samples measured using DLS with the mean value of triplicate measurements used.

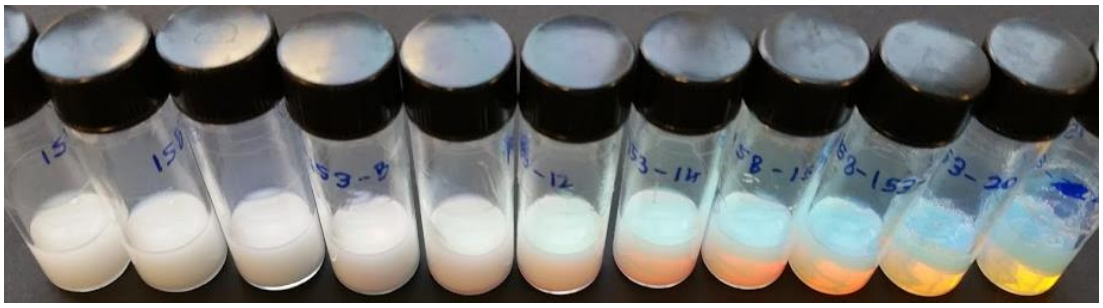

Figure A.2 Photograph (digital image) of tyndall scattering in PNA160. Sample dispersed from 2 to 22 wt% from left to right in 2wt% increments.

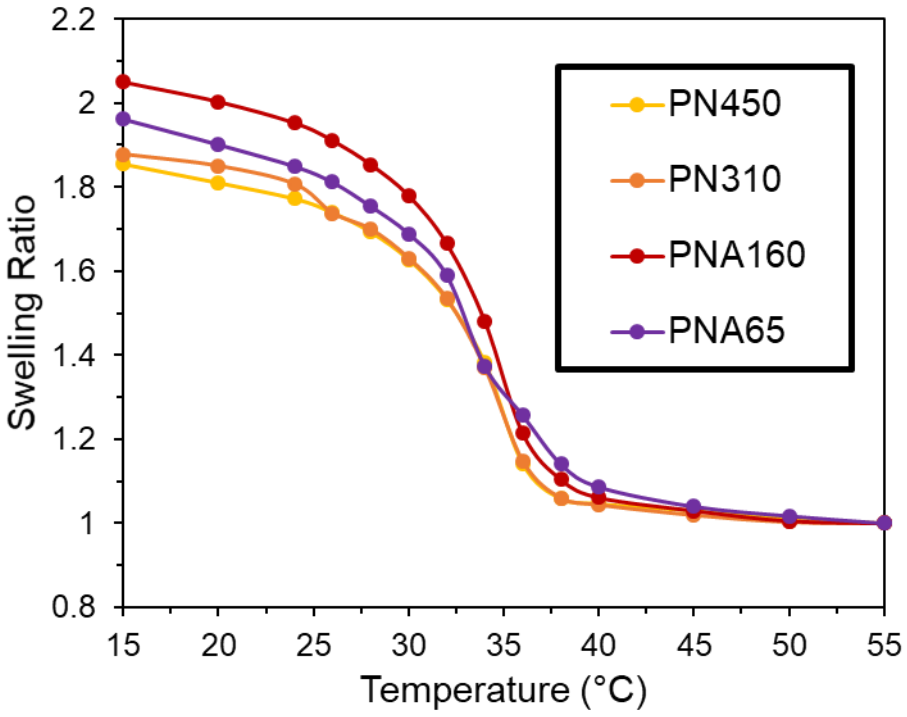

Figure A.3 Swelling ratio vs temperature of different sized nanogels. Swelling ratio equals hydrodynamic diameter at given temperature divided by hydrodynamic diameter at 55 °C. Samples measured using DLS with the mean value of triplicate measurements used.

Table A.1 Aggregation temperature in degrees Celsius (°C) of nanogels at 1 mg ml^{-1} in NaCl solutions measured by DLS. A dash represents no aggregation in the temperature range measured (20 to 55 °C)

[NaCl] (M)	1	0.1	0.01	0.001	0.0
PN400	23	34	35	-	-
PN310	23	34	35	-	-
PN160	23	34	35	-	-
PN60	23	34	35	-	-

Table A.2 Hydrodynamic diameter and PdI of nanogels. All measurements made using DLS with aqueous 1 mg ml^{-1} samples measured in triplicate.

	Synthesis[a]				Dispersal[b]				Sonication[c]
	PNA65	PNA160	PNA310	PNA450	PNA65	PNA160	PNA310	PNA450	PNA450
Hydrodynamic Diameter (nm)	60	160	310	450	65	160	310	890	450
PdI	0.13	0.03	0.01	0.02	0.13	0.02	0.01	0.63	0.03

[a]measured after synthesis and purification of nanogel.
[b]measured after dispersion of lyophilised nanogel.
[c]measured after 30 minutes sonication of aqueous dispersion in a sonication bath.

Table A.3 k value for each nanogel sample

Sample	k (20 °C)[a]
PNA450	0.091
PNA310	0.106
PNA160	0.134
PNA65	0.282

[a] k value determined from the fitting of the Bachelor equation ($\eta_{rel}=5.9(kc)^2+2.5(kc)+1$) to relative viscosity data at 20 °C.

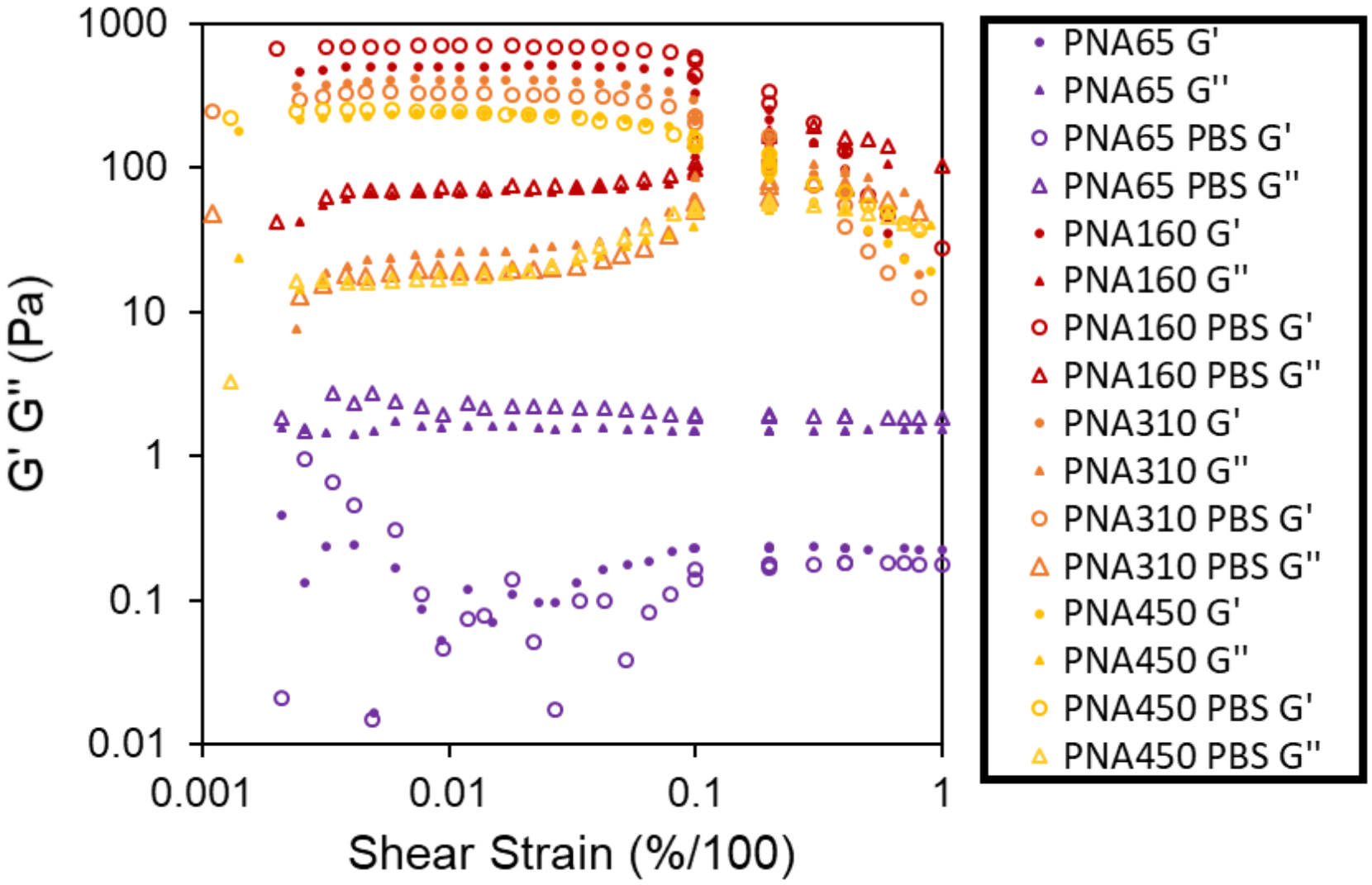

Figure A.4 Amplitude sweep for each nanogel sample as a 12 wt% aqueous dispersion. G' (circle), G'' (triangle), water (filled symbol), PBS (open symbol).

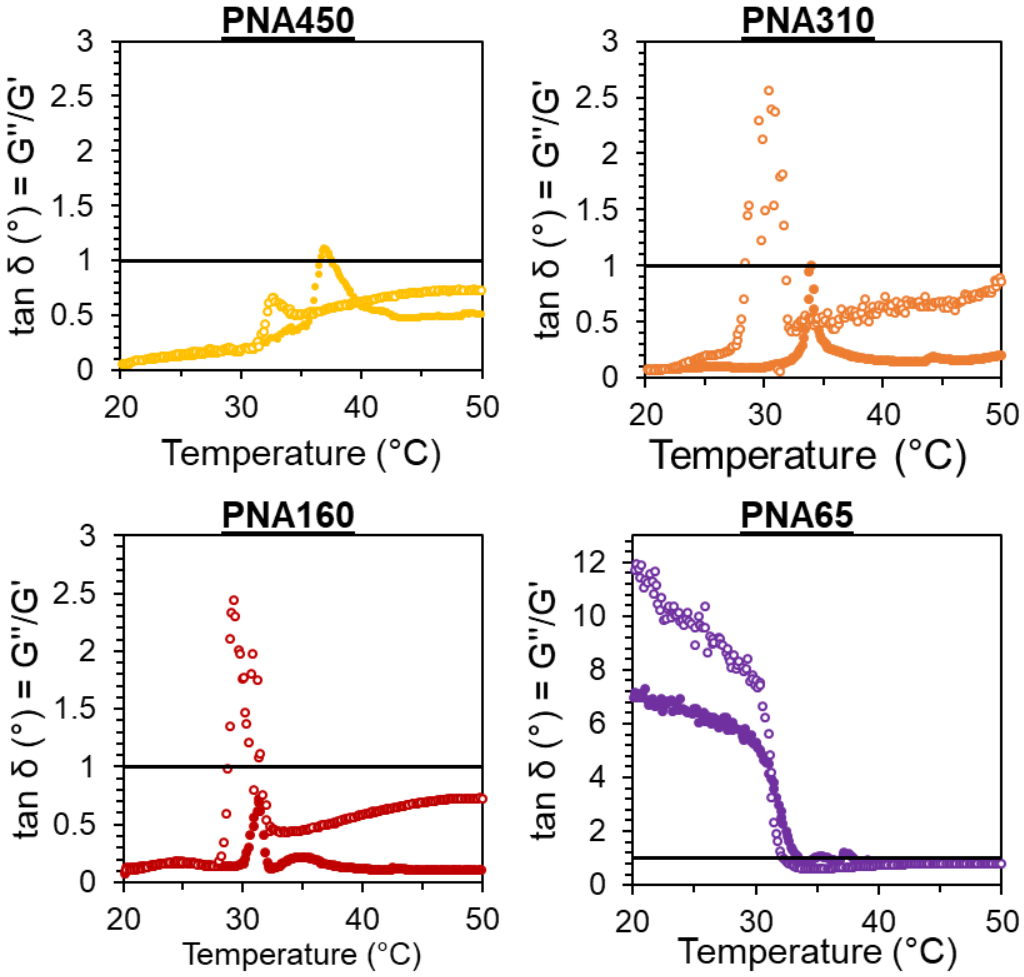

Figure A.5 Dynamic temperature sweep Tan δ values for each nanogel in water (closed circle) and PBS (open circle). Tan δ (°) = 1 shown as black line.

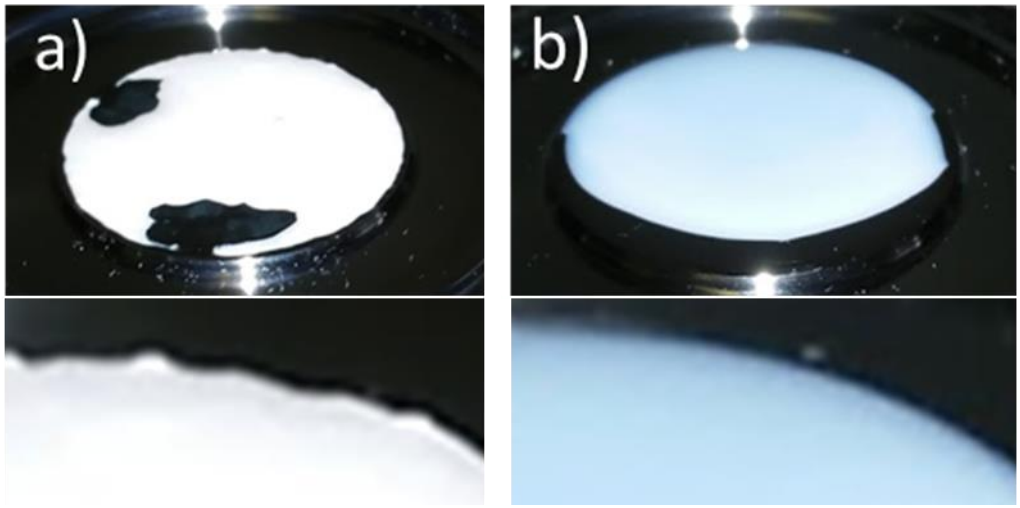

Figure A.6 Photographs (digital images) of aqueous samples at 50 °C after dynamic temperature sweep for a) PNA450 (visible solid aggregate particles present within liquid) b) PNA310 (liquid). (Top) original image and (bottom) enlarged image.

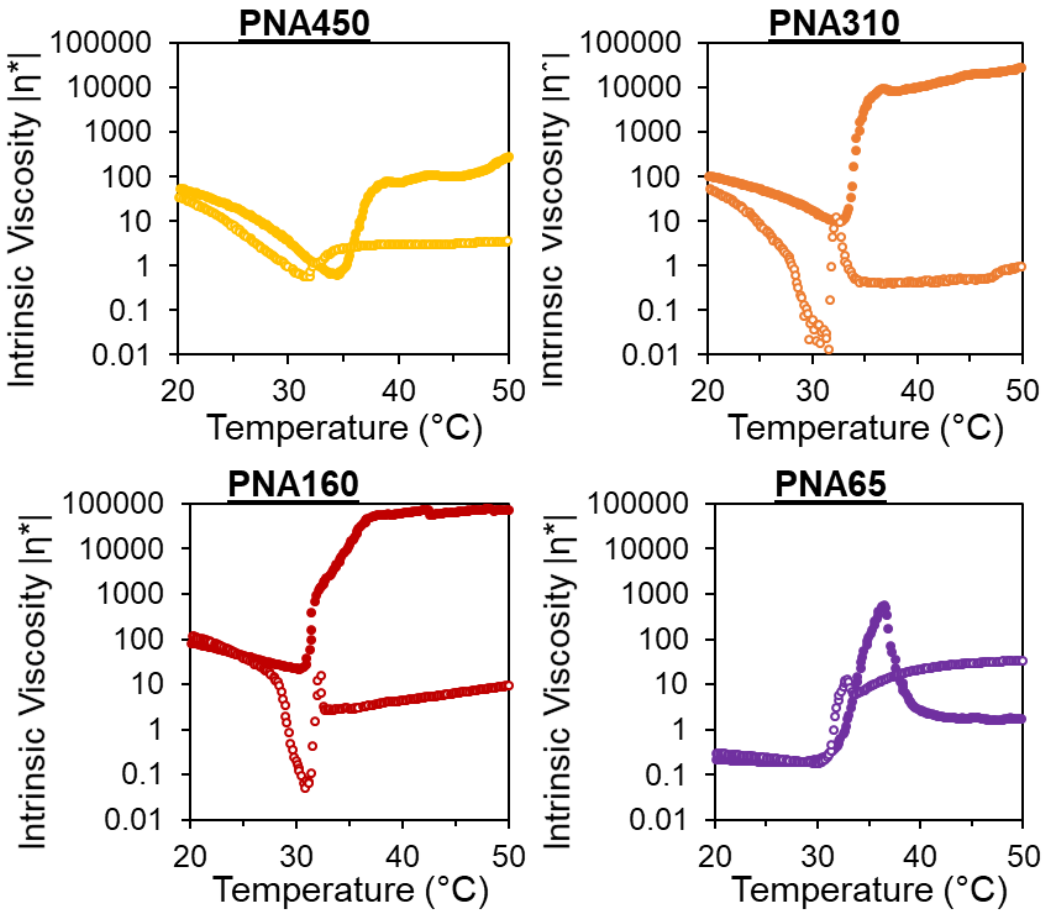

Figure A.7 Dynamic temperature sweep intrinsic viscosity values for each nanogel in water (closed circle) and PBS (open circle).

Figure A.8 Photograph (digital image) of PNA65-50 cylindrical aggregate nanogel depot held inside 150 µm pore size mesh contained suspended in 200 mL of release media (PBS, 1X strength, pH 7.4).

Table A.4 Correlation coefficient (R_c) and dissolution constant (k) values.

Formulation	R_c	k
PNA65-33	2.08	0.9942
PNA65-50	3.17	0.9988
PNA65-66	5.97	0.9872
PNA160-33	4.13	0.9995
PNA160-50	14.69	0.9972
PNA160-66	15.15	0.9837
PNA310-33	5.56	0.9950
PNA310-50	12.80	0.9813
PNA310-66	11.82	0.9949
PNA450-33	8.88	0.9971
PNA450-50	8.31	0.9964
PNA450-66	12.14	0.9964

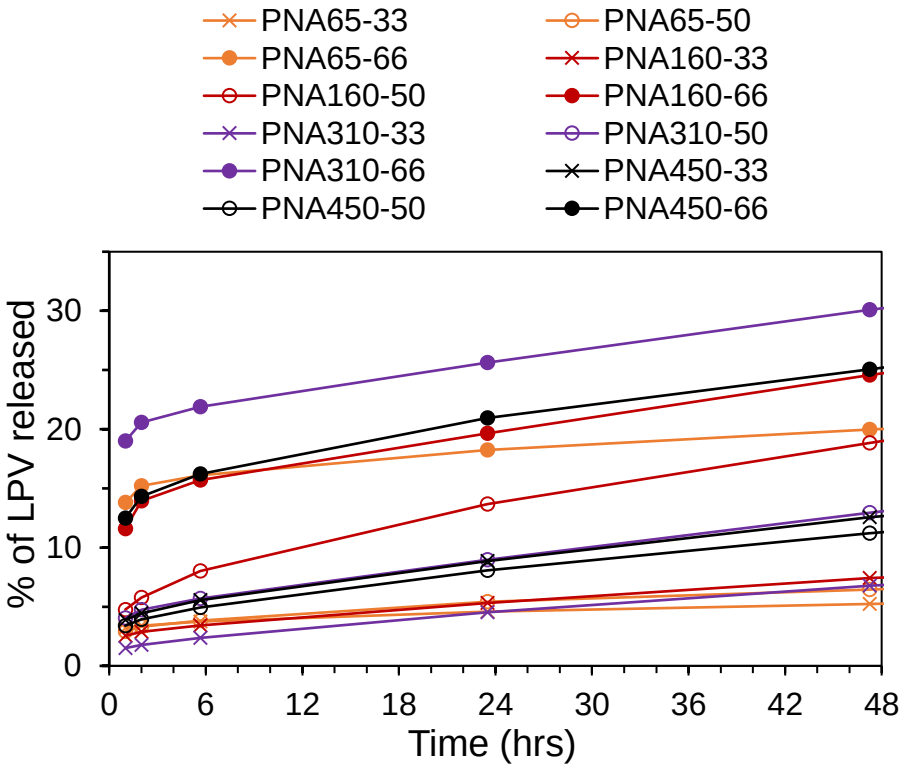

Figure A.9 Cumulative % release of LPV drug from aggregated nanogel discs over first 48 hours. Burst release complete within one hour, with no further dramatic rise in total cumulative release. Determined using duplicate HPLC measurments.

4.6. References

1 R. H. Pelton and P. Chibante, *Colloids and Surfaces*, 1986, **20**, 247–256.

2 X. Wu, R. H. Pelton, a. E. Hamielec, D. R. Woods and W. McPhee, *Colloid Polym. Sci.*, 1994, **272**, 467–477.

3 R. Pelton, *Macromol. Symp.*, 2004, **207**, 57–65.

4 A. Fernández-Barbero, A. Fernández-Nieves, I. Grillo and E. López-Cabarcos, *Phys. Rev. E - Stat. Physics, Plasmas, Fluids, Relat. Interdiscip. Top.*, 2002, **66**, 10.

5 N. Vogel, M. Retsch, C. A. Fustin, A. Del Campo and U. Jonas, *Chem. Rev.*, 2015, **115**, 6265–6311.

6 M. Stieger, W. Richtering, J. S. Pedersen and P. Lindner, *J. Chem. Phys.*, 2004, **120**, 6197–6206.

7 B. R. Saunders, *Langmuir*, 2004, **20**, 3925–3932.

8 R. Acciaro, T. Gilányi and I. Varga, *Langmuir*, 2011, **27**, 7917–7925.

9 W. McPhee, K. C. Tam and R. Pelton, *J. Colloid Interface Sci.*, 1993, **156**, 24–30.

10 I. Varga, T. Gilányi, R. Mészáros, G. Filipcsei and M. Zrínyi, *J. Phys. Chem. B*, 2001, **105**, 9071–9076.

11 L. Arleth, X. Xia, R. P. Hjelm, J. Wu and H. U. Zhibinc, *J. Polym. Sci. Part B Polym. Phys.*, 2005, **43**, 849–860.

12 M. Andersson and S. L. Maunu, *J. Polym. Sci. Part B Polym. Phys.*, 2006, **44**, 3305–3314.

13 G. R. Deen, T. Alsted, W. Richtering and J. S. Pedersen, *Phys. Chem. Chem. Phys.*, 2011, **13**, 3108–3114.

14 G. R. Deen and J. S. Pedersen, *Cogent Chem.*, 2015, **1**, 1–15.

15 G. Romeo, A. Fernandez-Nieves, H. M. Wyss, D. Aciernoand and D. A. Weitz, *Adv. Mater.*, 2010, **22**, 3441–3445.

16 J. Zhou, G. Wang, L. Zou, L. Tang, M. Marquez and Z. Hu, *Biomacromolecules*, 2008, **9**, 142–148.

17 Z. Hu and X. Xia, *Adv. Mater.*, 2004, **16**, 305–309.

18 W. Xiong, X. Gao, Y. Zhao, H. Xu and X. Yang, *Colloids Surf. B. Biointerfaces*, 2011, **84**, 103–10.

19 H. Senff and W. Richtering, *J. Chem. Phys.*, 1999, **111**, 1705–1711.

20 R. Pelton, *Adv. Colloid Interface Sci.*, 2000, **85**, 1–33.

21 M. Rasmusson and B. Vincent, *React. Funct. Polym.*, 2004, **58**, 203–211.

22 H. Wang, X. Wu, Z. Zhu, C. S. Liu and Z. Zhang, *J. Chem. Phys.*, 2014, **140**, 2908.

23 A. N. S. John, V. Breedveld and L. A. Lyon, *Bioengineering*, 2007, **111**, 7796–7801.

24 R. Shu, W. Sun, Y. Liu, T. Wang, C. Wang, X. Liu and Z. Tong, *Colloids Surfaces A Physicochem. Eng. Asp.*, 2013, **436**, 912–921.

25 Y. Zhao, Y. Cao, Y. Yang and C. Wu, *Macromolecules*, 2003, **36**, 855–859.

26 K. Kratz, T. Hellweg and W. Eimer, *Polymer (Guildf).*, 2001, **42**, 6631–6639.

27 A. M. Howe, S. Desrousseaux, L. S. Lunel, J. Tavacoli, H. N. Yow and A. F. Routh, *Adv. Colloid Interface Sci.*, 2009, **147**–**148**, 124–131.

28 B. H. Tan, R. H. Pelton and K. C. Tam, *Polymer (Guildf).*, 2010, **51**, 3238–3243.

29 N. C. Woodward, B. Z. Chowdhry, M. J. Snowden, S. A. Leharne, P. C. Griffiths and A. L. Winnington, *Langmuir*, 2003, **19**, 3202–3211.

30 G. Zhou, Y. Zhao, J. Hu, L. Shen, W. Liu and X. Yang, *React. Funct. Polym.*, 2013, **73**, 1537–1543.

31 D. M. Öle Kiminta and P. F. Luckham, *Polymer (Guildf).*, 1995, **36**, 4827–4831.

32 P. Webb, *Eur. J. Appl. Physiol. Occup. Physiol.*, 1992, **64**, 471–476.

33 R. Lenhardt and D. I. Sessler, *Anesthesiology*, 2006, **105**, 1117–1121.

34 L. Lyons, *Guidelines for the storage of essential medicines and other health commodities*, Arlington, 2003.

35 T. W. Hartgill, T. K. Bergersen and J. Pirhonen, *Acta Physiol.*, 2011, **201**, 467–474.

36 X. Huang and C. S. Brazel, *J. Control. Release*, 2001, **73**, 121–136.

37 A. Hatefi and B. Amsden, *J. Control. Release*, 2002, **80**, 9–28.

38 M. V. S. Varma, A. M. Kaushal, A. Garg and S. Garg, *Am. J. Drug Deliv.*, 2004, **2**, 43–57.

39 R. Gurny, E. Doelker and N. A. Peppas, *Biomaterials*, 1982, **3**, 27–32.

40 X. Tongwen and H. Binglin, *Int. J. Pharm.*, 1998, **170**, 139–149.

41 L. C. Graton and H. J. Fraser, *J. Geol.*, 1935, **43**, 785–909.

42 H. Senff and W. Richtering, *Colloid Polym. Sci.*, 2000, **278**, 830–840.

43 U. Gasser, J. S. Hyatt, J. J. Lietor-Santos, E. S. Herman, L. A. Lyon and A. Fernandez-Nieves, *J. Chem. Phys.*, 2014, **141**, 34901.

44 B. R. Saunders and B. Vincent, *Adv. Colloid Interface Sci.*, 1999, **80**, 1–25.

45 N. Al-manasir, S. Fanaian, K. Zhu, B. Nyström, G. Karlsson and A. Kjøniksen, *J. Phys. Chem. B*, 2009, **113**, 11115–11123.

46 M. Rasmusson, A. Routh and B. Vincent, *Langmuir*, 2004, **20**, 3536–3542.

47 Q. Wang, Y. Zhao, Y. Yang and H. Xu, *Colloid Polym. Sci.*, 2007, **285**, 515–521.

48 Y. Zhao, C. Zheng, Q. Wang, J. Fang, G. Zhou, H. Zhao, Y. Yang, H. Xu, G. Feng and X. Yang, *Adv. Funct. Mater.*, 2011, **21**, 2035–2042.

49 C. G. de Kruif, E. M. F. van Iersel, A. Vrij and B. W. Russel, *J. Chem. Phys.*, 1985, **83**, 4717–4725.

50 V. Wintgens and C. Amiel, *Macromol. Chem. Phys.*, 2008, **209**, 1553–1563.

51 A. Y. Malkin and A. I. Isayev, in *Rheology - Concepts, Methods and Applications*, ChemTec Publishing, Toronto, 2nd edn., 2012.

52 S. Minami, T. Watanabe, D. Suzuki and K. Urayama, *Polym. J.*, 2016, **48**, 1079–1086.

53 J. Luo, G. Yuan, C. Zhao, C. C. Han, J. Chen and Y. Liu, *Soft Matter*, 2015, **11**, 2494–2503.

54 G. K. Batchelor, *J. Fluid Mech.*, 1977, **83**, 97–117.

55 C. Pellet and M. Cloitre, *Soft Matter*, 2016, **12**, 3710–3720.

56 J. Brijitta, B. V. R. Tata and T. Kaliyappan, *J. Nanosci. Nanotechnol.*, 2009, **9**, 5323–5328.

57 B. H. Tan, K. C. Tam, Y. C. Lam and C. B. Tan, *Adv. Colloid Interface Sci.*, 2005, **113**, 111–120.

58 M. S. Wolfe, *Prog. Org. Coatings*, 1992, **20**, 487–500.

59 C. K. Han and Y. H. Bae, *Polymer (Guildf).*, 1998, **39**, 2809–2814.

60 S. Chen, J. Long and Y. Dan, *J. Appl. Polym. Sci.*, 2011, **121**, 3322–3331.

61 T. G. Mezger, in *The Rheology Handbook: For Users of Rotational and Oscillatory Rheometers*, Vincentz Network, Hannover, 4th ed., 2014, pp. 114–171.

62 K. Qian, Y. Ma, J. Wan, S. Geng, H. Li, Q. Fu, X. Peng, X. Kan, G. Zhou, W. Liu, B. Xiong, Y. Zhao, C. Zheng, X. Yang and H. Xu, *J. Control. Release*, 2015, **212**, 41–49.

63 A. Yethiraj, *Soft Matter*, 2007, **3**, 1099.

64 Y. Wang, J. L. Robertson, W. B. Spillman and R. O. Claus, *Pharm. Res.*, 2004, **21**, 1362–1373.

65 P. Liu, O. De Wulf, J. Laru, T. Heikkilä, B. van Veen, J. Kiesvaara, J. Hirvonen, L. Peltonen and T. Laaksonen, *AAPS PharmSciTech*, 2013, **14**,

748–756.

66 S. A. Abouelmagd, B. Sun, A. C. Chang, Y. J. Ku and Y. Yeo, *Mol. Pharm.*, 2015, **12**, 997–1003.

67 U. Bhardwaj and D. J. Burgess, *Int. J. Pharm.*, 2010, **388**, 287–294.

68 P. L. Ritger and N. A. Peppas, *J. Control. Release*, 1987, **5**, 23–36.

69 B. Jeong, Y. H. Bae and S. W. Kim, *Macromolecules*, 1999, **32**, 7064–7069.

70 M. Giardiello, N. J. Liptrott, T. O. McDonald, D. Moss, M. Siccardi, P. Martin, D. Smith, R. Gurjar, S. P. Rannard, A. Owen, *Nat. Commun.*, 2016, **7**, 13184.

71 J. Shen and D. J. Burgess, *J. Pharm. Pharmacol.*, 2012, **64**, 986–996.

72 H. Hyun, Y. H. Kim, I. B. Song, J. W. Lee, M. S. Kim, G. Khang, K. Park and H. B. Lee, *Biomacromolecules*, 2007, **8**, 1093–1100.

73 A. D'Avolio, L. Baietto, M. Siccardi, M. Sciandra, M. Simiele, V. Oddone, S. Bonora and G. Di Perri, *Ther. Drug Monit.*, 2008, **30**, 662–669.

Chapter 5

Biodegradable Nanogels

5.1. Introduction

The polyNIPAM nanogels developed for use as an ISFI in previous chapters show an inherent weakness; their lack of degradability. This final results chapter will explore the development of nanogels which are capable of undergoing degradation at a depot injection site in the body.

5.1.1. Degradable Nanogels

Biodegradable ISFIs solidify through different mechanisms such as thermoplastic setting pastes, in situ cross-linking, in situ polymer precipitation and in situ solidifying organogels.[1] PolyNIPAM nanogels can solidify via in situ precipitation to form an aggregate, as we have demonstrated in previous work.[2] In order for these solidified nanogels to be removed from the injection site through renal excretion after having served their purpose, the cross-linked polymer network must be degraded *in vivo* into low molecular weight polymers (~40 kDa or less),[3] or smaller nanogels (~20 nm or less).[4] The molecular weight of the polymer in a nanogel network can be degraded by either the scission of the backbone of the polymer or cleavage of bonds in the cross-linkers. The carbon-carbon backbone of polyNIPAM is extremely resistant to degradation, however, a range of studies have attempted to incorporate degradability into this backbone through strategies such as the insertion of degradable polymer blocks, and discrete insertion of main-chain degradable groups.[5] The most appropriate technique for complete removal of a large mass of polymer from the body via a degradable backbone is the insertion of multiple main-chain degradable functionalities via a comonomer, due to the fact that it allows the polymer to degrade into significantly lower molecular weight polymers.[6,7] In terms of free radical polymerisation (FRP), where a radical is generated and transferred from monomer to monomer as they are added to the end of a growing polymer chain, many ring opening comonomers are able to introduce a degradable polyester unit into the backbone.[8] This has included the synthesis of enzymatically degradable linear polyNIPAM in toluene, where proteinase K was used in conjunction with comonomer 2-methylene-1,3-dioxepane, which introduces an ester into the polymer backbone.[9] Ren and Agarwal also synthesised degradable polyNIPAM-co-ester polymers, however, the ring opening comonomer had a low reactivity, and polymerisation was conducted in anisole.[10] Therefore, the degradable units were not distributed evenly throughout the polymer. Degradation

would lead to polymer fragments with a broad range of molecular weights, including those with a molecular weight greater than is required for renal excretion (~40 kDa) *in vivo*. Precipitation polymerisation is a common and simple method used to produce nanogels, however, this method is also highly sensitive to the solvent it is conducted in, as such the modification of this synthesis to create a nanogel structure in solvents other than water such as anisole may not be possible. This likely explains why polyNIPAM polymers which contain a degradable backbone via a ring opening comonomer have not reached widespread usage. There also currently appears to be no reports in literature of any other simple routes to synthesise polyNIPAM nanogels with a biodegradable polymer backbone.

The second way in which nanogel degradation can occur *in vivo* is via the cross-links between the polymer chains which form the nanogel polymer network. A range of different degradable cross-linkers exist which can degrade in response to various conditions, and can also be incorporated successfully into a nanogel structure during synthesis. These include the synthesis of nanogels with glycolate ester based biodegradable cross-linking agents, which are able to degrade hydrolytically,[11] ketal cross-linked nanogels which degrade in response to a low pH,[12] enzymatic degradation using dextran based cross-linking agents,[13] and many others.[14–16] PolyNIPAM based degradable nanogels have previously been synthesised, for example with the inclusion of a cross-linking agent containing a vicinal diol.[17] One form of biodegradable cross-linking agent which has been employed in numerous polyNIPAM nanogels is that of N,N'-bis(acryloyl)cystamine (BAC), which contains a biodegradable disulphide bond.[18–21] BAC is similar in structure to the more commonly used non degradable cross-linking agent N,N′-methylenebis(acrylamide)(BIS), (figure 5.1, a). Disulphide bonds undergo reduction under physiologically relevant reducing conditions.[20] The main disulphide bond reducing agent in the body is glutathione (GSH), which is found at a concentration of 2-20 μM in the extracellular environment, and 0.5-10 mM in the intracellular environment.[22,23] Hence disulphide bonds rapidly cleave within the highly reductive environment of cells,[24] but more slowly in extracellular fluid.[25,26] In this process GSH is oxidised to form the dimer glutathione disulphide (GSSG), cleaving a disulphide bond into two thiols (figure 5.1, b),[23] potentially allowing the polymer network cross-linked by disulphide bonds in a BAC cross-linked nanogel to be slowly degraded in an extracellular environment, to

generate low molecular weight polymers which can be eliminated from the body. The reductant dithiothreitol (DTT), is often used for *in vitro* reduction of disulphide bonds, mimicking the role of GSH in the body,[19,21,22] with reduction of the disulphide bond achieved via a thiol-disulphide exchange reaction driven by the formation of a six membered ring in DTT (figure 5.1, c).[27,28]

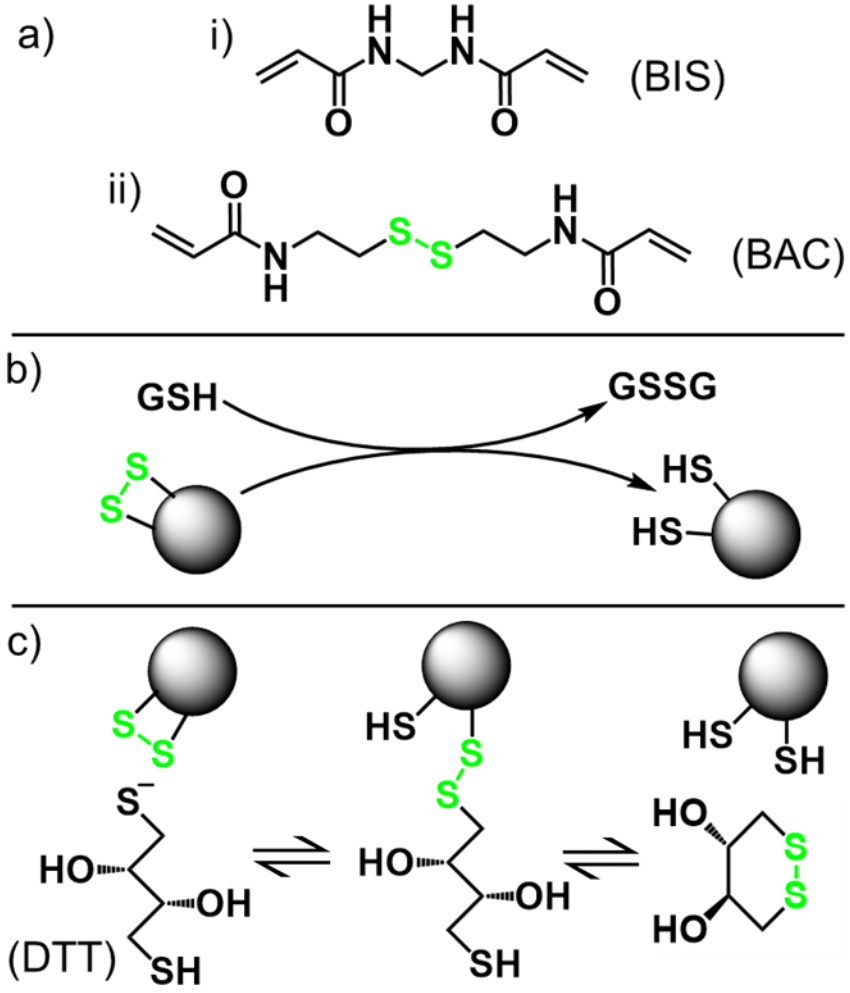

Figure 5.1 Disulphide bond chemistry a) comparison of cross-linking agent chemical structure of i) N,N′-methylenebis(acrylamide)(BIS) and ii) N,N'-bis(acryloyl)cystamine (BAC), b) schematic showing reduction of nanogel disulphide bond into thiols by GSH, c) disulphide exchange reaction between nanogel disulphide bond and dithiothreitol (DTT).

5.1.2. Obstacles to Degradation

PolyNIPAM nanogels cross-linked with the degradable cross-linking agent (1,2-dihydroxylethylene)bisacrylamide (DHEA), have previously been reported to give incomplete degradation.[17] It was hypothesised that non-degradable cross-linking is introduced through a chain transfer reaction. PolyNIPAM contains a hydrogen atom

on the tertiary carbon of the polymer main chain, which can be abstracted in a chain transfer reaction.[17,27] In replacing the NIPAM monomer with N-isopropylmethacrylamide (NIPMAM), (figure 5.2), which is identical in structure except for a methyl group in place of the hydrogen atom on the tertiary carbon of the main polymer chain,[29] fully degradable nanogels could be synthesised.[17]

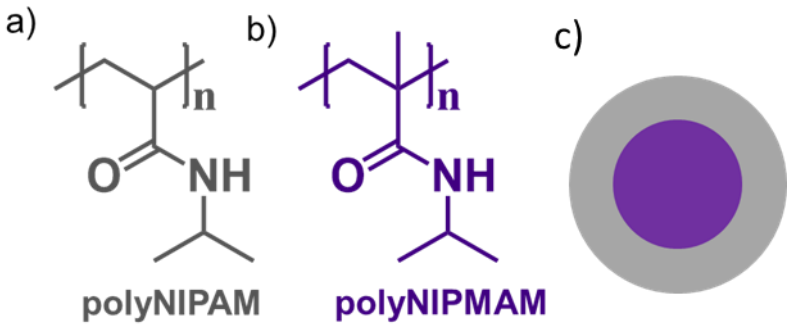

Figure 5.2 Chemical structure of a) poly(N-isopropylacrylamide) (polyNIPAM), b) Poly(N-isopropylmethacrylamide) (polyNIPMAM) and c) a core-shell structure.

PolyNIPMAM has an LCST between 38 to 44 °C (above body temperature),[30,31] so it would be unable to aggregate in response to body temperature to form a depot, as the aggregation temperature of polyNIPMAM nanogels is around 46 °C.[32] However by combining NIPMAM and NIPAM monomers, Fundueanu *et al.* recently showed that the LCST can be tuned by varying the copolymer composition. It was also found that a 60:40 mol% ratio of NIPAM to NIPMAM gave nanogels with a VPTT of 36.8 °C, just below body temperature.[33] Weise *et al.* similarly showed that a 50:50 mol% ratio gave nanogels with a VPTT of 38 °C. They also synthesised a nanogel with a polyNIPAM core and polyNIPMAM shell structure (figure 5.2, c). The core-shell structure had a higher aggregation temperature (40 °C) than the copolymer nanogel composed of the same mol% of each monomer (36 °C).[32] Therefore, aggregation temperature was more dependent on the VPTT of the polyNIPMAM shell than the polyNIPAM core. Hence it may be possible to synthesise a nanogel where the monomer in the core and shell are switched, to give a nanogel compromised of a polyNIPMAM core, and a polyNIPAM shell. The aggregation temperature of this nanogel would likely remain closer to polyNIPAM than polyNIPMAM, allowing aggregation at a temperature below 37 °C when at physiological ionic strength. Nanogels consisting of polyNIPMAM with the degradable cross-linking agent BAC

have also previously been synthesised by Gaulding *et al.*[21] Again incomplete degradability was observed. This time it was attributed to the elevated temperature of synthesis (80 °C) allowing the disulphide bond of the BAC cross-linking agent to participate in various reactions, such as attack by a radical to form a thioether. These non-degradable cross-links also prevented the nanogel from fully degrading if a significant amount of the non-degradable cross-links present. However, fully degradable nanogels were synthesised by conducting low temperature redox-initiated polymerisation (50 °C) with the addition of N,N,N′,N′-tetra-methylethylenediamine (TEMED). This avoids unwanted reactions with the disulphide bond which occur at higher temperature.[21] To summarise, both polyNIPAM, and BAC can potentially prevent nanogels fully degrading due to the chain transfer reactions which can occur. The non-degradable cross-links introduced by NIPAM polymerisation can be eliminated by replacing the monomer with NIPMAM, and the non-degradable cross-links introduced by BAC can be eliminated by conducting the reaction at a lower temperature.

5.1.3. Monitoring Nanogel Degradation

The degradation of nanogels has previously been monitored using a range of techniques including asymmetric flow field flow fractionation,[17,21] dynamic light scattering,[11,12] atomic force microscopy,[27] scanning electron microscopy,[20,34] transmission electron microscopy[19], visual turbidity[21] and indirectly through enhanced drug or dye release.[18,20] Monitoring degradation through dynamic light scattering is particularly useful, as degradation can be monitored *in situ*. Chen *et al.* and Leber *et al.* showed that the count rate of a nanogel sample drops as the nanogel degrades.[11,12] Count rate is measured in kilo counts per second, and gives a measure of the fluctuation in scattered light intensity measured over time.[35] The count rate is a function of particle size, concentration and particle to medium refractive index.[36] Assuming the particles do not change in size or concentration, through processes such as aggregation or sedimentation, then a drop in count rate over time can be attributed to a change in particle to medium refractive index due to particle degradation, as polymeric material is lost from the particle and replaced by solvent. Zou *et al.* showed that the count rate of a degradable particle remained constant over time in a control sample, but gradually decreased in the presence of an enzymatic degradation species.[37]

5.1.4. Aims

The main aim of this chapter is to synthesise polyNIPMAM core – polyNIPAM shell nanogels which are fully degradable whilst aggregating below 37 °C under physiological ionic strength, so as to be able to form a degradable aggregate drug delivery depot when injected into the body. This is not something which has previously been achieved, and would potentially give an ISFI which doesn't suffer from burst release whilst also not requiring microsurgery for removal after having served its purpose. To achieve the main aim of this chapter the following objectives will be achieved:

- Determine the mol% ratio of NIPMAM monomer used in the synthesis of the particle core and NIPAM monomer in the shell which minimises the polyNIPAM in the shell to reduce the amount of non-degradable cross-links introduced by NIPAM polymerisation, whilst retaining a polyNIPAM shell large enough to allow the particle to aggregate below 37 °C under physiological ionic strength.
- Investigate the effect of the core-shell structure on the colloidal stability of the nanogels by testing both polyNIPAM and polyNIPMAM in the cores and shells and looking at the change in aggregation temperature of each nanogel.
- Select the degradation conditions which allow slow degradation of the nanogel particle to gain further insight into how degradation occurs. The structure of nanogels changes with increasing temperature as they de-swell, so these degradation conditions will also be used to look at the effect of temperature on degradation rate of the nanogels.

5.2. Results and Discussion

5.2.1. Degradable Nanogel Synthesis and Characterisation

To create a nanogel which was both degradable and able to aggregate below 37 °C at physiological ionic strength, a series of core-shell nanogels were produced with a polyNIPMAM core and polyNIPAM shell, (table 5.1). The mol% of NIPAM and NIPMAM used varied in order to minimise the polyNIPAM content in the shell with the aim of potentially reducing the amount of non-degradable cross-links introduced by NIPAM polymerisation, whilst retaining a polyNIPAM shell with a thickness great

enough to allow aggregation below 37 °C at physiological ionic strength, due to the underlying core with a higher aggregation temperature. The full composition of reactants used to create these nanogels can be found in (table M.5.1, Methods), The molar concentration ratio of monomer, cross-linker, and initiator was kept constant between samples and across core and shell stages of synthesis. These nanogels consisted of a decreasing mol% NIPMAM monomer used to create the core, compared to increasing mol% of NIPAM used for the synthesis of the shell. (The samples are named with the monomer in the core, followed by the monomer in the shell, followed by CS to represent the core-shell nature of the sample, and the ratio of mol% monomer used to create the core and shell. PNIPAM is abbreviated to PAM and PNIPMAM is abbreviated to MAM. For example "MAM/PAM CS 100/0"). The mol% of NIPMAM used decreased from 100, 70, 50, 30 to 15 mol% (MAM/PAM CS 100/0, MAM/PAM CS 70/30, MAM/PAM CS 50/50, MAM/PAM CS 30/70, MAM/PAM CS 15/85) respectively. In addition to these samples, a nanogel of 100 mol% NIPAM (PAM/MAM CS 100/0) was produced. A visual representation of the samples can be seen in figure 5.3. All nanogels showed a characteristic deswelling with increasing temperature (figure 5.4), and had a hydrodynamic diameter in the range of 86-208 nm at 25 °C, with no strong trends in nanogel size observed, (table 5.1). The PdI of all samples was also low (≤ 0.03), suggesting a single population of low dispersity samples were synthesised. The core-shell nanogels tended to be similar in size (149-208 nm), and all the nanogel samples were larger than the nanogels consisting of 100 mol% NIPAM, (PAM/MAM CS 100/0) (86 nm), despite the same total moles of monomer being used for each nanogel. This suggests the 100 mol% NIPAM nanogel may be more densely cross-linked and hence limited in the size it is able to swell to, or a smaller number of larger nanoparticles are formed when NIPMAM monomer is used in the synthesis.

Table 5.1 Composition and properties of core shell nanogels degradable into short polymer fragments produced using the monomers NIPAM and NIPMAM.

Sample	NIPMAM mol%[a]	NIPAM mol%[a]	Cross-linker Core/shell	Hydrodynamic Diameter[b] (nm)	PdI	Swelling Ratio[c]	Aggregation Temperature (°C)
MAM/PAM CS 100/0	100	0	BAC/BAC	152	0.02	1.31	43
MAM/PAM CS 70/30	70	30	BAC/BAC	201	0.02	1.36	41
MAM/PAM CS 50/50	50	50	BAC/BAC	149	0.01	1.30	38
MAM/PAM CS 30/70	30	70	BAC/BAC	167	0.02	1.21	37
MAM/PAM CS 15/85	15	85	BAC/BAC	166	0.01	1.21	34
PAM/MAM CS 100/0	0	100	BAC/BAC	86	0.03	1.19	34
PAM/MAM CS 50/50	50	50	BAC/BAC	208	0.03	1.38	42
PAM/MAM CS 50/50 BIS[d]	50	50	BAC/BIS	208	0.01	1.76	41

[a] mol% based on total moles of NIPMAM and NIPAM, excludes moles of cross-linker and initiator used (see table M.5.1, methods, for complete mol% composition of reactants)
[b] Hydrodynamic diameter of an aqueous dispersion at 25 °C and 1 mg ml^{-1} using DLS with the mean value of triplicate measurements.
[c] Swelling ratio calculated using H_d (Hydrodynamic diameter). H_d (25 °C)/H_d (55 °C).
[d] Control sample created using a core crosslinked with non-degradable N,N′-methylenebis(acrylamide) (BIS) crosslinker.

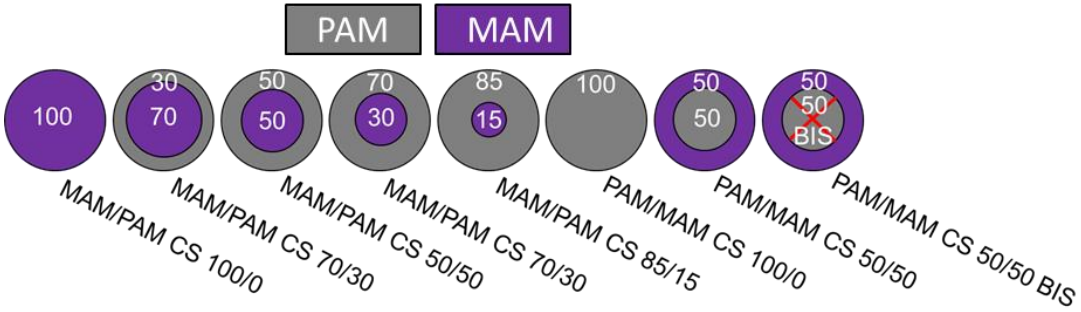

Figure 5.3 Illustration of the core shell structure and monomer composition of the degradable nanogel samples. NIPAM monomer shown in grey, and NIPMAM monomer in purple.

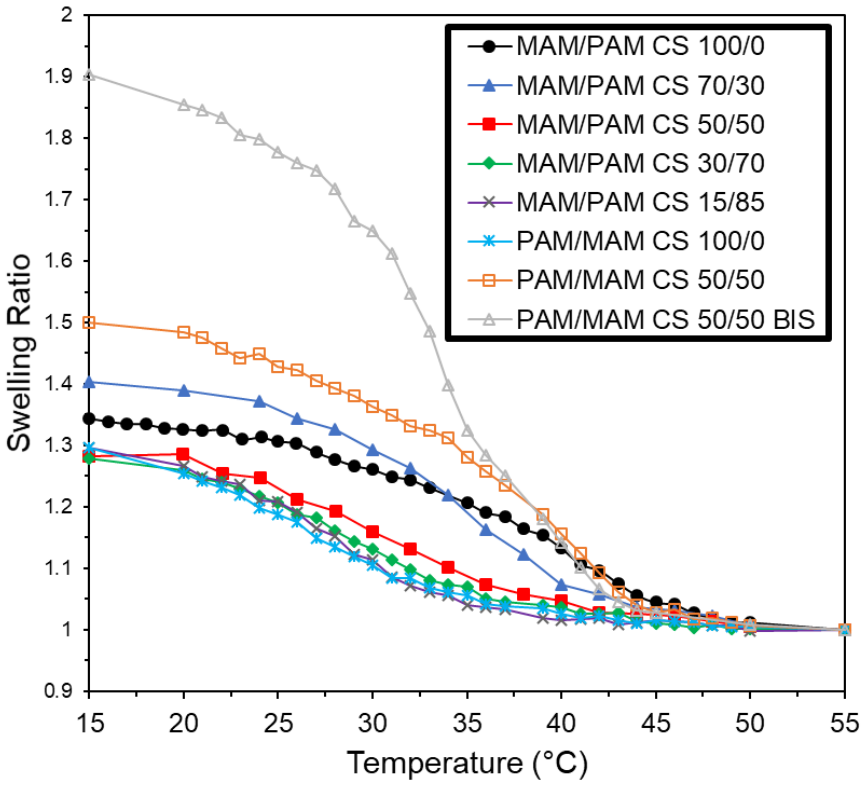

Figure 5.4 Swelling ratio of nanogel samples with temperature. Swelling ratio calculated using H_d (Hydrodynamic diameter) of nanogel at given temperature (T). H_d (T)/H_d (55 °C). Hydrodynamic diameter provided by DLS measurements on a 1 mg ml^{-1} aqueous dispersion using the mean value of triplicate measurements.

This range of nanogels all have a similar swelling ratio (1.19-1.36) at 25 °C with the exception PAM/MAM CS 50/50 BIS, with a decrease in swelling ratio as the mol% of PAM used in the synthesis increases (figure 5.5). Varga *et al.* showed for polyNIPAM nanogels, swelling ratio was linked to cross-linking density,[38] and more recently this was shown to be applicable to polyNIPMAM nanogels.[21] Particles with a higher cross-linking density are more constrained, and therefore have a lower swelling ratio. Nanogels with a greater PAM mol% hence can be considered to contain a higher overall cross-linking density due to their lower swelling ratio. In other studies, nanogels which were synthesised with PAM or MAM monomer contained a heterogeneous or homogeneous distribution of cross-linking, depending on the cross-linking agent and polymerisation conditions used.[21,39] PAM also undergoes polymerisation at a different rate to MAM, leading to a different reactivity ratio of monomer and cross-linking agent.[40,41] Therefore the swelling ratio could be due to

differences in the distribution of the cross-linking with each of the two monomers giving a different internal nanogel structure. A study using a different cross-linking agent, (1,2-dihydroxylethylene)-bisacrylamide), showed that it was distributed more homogeneously through a polyNIPMAM than a polyNIPAM nanogel.[17] Studies into the reaction kinetics, and internal structure of the nanogels would be required to provide further insight into the reason behind the increasing cross-linking density for nanogels synthesised with greater mol% of PAM monomer with BAC cross-linking agent compared to MAM monomer, and whether more homogeneous cross-linking occurs in the nanogel of one of the polymers over the other.

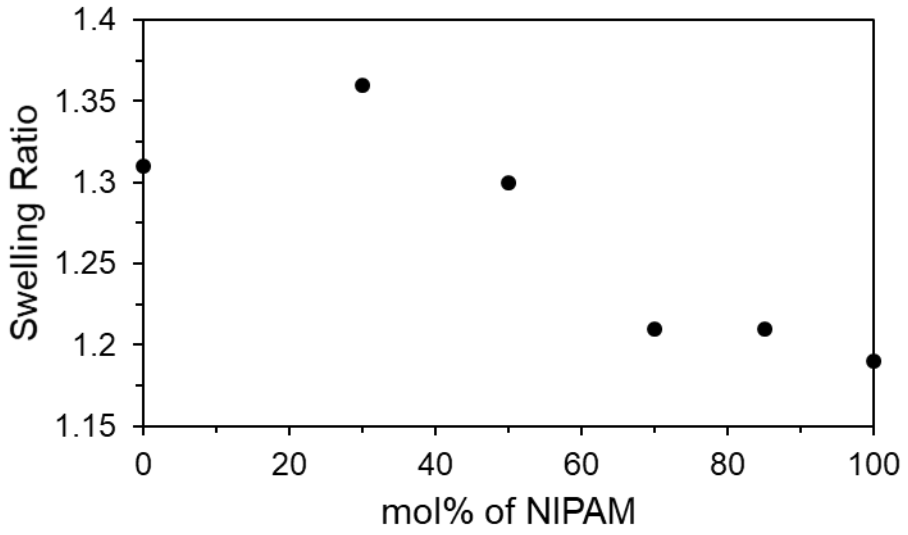

Figure 5.5 Swelling ratio of nanogel compared to mol% of NIPAM (as a mol% of NIPAM and NIPMAM) used in synthesis. Swelling ratio calculated using H_d (Hydrodynamic diameter). H_d (25 °C)/H_d (55 °C)

The aggregation temperature of the nanogels in PBS (1X strength, pH 7.4) was found by heating them in 1 °C intervals to determine the temperature at which the particles aggregated. This temperature was indicated by a dramatic rise in hydrodynamic diameter and sample dispersity value (figure A.1, Appendix).[32] The aggregation temperature of 100 mol% MAM nanogel (MAM/PAM CS 100/0) was 43 °C, while for the 100 mol% PAM nanogel (PAM/MAM CS 100/0) it was 34 °C, (figure 5.6). For the samples of increasing mol% MAM used to create the nanogel core, the aggregation temperature also increases between these two temperature values.

Therefore despite polyNIPMAM being contained within the core of the particle, it still exerts some influence on the overall aggregation temperature as seen previsouly.[32] Some interpenetration exists between the core and shell of polyNIPAM core, polyNIPMAM shell nanogels,[42] hence it is reasonable to assume this interpenetration exists when the monomer in the core and shell is switched around. As the polyNIPAM shell collapses with temperature, the interpenetrating polyNIPMAM core is likely able to provide a degree of colloidal stability, shifting the aggregation temperature higher and towards that of polyNIPMAM particles (43 °C), compared to polyNIPAM particles (34 °C). There was no increase in aggregation temperature upon moving from a 100 mol% polyNIPAM nanogel (PAM/MAM CS 100/0) to a nanogel with a 15 mol% polyNIPMAM core (MAM/PAM CS 15/85), likely due to the shell being too thick for the interpenetrating core to provide any colloidal stability upon shell collapse.

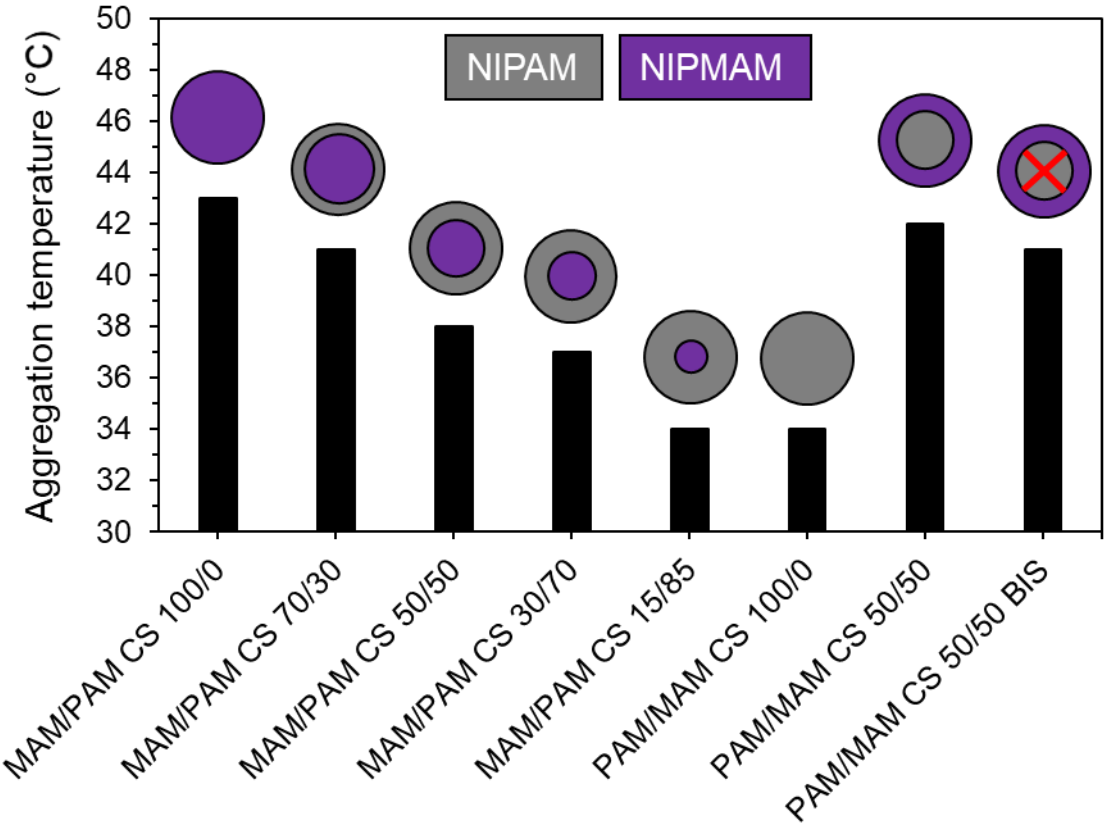

Figure 5.6 Aggregation temperature of nanogel and core-shell nanogels synthesised with NIPAM and NIPMAM monomers.

Two samples were synthesised in which the monomer used in the core and the shell was reversed compared to the previous samples. The first of these, (PAM/MAM CS 50/50), consisted of 50 mol% of NIPAM monomer to create the core, and 50 mol% NIPMAM for the shell, to assess the effect on the colloidal stability of the particle when the monomer in the core was switched to the shell and vice versa. The second (PAM/MAM CS 50/50 BIS) had the same mol% values, however, BIS was used in place of BAC in the synthesis of the core, to create a nanogel with only a degradable shell as a control sample (table 5.1, figure 5.3). These samples also showed a characteristic deswelling with rise in temperature (figure A.1, Appendix) and low PdI values (table 5.1). Comparing PAM/MAM CS 50/50 to MAM/PAM CS 50/50, having a shell consisting of polyNIPMAM as opposed to polyNIPAM gave an aggregation temperature 4 °C higher, (figure 5.6). This aggregation temperature (42 °C), for the PAM/MAM CS 50/50 sample was very close to that of the sample consisting of 100 mol% MAM monomer, MAM/PAM CS 100/0 (43 °C), despite a significant polyNIPAM core being present. The difference between PAM/MAM CS 50/50 and MAM/PAM CS 50/50 is that the core, rather than shell collapses in PAM/MAM CS 50/50. This suggests that when the core collapses at elevated temperature, the nanogel shell allows the particle to remain colloidally stable, whereas when the shell collapses, the core can only provide limited colloidal stability to the nanogel. This is because steric stabilisation is provided be solvated polymer on the surface of the nanogel.[43] So the aggregation temperature is unaffected by the polymer in the core becoming unsolvated. However, when the shell becomes insoluble and collapses into the core, the still solvated core is only able to somewhat penetrate through the collapsed shell to provide solvated polymer on the nanogel surface, hence the lower aggregation temperature. This behaviour of PAM/MAM CS 50/50 could find potential use in systemic drug delivery of poorly water-soluble drug, as polymeric hydrophobic core, hydrophilic shell vehicles which are colloidally stable at physiological temperature and ionic strength have previously used to encapsulate and deliver poorly water-soluble drugs.[44–46] The sample MAM/PAM CS 30/70 has an aggregation temperature of (37 °C); with the main aim being to synthesise a nanogel which is able to aggregate under physiological conditions to form a drug delivery

depot, therefore nanogels synthesised with a 30 mol% or below NIPMAM core are able suitable for an aggregate drug delivery depot.

The swelling ratio of the PAM/MAM CS 50/50 BIS (1.76) was significantly larger than any other sample (table 5.1), likely due to this being the only sample with a BIS cross-linking agent being incorporated into the core of the nanogel. BIS cross-linke has been shown to be incorporated inhomogeneously in polyNIPAM nanogel synthesis, changing the swelling ratio compared to homogeneous incorporation from a controlled feed.[39] Therefore the reactivity ratio of NIPAM with BAC may have a different reactivity compared with BIS, due to the difference in swell ratio. To investigate this, the reaction kinetics of NIPAM with each cross-linking agent were investigated by monitoring the evolution of hydrodynamic diameter and PdI over the first five hours of the reaction. Samples PAM-BIS and PAM-BAC were synthesised using the same molar concentration of monomer, cross-linking agent and initiator as other samples (table M.5.1, methods), to create polyNIPAM nanogels cross-linked with BIS and BAC respectively. It can be seen in figure 5.7 that for PAM-BIS the hydrodynamic diameter of the particles remains constant, and the PdI remains low and constant, whereas in PAM-BAC, PdI decreases from an initially high value, and the hydrodynamic diameter increases and then begins to plateau over the first 5 hours of the reaction. This suggests that the PAM-BIS reaction is completed within the first hour, as seen previously,[47] however the PAM-BAC reaction proceeds more slowly, with polymerisation and hence particle growth continuing for ~5 hours. This may have had some effect on the samples synthesised with NIPAM and BAC in the core of the nanogel, where ideally polymerisation of the core would have been conducted for a longer time period to ensure all of the monomer was converted into polymer before commencing polymerisation of the shell. The effect of this is there was likely a less defined transition from core to shell in the nanogels as some of the core monomer was left to join the polymerisation with the shell monomer.

During the synthesis, precursor particles form, which both aggregate, and grow to achieve colloidally stable polymer particles.[48,49] This process leads to an increase in particle size until the polymerisation is complete.[47] The PdI of PAM-BAC is also initially high due to the existence of growing particles, precursor particles and oligomers, and aggregation between these species during synthesis.[49–51] The PdI

stabilises (at a low value for monodisperse particles) when the polymerisation reaches completion, with no further precursor particles forming, or aggregation taking place between particles once they are colloidally stable. Hence it can be concluded that polymerisation of NIPAM proceeds more slowly with BAC than BIS. This gives particles of lower swelling ratio, and hence higher cross-link density, which is likely due to more homogeneous cross-linking occurring.

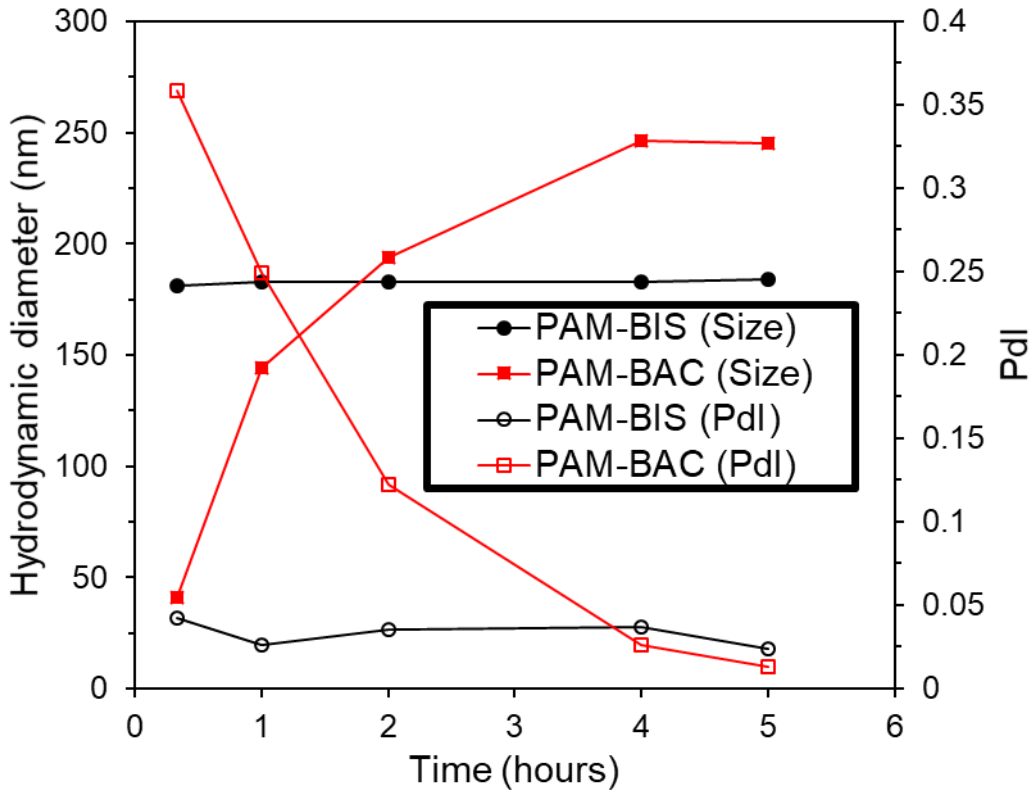

Figure 5.7 Kinetic study of polyNIPAM nanogel synthesis with BIS (PAM-BIS) and BAC (PAM-BAC) cross-linking agents showing evolution of nanogel particle hydrodynamic diameter and PdI over time during the polymerisation reaction. Samples measured using DLS with the mean value of triplicate measurements used.

5.2.2. Nanogel Degradation

In order to completely degrade particles into short polymer fragments over a measurable time period, DTT was used in excess (150 mM, ~350 equivalents of DTT for each cross-link) at pH 10 to degrade the nanogel particles. It was found that all nanogels showed a high degree of degradability. DLS was used to measure the mean count rate in kilo counts per second (k.c.p.s.) of the sample before and after degradation, keeping the attenuator value and measurement position of the laser fixed for a specific sample before and after degradation. The mean count rate of each nanogel

was reduced to 0.9 – 6.7 % of its original value after degradation for all samples except PAM/MAM CS 50/50 BIS, which only degraded to 48.1% of its original count rate, due to its non-degradable core, (table 5.2).

Table 5.2. Mean count rate reduction upon sample degradation of 1 mg ml^{-1} aqueous dispersion with 150 mM DTT at pH 10.

Sample	% of original count rate after degradation
MAM/PAM CS 100/0	0.9
MAM/PAM CS 70/30	1.8
MAM/PAM CS 50/50	5.5
MAM/PAM CS 30/70	1.0
MAM/PAM CS 15/85	1.3
PAM/MAM CS 100/0	1.2
PAM/MAM CS 50/50	6.7
PAM/MAM CS 50/50 BIS	48.1

This is expected as only the shell can degrade, leaving a non-degraded core with a significant count rate. Previous work by Gaulding *et al.* showed that polyNIPMAM nanogels cross-linked with BAC were not fully degradable unless low temperature redox polymerisation was employed.[21] With dispersion polymerisation conducted overnight at 80 °C leading to only partially degradable particles. Therefore, a lower temperature and reaction time of 70 °C and 4 hrs respectively appears to have significantly reduced the proposed chain transfer reactions which involve the di-sulphide bond. With polyNIPAM nanogels also showing a high degree of degradability, the proposed chain transfer reactions occurring from proton abstraction from the polymer backbone,[17] may also have been reduced with a shorter reaction time. The polyNIPAM nanogel kinetic study samples PAM-BIS and PAM-BAC containing BIS and BAC cross-linking agent respectively were degraded with DTT at each timepoint in the reaction. PAM-BIS showed no degradation as expected, whilst PAM-BAC remained completely degradable in the first 5 hours of polymerisation, with a negligible measurable count rate after particle degradation (figure 5.8). It is clear that the causes of this underlying hindrance to complete nanogel degradation requires further investigation, to determine how a greater reaction duration and higher synthesis temperature reduce the amount of degradation that can occur within the particle.

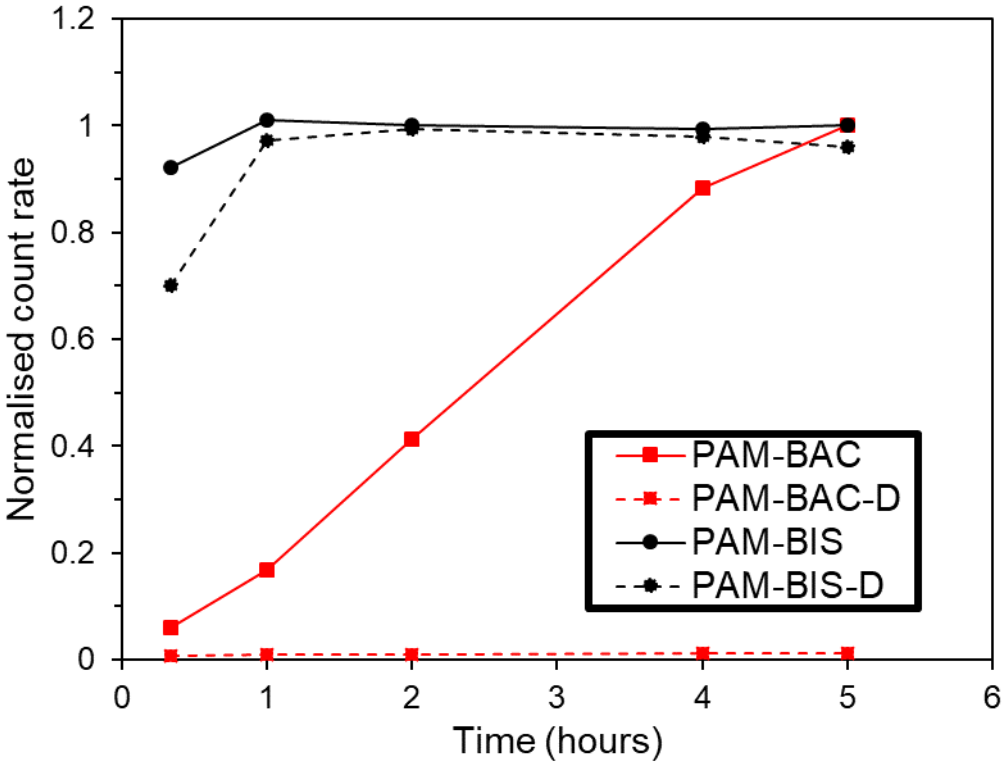

Figure 5.8 During polyNIPAM nanogel synthesis sample was terminated at each time point and a normalised count rate was measured for kinetic study with BIS (PAM-BIS) and BAC (PAM-BAC) cross-linking agent. Each PAM-BAC and PAM-BIS sample was then degraded using the addition of 150 mM DTT to degrade the nanogel particles giving PAM-BIS-D and PAM-BAC-D. Samples measured using DLS with the mean value of triplicate measurements used.

To study the degradation process more in depth, and the effect of temperature on degradation rate, the pH of the dispersion was lowered from pH 10 to pH 7 to give a much longer degradation period. The thiols of DTT have a pK_a of 9.2 and 10.1 respectively. Therefore at a pH lower than ~9, less of the of DTT exists in the active thiolate form which is able to initiate the di-sulphide exchange reaction and cleave the di-sulphide bonds contained within the nanogel. Hence degradation occurs more slowly at lower pH. This time dependence of degradation with pH can be seen visually in figure 5.9. Two turbid dispersions of MAM/PAM CS 50/50 at 1 mg ml^{-1} at pH 7 were formed with 150 mM DTT. When a volume of NaOH solution was added which increased the pH to 10, and the sample was shaken, rapid degradation occurred, indicated by the significant change in turbidity of the solution. When the equivalent volume of water rather than NaOH solution was added, no change in turbidity was initially seen, due to the much slower rate of degradation at pH 7. Hence the decrease

in mean count rate with degradation of the sample could be monitored over a longer time period at pH 7 to gain an understanding of the degradation process. The time taken for complete degradation to occur could also be changed by changing the molarity of DTT present at pH 7. MAM/PAM CS 50/50 was degraded with 150, 15 and 1.5 mM solutions of DTT. Complete degradation occurred within 16 hours with 150 and 15 mM DTT solutions, however degradation took up to 46 hours with 1.5 mM DTT, (figure A.2, Appendix).

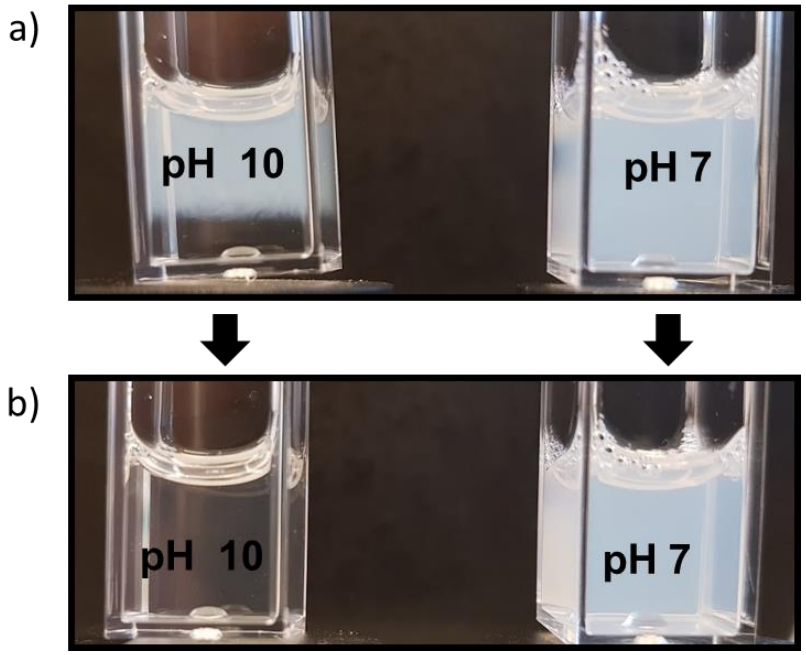

Figure 5.9 Change in turbidity caused by degradation of MAM/PAM CS 50/50 at 1 mg ml^{-1} with 150 mM DTT at a much faster rate at pH 10 than pH 7. a) Aqueous NaOH solution (0.1 M) (left) and water (right) added to dispersion, b) dispersion after shaking for 2 seconds.

The degradation of MAM/PAM CS 50/50 over time was monitored using 150 mM DTT and a pH of 7, allowing a long enough degradation time to create a detailed degradation profile using DLS, (figure 5.10). The count rate of the sample decreased over a 14 hour period of degradation. In this period the PdI remained low and increased slightly at the end of the degradation period at ~11 hours. The hydrodynamic diameter of the particles continuously increased over the degradation period by 72%. This can be explained by the effects caused from cross-link scission in the nanogels. Previous work has showed that the size a nanogel is able to swell to is constrained by the density of cross-linking present.[47,52] Therefore, as cross-links are broken over time, the polymer network is less restrained and so able to swell to a larger hydrodynamic diameter in the first 13 hours of degradation.[17] After 13 hours, the scattering intensity became too low to continue measuring the hydrodynamic diameter, as essentially all

particles have now dissolved into oligomers with low scattering cross sections as all cross links are broken by the end of the degradation period.[17] The count rate dropped in a similar manner to that seen for the degradation of particles in other work where the count rate gradually dropped to less than 35% of original value.[12,37] The decrease can be explained by the fact that polymer chains were progressively lost from the particle over time, as cross-link scission occurred. This effect, combined with the swelling of the particle, reduced the refractive index difference between the particle and solvent, and hence the scattering intensity decreased, leading to a dramatic decrease in the count rate measured over 13 hours, to the point at which essentially all particles had degraded into oligomers. Finally, the PdI remained low throughout the degradation period, suggesting all nanogel particles degraded and swelled at the same rate. Towards the end of the degradation after ~12 hours the PdI increased, likely due to the complete disintegration of individual particles into smaller fragments and finally oligomers at slightly different times. Again, the scattering intensity was too low to continue measuring PdI after ~13 hours of degradation to give reliable data (count rate below measurable range) as it was likely no particles were left to scatter enough light for sample measurements, so at this point, measurements were simply being made on low levels of contamination in the sample, such as from dust.

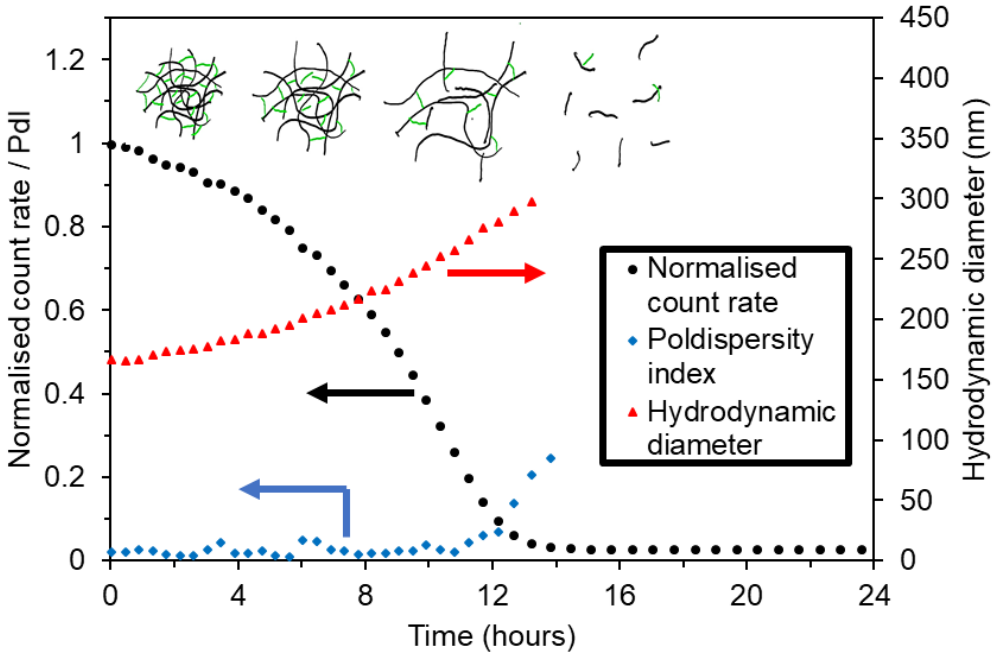

Figure 5.10 Degradation of MAM/PAM CS 50/50 at pH 7, 25 °C, with 150 mM DTT. Count Rate, PdI and hydrodynamic diameter were monitored over time. Samples measured using DLS with the mean value of triplicate measurements used.

Due to the deswelling behaviour of polyNIPAM/polyNIPMAM nanogels in response to increasing temperature, it was expected that this would influence the rate of degradation of the nanogels, as the particles become a denser polymer network with increasing temperature. The degradation of MAM/PAM CS 50/50 with DTT at pH 7 was monitored with sealed cuvettes at different temperatures, (figure 5.11). Upon increasing the temperature from 10 to 25 °C, normalised count decreased over a shorter time frame indicating that the rate of degradation had increased, with degradation time reduced from 1.6 to 0.6 days (figure 5.11, a). However, when temperature was increased from 25 to 40 °C, the rate of count rate decrease over time was dramatically lower, which indicates the degradation rate decreased dramatically at higher temperature, (figure 5.11, b), with an increase in degradation time from 0.6 to 4 days on moving from 25 to 32.5 °C. This can be explained by the fact that at low temperature (10 to 25 °C) polyNIPAM/polyNIPMAM nanogels remain hydrophilic in nature, containing a high degree of water,[53] with little change in swelling as the temperature increases, (figure A.1, Appendix). Therefore the increase in degradation rate with temperature can be attributed to a faster thiol-disulphide exchange reaction rate occurring at higher temperature.[54] The degradation rate decreased above 25 °C, as polyNIPAM/polyNIPMAM nanogels start to dramatically deswell as the temperature increases towards the LCST of the polymers contained in MAM/PAM CS 50/50 (figure 5.4),[30,55] and a decrease in water content occurs as the nanogel environment becomes more hydrophobic in nature. This creates an environment where the disulphide bonds are less solvent accessible, so that they are more difficult to reduce with DTT.[56] Ainavarapu *et al.* showed that the reduction of solvent inaccessible di-sulphide bonds in 100 mM DTT was very slow compared to solvent accessible di-sulphide bonds.[57] Hence the degradation rate of the MAM/PAM CS 50/50 decreases when increasing the temperature above 25 °C. A similar effect would be expected for GSH *in vivo*, as GSH is also a highly water soluble reducing agent which resides in an aqueous environment like DTT.[58]

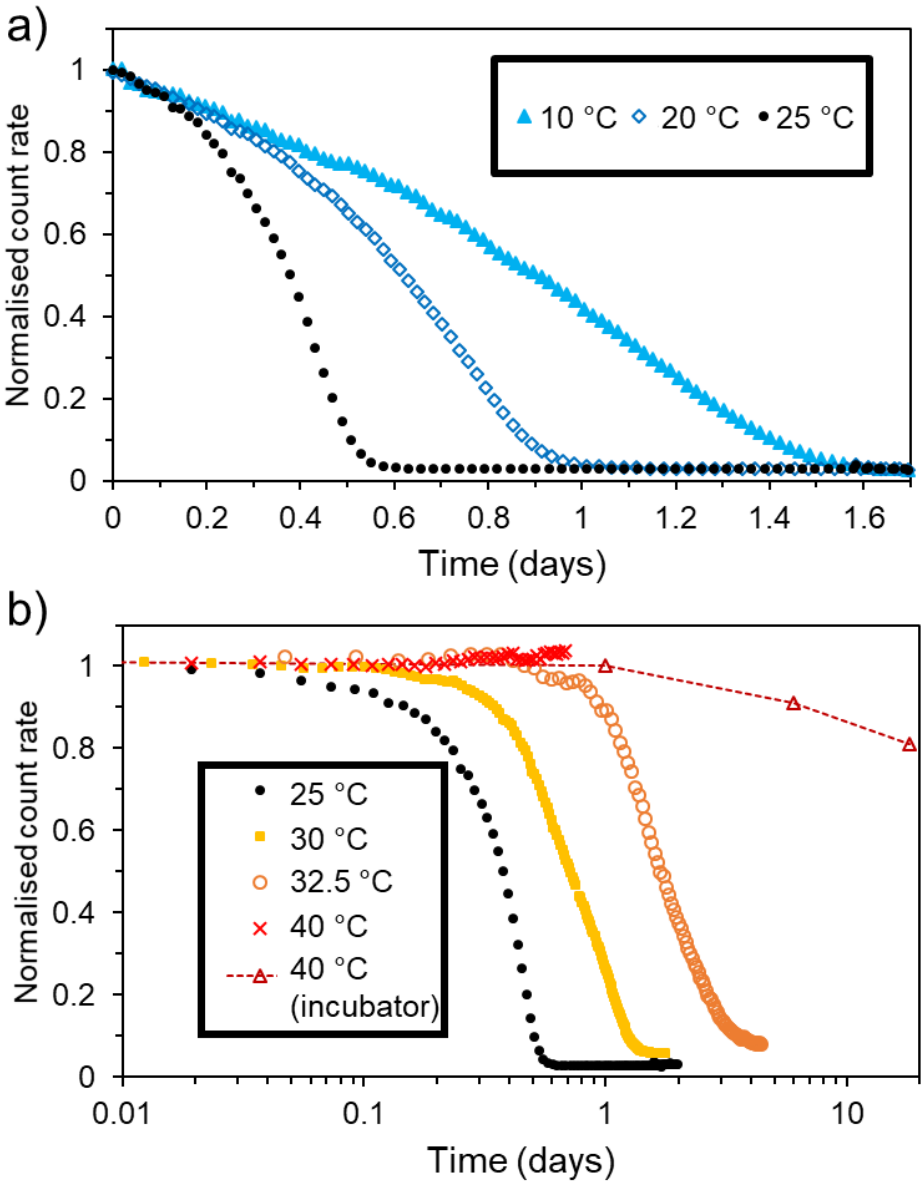

Figure 5.11 Time dependence of count rate for MAM/PAM CS 50/50 at pH 7, with degradation conducted in 150 mM DTT at different temperatures, a) 10, 20 and 25 °C, (linear time scale) b) 25, 30, 32.5 and 40 °C (logarithmic time scale). Samples measured using DLS with the mean value of triplicate measurements used.

At 40 °C no decrease in count rate was seen in the first day, suggesting little or no degradation occurs at this temperature on this timescale. Therefore, a sample was held at 40 °C in an incubator and transferred at specific times into the measuring chamber of the DLS equipment preheated to the same temperature to measure over a longer time period. The count rate began to decrease over the first 18 days, dropping to 81% of its initial value, (figure 5.11, b), suggesting degradation slowly takes place. The loss of polymer and increase in swelling with disulphide bond scission on the surface of

the particle likely slowly exposes disulphide bonds further into the interior of the particle over time, so that at 40 °C the particles are degraded very slowly. DTT is not stable for a long time in reduced form,[56] however by conducting the degradation at pH 7, the reducing activity of DTT was likely prolonged, due to only a small fraction of the DTT being present in reduced form at a given time. However, although DTT was present in excess, it is likely that DTT would still lose it reducing power over the 18 days the experiment was conducted. Hence although it's likely that degradation takes place slowly at 40 °C, this requires further investigation, where DTT is replaced continuously or at given timepoints, and stabilised, for example with egtazic acid to reduce the loss of reducing power.[59] A nanogel control would also need to be performed in a future study to ensure nanogels were not undergoing sedimentation at elevated temperature over an extended time period.

The dramatic effect on degradation rate with temperature enable nanogels to be created, which in the short term remain relatively stable in a highly water soluble reducing agent at 40 °C, but rapidly degrade at 25 °C. This can be demonstrated by initiating degradation for two samples of MAM/PAM CS 50/50 at 25 °C (**I**) and 40 °C (**II**) respectively, (figure 5.12). After 0.66 days, for the sample at 25 °C (**I**), the count rate has dropped to 2.9% of its original value and the hydrodynamic diameter has increased as the particle has swollen and disintegrated. In the same period of time, the sample at 40 °C (**II.a**) has maintained its starting count rate and particle hydrodynamic diameter, suggesting no significant degradation has occurred. When this sample is then cooled to 25 °C (**II.b**), the count rate and hydrodynamic diameter change at the same rate as sample (**I**). The degradation process is effectively 'switched on' by the 15 °C drop in temperature.

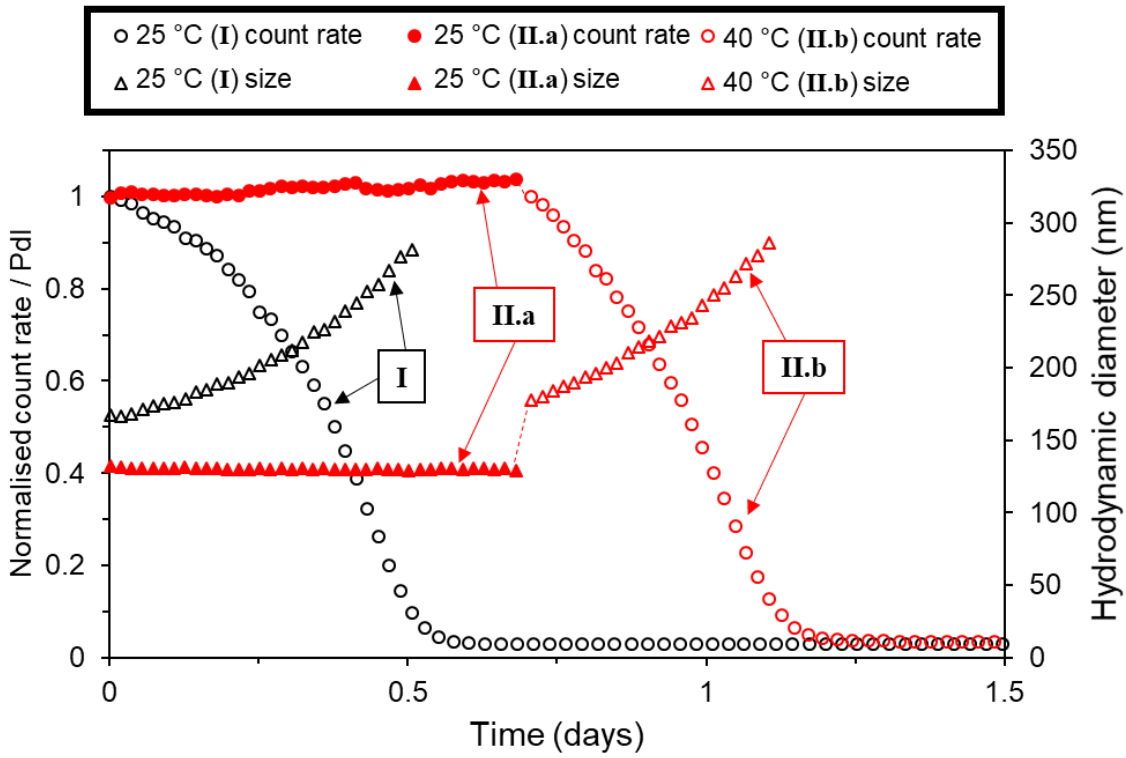

Figure 5.12 Time dependence of count rate and hydrodynamic diameter for MAM/PAM CS 50/50 at pH 7, with degradation conducted in 150 mM DTT at 25 °C (**I**), or at 40 °C (**II.a**), followed by a reduction in temperature to 25 °C (**II.b**). Samples measured using DLS with the mean value of triplicate measurements used.

5.3. Conclusion

The degradable cross-linking agent BAC, which contains a disulphide bond was successfully utilised in the synthesise of degradable nanogels based on NIPAM and NIPMAM. Single monomer nanogels, and core-shell nanogels of the two different monomers were produced. For core-shell nanogels the aggregation temperature was shown to be dependant not only on the LCST of the respective monomers, but also to be more sensitive to the LCST of the shell than the core. A nanogel was also synthesised which contained a collapsed hydrophobic core, whilst also remaining colloidally stable under physiological conditions due to its higher LCST shell (PAM/MAM CS 50/50). This may be useful for the delivery of poorly water-soluble drug. All the nanogels synthesised were shown to be essentially completely degradable, despite previous published work by others sometimes leading to only partially degradable nanogels when BAC cross-linking agent, or NIPAM monomer

were employed using a longer reaction time or higher temperature. The effect of temperature and reaction time on the formation on non-degradable cross-links in the synthesis requires a more in-depth study. It was shown that the degradation process could be monitored over time using DLS to measure sample mean count rate, particle hydrodynamic diameter, and PdI. The particles swell and appear to degrade at a constant rate to one another over the degradation period. Temperature was also shown to have a great effect on the rate of particle degradation, with degradation occurring in less than a day at 25 °C under reducing conditions, but over a week at 40 °C. The exact rate of degradation at 40 °C is yet to be determined. With the reduction in normalised count rate from 100% to 80% in 2 weeks, the degradation rate appears to be increasing and it would be expected that degradation into polymer fragments would eventually occur fully. This may allow the depot to provide long-term sustained release of drug before being degraded and removed from the body, however this requires further investigation.

5.4. Materials and Methods

5.4.1. Materials

N-Isopropylacrylamide (NIPAM, ≥99%), N-isopropylmethacrylamide (NIPMAM, 97%), N,N-methylenebis(acrylamide) (BIS, 99%), potassium persulfate (KPS, ≥99%), sodium chloride (NaCl, ≥99.5%), anhydrous sodium hydroxide pellets (NaOH, analysis grade), sodium dodecyl sulphate (SDS, ≥99%) were purchased from Sigma-Aldrich Company Ltd, Gillingham (Dorset) UK, a subsidiary of Merck KGaA, Darmstadt, Germany. Phosphate buffered saline tablets (Bioreagent), hydrochloric acid 37% (HCl, analytical grade), were purchased from Fischer Scientific UK, Loughborough, UK, a part of Thermo Fisher Scientific. N,N′-Bis(acryloyl)cystamine (BAC, 98%) was purchased from Alfa Aesar, Lancashire, UK, a subsidiary of Thermo Fisher Scientific, Waltham (Massachusetts), USA. 1,4-Dithiothreitol (DTT, 97%) was purchased from Manchester organics Ltd., Runcorn, UK, a subsidiary of Navin Fluorine International Ltd., Mumbai, India. Type I distilled water obtained from a water purification system with a resistivity of >18 MΩ cm−1 (PURELAB option R, Veolia). Spectra/por 2 (MWCO = 12-14 kDa) dialysis tubing was purchased from Spectrum Europe B.V., Breda, The Netherlands.

5.4.2. Synthesis of Degradable PolyNIPAM Nanogels

The polyNIPAM nanogels were synthesized by dispersion polymerisation. The composition used in the synthesis of each nanogel can be found in table M.5.1. For the synthesis of the core, the NIPAM or NIPMAM monomer, BIS or BAC cross-linking agent and SDS surfactant were dissolved in distilled water in a 250 mL two-neck round bottom flask equipped with a stir bar and reflux condenser. This was then sealed and nitrogen was bubbled through the aqueous solution for 1 hour whilst stirring (400 rpm) to remove dissolved oxygen. The solution was then heated to 70 °C. Separately KPS initiator was dissolved in distilled water and degassed with N_2 for 1 hour before being transferred to the flask containing the monomers. The reaction was maintained under a N_2 atmosphere for 1 hours at 70 °C before further addition of the shell monomer, cross-linking agent and SDS which were separately sealed and degassed with nitrogen for 1 hour whilst stirring (400 rpm), and further KPS initiator. After a further 3 hours at 70 °C the solution was cooled down to room temperature. Where only a core was synthesized, the reaction was simply conducted for 4 hours to give the same total reaction time. To remove unreacted impurities, the nanogel suspension was dialyzed for 5 days using regenerated cellulose dialysis tubing (12-14 kDa MWCO, Spectrum Labs), replacing the distilled water every 12 hours. The purified suspension was then lyophilized (Virtis Benchtop K with ultra-low temperature condenser) and stored in a desiccator.

For the kinetics study, the same reaction conditions were used, however samples were taken from the reaction at specific time intervals and terminated by immediately cooling the sample to 0 °C in and ice bath whilst simultaneously bubbling air into the solution.

Table M.5.1 Nanogel reactants composition.

Sample	Monomer[a] (93 mol%)		BAC (5 mol%)		KPS[b] (2 mol%)		SDS		Water[d]	
	NIMAM mol%	NIPAM mol%	Core mol%	Shell mol%	Core mol%	Shell mol%	Core mg	Shell mg	Core mL	Shell mL
MAM/PAM CS 100/0	93	0	5	-	2	-	80	-	140	-
MAM/PAM CS 70/30	65.1	27.9	3.5	1.5	1.4	0.6	56	24	98	42
MAM/PAM CS 50/50	46.5	46.5	2.5	2.5	1	1	40	40	70	70
MAM/PAM CS 30/70	27.9	65.1	1.5	3.5	0.6	1.4	24	56	42	98
MAM/PAM CS 15/85	13.9	79.1	0.75	4.25	0.3	1.7	12	68	21	119
PAM/MAM CS 100/0	0	93	5	-	2	-	80	-	140	-
PAM/MAM CS 50/50	46.5	46.5	2.5	2.5	2.5	2.5	40	40	70	70
PAM/MAM CS 50/50 BIS	46.5	46.5	2.5	2.5	2.5[c]	2.5	40	40	70	70
PAM-BAC		93	5	-	2	-			140	-
PAM-BIS		93	5	-	2	-			140	-

[a] 34.7 mmol of total monomer used in synthesis
[b] 9.38 mg/ml aqueous solution
[c] 2.5 mol% BIS
[d] 160 ml reaction volume, which includes a total addition of 20 ml aqueous KPS.

5.4.3. Characterisation of Degradable PolyNIPAM Nanogels

Dynamic light scattering (DLS) measurements were performed at 25 °C with a 1 mg ml^{-1} nanogel dispersion using an equilibration time of 600 seconds, unless otherwise stated, with a Malvern Zetasizer Nano ZS (running Malvern Zetasizer software V7.12) (Malvern Instruments, Malvern, UK) with 633 nm He–Ne laser and the detector positioned at 173°. 1 cm path length disposable polystyrene cuvettes were used for measurements. Measurements were repeated in triplicate to give a mean Z-average diameter and polydispersity index (PdI) value. Adjustments of dispersion pH were made with NaOH and HCl solutions, and dispersion pH measurements were made with a HI-11310 pH Edge Electrode (HANNA Instruments, Bedfordshire, UK).

5.4.4. Nanogel Degradation Studies

Nanogels were degraded as a 1 mg ml^{-1} pH 10 aqueous dispersion using 150 mM DTT where immediate degradation was required, pH adjustments were made using 0.1M NaOH solution. DLS was used to measure the mean count rate of a degraded and non-degraded sample at the same attenuator value and measurement position. For long term monitoring of degradation, a 1 mg ml^{-1} pH 7 aqueous dispersion of the nanogels was used with 150 mM of DTT unless otherwise stated. The attenuator value was fixed at a value found to be suitable for the dispersion at the start of the degradation, and the measurement position of the laser was fixed at 4.65 mm (centre of the cuvette). For degradation over 6 hours, or at elevated temperatures, the measurement cuvette was sealed to prevent solvent evaporation over time. For the measurement on the sample held in a cuvette at 40 °C, which was transferred between an incubator and a DLS measuring chamber for measurements, the DLS sample chamber was preheated to 40 °C for 10 minutes.

5.5. Appendix

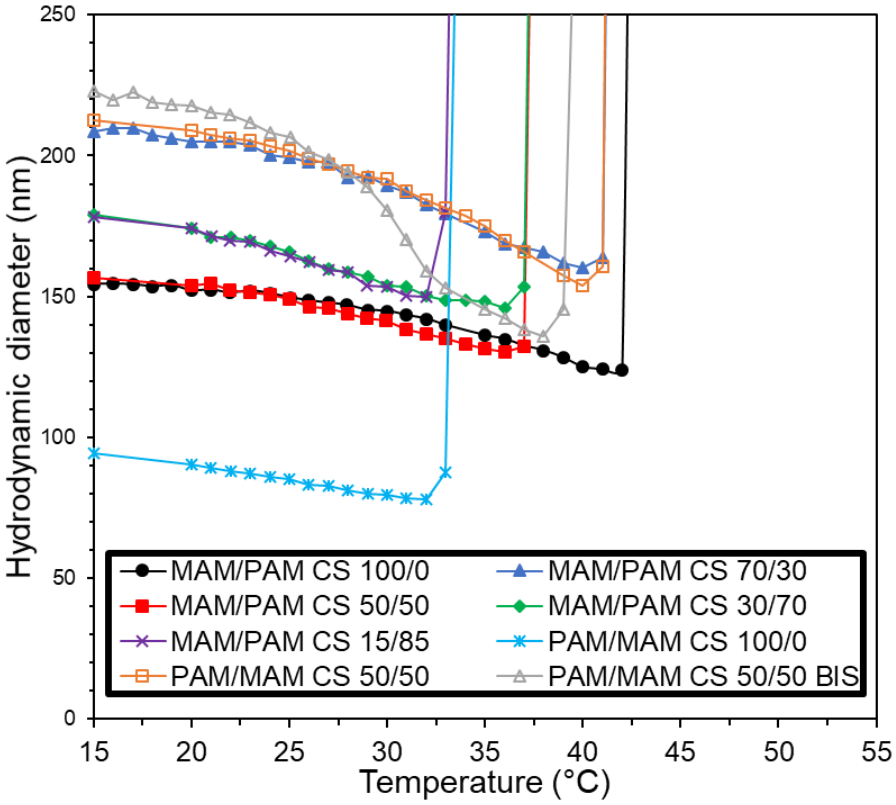

Figure A.1 Stability of nanogel samples in PBS (1X strength, pH 7.4) with increasing temperature. Aggregation temperature reached when dramatic increase in hydrodynamic diameter observed. Hydrodynamic diameter provided by DLS measurements on a 1 mg ml^{-1} PBS dispersion.

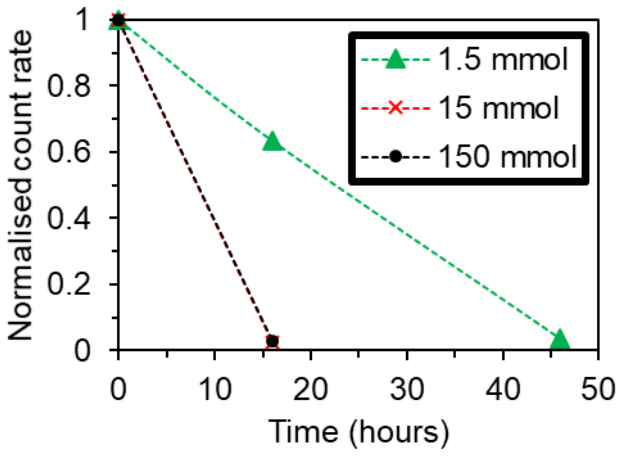

Figure A.2 Reduction in count rate over time of MAM/PAM CS 50/50 as a 1 mg ml^{-1} pH 7 aqueous dispersion in the presence of different concentrations of DTT.

5.6. References

1 A. Hatefi and B. Amsden, *J. Control. Release*, 2002, **80**, 9–28.

2 A. R. Town, M. Giardiello, R. Gurjar, M. Siccardi, M. E. Briggs, R. Akhtar and T. O. McDonald, *Nanoscale*, 2017, **9**, 6302–6314.

3 M. Patenaude and T. Hoare, *ACS Macro Lett.*, 2012, **1**, 409–413.

4 E. Sharmin, in *Nanogels for Biomedical Applications*, eds. A. Vashist, A. K. Kaushik, S. Ahmad and M. Nair, The Royal Society of Chemistry, London, 1st edn., 2018, pp. 29–49.

5 V. Delplace and J. Nicolas, *Nat. Chem.*, 2015, **7**, 771–784.

6 D. J. Siegwart, S. A. Bencherif, A. Srinivasan, J. O. Hollinger and K. Matyjaszewski, *J. Biomed. Mater. Res. - Part A*, 2008, **87**, 345–358.

7 J.-F. Lutz, J. Andrieu, S. Uzgun, C. Rudolph and S. Agarwal, *Macromolecules*, 2007, **40**, 8540–8543.

8 S. Agarwal, *Polym. Chem.*, 2010, **1**, 953.

9 L. F. Sun, R. X. Zhuo and Z. L. Liu, *Macromol. Biosci.*, 2003, **3**, 725–728.

10 L. Ren and S. Agarwal, *Macromol. Chem. Phys.*, 2007, **208**, 245–253.

11 Y. Chen, M. J. van Steenbergen, D. Li, J. B. van de Dikkenberg, T. Lammers, C. F. van Nostrum, J. M. Metselaar and W. E. Hennink, *Macromol. Biosci.*, 2016, **16**, 1122–1137.

12 N. Leber, L. Kaps, M. Aslam, J. Schupp, A. Brose, D. Schäffel, K. Fischer, M. Diken, D. Strand, K. Koynov, A. Tuettenberg, L. Nuhn, R. Zentel and D. Schuppan, *J. Control. Release*, 2017, **248**, 10–23.

13 G. Aguirre, J. Ramos and J. Forcada, *Soft Matter*, 2013, **9**, 261–270.

14 L. Nuhn, N. Vanparijs, A. De Beuckelaer, L. Lybaert, G. Verstraete, K. Deswarte, S. Lienenklaus, N. M. Shukla, A. C. D. Salyer, B. N. Lambrecht, J. Grooten, S. A. David, S. De Koker and B. G. De Geest, *Proc. Natl. Acad. Sci.*, 2016, **113**, 8098–8103.

15 P. D. Thornton, S. M. R. Billah and N. R. Cameron, *Macromol. Rapid Commun.*, 2013, **34**, 257–262.

16 M. Gulfam, T. Matini, P. F. Monteiro, R. Riva, H. Collins, K. Spriggs, S. M. Howdle, C. Jérôme and C. Alexander, *Biomater. Sci.*, 2017, **5**, 532–550.

17 M. H. Smith, E. S. Herman and L. A. Lyon, *J. Phys. Chem. B*, 2011, **115**, 3761–3764.

18 H. Yang, Q. Wang, S. Huang, A. Xiao, F. Li, L. Gan and X. Yang, *ACS Appl. Mater. Interfaces*, 2016, **8**, 7729–7738.

19 Y. Zhan, M. Gonçalves, P. Yi, D. Bora Capelo, Y. Zhang, J. O. Rodrigues, C. Liu, H. Tomá, Y. Li and P. He, *J. Mater. Chem. B*, 2015, **3**, 4221–4230.

20 X. Zhang, S. Lu, C. Gao, C. Chen, X. Zhang and M. Liu, *Nanoscale*, 2013, **5**,

6498–6506.

21 J. C. Gaulding, M. H. Smith, J. S. Hyatt, A. Fernandez-Nieves and L. A. Lyon, *Macromolecules*, 2012, **45**, 39–45.

22 F. Meng, W. E. Hennink and Z. Zhong, *Biomaterials*, 2009, **30**, 2180–2198.

23 B. Gyarmati, Á. Némethy and A. Szilágyi, *Eur. Polym. J.*, 2013, **49**, 1268–1286.

24 G. Saito, J. A. Swanson and K. D. Lee, *Adv. Drug Deliv. Rev.*, 2003, **55**, 199–215.

25 M. C. Yi and C. Khosla, *Annu Rev Chem Biomol Eng.*, 2016, **7**, 197–222.

26 F. G. Ottaviano, D. E. Handy and J. Loscalzo, *Circ. J.*, 2008, **72**, 1–16.

27 R. Singh and G. M. Whitesides, in *Sulphur-Containing Functional Groups (1993)*, eds. S. Patai and Z. Rappoport, John Wiley & Sons, Inc., 2010, pp. 633–658.

28 W. W. Cleland, *Biochemistry*, 1964, **3**, 480–482.

29 S. Fujishige, K. Kubota and I. Ando, *J. Phys. Chem.*, 1989, **93**, 3311–3313.

30 D. Duracher, A. Elaïssari and C. Pichot, *Colloid Polym. Sci.*, 1999, **277**, 905–913.

31 E. I. Tiktopulo, V. N. Uversky, V. B. Lushchik, S. I. Klenin, V. E. Bychkova and O. B. Ptitsyn, *Macromolecules*, 1995, **28**, 7519–7524.

32 S. Wiese, Y. Tsvetkova, N. J. E. Daleiden, A. C. Spieß and W. Richtering, *Colloids Surfaces A Physicochem. Eng. Asp.*, 2016, **495**, 193–199.

33 G. Fundueanu, M. Constantin, S. Bucatariu and P. Ascenzi, *Macromol. Chem. Phys.*, 2016, **217**, 2525–2533.

34 L. Nuhn, L. Braun, I. Overhoff, A. Kelsch, D. Schaeffel, K. Koynov and R. Zentel, *Macromol. Rapid Commun.*, 2014, **35**, 2057–2064.

35 J. Smeraldi, R. Ganesh, J. Safarik and D. Rosso, *J. Environ. Monit.*, 2012, **14**, 79–84.

36 V. V. Vysotskii, O. Y. Uryupina, A. V. Gusel'nikova and V. I. Roldugin, *Colloid J.*, 2009, **71**, 739–744.

37 K. Zou, Q. Liu, J. Chen and J. Du, *Polym. Chem.*, 2014, **5**, 405–411.

38 I. Varga, T. Gilányi, R. Mészáros, G. Filipcsei and M. Zrínyi, *J. Phys. Chem. B*, 2001, **105**, 9071–9076.

39 R. Acciaro, T. Gilányi and I. Varga, *Langmuir*, 2011, **27**, 7917–7925.

40 D. Duracher, A. Elaïssari and C. Pichot, *J. Polym. Sci. Part A Polym. Chem.*, 1999, **37**, 1823–1837.

41 M. H. Kwok, Z. Li and T. Ngai, *Langmuir*, 2013, **29**, 9581–9591.

42 I. Berndt, J. S. Pedersen, P. Lindner and W. Richtering, *Langmuir*, 2006, **22**, 459–468.

43 T. F. Tadros, *Polym. J.*, 1991, **23**, 683–696.

44 S. A. Abouelmagd, B. Sun, A. C. Chang, Y. J. Ku and Y. Yeo, *Mol. Pharm.*, 2015, **12**, 997–1003.

45 B. G. Yu, T. Okano, K. Kataoka and G. Kwon, *J. Control. Release*, 1998, **53**, 131–136.

46 E. V Batrakova, T. K. Bronich, J. A. Vetro and A. V Kabanov, in *Nanoparticulates as Drug Carriers*, ed. V. P. Torchilin, Imperial College Press, London, 2006, pp. 57–93.

47 X. Wu, R. H. Pelton, a. E. Hamielec, D. R. Woods and W. McPhee, *Colloid Polym. Sci.*, 1994, **272**, 467–477.

48 S. Kawaguchi and K. Ito, in *Advances in Polymer Science*, Springer-Verlag Berlin Heidelberg, 2005, vol. 175, pp. 299–328.

49 R. Pelton, *Adv. Colloid Interface Sci.*, 2000, **85**, 1–33.

50 G. R. Hendrickson, M. H. Smith, A. B. South and L. A. Lyon, *Adv. Funct. Mater.*, 2010, **20**, 1697–1712.

51 S. Nayak and L. Andrew Lyon, *Angew. Chemie - Int. Ed.*, 2005, **44**, 7686–7708.

52 C. Obeso-Vera, J. M. Cornejo-Bravo, A. Serrano-Medina and A. Licea-Claverie, *Polym. Bull.*, 2013, **70**, 653–664.

53 R. Pelton, *J. Colloid Interface Sci.*, 2010, **348**, 673–674.

54 A. Fava, A. Iliceto and E. Camera, *J. Am. Chem. Soc.*, 1957, **79**, 833–838.

55 H. M. Crowther and B. Vincent, *Colloid Polym. Sci.*, 1998, **276**, 46–51.

56 I. B. Santarino, S. C. B. Oliveira and A. M. Oliveira-Brett, *Electrochem. commun.*, 2012, **23**, 114–117.

57 S. R. K. Ainavarapu, A. P. Wiita, H. H. Huang and J. M. Fernandez, *J. Am. Chem. Soc.*, 2008, **130**, 436–437.

58 A. Garcia, N. D. Eljack, M. A. Sani, F. Separovic, H. H. Rasmussen, W. Kopec, H. Khandelia, F. Cornelius and R. J. Clarke, *Biochim. Biophys. Acta - Biomembr.*, 2015, **1848**, 2430–2436.

59 E. B. Getz, M. Xiao, T. Chakrabarty, R. Cooke and P. R. Selvin, *Anal. Biochem.*, 1999, **273**, 73–80.

Chapter 6

Conclusions and Future Work

6.1. Conclusions

The main aim of this research was to investigate polyNIPAM nanogels for use as an in situ forming implant (ISFI). Three different solidification concepts were explored, and it was found that solidification to form a drug depot could be achieved using the combined dual stimulus of physiological temperature and ionic strength to trigger the aggregation of nanogel particles in a concentrated polyNIPAM nanogel dispersion to form a solid drug depot at the injection site. The nanogels were also able to rapidly and responsively aggregate at the injection site after being injected through a standard 18G needle, resulting in a small burst release compared to other ISFI systems. This dual triggered solidification of polyNIPAM nanogels is a novel ISFI technology. Further research then expanded on this nanogel based ISFI to gain a greater understanding and further optimisation for its use as an ISFI. The system was able to meet the aims set out in the research objectives (Chapter 1, section 1.6), which could potentially allow it to be developed towards a commercially and clinically viable ISFI, whilst also potentially offering better performance than other ISFIs. The nanogel system was able to efficiently entrap a hydrophobic drug or solid drug nanoparticle (SDN) payload with a burst release as low as 0.5% of the cumulative release achievable. A high drug loading was also possible, with depots remaining mechanically stable with up to 66 wt% loading with SDNs. Drug release from the depot was also maintained for over 120 days in the *in vitro* release. This release rate could also be tuned, depending on the ratio of polyNIPAM and polyNIPAM-co-allylamine nanogel used in the depot formulation, or the size of the polyNIPAM nanogels used. The nanogels also presented no cytotoxicity in the limited preliminary studies conducted. Finally, nanogels created with a biodegradable di-sulphide cross-linking agent were demonstrated to be degradable in a physiological environment.

Using polyNIPAM in its nanogel form also gave four important advantages for this ISFI. These are (1) the colloidal stability of nanogels can be tailored by their synthesis conditions, as such, so they can be synthesised so that they are no longer colloidally stable above the VPTT at increased ionic strength. This allows triggered aggregation to occurs via the dual triggers of the temperature and ionic strength of the depot injection site, (2) the large surface area of polyNIPAM nanogels compared to bulk hydrogels allows rapid aggregation at the depot site, entrapping the payload, and avoiding the larger burst release seen in the slow gelation of other ISFI systems,

(3) Incorporation of a comonomer in the nanogel synthesis allows easy tuning of the release rate of drug, (4) sheer thinning behaviour of the nanogel allows easy injection of the material. A short summary of each results chapter can be found below.

6.1.1. Chapter 2

Chapter 2 explored three concepts for in situ solidification of a polyNIPAM nanogel dispersion. These concepts were pH enhanced thermally triggered gelation to form a shrunken gel, charge based colloidal gel network formation, and dual temperature and ionic strength triggered aggregation. The comonomers allylamine and acrylic acid were successfully incorporated into the nanogel synthesis to give pH responsive and oppositely charged nanogels required for pH or charge based gelation. Polyvinylpyrrolidone (PVP) stabilised nanogels were used for these two gelation concepts in order to prevent aggregation of the nanogels at physiological temperature and ionic strength. However, PVP also appeared to disrupt the interactions between nanogels which allowed solidification via these mechanisms. Conversely, in the dual temperature and ionic strength triggered aggregation concept, PVP allowed aggregation of concentrated polyNIPAM nanogel dispersions when heated in the absence of the ionic strength trigger, which was undesirable. However, a concentrated dispersion of surfactant free nanogels and nanogels synthesised with sodium dodecyl sulphate (SDS) were shown to responsively aggregate only under the dual-stimuli of physiological ionic strength and temperature. This behaviour allowed the rapid formation of an aggregate depot for drug delivery, as required to act as an ISFI. Hence the aggregation concept using surfactant free and SDS based nanogels were used in subsequent chapters for further testing and development as an ISFI.

6.1.2. Chapter 3

In Chapter 3, surfactant free polyNIPAM and polyNIPAM-co-allylamine nanogels of approximately 550 nm hydrodynamic diameter were successfully synthesised and characterised. As a concentrated dispersion these nanogels could be injected through an 18G needle into subcutaneous tissue and a subcutaneous tissue mimic to rapidly form an aggregate depot. They were also found to entrap a model payload of oil red dyed polystyrene particles upon aggregating to form a depot. The depot was found to vary in density and water content depending on the ratio of polyNIPAM to polyNIPAM-co-allylamine nanogels used. Poorly water soluble drug lopinavir (LPV) in either its powder or SDN form were loaded into the depot for *in vitro* release studies.

This gave a tuneable drug release rate with polyNIPAM-co-allylamine nanogels giving a greater release rate. Sustained release from the depots was also possible for over 120 days, with burst release as low as 0.5% for LPV, and 3.4% for the SDN form of the drug. Release was also shown to occur through Fickian diffusion of drug through the depot matrix. Finally no cytotoxicity was seen in ATP and MTT assays conducted on the nanogels.

6.1.3. Chapter 4

Chapter 4 focused on polyNIPAM nanogels of four different hydrodynamic diameters (65, 160, 310 and 450 nm). These were synthesised using dispersion polymerisation with different concentrations of SDS. As a dilute dispersion in water all the nanogels showed the same swelling ratio in response to temperature, and the same aggregation temperature in higher ionic strength phosphate buffered saline (PBS). As a concentrated dispersion it was shown that dramatic changes in the phase transitions and rheological properties were seen for different nanogel sizes at different temperatures and dispersion concentrations in water and PBS. Swollen gel, shrunken gel, liquid and phase separated (aggregate) phases were all possible under specific combinations of temperature, solvent and dispersion concentration. The smallest nanogels PNA65 showed the most unusual phase and rheological behaviour, which was highly likely due to its different internal structure compared to the larger nanogels. Previous studies have shown a homogeneous internal structure for nanogels of this size (around 65 nm), compared to the increasing core-shell natured structure of the other nanogels with increasing size. When LPV SDNs were loaded into the nanogel depots in an *in vitro* release study, the release rate of drug from the nanogel depot was also tuneable by changing the size of the nanogel used to form the depot. The release rate of drug could also be tuned in a linear fashion by changing the % loading of SDN, or the size of the nanogel used to form the depot. All sizes of nanogel also gave a low burst release of <5% with a 50 wt% payload of LPV SDNs, and a sustained release of drug over the 15 days of the release experiment. The 65 nm diameter nanogels (PNA65) were found to be the most suitable of the different sized nanogels for an ISFI, as a depot with a 66 wt% loading of LPV SDN's remained mechanically stable across the entire release period. Unlike the other nanogels, at a temperature below 35 °C and a high dispersion concentration these nanogels also remained a liquid rather than a swollen gel, which is easier to formulate with drug and inject through a needle.

6.1.4. Chapter 5

Biodegradable nanogels were successfully synthesised using the cross-linking agent N,N'-bis(acryloyl)cystamine (BAC), which contains a degradable di-sulphide bond. These nanogels were synthesised using the monomers NIPAM or N-isopropylmethacrylamide (NIPMAM). Single monomer nanogels, and core-shell nanogels of the two different monomers were produced. The aggregation temperature of the core-shell nanogels was dependant on the ratio of each monomer used in the synthesis, as well as which monomer was used in the core and shell of the nanogel, with aggregation temperature being more sensitive to the LCST of the monomer used in the shell than the core. A nanogel was also synthesised which under physiological conditions contained a collapsed hydrophobic core, whilst also remaining colloidally stable due to its higher LCST shell (PAM/MAM CS 50/50). This may be useful for the delivery of poorly water-soluble drug. Degradation of the particles with the reductant dithiothreitol (DTT) was monitored over time using dynamic light scattering to monitor the mean count rate, hydrodynamic diameter and PdI of the sample. All nanogels synthesised were essentially fully degradable, despite only partial degradation seen in previous studies with different reaction times and temperatures.[1,2] This is likely due to shorter reactions times and lower temperatures, which is something that could be investigated further in the future. The degradation rate was shown to be strongly dependent on the temperature dependent swelling behaviour of the nanogels. Full degradation occurred in less than a day at 25 °C under reducing conditions, but over a week at 40 °C. Higher temperature causes the nanogels to deswell, so that the di-sulphide bonds are less accessible to water soluble reductants. This gives a much lower rate of degradation at a higher temperature, which would be required if a nanogel depots was to medicate a patient over a period of months.

6.2. Future Work

There are several areas where the research and development conducted could be expanded upon further. In Chapter 2, PVP appeared to prevent the colloidal interactions which allow the solidification of polyNIPAM nanogels triggered by a change in pH to form a shrunken gel, or through oppositely charged nanogels self-assembling into a gel. Versions of these nanogels could be synthesised without PVP, and despite the loss of colloidal stabilisation at physiological ionic strength without the steric stabilisation provided by PVP, may still be able to solidify into a gel

without aggregating. This would give alternative methods of solidification and a solid phase with different properties. The ISFI would consist of a shrunken gel like phase, potentially giving different drug release rates and biocompatibilities to the aggregate phase of an ISFI based on a nanogel aggregate depot.

In Chapter 3 the delivery of the poorly water soluble drug LPV and the SDN form of the drug were demonstrated. Release of other drug payloads could be tested. This could include the combination of two or more drugs, as required in combination therapies such as those used to treat cancer,[3] and HIV.[4,5] Release of other nanomedicine delivery vehicles could also be tested.[6,7] The release of hydrophilic drug, which would have a much lower affinity for the depot, and so potentially a much greater release rate could be explored. The biocompatibility of the nanogels could also be tested to a greater extent than the cytotoxicity assays performed in this chapter. The biocompatibility of implantable biomaterials covers a range of aspects which must be considered beyond simply looking at the biocompatibility of the biomaterial in question without considering the effects of injection and implantation. Inflammation, wound healing, and foreign body response should be considered alongside cytotoxicity of the biomaterials.[8] Inflammation response has previously been observed in polyNIPAM in bulk hydrogel, reaching a peak after 30 days,[9] so this could cause potential biocompatibility issues, which would need to be assessed *in vivo*. This inflammation response may be due to polyNIPAM having a more hydrophobic nature above the VPTT, as the more hydrophobic a polymer is, the more monocytic adhesion occurs,[10] which can induce inflammation and other unwanted effects.[11] However, it is important to remember that although polyNIPAM is often described as hydrophobic above its LCST, it's actually more accurate to consider it as partially dehydrated, as many studies have shown it is still surrounded by 20-50 wt% water.[12] Hence it shouldn't be assumed that the hydrophobicity of aggregates will cause biocompatibility issues. Due to the nanogels being nanoparticulate, phagocytosis may also occur, with particles in the size range of the polyNIPAM nanogels previously being demonstrated to be internalised by cells.[13] This phagocytic activity could be investigated.[14]

It was assumed in Chapter 4 that nanogels of different sizes synthesised with SDS had heterogeneous or homogeneous cross-linking density based on their size, as previously reported in literature.[15–22] This could be confirmed using characterisation techniques such as small angle x-ray scattering,[23] or multi angle light scattering,[2] to determine the radius of gyration of the nanogels, giving the density distribution within the nanogels.

This could help substantiate the idea of the smallest nanogel (PNA65) having a low homogeneous cross-linking density, rather than a higher cross-linked core. This would help reinforce the proposal of the smaller nanogel particles having greater deformability and the associated difference in phase and rheological data. It is likely this was the cause of observations such as PNA65 existing as a liquid rather than swollen gel phase at high dispersion concentration and low temperature. Also the fact PNA65 had greater mechanical stability as a depot, where the smaller nanogels potentially deform around the payload to form a cohesive network unlike the larger less deformable nanogels. As the different sized nanogels showed different rates of release of hydrophobic drug, likely due to the size of the porous water filled pores in the matrix,[24–26] it would also be useful to be able to measure the porosity and size of the pores to provide further evidence for the theory underpinning this observation. This could be done through techniques such as cryogenic SEM, AFM and mercury intrusion porosimetry.[27]

In Chapter 5 BAC cross-linked nanogels were demonstrated to be fully degradable with the reduction agent DTT at different temperatures. However, a degradation experiment closer to *in vivo* conditions would be more desirable. The degradation on nanogels with GSH at 37 °C could be monitored in an aqueous dispersion using DLS to determine the timescale of degradation of nanogels under these conditions. More importantly, weight loss from an aggregate depot could be monitored over time, and an in vitro release experiment in the presence of a reducing agent could be conducted to find the effect of the degradation on the release rate of drug over time. The rate of polymer degradation could then be factored into a mathematical model which has previously been used to describe drug release from cylindrical depots based on both diffusion and degradation.[28] The degraded fragments of polymer created from the nanogel degradation could also be analysed, to find the average molecular weight and branching of the degraded polymer fragments to determine how complete the degradation of the nanogels is. Analysis could be performed using a technique such as size exclusion (gel permeation) chromatography.[29] Finally the degradable nanogels could be tested for specific applications. For example the concentration of the reductant GSH is often higher in tumour tissue,[30] and so if the ISFI was injected at the site of a tumour, this might allow a responsive faster rate of local release of drug at the site of the tumour. This is because the tumour would be creating a higher concentration of GSH to enable faster degradation of the depot, and hence a higher drug release rate.

6.3. References

1 J. C. Gaulding, M. H. Smith, J. S. Hyatt, A. Fernandez-Nieves and L. A. Lyon, *Macromolecules*, 2012, **45**, 39–45.

2 M. H. Smith, E. S. Herman and L. A. Lyon, *J. Phys. Chem. B*, 2011, **115**, 3761–3764.

3 R. B. Mokhtari, T. S. Homayouni, N. Baluch, E. Morgatskaya, S. Kumar, B. Das and H. Yeger, *Oncotarget*, 2017, **8**, 38022–38043.

4 V. Pirrone, N. Thakkar, J. M. Jacobson, B. Wigdahl and F. C. Krebs, *Antimicrob. Agents Chemother.*, 2011, **55**, 1831–1842.

5 E. J. Arts and D. J. Hazuda, *Cold Spring Harb. Perspect. Med.*, 2012, **2**, a007161.

6 J. M. Caster, A. N. Patel, T. Zhang and A. Wang, *Wiley Interdiscip. Rev. Nanomedicine Nanobiotechnology*, 2017, **9**, e1416.

7 T. O. McDonald, M. Siccardi, D. Moss, N. Liptrott, M. Giardiello, S. Rannard and A. Owen, in *Nanoengineering - Global Approaches to Health and Safety Issues*, Elsevier, Amsterdam, 2015, pp. 173–223.

8 J. C. Wright and D. J. Burgess, *Long Acting Injections and Implants*, Springer-Verlag, Berlin, 2012.

9 R. Zhu, G. Wu, X. Liu, D. Shi, B. Cao, R. Gu, J. Xiao and H. Liao, *RSC Adv.*, 2015, **5**, 28023–28029.

10 A. Hezi-Yamit, C. Sullivan, J. Wong, L. David, M. Chen, P. Cheng, D. Shumaker, J. N. Wilcox and K. Udipi, *J. Biomed. Mater. Res. - Part A*, 2009, **90**, 133–141.

11 F. G. P. Welt and C. Rogers, *Arterioscler. Thromb. Vasc. Biol.*, 2002, **22**, 1769–1776.

12 R. Pelton, *J. Colloid Interface Sci.*, 2010, **348**, 673–674.

13 H. Hillaireau and P. Couvreur, *Cell. Mol. Life Sci.*, 2009, **66**, 2873–2896.

14 N. Platt and P. Fineran, in *Methods in Cell Biology*, Elsevier Ltd, 2015, vol. 126, pp. 287–304.

15 X. Wu, R. H. Pelton, a. E. Hamielec, D. R. Woods and W. McPhee, *Colloid Polym. Sci.*, 1994, **272**, 467–477.

16 R. Pelton, *Macromol. Symp.*, 2004, **207**, 57–65.

17 A. Fernández-Barbero, A. Fernández-Nieves, I. Grillo and E. López-Cabarcos, *Phys. Rev. E - Stat. Physics, Plasmas, Fluids, Relat. Interdiscip. Top.*, 2002, **66**, 10.

18 M. Stieger, W. Richtering, J. S. Pedersen and P. Lindner, *J. Chem. Phys.*, 2004, **120**, 6197–6206.

19 B. R. Saunders, *Langmuir*, 2004, **20**, 3925–3932.

20 R. Acciaro, T. Gilányi and I. Varga, *Langmuir*, 2011, **27**, 7917–7925.

21 L. Arleth, X. Xia, R. P. Hjelm, J. Wu and H. U. Zhibinc, *J. Polym. Sci. Part B Polym. Phys.*, 2005, **43**, 849–860.

22 M. Andersson and S. L. Maunu, *J. Polym. Sci. Part B Polym. Phys.*, 2006, **44**, 3305–3314.

23 G. R. Deen, T. Alsted, W. Richtering and J. S. Pedersen, *Phys. Chem. Chem. Phys.*, 2011, **13**, 3108–3114.

24 R. Gurny, E. Doelker and N. A. Peppas, *Biomaterials*, 1982, **3**, 27–32.

25 M. V. S. Varma, A. M. Kaushal, A. Garg and S. Garg, *Am. J. Drug Deliv.*, 2004, **2**, 43–57.

26 X. Tongwen and H. Binglin, *Int. J. Pharm.*, 1998, **170**, 139–149.

27 H. M. Rootare, in *Advanced Experimental Techniques in Powder Metallurgy*, eds. J. S. Hirschhorn and K. H. Roll, Springer US, Boston, MA, 1970, pp. 225–252.

28 D. Jones, in *Rapra Review Reports*, Volume 15., 2004.

29 B. Dušan, *J. Sep. Sci.*, 2010, **33**, 315–335.

30 S. C. Barranco, R. R. Perry, M. E. Durm, M. Quraishi, A. L. Werner, S. G. Gregorcyk and P. Kolm, *Dis. Colon Rectum*, 2000, **43**, 1133–1140.